Development of Water-Stable Metal-Organic Frameworks for Oil-Water Separation and Toxic Chemical Sensing

A Dissertation Submitted to the

Indian Institute of Technology Guwahati

as Partial Fulfilment for the Degree of

DOCTOR of PHILOSOPHY

in

CHEMISTRY

by

Abhijeet Rana

Roll No. 206122010

DEPARTMENT OF CHEMISTRY

INDIAN INSTITUTE OF TECHNOLOGY GUWAHATI

GUWAHATI-781039

INDIA

February 2025

DECLARATION:

I hereby affirm that the thesis titled as "**Development of Water-Stable Metal-Organic Frameworks for Oil-Water Separation and Toxic Chemical Sensing**" is the culmination of my research conducted at the Department of Chemistry, Indian Institute of Technology Guwahati. I conducted this research under the guidance of Prof. Shyam P. Biswas. I confirm that this work has not been previously submitted to any other institution or university. I have duly acknowledged collaborative efforts in obtaining results and have appropriately credited materials sourced from other references in the thesis.

Adhering to scientific traditions, I assert that all information presented in this thesis is accurate to the best of my knowledge.

IIT Guwahati

February 2025

Abhijeet Rana

Candidate

Prof. Shyam P. Biswas
Associate Professor
Department of Chemistry
Indian Institute of Technology Guwahati
Guwahati – 781039, India
Tel: +91-361-258 3309
Email: sbiswas@iitg.ac.in

CERTIFICATE

This is to certify that the work presented in the thesis entitled "**Development of Water-Stable Metal-Organic Frameworks for Oil-Water Separation and Toxic Chemical Sensing**" by Mr. Abhijeet Rana, was carried out by the candidate at the Department of Chemistry, Indian Institute of Technology Guwahati, under my supervision and has not been submitted elsewhere for a degree.

IIT Guwahati
February 2025

Shyam Biswas

Thesis supervisor
Department of Chemistry
Indian Institute of Technology Guwahati
Guwahati – 781039, Assam, India

ACKNOWLEDGEMENT

I would like to express my heartfelt gratitude to everyone who played a crucial role in the successful completion of this dissertation. First and foremost, I extend my sincere thanks to my supervisor, Prof. Shyam P. Biswas, for introducing me to the fascinating field of Metal-Organic Frameworks (MOFs). His unwavering motivation, encouragement, and continuous guidance were invaluable throughout this scientific journey, and his support has been instrumental in shaping this thesis.

I also take this opportunity to convey my deep appreciation to the members of my doctoral committee Prof. A. S. Achalkumar, Prof. Gopal Das, and Dr. Animesh Das for their insightful suggestions and guidance during the course of my research.

I am deeply grateful to our collaborators Dr. Amarajothi Dhakshinamoorthy, Dr. Matthias Vandichel, Dr. Felix Steinke, Prof. Uttam Manna, Prof. Aditya N. Panda, Dr. Asamanjoy Bhunia, and Prof. Debasis Manna whose contributions significantly enriched my research.

My sincere thanks to Dr. Kamlesh Kumar and Dr. Arindam Indra for their valuable suggestions during my MSc project and internship. I would also like to thank the Department of Chemistry and the Central Instrument Facility (CIF) at IIT Guwahati for providing access to the sophisticated instruments essential for the characterization of my compounds. Special thanks go to the faculty and staff members of the Department of Chemistry for their support, as well as the technical officers and operators at the Chemistry Department and CIF who assisted in data collection.

I am grateful to Banaras Hindu University, Dharamsala Mahavidyalaya, Madhuban Mahavidyalaya, and Malapada High School for shaping my educational journey. I also extend my heartfelt appreciation to my lab seniors: Dr. Rana Dalapati, Dr. Mostakim SK, Dr. Aniruddha Das, Dr. Soutick Nandi, Dr. Chiranjib Gogoi, Mr. Masud Alam, Dr. Subhrajyoti Ghosh, and Pranam Daa for their expert guidance and invaluable support during this work.

I would like to acknowledge my lab colleagues: Dr. Paltan Laha, Srijan, Sakir, Nazir, Arindam, Priti, Jyotismita, Yashi, Prasanjeet, and Sarif for their unwavering help and camaraderie. They are more than just colleagues; they are like family. The supportive and joyful atmosphere they created in the lab inspired me to work with enthusiasm and dedication. I also express my thanks to Arpa Banik, Gyanesh Mishra, Ananya Hazarika, Arunabha Dutta and Soutrick Bhandari for their contributions during their master's and internship project work.

I am deeply grateful to my friends: Alapna, Somya, Biswamohan, Jugal, Arup, Priyam, Neha, Pallavi, Dinabandhu, Satyajit, Chita, Pabitra, Swarup Daa, Soumen Daa, Amit Bhaiya, and Avishek for their unasked help and constant support during my research. I also thank my friends from my MSc days Prattay, Palak, Soumya, Banamali, Shekhar, Nilotpal, Anajali, Saswata, and Swatee for their positive motivation at that time. I extend my love to Somya Bhai, Saroj Bhai, Sonali, Sarvani, and Praveen from Utkal Samaj, Banaras Hindu University. I also cherish the memories with my school friends Sourav, Tapan, Mani, Chintu, Butu, Bunty, Raju, and Raja who have been an important part of my journey.

I am forever indebted to my teachers and professors from school, college, and university, whose guidance helped shape my career. Special thanks go to my school teachers, Nilamani Sir and Hari Sir, for their encouragement during my early years. I am also grateful to my college senior, Bramha Bhai, for his invaluable support and encouragement to pursue a career in research. I am deeply thankful to my chemistry teacher, Mr. Jayanta Kumar Sahoo, for his wise advice and support during my graduation.

I express my sincere gratitude to the Ministry of Human Resource Development (MHRD), Government of India, and the Prime Minister Research Fellowship (PMRF) for their financial and research support throughout my journey.

I owe a deep debt of gratitude to my family: my parents, Niranjan Rana and Premalata Rana; my elder brothers, Kiran Rana, Debendra Rana, and Sujit Rana; and my sisters-in-law, Babina Rana, Sarojini Rana, and Monali Swain for their unconditional love, sacrifices, and unwavering support during my academic career. I express my love to my niece, Gayatri, and my nephew, Trilochana, whose smiles have brought immeasurable joy into my life.

I also dedicate this work to the memory of my late grandparents Jeje and Jejema Bhobani Rana and Tulasi Rana, and my Aja and Aai Markanda Rana and Purnima Rana for their endless love and affection.

My heartfelt thanks go to my uncles: Narendra Rana, Suresh Rana, Golakh Rana, Alekh Rana, Aruna Rana, Babaji Rana, Damburu Rana, Jaganath Rana, Bunu Rana, Makara Rana, Kuna Rana, Sukadeva Rana, Udhaba Chandra Rana, Surendra Rana, and Akshaya Rana and my aunts: Sara Rana, Pramila Rana, Sumitra Rana, Malati Rana, Tila Rana, Soudamini Rana, Lalita Rana, Pramila Rana, Urmila Rana, and Nirmala Rana for their unwavering support. I am deeply grateful to my cousins: Somi Di, Tiki Dei, Jali Dei, Mili Dei, and Laxmi Dei, Sipu Bhai, Gopal Bhai, Kunu Bhai, Mahani Bhai, Babu Bhai, Ravi Bhai, Ranka Bhai, Jatuli Bhai, Bapun, Ravi, Dipun, Bunty, Gourav, Pinku, Puja, Khusi, Lucky, Liza, and Lucky for their companionship and love.

Finally, I would like to express my deepest gratitude to the Almighty Lord Jagannath, Maa Biraja, Maa Kamakhya, Narasingha Bhagwan, and Gramadevi Maa Basulai for bestowing upon me the strength and determination to overcome life's challenges and successfully complete this dissertation. Although many individuals have contributed to this work, their efforts, even if not always explicitly mentioned, are deeply appreciated and sincerely acknowledged.

Abhijeet Rana

DEDICATED TO MY FAMILY

TABLE OF CONTENTS

Ph.D. Synopsis Report

Thesis Title: Development of Water-Stable Metal-Organic Frameworks for Oil-Water Separation and Toxic Chemical Sensing

Name of the Candidate: Abhijeet Rana
Roll No.: 206122010
Thesis Supervisor: Prof. Shyam P. Biswas
Department: Chemistry
Institute: Indian Institute of Technology Guwahati, Assam, India

Thesis Overview:

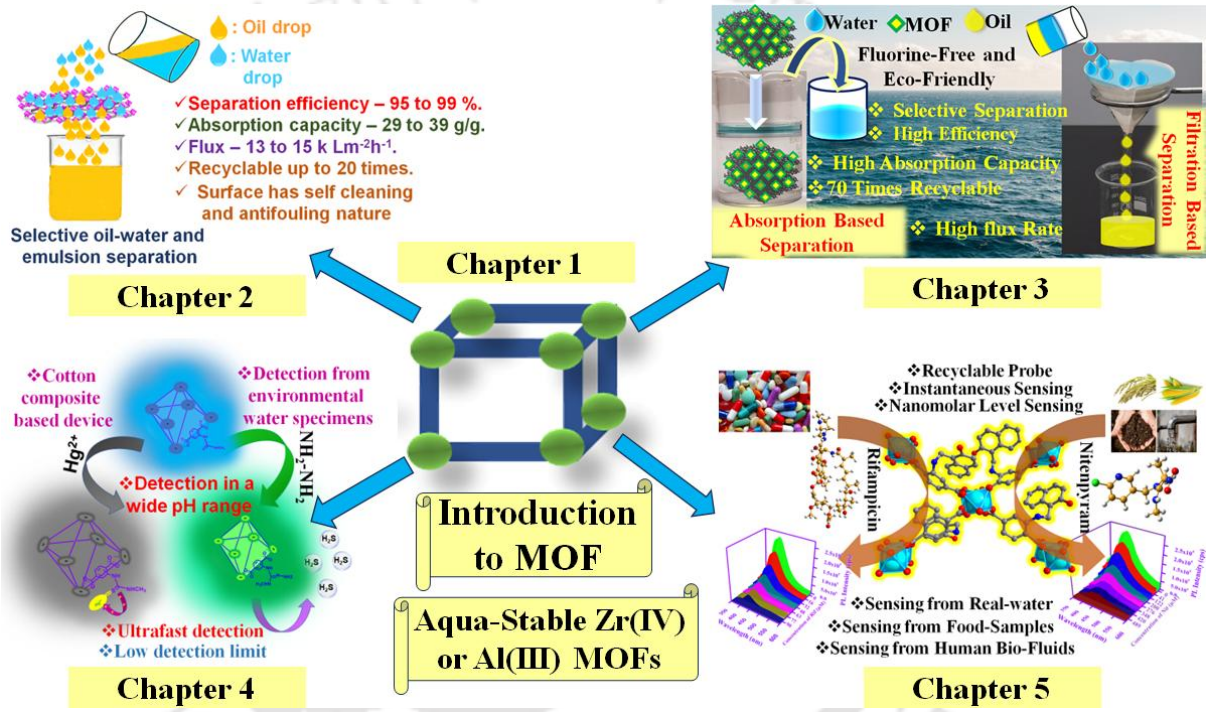

Chapter 1: Evolution of Metal-Organic Frameworks (MOFs) and Their Applicability

MOFs have emerged as a transformative class of materials, attracting considerable attention since late 1990s although discovered earlier. These materials are constructed by linking organic molecules with metal ions or clusters, forming highly crystalline, porous networks with a broad spectrum of potential uses. MOFs offer distinct advantages over traditional porous materials like zeolites, primarily due to their customizable nature. Their properties can be fine-tuned by carefully selecting specific metal ions and organic linkers, and their structure can be modified even after synthesis. This chapter provides a comprehensive overview of the evolution and development of MOFs, examining various synthesis techniques and showcasing their wide array of applications, including catalysis, gas storage, drug delivery, luminescent sensing, carbon capture, chemical detection, oil-water separation, self-cleaning and antibacterial properties. The discussion emphasizes the role of precise structural modifications, particularly the incorporation of specific functional groups in the linker components, which enhance the performance of MOFs in targeted applications. These include detecting bio-active compounds and pollutants, as well as enabling efficient oil-water separation. The flexibility in designing MOFs for specialized purposes underscores their potential as highly versatile materials capable of addressing specific scientific and environmental challenges, making them invaluable in advancing numerous technological fields.

Chapter 2: Superhydrophobic Self-Cleaning Composite of a Metal–Organic Framework with Polypropylene Fabric for Efficient Removal of Oils from Oil–Water Mixtures and Emulsions

This chapter provides the detailed synthesis, characterization and application of a new hydrophobic Hf(IV) based MOF with DUT-52 structure bearing the rigid 1-(2,2,2-trifluoroacetamido)naphthalene-3,7-dicarboxylic acid (H_2L^1) ligand was prepared and its solid structures were characterized with the help of X-ray powder diffraction technique. The other characterization methods like thermogravimetric analysis and Fourier transform infrared spectroscopy were applied to verify the phase purity of the compound. Indexing of the slow scan PXRD pattern was carried out in comparison with the parent DUT-52 MOF in order to know the lattice parameters of our as-synthesized MOF material.

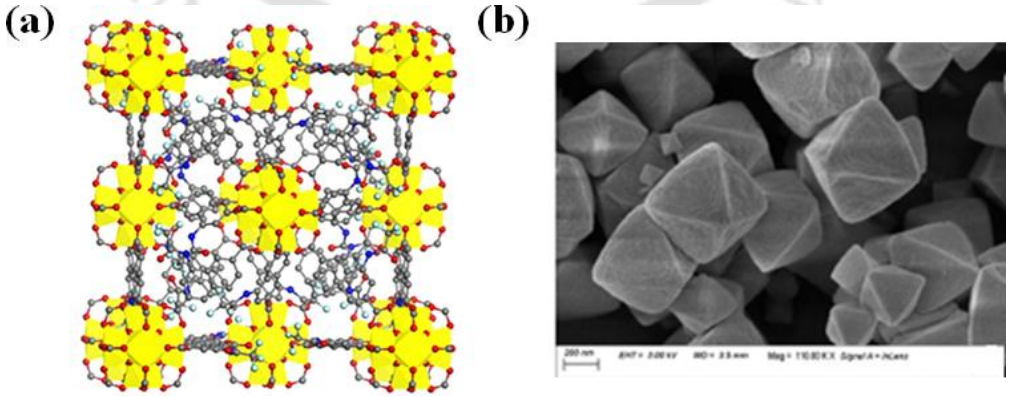

Figure 1. (a) Cubic framework structure of **1′** and (b)FE-SEM image of **1′**.

As-synthesized (**1**) and activated (**1′**) compounds are thermally stable up to 310 °C in air atmosphere. The BET surface area of **1′** was found to be 884 $m^2 g^{-1}$**.** The in-situ synthesis

of this hydrophobic MOF was again prepared and immobilized on the surface of PP fabric of a N95 mask. The surface immobilization of PP fabric of a N95 mask was confirmed by FT-IR, EDX, FESEM, water contact angle measurement (WCA) and BET surface area measurement. The surface area of PP fabric before and after immobilization was found to be 0 and 257 $m^2 g^{-1}$. The contact angle before and after surface modification was found to be 0° and 160° respectively. The superhydrophobic PP fabric (**1′@PP**) possesses remarkable efficiency towards both heavy and light oil separation from oil-water mixture (95 to 99 %). The efficiency of oil-water separation was remained unaltered even in harsh conditions like in different environmental water samples and pH solutions. The hydrophobic nature of synthesized MOF material inspired us to examine its self-cleaning nature. The material displays good self-cleaning nature for various real field applications.

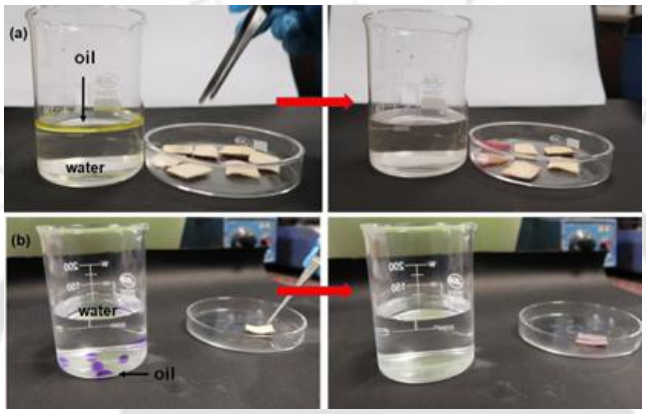

Figure 2 Digital photographs of the discriminative absorption-based separation of (a) floating oil and (b) underwater oil by **1'@PP** composite. Light and heavy oils were coloured with yellow and red for better visualization effect.

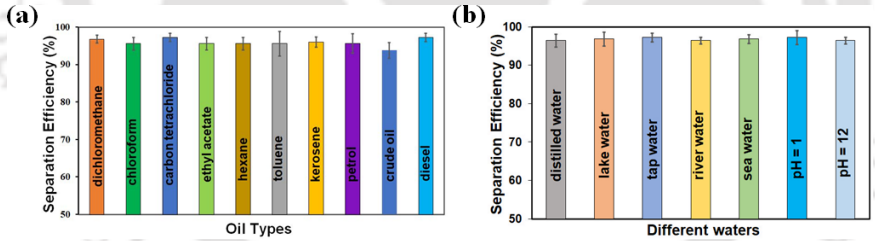

Figure 3 (a) Separation efficiency (%) of **1'@PP** towards various oils from oil-water mixtures presented by error bar plot. (b) Separation efficiency (%) of **1'@PP** towards chloroform from different real water samples to show its applicability in various environmental water bodies.

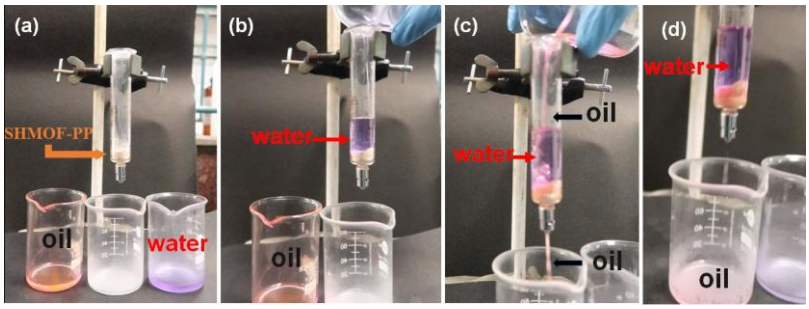

Figure 4 Digital photographs of selective separation of heavy oil by gravity driven method of separation by **1'@PP** (chloroform: red, water: violet).

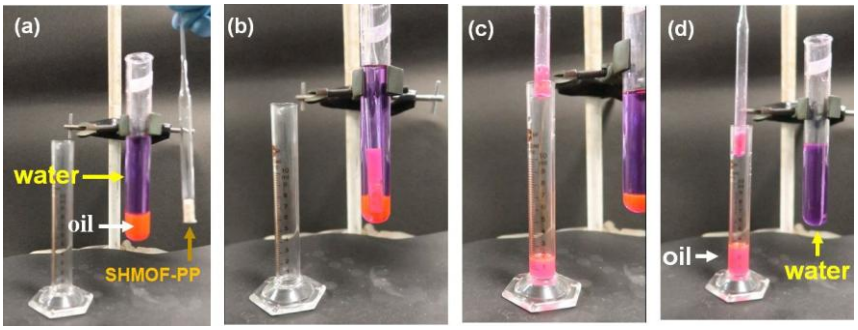

Figure 5 Digital photographs of separation of sedimentary oil by antigravity method of separation by **1'@PP** Oil and water were coloured with red and violet for better visualisation.

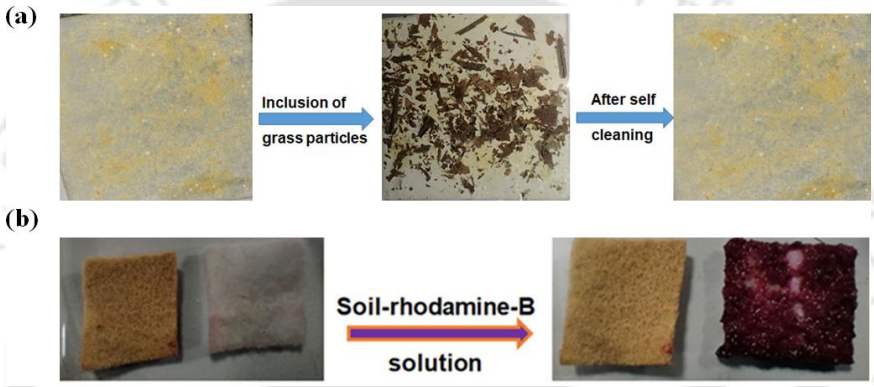

Figure 6 (a) Digital images of **1'@PP** coated glass slide displaying self-cleaning nature. (b) Digital images of **1'@PP** composite and PP-fabric before and after antifouling experiment.

Chapter 3: An Eco-Friendly Approach by Nonfluorous Self-Cleaning Metal-Organic Framework Composite and Membrane for Oil-Water Separation

In this chapter, a superhydrophobic Zr-UiO-66 (**2'**) metal-organic framework was synthesized palamitamidoterephthalic acid (H_2L^2, (H_2L^2: BDC-NH-CO-$(CH_2)_{14}$-CH_3)) linker and zirconium salt. Using the fluorine-free superhydrophobic **2'** MOF a robust **2'@sponge** composite and an **2'@silk** membrane were designed using PDMS-co-PMHS polymer. Initially, the sponge was coated with polydopamine hydrochloride (PDA) followed by dipping into the suspension of PDMS-co-PMHS polymer and **2'**. An enhancement in water contact angle (WCA) from 106 ± 1 to 169 ± 1 was found by the surface drafting of **2'** particles.

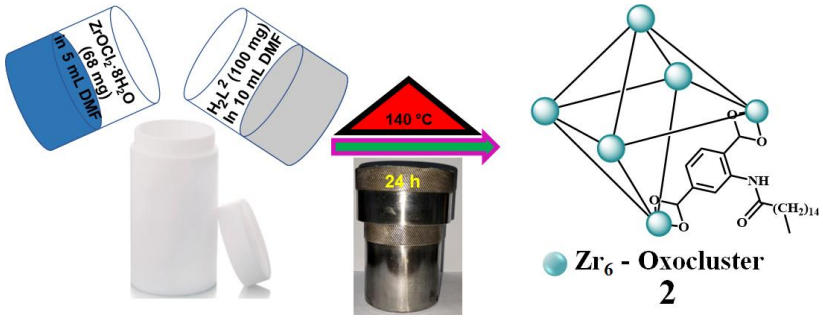

Scheme 1 Detailed synthesis route of compound **2**.

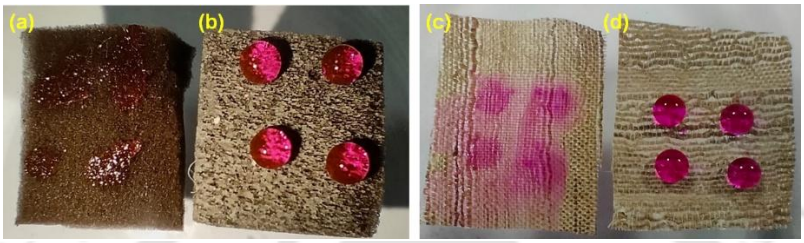

Figure 7 Digital image of beaded water droplets on the surface of (a) polymer-coated sponge, (b) **2′@sponge** composite, (c) polymer-coated membrane and (d) **2′@silk** membrane.

The superhydrophobic composite and membrane displayed a remarkable oil-water separation with 70-time recyclability and a very fast flux rate. The separation efficiency of both the composite and membrane is over 99 % and the composite has an absorption capacity of 43.8-97.2 $g \cdot g^{-1}$ and the membrane has a flux rate of 58263-47416 $Lm^{-2}h^{-1}$ for different oils. The membrane and composite are maintaining their native property of hydrophobicity and crystallinity of drafted MOF particles even after 70 times of oil-water separation experiments. Both the composite and membrane maintain the self-cleaning and anti-fouling properties in soil and dye suspension. The mechanism of oil-water separation was also supported by the ESP diagram of all the possible molecules present in crude oil. The separation of crude oil was also performed. The recyclability of the material towards crude oil was also 70 times. The fluorine-free eco-friendly nature, recyclability harsh conditions and applicability towards the separation of crude oil made this work unique in the field of oil-water separation.

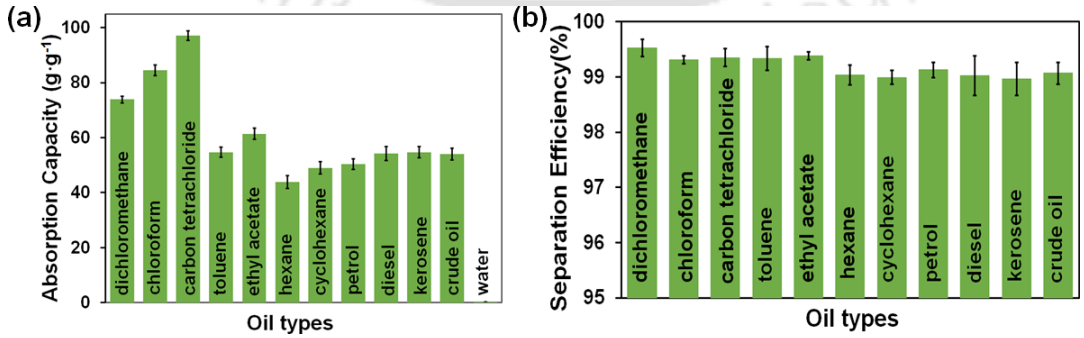

Figure 8 (a) Absorption capacity of **2′@sponge** composite in $g \cdot g^{-1}$. (b) Separation efficiency of **2′@sponge** composite in percentage.

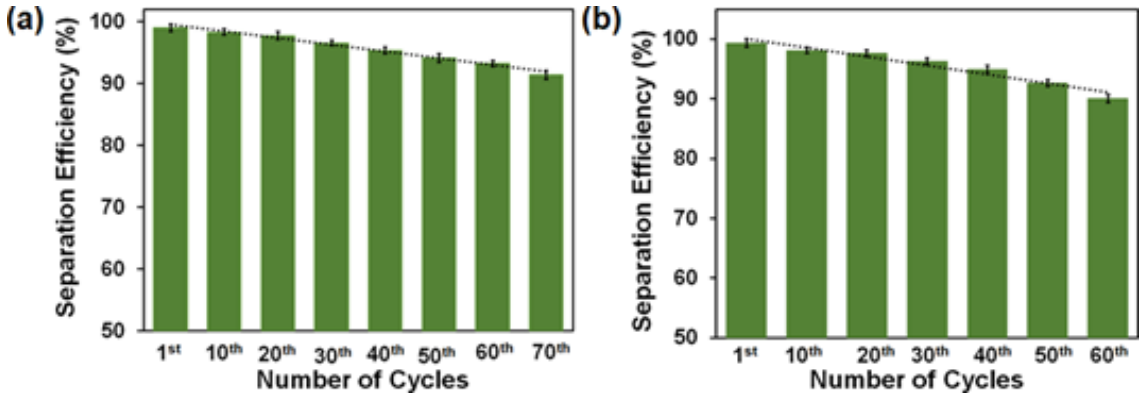

Figure 9 Reusability of (a) **2′@sponge** and (b) **2′@silk** composite for oil/water separation experiments (model oil: petrol).

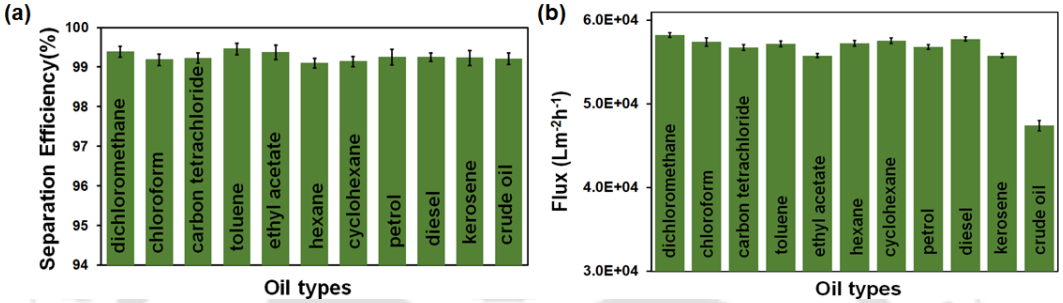

Figure 10 (a) Separation efficiency of **2′@silk** membrane towards various oils in percentage. (b) Flux of oil-water separation by different oils in $Lm^{-2}h^{-1}$.

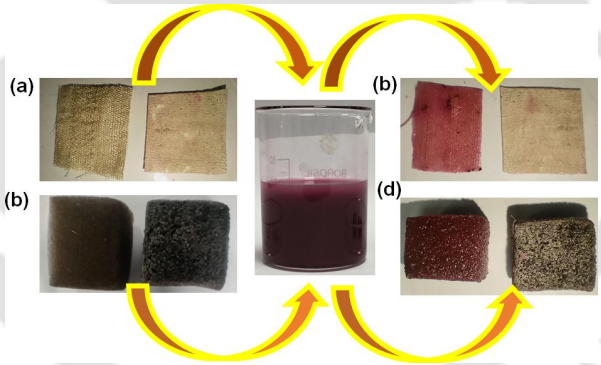

Figure 11 Digital images of **2′@silk** membrane and polymer-coated silk (a) before and (b) after self-cleaning and **2′@sponge** composite (c) before and (d) after self-cleaning.

Chapter 4: Electrophilicity Modulated Targeted Luminescence of MOF-Coated Cotton Composite for Dual Analyte Detection in Aqueous Medium

In this work, a new hafnium (Hf) metal-organic framework and bearing the rigid amine functionalized 2-aminoterephthalic acid ($H_2BDC\text{-}NH_2$) ligand was prepared and thereafter, post-synthetically modified with methylisocyanate to introduce a thioureido functionalization. The solid structure of MOF was characterized with the help of X-ray powder diffraction technique. Other characterization methods like thermogravimetric analysis and Fourier transform infrared spectroscopy were applied to verify the phase purity of the compound. The activated (**3**) compound is thermally stable up to 400 °C in N_2

atmosphere, whereas the stability of **3'** was between 350 to 400 °C. The BET surface area of **3'** was found to be 512 m^2g^{-1}.

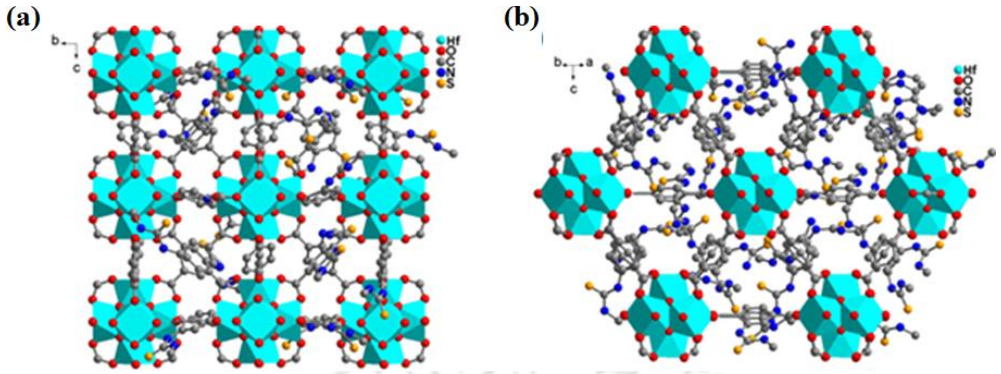

Figure 12 Framework structure of **3** with Hf atoms shown as cyan polyhedra.

Fluorescence titration experiments showed that **3'** exhibits highly selective and sensitive fluorescence turn-off and turn-on behavior towards mercury (Hg^{2+}) and hydrazine (NH_2-NH_2) respectively. A good feature of a chemical sensor is to produce a detectable change towards the target analytes and with our probe, a 91% quenching and 28-fold increment in fluorescence emission intensity were observed for Hg^{2+} and NH_2-NH_2 respectively. The interference experiments suggested that other cations did not interfere with detecting Hg^{2+} and, the probe was sufficiently selective towards NH_2-NH_2 over the competitive analytes. Moreover, short response times (10 s and 50 s) were shown by the probe **3'** for Hg^{2+} and NH_2-NH_2 detection, respectively.

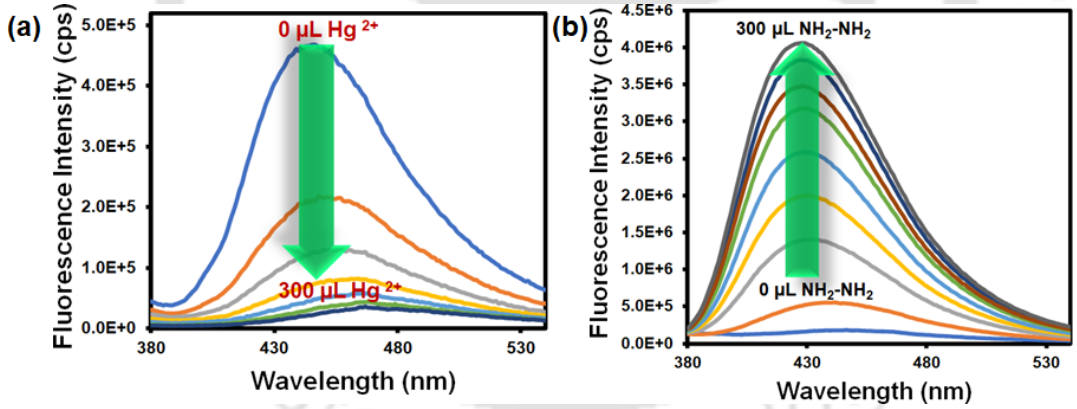

Figure 13 Change in fluorescence emission intensity of probe **3′** after the incremental addition of 300 µL of aqueous 10 mM (a) Hg^{2+} and (b) NH_2-NH_2 solution.

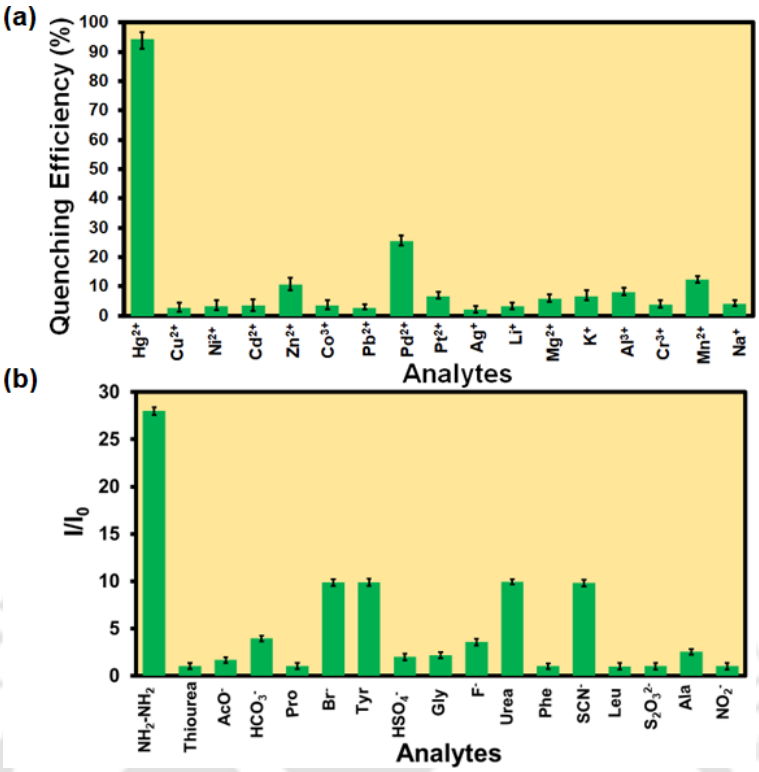

Figure 14 Comparative selectivity bar plots of probe **3′** towards (a) Hg^{2+} and (b) NH_2-NH_2 with their respective congeners (plots are shown with standard deviations of 3 measurements).

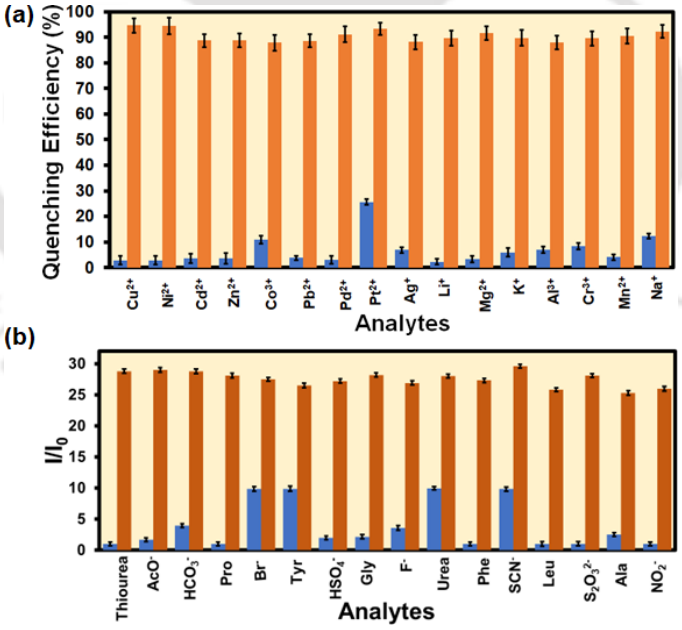

Figure 15 Comparative selectivity bar plot (with standard deviations) of probe **3′** towards (a) Hg^{2+} and (b) NH_2-NH_2 in the presence of their respective congeners. Brown bars represent the quenching efficiency towards Hg^{2+} and fold increment in the case of NH_2-NH_2 and the blue bars belong to the competitive analytes.

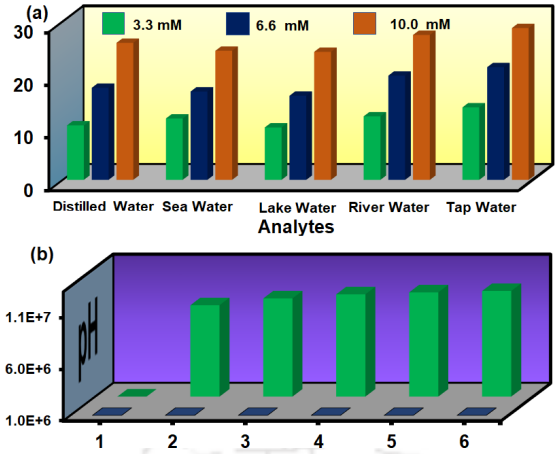

Figure 16 (a) Detection of hydrazine in environmental water specimens at different concentrations. (b) Detection of hydrazine in various pH solutions.

The detection limits were found to be 4.0 nM and 1.9 nM, by our probe for Hg^{2+} and NH_2-NH_2, respectively, which is lower than the maximum acceptable concentration of Hg^{2+} ion as regulated by WHO and US environment protection agency. The response time and LOD of our probe are much lower than the other previously reported probes for Hg^{2+} and NH_2-NH_2 to date. Probe **3'** can also be effectively used for on-site detection of Hg^{2+} and NH_2-NH_2 by using portable MOF-coated cotton composite. The experimental studies about the possible sensing mechanism revealed that the soft-soft interaction between the sulfur atom of the probe and Hg^{2+} is the reason behind the turn-off behavior of our probe in the presence of Hg^{2+}. The nucleophilic attack of hydrazine to the moderate electrophilic thiourea center of our probe caused a drastic increment in fluorescence emission intensity.

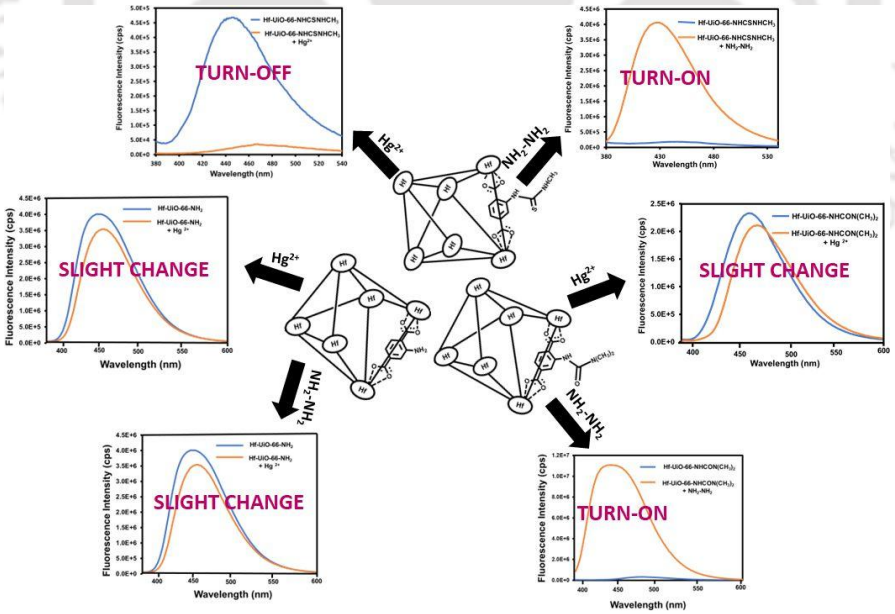

Figure 17 Schematic representation of the change in fluorescence emission intensity of **3**, **3'** and Hf-UiO-66-NHCON$(CH_3)_2$ before and after the addition of Hg^{2+} and NH_2-NH_2.

Chapter 5: Design of Functionalized Luminescent MOF Sensor for Precise Monitoring of Tuberculosis Drug and Neonicotinoid Pesticide from Human Body-Fluids and Food Samples to Protect Health and Environment

The advancement of health science, crop protection, and agricultural research has hastened the production and use of medications, pesticides, and insecticides. The excessive use of pharmaceutical drugs and pesticides brings them to our natural environment (water, soil and agricultural products). The presence of such toxic contaminants in our natural environment directly affects the health of humans and animals. Therefore, detecting and precisely monitoring such active contaminants is essential for protecting our health and environment. In this chapter, we present the judicious design and detailed synthesis of a physiochemically stable luminescent metal-organic framework (MOF) with 2-hydroxy naphthalene functionalization for the selective, fast and nanomolar recognition of tuberculosis drug (rifampicin) and pesticide (nitenpyram). This work is the first-ever luminescent MOF-based nanomolar sensing of nitenpyram and rifampicin in an aqueous medium.

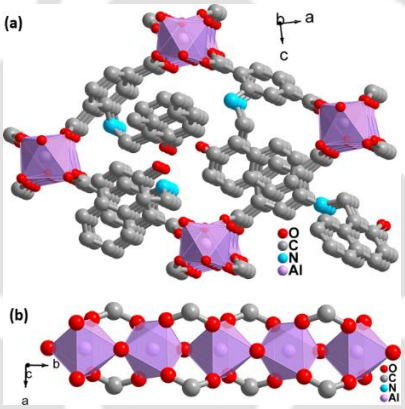

Figure 18 (a) 3D network structure of **4**. (b) 1D inorganic linear chain in the structure of **4**.

This MOF-based sensor could detect rifampicin and nitenpyram instantaneously within 5 s. Pharmaceutical drugs and pesticides have lethal effects even in deficient concentrations. Our probe has an ultralow detection limit towards the sensing of nitenpyram (13.8 nM) and rifampicin (11.7 nM), which is an essential advantage of our probe to detect such lower concentration of nitenpyram and rifampicin for real-world application over the previously reported probes. The overdoses of drugs (rifampicin) into the human body could have toxic effects. Therefore, an ideal probe should be able to detect the targeted analyte from human body fluids. This issue could be addressed with the help of our probe, as it can detect and monitor rifampicin from human blood serum and urine with good accuracy and precision. The presence of pesticides and drugs in environmental waters could harm the health of humans and animals, too. As a result, we performed the detection of nitenpyram and rifampicin from environmental water samples (lake, river, tap and distilled water). Moreover, nitenpyram could also contaminate the soil and agricultural products (crops). Therefore, we have precisely quantified this neonicotinoid pesticide (nitenpyram) from soil and food samples (corn and rice) with the help of our probe. This probe could detect both these analytes (rifampicin and nitenpyram) multiple times due to its recyclable nature, which is an advantage over the single-use probes from an economical point of view. Systematic analytical experiments were performed to understand the exact mechanism of fluorescence quenching. We believe that this work will provide a detailed idea from the

synthesis of functional luminescent MOF to the application of selective sensing of rifampicin and nitenpyram. It could be useful for the biomedical remediation and safeguarding of human health.

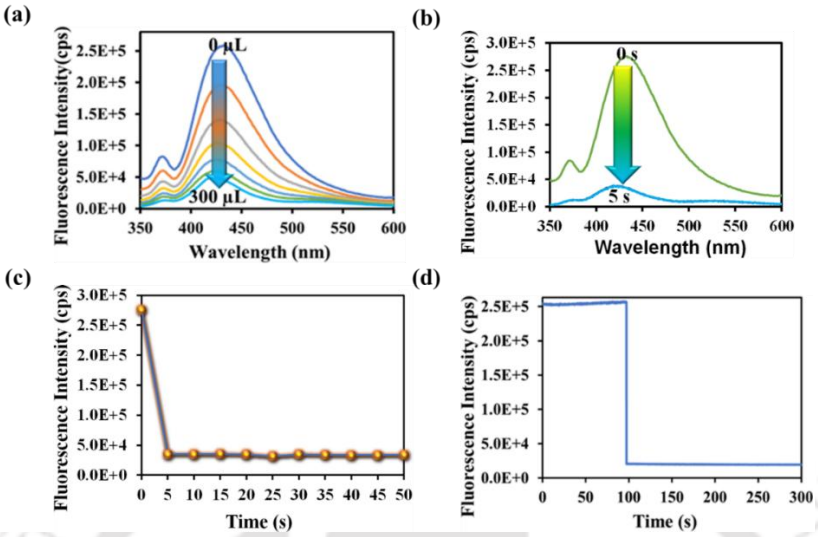

Figure 19 (a) PL emission intensity plot for **4′** with incrementally added rifampicin. (b) Time-dependent PL emission intensity of **4′** in the presence of 300 µL of 1 mM rifampicin. (c) PL emission intensity of the probe with variation in time after adding 300 µL, 1 mM rifampicin. (d) Fluorescence kinetic study of the probe by recording the PL intensity at 430 nm with variation in time after the addition of 300 µL, 1 mM rifampicin.

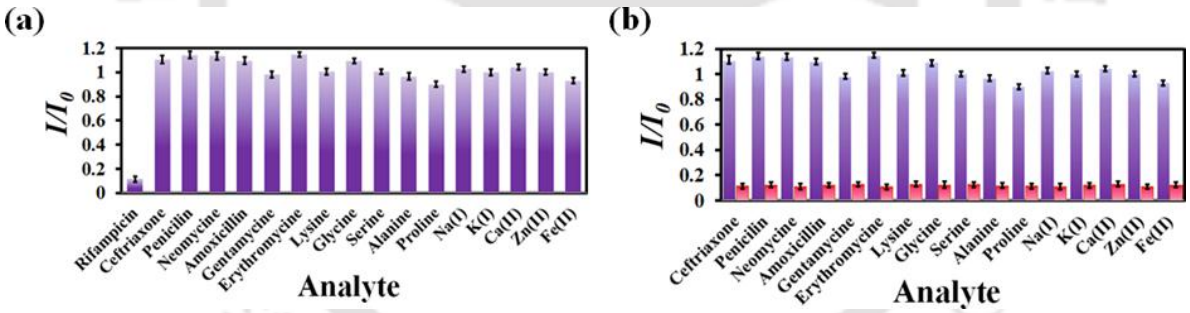

Figure 20 (a) Selectivity plot for rifampicin over its congeners. (b) Selectivity plot for rifampicin in the coexistence of the competitive analytes.

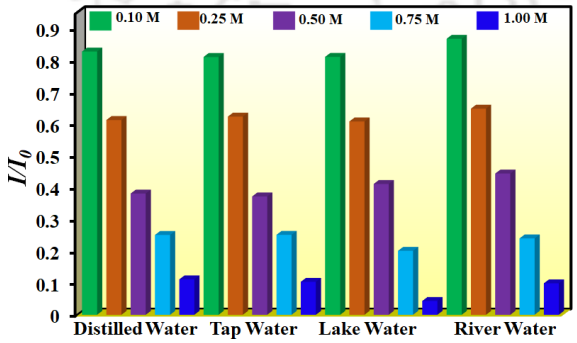

Figure 21 Bar plot depicting the detection of rifampicin from real water specimens by **4′**.

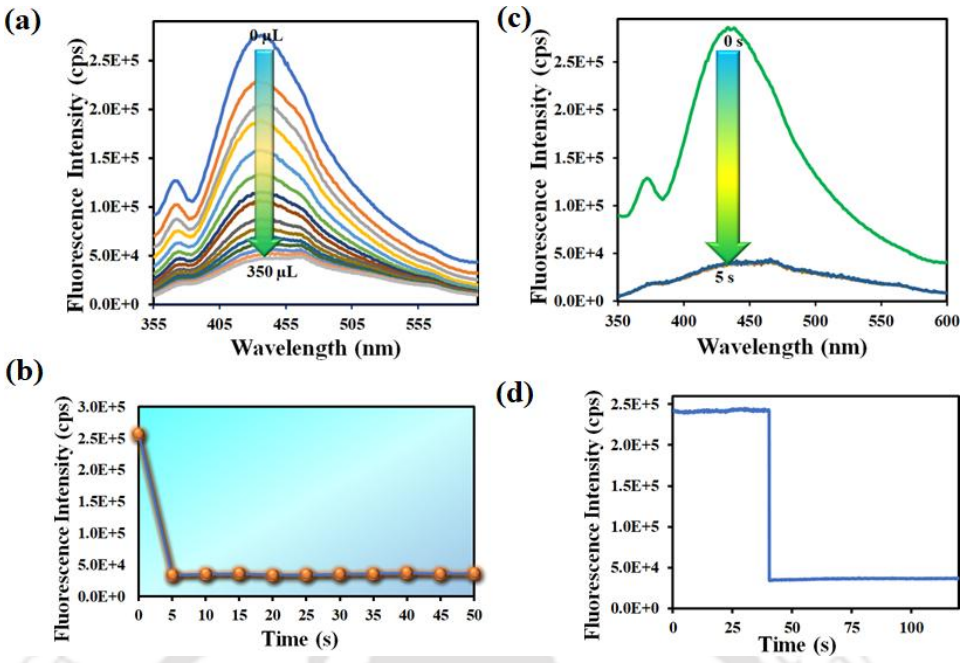

Figure 22 PL emission intensity plot for **4′** with incrementally added nitenpyram. (b) Time-dependent PL emission intensity of **4′** in 350 µL of 1 mM nitenpyram. (c) PL emission intensity of the probe by changing the time after adding 350 µL, 1 mM nitenpyram. (d) Fluorescence kinetic study of the probe by recording the PL intensity at 430 nm by changing the time after the addition of 350 µL, 1 mM nitenpyram.

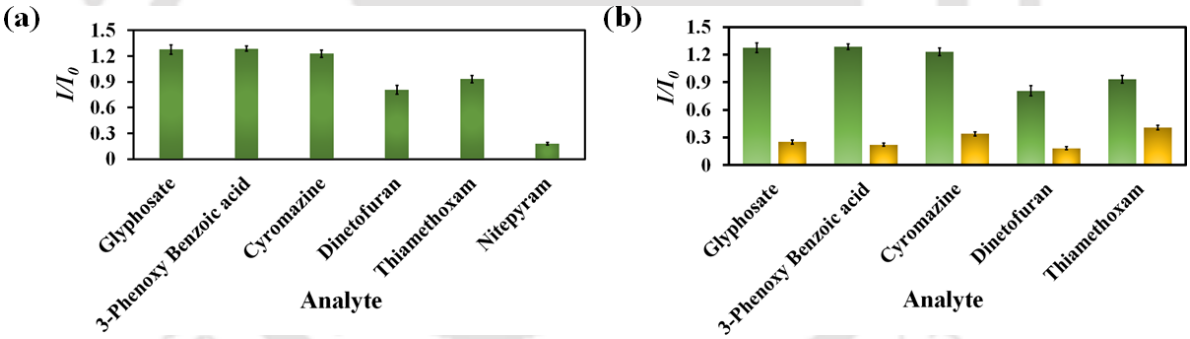

Figure 23 (a) Selectivity plot for nitenpyram over its congeners. (b) Selectivity plot for nitenpyram in the coexistence of the competitive analytes.

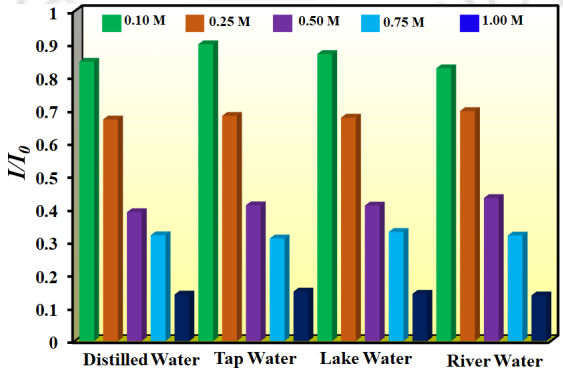

Figure 25 Bar plot depicting the detection of nitenpyram from real-water specimens by **4′**.

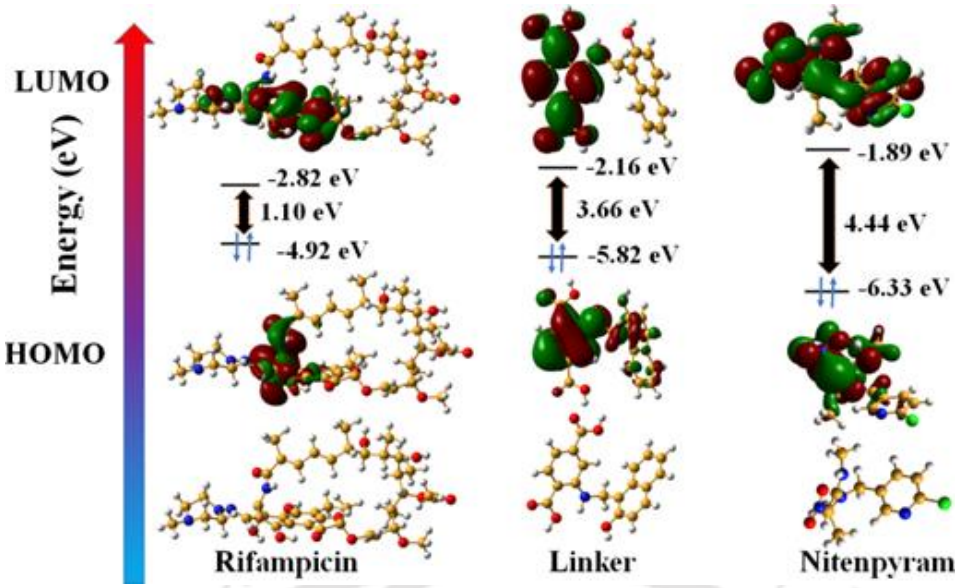

Figure 26 DFT based HOMO and LUMO energy levels of linker, rifampicin and nitenpyram.

Conclusion

The main theme of this thesis is centered on the development of various aqua-stable MOFs and their utilization for oil-water separation and toxic chemical sensing in environmental safety. It embraces comprehensive discussions on the intricate structures of diverse functionalized Zr(IV) and Al(III) metal ion containing MOFs. Here, the functionality of a MOF was deliberately integrated into the MOF linker, enabling its practical application in the fluorescence-based detection and quantification of environmental contaminants and organo-toxins. Additionally, the thesis investigates the synthetic methodology of a hydrophobic MOF designed for the selective and efficient adsorption of oil from marine oil-spillage. We assert that the findings presented in this thesis hold significant importance for promoting the sustainable development of a clean environment and contribute to the accurate monitoring of toxic environmental contaminants.

Evolution of Metal-Organic Frameworks and Their Applicability

Metal-organic frameworks (MOFs) have emerged as a transformative class of materials, attracting considerable attention in the late 1990s although discovered before. These materials are constructed by linking organic molecules with metal ions or clusters, forming highly crystalline, porous networks with a broad spectrum of potential uses. MOFs offer distinct advantages over traditional porous materials like zeolites, primarily due to their customizable nature. Their properties can be fine-tuned by carefully selecting specific metal ions and organic linkers, and their structure can be modified even after synthesis. This chapter provides a comprehensive overview of the evolution and development of MOFs, examining various synthesis techniques and showcasing their wide array of applications, including catalysis, gas storage, drug delivery, luminescent sensing, carbon capture, chemical detection, oil-water separation, self-cleaning and antibacterial properties. The discussion emphasizes the role of precise structural modifications, particularly the incorporation of specific functional groups in the linker components, which enhance the performance of MOFs in targeted applications. These include detecting bio-active compounds and pollutants, as well as enabling efficient oil-water separation. The flexibility in designing MOFs for specialized purposes underscores their potential as highly versatile materials capable of addressing specific scientific and environmental challenges, making them invaluable in advancing numerous technological fields.

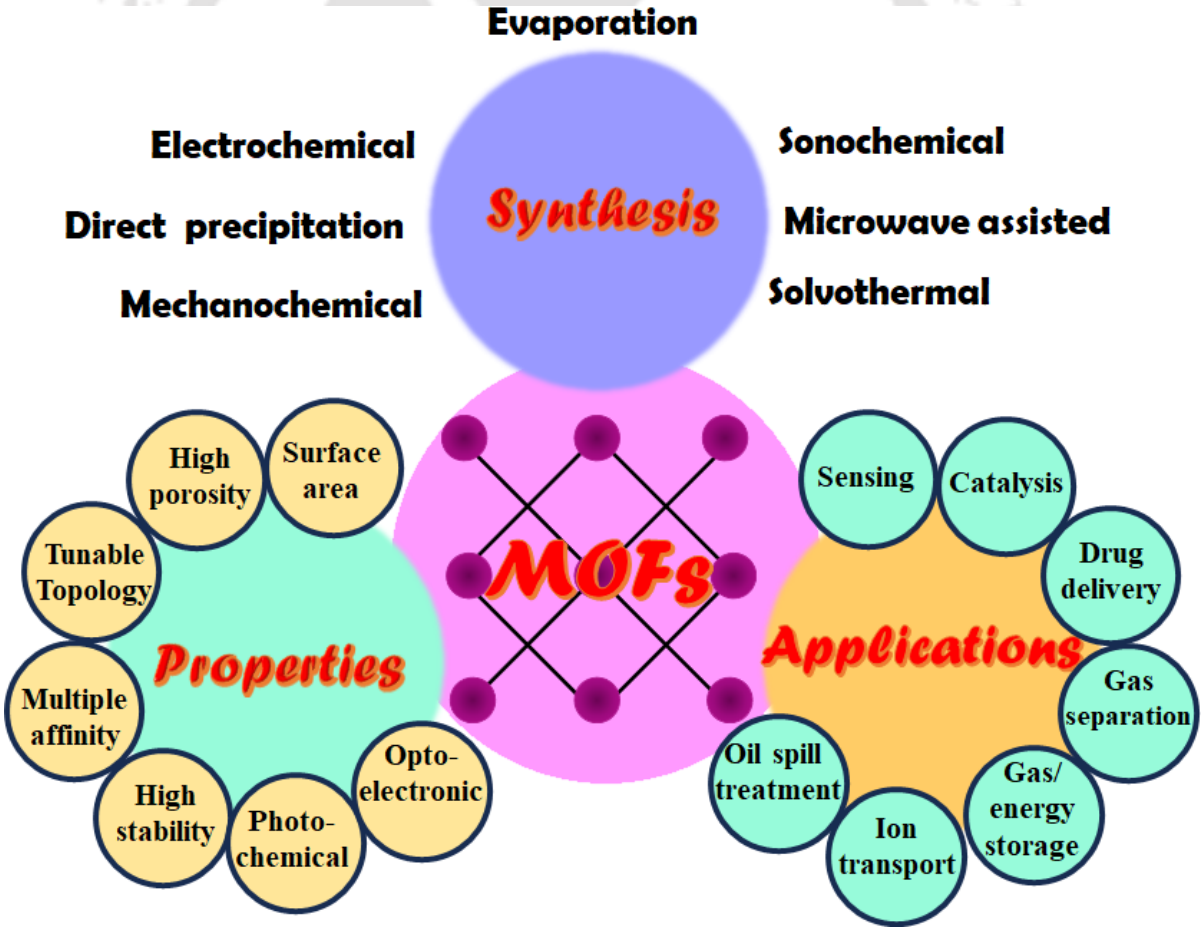

1.1 Introduction

The history of coordination chemistry, coordination polymers, and metal-organic frameworks (MOFs) reflects the continuous evolution of inorganic and organic chemistry, with each development building upon previous discoveries. The foundation of coordination chemistry was established in the early 19th century, primarily through the work of Swiss chemist Alfred Werner. In 1893, Werner proposed the concept of coordination compounds,[1] introducing the idea of coordination bonds between metal ions and organic molecules known as ligands. This ground breaking work revolutionized the understanding of metal-ligand interactions, earning Werner the Nobel prize in chemistry in 1913. Coordination compounds typically consist of a central metal ion bonded to one or more ligands through coordinate covalent bonds, forming stable complexes. Early examples of such complexes, like $[Cu(NH_3)_4]^{2+}$ and $[Fe(CN)_6]^{4-}$, demonstrated the variety of bonding interactions and geometries that metal ions could form with ligands.[2-5] This laid the groundwork for further exploration into these complexes structural properties and reactivity, influencing fields such as catalysis and material science.

By the mid-20th century, coordination chemistry evolved to include coordination polymers formed by repeating metal-ligand units that create extended one-, two-, or three-dimensional networks. This development was driven by the need to explore materials with unique properties such as conductivity, magnetism, and porosity. The 1960s and 1970s saw the emergence of coordination polymers composed of metal ions or clusters linked by organic ligands. However, early coordination polymers often lacked the structural rigidity and order that would later be seen in MOFs.[6] Pioneering work by researchers such as J. M. Lehn, who won the Nobel prize in chemistry in 1987, emphasized the importance of molecular assembly, which led to the synthesis of more defined coordination polymers.[7] These materials, often considered inorganic-organic hybrids, began to show potential applications in catalysis, magnetism, and gas adsorption.

In 1756, Swedish chemist Prof. Axel Frederik Cronstedt discovered natural zeolites, porous materials that have been widely used due to their ability to adsorb and separate molecules.[8] However, zeolites have limitations, particularly in their inability to modify pore size and incorporate functional groups to meet specific needs. This limitation sparked further efforts to develop materials with tunable porosity. In the 1990s, Prof. Robson and Prof. Hoskins synthesized the first functionalized microporous coordination polymer, a porous cage formed between Cu(I) metal nodes and TCTPM (4,4′,4″,4‴-tetracyanotetraphenylmethane), which demonstrated the possibility of modifying pore volumes and incorporating different sized linkers to create materials with tunable porosity.[9] This was a pivotal moment in the development of more versatile coordination-based materials.

The discovery of MOFs is deeply rooted in the pioneering work of Prof. O. M. Yaghi, who, in 1999, introduced a solvothermal synthesis method to create a highly porous, crystalline organic-inorganic hybrid framework known as MOF-5.[10] This material, with porosity comparable to activated carbon and zeolite, exhibited a Langmuir surface area of 3800 m^2/g. MOF-5 was a zinc-based framework with a pcu-topology, synthesized by heating a mixture of $Zn(CH_3COO)_2$ and benzene-1,4-dicarboxylic acid in DMF. This marked the beginning of reticular chemistry, which continues to influence the development of new materials with tailored properties.

Today, MOFs are defined as a class of giant coordination polymers that combine organic linkers and metal ions in a network structure, which can extend in one, two, or three dimensions.[11-12] Since the synthesis of MOF-5, over 1,13,000 of MOF structures have been reported, demonstrating these material's vast diversity and versatility.[13] MOFs have become a focal point in the fields of inorganic chemistry and material science due to their tunable surface

area, porosity, and functionality.[14] Their exceptional physicochemical stability, catalytic activity, and ability to selectively detect analytes have made them highly desirable for a variety of applications, including chemical separation, gas storage, drug delivery, and luminescence sensing.[15-20] Luminescent MOFs, in particular, have gained significant attention due to their high selectivity, fast response, reversibility, and operability.[21-24] They have successfully detected a wide range of substances, such as cations, anions, bio-active molecules, reactive oxygen and nitrogen species, and volatile organic compounds.[25-28]

MOFs are unique among porous materials. Their surface area typically ranges from 1000 to 10,000 m^2/g,[29] and their porosity can be finely tuned by altering the size and functional groups of the organic linkers.[30] Unlike traditional porous materials like zeolites or activated carbon, MOFs can be post-synthetically modified, offering flexibility for tailoring their properties to meet specific needs.[31] This ability to modify the framework after synthesis makes MOFs especially versatile as adsorbent materials.

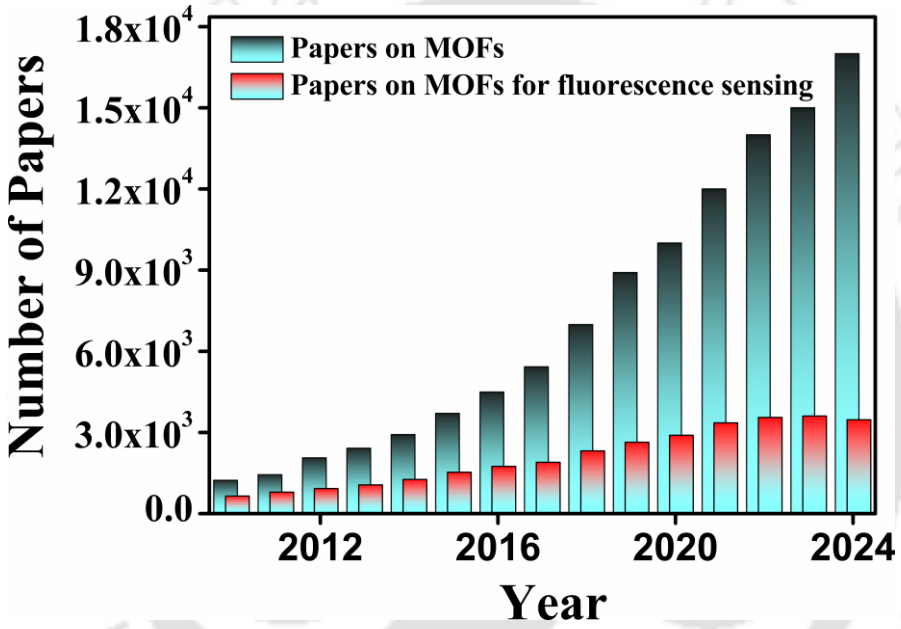

Figure 1.1 Number of research papers per year from 2010-2024 on the topics of "metal-organic framework" and "metal-organic framework for fluorescence sensing". The figure was drawn using Scifinder's database. Search was conducted in December 2024. The search employed keywords such as "metal-organic framework" and "water-stable metal-organic framework," specifically focusing on applications in fluorescence sensing.

Another notable feature of MOFs is their outstanding physicochemical stability. The stability of these materials depends on the metal ion used and the strength of the metal-linker bonds. MOFs synthesized with high oxidation state metals, such as Cr(III), Fe(III), Ti(IV), Al(III), Zr(IV), and Hf(IV), tend to exhibit better stability.[32-37] However, despite the advancements in developing stable MOFs, their application in industrial settings is still limited by factors such as stability under extreme conditions (e.g., highly acidic or basic environments, high temperatures, or moisture). This presents an ongoing challenge in the field: the need to develop ultra-stable MOFs that can withstand the demanding conditions found in industrial processes.

In recent years, the synthesis of superhydrophobic MOFs has garnered considerable interest, particularly for applications such as oil-water separation, self-cleaning, dye removal, anti-icing, and corrosion resistance.[38-43] While over 1,13,000 of MOF structures are known, only around 100 are hydrophobic, and fewer than 30 are superhydrophobic.[44-46] Very few of these materials

have been utilized in practical applications like oil-water separation, making this a promising area for future research.

In this thesis, I have focused on the synthesis, characterization, and application of Zr(IV) and Al(III)-based MOFs from the UiO (University of Oslo) and MIL (Material of Institute Lavoisier) series, such as UiO-66 and MIL-53. These materials are particularly appealing due to the high oxidation state of zirconium and aluminium, which contributes to the synthesis of highly stable MOFs and their non-toxic and eco-friendly nature. Over the past decade, the UiO and MIL series have been the subject of significant research, and these materials have shown great promise in various applications, including sensing and oil-water separation. This research aims to explore and expand the potential of UiO and MIL-type MOFs for these applications.

1.2 Essential Roles of MOFs in Tackling Modern Water Pollution

The modern lifestyle has contributed significantly to water pollution through various sources such as industrial waste, agricultural runoff, untreated sewage, plastic waste, oil spills, mining, and biomedical waste.[47-48] Industrial growth and urbanization release toxic chemicals and heavy metals into water bodies, while agriculture contributes to contamination through the runoff of chemicals. Inadequate sanitation and waste management exacerbate the issue, particularly in developing regions. Plastic pollution and oil spills harm marine ecosystems, and mining activities introduce hazardous substances into water. Deforestation reduces the natural ability of ecosystems to filter water, while climate change worsens the situation with altered rainfall and flooding patterns. Water pollution leads to severe health risks, including waterborne diseases and long-term illnesses like cancer. It also damages biodiversity, disrupts ecosystems, and results in economic losses in sectors such as fishing and tourism.[49-50] This pollution reduces access to clean water and threatens food security. Minimizing environmental pollution while maintaining the comforts of modern life represents one of the foremost challenges for environmental scientists in the 21st century. Consistent and comprehensive monitoring of domestic and urban water pollution is crucial to understanding its dynamics and mitigating its impact. Regular water quality surveillance is essential to ensure that human health and ecological integrity are preserved in the face of increasing pollution levels.

Among the various sources of water pollution, oil spills are considered one of the most severe due to the large quantities of oil released into the environment.[51-52] The volume of oil spilled during such incidents is often immense, causing widespread contamination of water bodies. Oil spills are very harmful to the environment, affecting rivers, oceans, and coastal areas.[53] They damage delicate underwater ecosystems and harm places where animals live, like coral reefs, beaches, tidal flats, salt marshes, and mangrove forests.[54-55] Oil contains harmful chemicals that can poison sea creatures, suffocate plants, and disturb the food chain. Coral reefs, which are vital for sea life and tourism, can be badly damaged by oil.[56] Oil also affects beaches and tidal flats, harming plants and animals. In mangrove forests, the oil on tree roots can kill the trees, stopping them from growing back for many years.[55] Oil spill contamination does not just harm the water, it also has an impact on the neighbouring land ecology, air humidity and the emission of greenhouse gases as a result of the burning of the oil.[57]

The birds and mammals are highest affects by the pollution arises from marine oil spill.[58-59] When oil gets on their feathers or fur, it can make it hard for them to stay warm, causing them to freeze or even drown. If animals swallow or breathe in oil, it can poison them, damage their organs, and make it hard for them to eat or reproduce.[59] Oil spills also greatly impact local businesses, especially tourism and fishing.[60] Oil makes beaches look dirty and unattractive, which highly affects tourism and leads to loss of income. Fish also become contaminated by oil, making them unsafe to eat and causing a drop in the fish population, leading to long-term

economic losses. Industries that rely on clean water, such as shipping and coastal businesses, are also affected.[60]

Oil spills can last for a long time. The oil stays in the environment for years, and ecosystems like coral reefs, salt marshes, and mangroves can take decades to recover.[61] Over time, repeated oil exposure weakens animals and plants, reducing the number of species.

Some of the largest oil spills in history have shown just how serious this problem is. The Exxon Valdez spill in 1989 released about 11 million gallons of crude oil in Pacific Ocean, affecting thousands of animals.[62] More than 250,000 seabirds, 2,800 sea otters, and over 300 harbor seals were killed, with the spill causing long-term damage to marine life and the local economy.[63] The economic loss was estimated at $7 billion due to the destruction of fisheries, tourism, and cleanup costs.[62] Similarly, the deepwater horizon spill in 2010 released around 4.9 million barrels (about 210 million gallons) of oil into the gulf of Mexico.[64] This spill killed thousands of marine animals, including dolphins, turtles, and fish, and damaged local industries,[65] causing an estimated $17 billion in economic loss from lost fishing revenues, tourism, and cleanup efforts.[66]

These past disasters show that oil spills are not only dangerous for nature but also for people's livelihoods. They remind us of the need for immediate action and long-term plans to clean up the environment, protect marine life, and support affected communities.

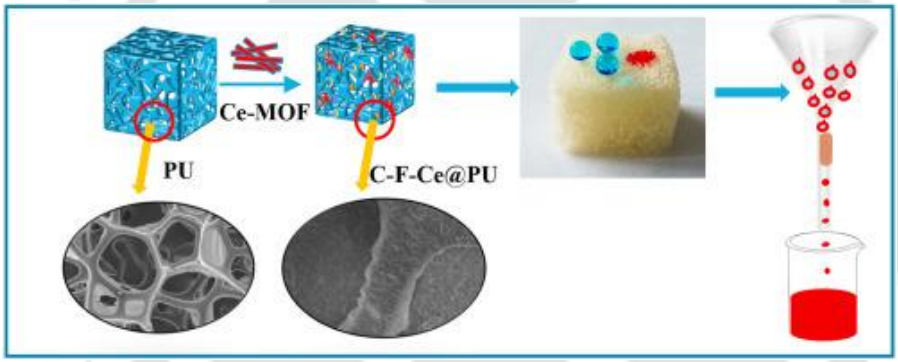

Figure 1.2 Graphical representation of MOF composite for selective separation of oil. This image was collected with permission from the ref. no. 72. Copyright 2023, Elsevier.

Oil spill cleanup uses different methods, like physical, mechanical, chemical, and biological techniques.[67] Each method has its own pros and cons.[68] Sorbent-based methods, which use materials to soak up or stick to oil, are especially useful because they are easy to use, quick to apply, and cause little harm to the environment.[69] Sorbents can be used on beaches, shorelines, and open waters without needing special tools.[70] They are affordable, biodegradable, and safer for marine life compared to chemical dispersants.[71] While sorbents may sink when they absorb too much oil, they are still a flexible and eco-friendly choice for cleaning up spills when used with other methods (Figure 1.2).[72] Designing porous hydrophobic MOFs can be a great way to remove oil spills from water effectively and repeatedly. Many recent studies have explored using hydrophobic polymers, MOFs, and other water-repellent materials to tackle environmental pollution caused by oil spills.

Water pollution caused by toxic water-soluble chemicals such as drugs, antibiotics, herbicides, pesticides, toxic heavy metals (e.g., mercury, cadmium, lead, arsenic, chromium, and manganese), and volatile organic compounds is a major global issue affecting the supply of clean drinking water. These chemicals can have harmful effects on plants, animals, and

aquatic ecosystems. Heavy metals, for instance, can cause mild to severe damage to living organisms, while pesticides and herbicides can disrupt biological processes within organisms. Given the hazardous nature of these pollutants, regular monitoring and removal are essential to protect the environment, ensure clean drinking water, and safeguard aquatic life.[73-76]

One of the most effective and efficient methods for detecting these contaminants in water is fluorescence sensing.[75, 77] Compared to other traditional techniques such as LC-MS, electrochemical detection, capillary electrophoresis, chromatography, atomic emission, absorption spectroscopy, and HPLC,[22, 78-79] fluorescence sensing is faster, more economical, and reliable.[80] This method uses fluorescence-based probes to identify and measure the concentration of harmful substances in water.

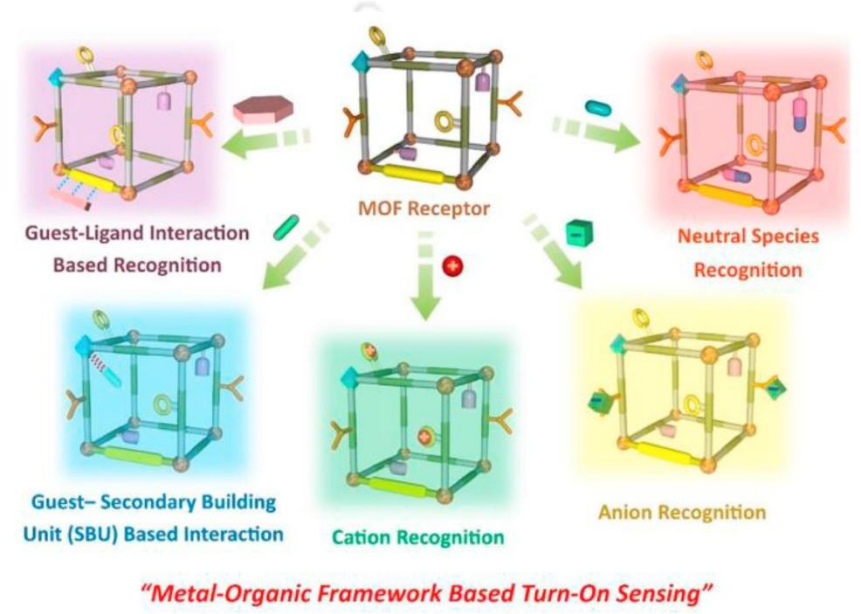

Figure 1.3 Graphical representation of MOF as a sensor. This image was collected with permission from the ref. no. 84. Copyright 2019, John Wiley and Sons.

For fluorescence sensing in aqueous environments, water-stable fluorescent probes must be used to selectively change their emission signals when in contact with targeted pollutants.[80-83] MOFs are a promising class of materials for this purpose. These materials are luminescent and porous, allowing them to adsorb toxic pollutants (Figure 1.3).[84] MOFs, particularly those made from zirconium (Zr(IV) and Al(III)), are highly stable in water, and their high porosity and diverse functionality make them ideal for monitoring and removing pollutants from water. Due to their high porosity, physicochemical stability, versatility, and reusability, thousands of Zr(IV) and Al(III)-based MOFs have been utilized over the past twenty years for fluorescence detection in aqueous environments and the adsorption of various pollutants.

1.3 Fundamental Principles and Strategies in MOF Synthesis

The structure of MOFs consists of two fundamental components: metal centers and organic linkers. The choice of metal and linker is entirely based on the framework's desired properties to suit specific applications. During the synthesis of MOFs metal centers act as a node and the organic linker, known as spacer connects those metal nodes two form a wide variety of MOF structures. Metal centers act as nodes connecting organic linkers, forming a stable framework that determines the MOF's topology (1D, 2D, or 3D).[85] The coordination between metal ions and linkers (ionic or covalent) influences the MOF's stability, porosity, and electronic properties, such as catalytic activity, magnetic behavior, and gas adsorption.[86] Transition metal

ions are commonly used because of the fact that transition metal ions are well-known to prefer different coordination numbers and geometries such as linear, tetrahedral, square planar, square-pyramidal, trigonal-bipyramidal and octahedral geometries.[85, 87] On the other hand, organic linkers act as the "spacer" of the framework. Organic linkers bridge metal centers, defining the MOF's structure, porosity, and surface area.[88-89] The linkers length, shape, and functional groups can be tailored to tune the MOF's properties, such as selective gas adsorption or catalytic activity. Linker's size and geometry control pore size and surface area, which are critical for gas storage, separation, and sensing applications.[90] Due to the infinite number of combinations of the metal cluster with linkers, there is an infinite number of possible network structures. Even the number of possible net topologies is infinite due to many topologically different vertices and the infinite ways of linkage of the vertices. For example, same metal center gives a different metal cluster according to the availability of their connectivity with carboxylic acid linkers (Figure 1.4).[91]

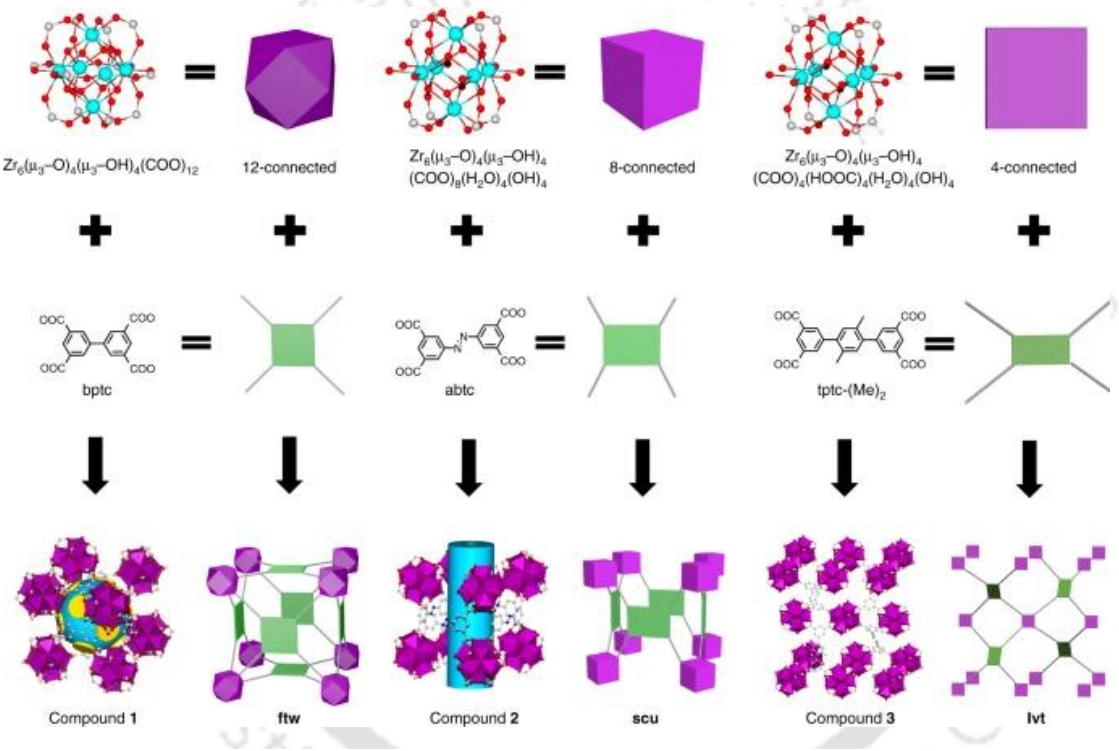

Figure 1.4 The node-and-connector approach to prepare MOFs. The adequate selection of the organic linker (linear in the case of terephthalic acid) and connection geometry of the metal cluster lead to the desired topology. Each framework topology has its characteristic pore size and available surface. Reproduced with permission from ref. 91. Copyright 2018, Nature.

However, using one metal node and different linkers can form MOFs with different structures. For example, in Figure 1.5, it was displayed that the use of Zr(IV) metal center with di, tri and tetra topic ligands could form 12, 8 and 6-connected framework structures.[92]

When looking at the structure of MOFs, it's important to focus on the secondary building units (SBUs), as they determine the overall shape of the framework.[93] Metal-cluster-based SBUs are usually small, finite units with extension points that create clear geometric shapes. These shapes are connected by linkers with multiple connection points, forming repeating frameworks. In a metal SBU, groups of metal atoms are connected either by M-X-M links (where X is a non-metal like N or O) or through a shared extension point, such as M-O-C-O-M in carboxylates.[94] For example, Figures 1.6a and 1.6b show metal atoms arranged in trigonal

and square planar shapes, respectively, while Figure 1.6c illustrates a tetrahedron of metal atoms around an oxo anion, and Figure 1.6d shows a dimetal paddlewheel SBU.[95] In all these cases, the linkers connect two metal ions through coordinating atoms, which helps control the direction of the linkers.[95] The geometry of the SBU depends on not just the metal and linker but also factors like the metal-to-linker ratio, solvents, and the source of anions needed to balance the metal's charge.

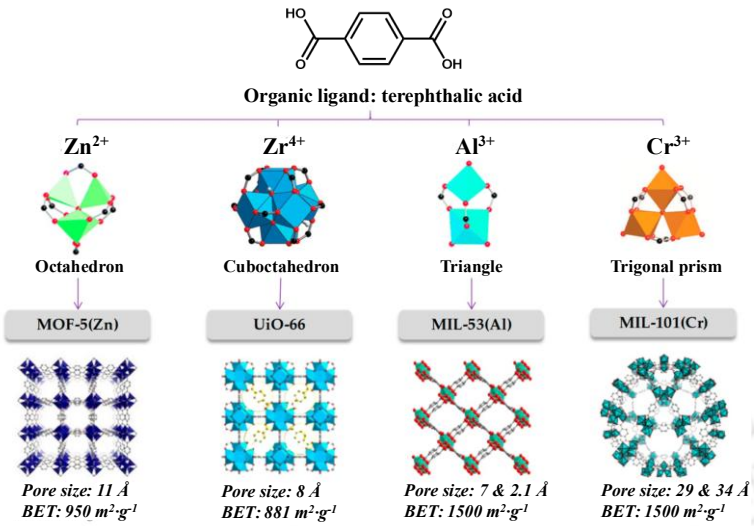

Figure 1.5 The node and connector approach to prepare MOFs. The adequate selection of the organic linker (linear in the case of terephthalic acid) and connection geometry of the metal cluster lead to the desired topology. Each framework topology has its characteristic pore size and available surface. Reproduced with permission from ref. 92. Copyright 2019, MDPI.

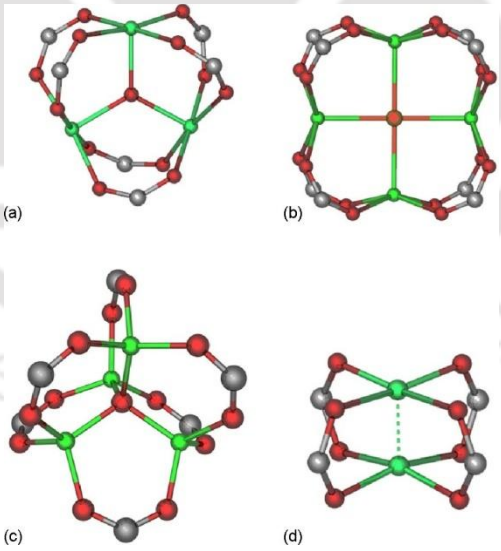

Figure 1.6 Structural representations of some SBUs, including (a) trigonal planar, (b) square planar, (c) tetrahedral, and (d) tetragonal paddlewheel. Reproduced with permission from ref. 95. Copyright 2009, Elsevier.

Once the synthesis of the SBU is achieved, it can be used to guide the assembly of ordered frameworks using rigid organic linkers, allowing for predictable chemistry in the resulting crystalline materials. Yaghi and his colleagues coined this approach "reticular synthesis"[96] defining it as the process of assembling carefully designed, rigid molecular building blocks

into predetermined, ordered structures (networks) that are held together by strong bonds.[96] In this approach, the combination of SBUs (serving as connectors) and organic linkers (serving as linkers) determines the final topology of the framework (Figure 1.7).[89] Reticular synthesis has been successfully applied to various MOF systems, including pillared paddlewheel MOFs, UiO-n, HKUST-1, and others.[97] For instance, as shown in Figure 1.7, a diamondoid network can be formed using 4-connected tetrahedral clusters and ditopic linkers, while a cubic network can be constructed using 6-connected octahedral clusters and ditopic linear linkers.

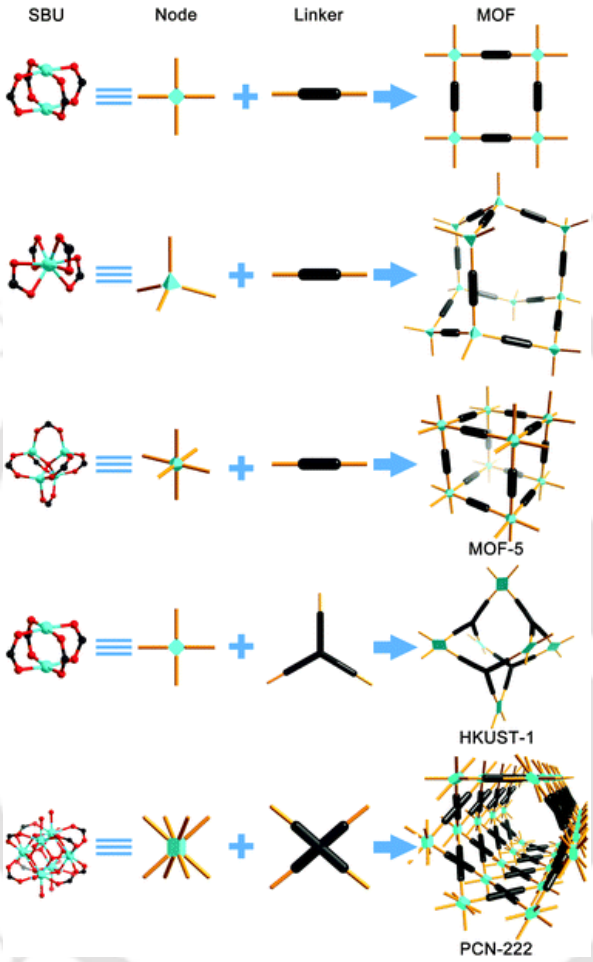

Figure 1.7 Graphical illustration of the construction of some representative coordination polymers/MOFs from SBUs and rigid linkers. Reproduced with permission from ref. 89. Copyright 2014, Royal Society of Chemistry.

The choice of linker with specific coordination sites is a key factor that influences a MOF's pore size, rigidity, stability, and geometry. Linkers are generally categorized in two ways: by their ionic nature (neutral, cationic, or anionic) and by the number of coordination sites they have (ditopic, tritopic, tetratopic, hexa-, or octatopic) (Figure 1.8). The selection of a linker typically follows the hard-soft acid-base theory. Soft metal ions tend to form stable frameworks with linkers that have soft binding sites (such as N-donors), while metal ions with a high positive charge prefer hard coordination centers (such as O-donors) (Figure 1.8).[94] A key feature of linkers is their rigidity, which helps maintain the open pore structure of the MOF even after guest molecules are removed.[98] This is why rigid organic linkers with phenyl rings are often preferred over flexible, long-chain compounds like alkanes. Linkers with multiple binding sites are also preferred because they can connect different metal centers to form extensive networks. Longer organic linkers, such as benzene-1,4-dicarboxylic acid (which

donates oxygen) or 4,4′-bipyridine (which donates nitrogen), are commonly used in MOF synthesis as they provide more space for adsorption. cationic linkers are rarely used because they have poor affinity for positively charged metal ions.[99]

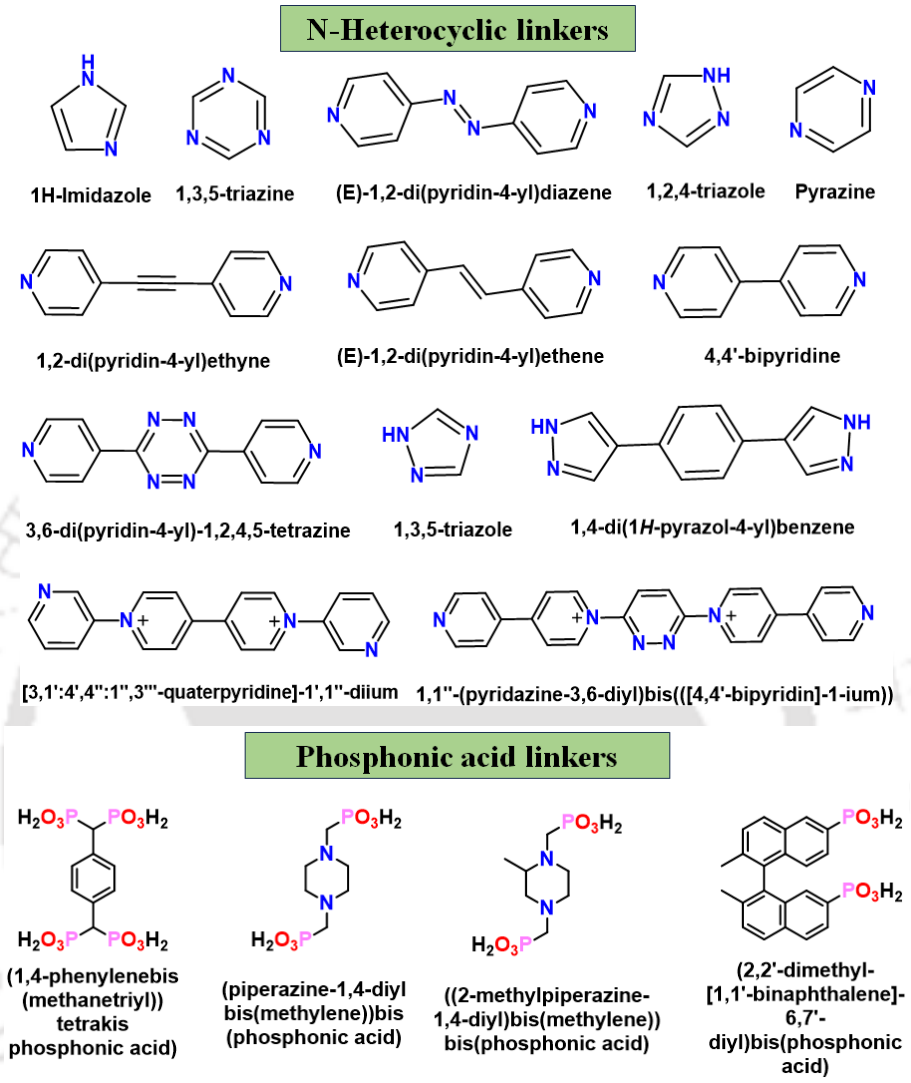

Ditopic carboxylate linkers

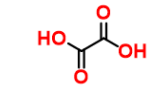
Ethanedioic acid

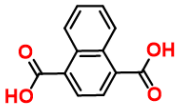
naphthalene-1,4-dicarboxylic acid

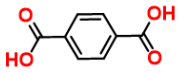
1,4-benzenedicarboxylic acid

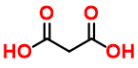
Propanedioic acid

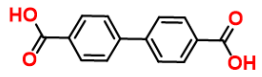
[1,1'-biphenyl]-4,4'-dicarboxylic acid

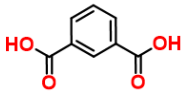
1,3-benzenedicarboxylic acid

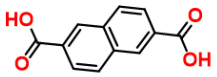
naphthalene-2,6-dicarboxylic acid

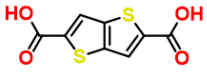
thieno[3,2-*b*]thiophene-2,5-dicarboxylic acid

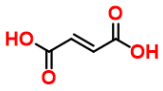
Fumaric acid

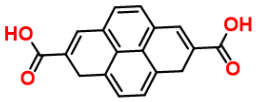
1,8-dihydropyrene-2,7-dicarboxylic acid

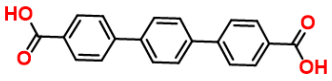
[1,1':4',1''-terphenyl]-4,4''-dicarboxylic acid

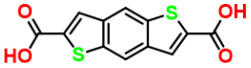
benzo[1,2-*b*:4,5-*b*']dithiophene-2,6-dicarboxylic acid

Tritopic carboxylate linkers

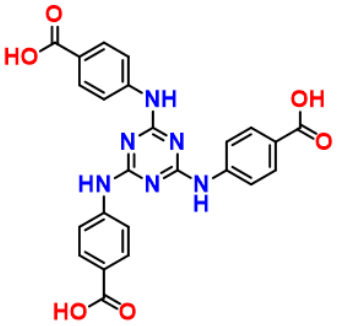
4,4',4''-((1,3,5-triazine-2,4,6-triyl)tris(azanediyl))tribenzoic acid

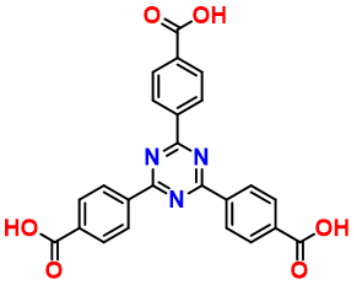
4,4',4''-(1,3,5-triazine-2,4,6-triyl) tribenzoic acid

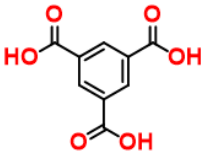
1,3,5-benzenetricarboxylic acid

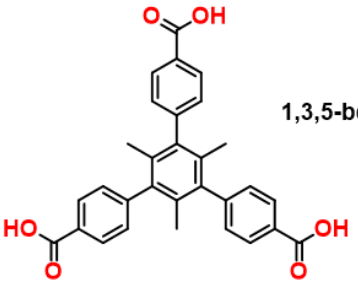
1,3,5-tris(4-carboxyphenyl)-2,4,6-trimethylbenzene

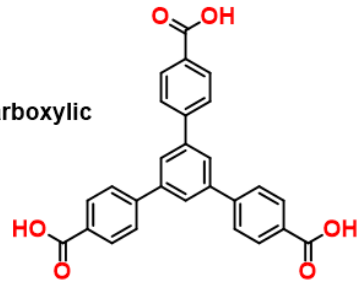
5'-(4-carboxyphenyl)-[1,1':3',1''-terphenyl] -4,4''-dicarboxylic acid

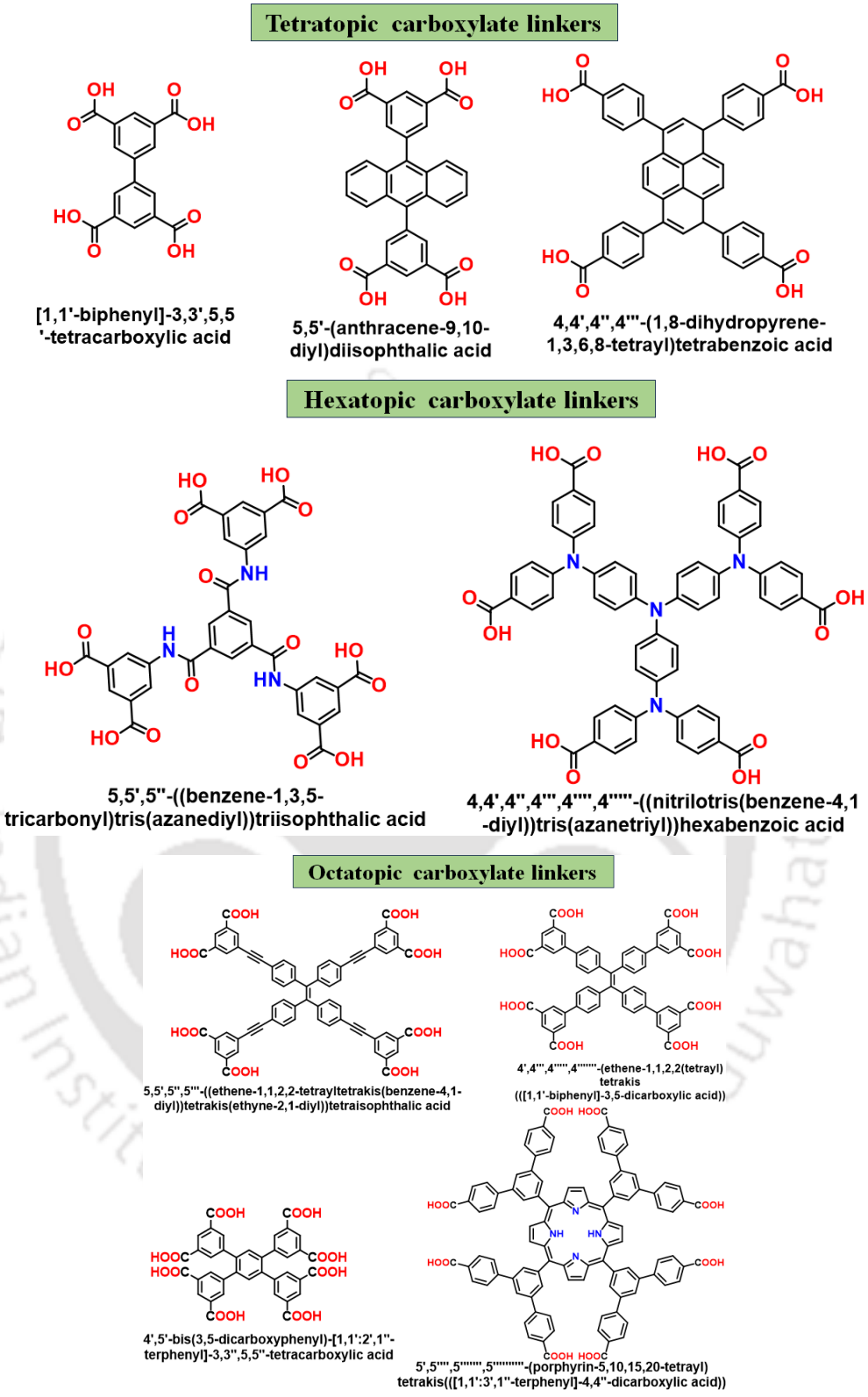

Figure 1.8 Different types of organic linkers that have been used for the synthesis of MOFs.

1.4 Different Synthesis Methods of MOFs

The ongoing advancements in the development of MOFs, which exhibit a wide range of crystal structures, porosities, and functional groups, have driven the evolution of numerous synthesis strategies. While the majority of MOFs are typically synthesized in the liquid phase, solid-state techniques have also been explored, although there are challenges in achieving single crystal

formation. One common method for growing MOF crystals involves the slow evaporation of the reaction solution, allowing crystals to form gradually over time.[100-101] Another traditional approach, the diffusion method, is often used to produce single crystals of MOFs. However, this method is known for being very slow, sometimes requiring weeks or even months to obtain crystals, and it often results in relatively low yields. The most widely used technique for MOF synthesis remains the solvothermal method, which is conducted under high pressure and temperature conditions. This method is considered the "classic" approach for producing MOFs, offering high yields and good crystallinity.[100] The solvothermal synthesis of MOFs can produce the desired framework for industrial applications as well. More recently, a variety of innovative synthetic methods have emerged, including slow evaporation, electrochemical synthesis, mechanochemical processes, microwave-assisted synthesis, sonochemical techniques, and post-synthetic modification strategies, each offering unique advantages and possibilities for MOF production (Figure 1.9).

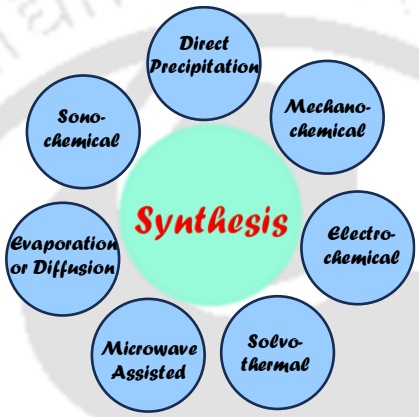

Figure 1.9 General synthesis methods of MOFs.

1.4.1 Evaporation and Diffusion Methods

In evaporation method, a reaction solution is prepared and allowed to evaporate slowly at room temperature or under controlled conditions, gradually forming MOF crystals as the solvent evaporates and the solute concentration increases.[100] This technique is simple and commonly used for producing large, well-formed crystals. However, it can take from several days to weeks for crystals to develop, and the yield is often low. Similarly, diffusion involves the controlled movement of components, such as metal salts or organic linkers, into a solvent, often in a gel-like or layered medium, causing the reactants to interact slowly and form crystals.[102] Although this method is effective for growing single crystals, it is also time-consuming, requiring weeks or even longer for completion, and typically results in low yields. While both methods are valuable for obtaining high-quality MOF crystals, they are not ideal for large-scale synthesis due to their slow processes and low efficiency.

1.4.2 Microwave-Assisted Method

Microwave-assisted synthesis is a widely adopted method for producing both organic and inorganic nanoporous materials, including metal clusters and MOFs. This technique utilizes electromagnetic radiation, specifically microwaves, to interact with the reactant molecules.[103] As the microwave radiation aligns with the dipoles of the molecules, it causes them to rotate, generating heat through molecular collisions.[104] This localized heating accelerates the reaction, facilitating the formation of the desired material. One of the main benefits of this approach is the reduction in reaction time compared to traditional methods like hydrothermal synthesis, leading to higher yields and improved crystallinity. Additionally, microwaves enhance the mobility of molecules, promoting nucleation (initial stage of crystal growth) which helps in producing crystals with more uniform shapes and sizes. This method enables precise control

over reaction parameters such as temperature and concentration, optimizing the properties of the resulting materials. Research has shown that microwave-assisted synthesis can significantly improve MOF production, with better yields and crystallinity observed in MOFs like UiO-66 and MIL-101 when compared to conventional techniques, making it a faster, more cost-effective choice for MOF synthesis.

1.4.3 Solvothermal Method

The solvothermal method is the most commonly used synthesis technique for MOFs and was initially developed for the synthesis of zeolites.[105] Today, it has become one of the most widely adopted methods for MOF synthesis. Solvothermal reactions are typically conducted in closed containers, such as sealed Pyrex tubes or stainless-steel autoclaves, which can withstand the high pressures generated by the evaporation of the solvent (Figure 1.10).[106] These reactions are performed using polar solvents with high boiling points, typically in the temperature range of 50 to 220 °C, and can last from several hours to several days. For reactions conducted at temperatures above 150 °C, Teflon-lined autoclaves are often employed to prevent corrosion and maintain reaction stability. The temperature and reaction time significantly influence the shape and size of the crystals, with longer reaction durations potentially leading to the decomposition of the final product.[107] Common solvents used in solvothermal MOF synthesis include dimethyl formamide (DMF), water (H_2O), diethyl formamide (DEF), dimethylacetamide (DMA), methanol (MeOH), acetonitrile (MeCN), and ethanol (EtOH), or combinations of these solvents. When water is used as the solvent, the process is referred to as a hydrothermal reaction, while the use of ionic liquids as solvents is known as an ionothermal method. At elevated temperatures, the dielectric constant of the solvent increases, which enhances the solvation of the reactants and facilitates the diffusion of the components due to a decrease in the solvent's viscosity.[108] Additionally, the cooling rate influences the crystal growth rate, which must be controlled and slow to ensure optimal crystal formation. After the MOF is synthesized, any encapsulated solvent molecules must be removed. This is typically carried out by stirring the MOF in a low boiling-point solvent and heating the material at high temperatures to obliterate the residual solvent. This approach has been widely used to synthesize various MOFs, including UiO-66, BUT-30, and DUT-52.[109-111] It has been extensively explored in recent studies due to its effectiveness in producing high-quality MOF crystals (Figure 1,10).[106]

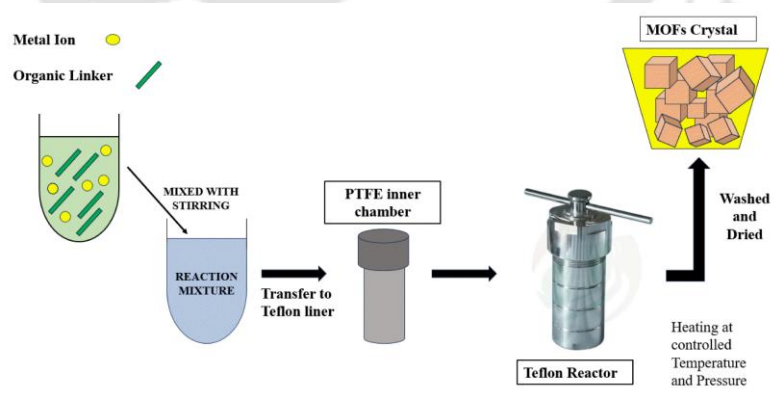

Figure 1.10 Schematic representation of hydrothermal/solvothermal synthesis of MOFs. Reproduced with permission from ref. 106. Copyright 2024, KSEE.

1.4.4 Electrochemical Method

The electrochemical synthesis of MOFs is a cutting-edge method that uses electrical current to facilitate the creation of MOFs.[104] This process involves applying an external electric field or

current to trigger the nucleation and growth of MOF crystals. Typically carried out in an electrolytic cell, metal ions are reduced at the cathode, while organic ligands undergo oxidation or reduction at the anode (Figure 1.11).[112] The metal ions then interact with the organic linkers to form the MOF structure. The metal precursors (e.g., metal salts) and organic ligands (e.g., carboxylates) are dissolved in an electrolyte solution, and when a voltage is applied, the metal ions are reduced at the cathode and combine with the ligands to form a coordination network, leading to the growth of MOF crystals. This technique provides precise control over various synthesis parameters, such as reaction time, temperature, and voltage, which can influence the crystals' size, shape, and morphology. One of the key benefits of electrochemical synthesis is its efficiency in controlling crystal growth, resulting in faster synthesis times compared to traditional solvothermal methods. It also allows for better control of the stoichiometry and uniformity of the MOF crystals, which can be performed at lower temperatures and pressures, reducing the need for specialized equipment.

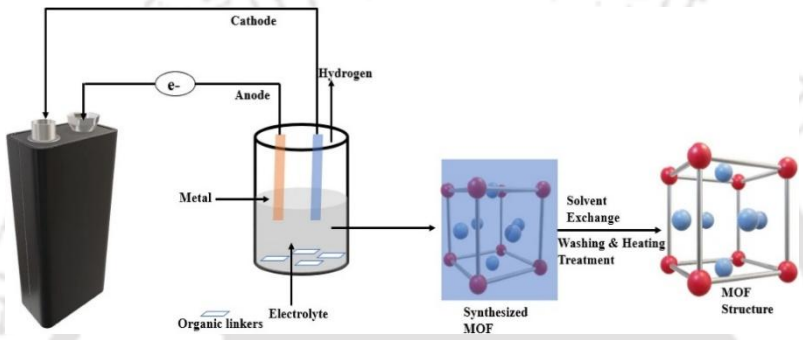

Figure 1.11 Electrochemical synthesis of MOFs. Reproduced with permission from ref. no. 112. Copyright 2023, Springer.

Electrochemical synthesis has been successfully applied to produce a variety of MOFs, including simple copper-based frameworks like Cu-BTC and more complex frameworks with adjustable properties.[113] This technique has potential applications in energy storage, catalysis, and sensing, as it allows for precise tailoring of the MOF structure and properties through the control of electrochemical conditions.[114] In conclusion, electrochemical synthesis is an efficient, scalable, and versatile method for producing high-quality MOFs suitable for various applications. However, this synthesis method requires a trained person in electrochemistry and an expensive electrochemical setup.

1.4.5 Mechanochemical Method

The solid-state synthesis of MOFs is a process in which reactants are manually ground, often using ball mills, to form coordination bonds at room temperature, eliminating the need for solvents.[115] This method facilitates the production of coordination polymers with varying dimensionalities, including 1D, 2D, and occasionally 3D structures. While the synthesis generally occurs without solvents, a small amount of solvent can sometimes be added to the reaction mixture to enhance the process further.[116] The mechanochemical approach significantly accelerates the reaction rate by improving mass transfer, reducing the particle size, promoting localized heating, and occasionally causing the reactants to melt in specific areas, all of which contribute to a more efficient reaction. This solid-state method is particularly appealing as a green chemistry technique due to its environmental benefits. It offers a sustainable alternative by avoiding harsh chemicals and solvents and producing MOFs with high purity, yield, and rapid reaction times.[117] This method has clear advantages over traditional solvothermal synthesis, which typically requires high temperatures and pressures, leading to potential environmental concerns, prolonged reaction times, and the formation of unwanted

by-products. In contrast, the mechanochemical process can avoid these by-products, ensuring a cleaner synthesis.

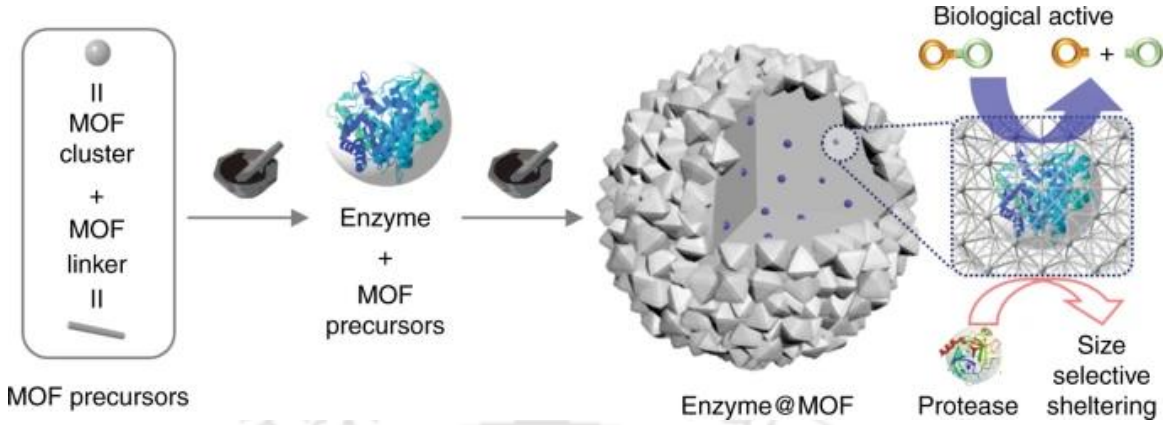

Figure 1.12 Schematic representation of the mechanochemical synthesis of UiO-66-NH_2, ZIF-8, and Zn-MOF-74. Reproduced with permission from ref. no. 119. Copyright 2019, Nature.

Furthermore, it is particularly advantageous when synthesizing MOFs containing sensitive functional groups, such as thermally or solvent-labile. The first use of this mechanochemical method to synthesize a Cu(II)-based MOF was reported by James et al., and since then, it has been successfully applied to the synthesis of various other MOFs, including HKUST-1, MOF-74, and ZIF-8.[117-118] One of the significant benefits of the mechanochemical approach is its ability to produce MOFs with different topologies compared to solvothermal methods. For example, a solvothermal reaction involving $Ni(OAc)_2 \cdot 4H_2O$ and 2-methyl imidazole in the presence of ZnO resulted in the formation of the BIT-12 MOF. However, a different topology, BIT-11, was produced when the mechanochemical method was employed. Three well-studied MOFs with different crystal structures and chemical compositions, UiO-66-NH_2, ZIF-8, and Zn-MOF-74 are used (Figure 1.12).[119] This demonstrates the ability of mechanochemical synthesis to offer novel structural outcomes that may not be achievable through conventional solvothermal approaches.

1.4.6 Direct Precipitation Method

The direct precipitation method is a simple and widely used technique for synthesizing metal-organic frameworks (MOFs). In this method, a metal salt and an organic ligand are directly mixed in a solvent, leading to the spontaneous formation of a metal-organic framework through precipitation.[120] The process typically occurs at room temperature or slightly elevated temperatures and does not require high pressure or complex equipment, making it a relatively straightforward approach for MOF synthesis.[121] During the reaction, the metal ions from the metal salt coordinate with the organic ligands, forming the MOF structure. The product precipitates out of the solution as the reaction progresses. The precipitate is then collected by filtration or centrifugation, washed to remove unreacted precursors or impurities, and dried to obtain the final MOF product. One of the key advantages of the direct precipitation method is its simplicity, cost-effectiveness, and scalability. It is beneficial for synthesizing MOFs without precise crystal size or morphology control. However, the process may result in lower crystallinity and yield than more complex techniques, such as solvothermal synthesis. Additionally, the precipitation rate and the final MOF quality can be influenced by factors such as the solvent, temperature, and concentration of the reactants.[122] This method has been successfully employed for synthesizing various MOFs, including well-known frameworks like MOF-5 and MIL-53.

1.4.7 Sonochemical Method

Intense ultrasonic radiation between 10 and 20 MHz is commonly employed in sonochemical synthesis to fabricate nanostructures, including MOFs. The primary advantage of this technique is its ability to offer a more energy-efficient, environmentally friendly, and ambient-temperature process for MOF synthesis, which contrasts with conventional methods such as the hydrothermal or solvothermal approaches.[123] These traditional methods often require high temperatures, solvents, and long reaction times, which can be energy-intensive and less sustainable. In contrast, sonochemical synthesis leverages ultrasonic waves to induce cavitation in a solvent, leading to localized high temperatures and microenvironmental pressures. This process accelerates nucleation and growth, resulting in uniform particles with fewer impurities and defects.[124] The first sonochemically synthesized MOF was reported by Qiu et al., who demonstrated that ultrasonic waves could significantly reduce synthesis time and enhance the yield of MOFs. This method also produces more uniform nucleation centers, promoting consistent crystallization and reducing unwanted by-product formation. Moreover, it is reported that by varying the reaction parameters, such as temperature and time, the morphologies and particle sizes of the resulting MOFs can be finely tuned, giving the technique a level of versatility that traditional methods may not offer. For example, in the synthesis of MOF-5 and HKUST-1, the ultrasonic process has been shown to produce highly crystalline structures with well-defined porosity, outperforming traditional methods in terms of crystallization time and product uniformity. Further advancements in sonochemical synthesis have led to the development of a wide range of other MOFs, such as MOF-177, MOF-556, and MOF-74.[125] Recent studies have shown that this method enhances the crystallinity and yield of the MOFs and allows for incorporating functional groups into the frameworks, making it possible to fine-tune the properties for specific applications, such as gas storage, catalysis, and sensing.[125] Sonochemical synthesis offers faster crystallization and energy efficiency. Still, it faces scalability, yield, particle control, and solvent compatibility challenges compared to solvothermal methods, which are more established and provide better control over particle size and morphology for larger-scale production.

1.4.8 Post-Synthetic Modification (PSM) Method

Incorporating specific functional groups into MOFs for specialized applications can be challenging due to the sensitivity and reactivity of these functionalities during MOF formation. An efficient solution to this issue is PSM, a technique first proposed by Hoskins and Robson in 1990.[126] In PSM, a MOF is synthesized first and then modified in a heterogeneous manner after the solid lattice has formed, unlike the direct synthesis of functionalized MOFs. This method offers significant advantages over pre-functionalization because it allows for better control over the type and quantity of functional groups incorporated into the framework. Additionally, PSM enables the functionalization of both the metal and organic components without compromising the framework's overall stability, making it an ideal approach for creating topologically identical but functionally distinct MOFs. Covalent modification is one of the most commonly used PSM techniques, where MOFs are functionalized for specific applications. For example, amino group-functionalized MOFs have been modified with reagents such as aldehydes, anhydrides, isocyanates, acyl chlorides, and alkyl bromides. Moreover, azide-functionalized MOFs undergo click reactions with alkynes, forming MOFs with tailored pore size and surface area (Figure 1.13).[127]

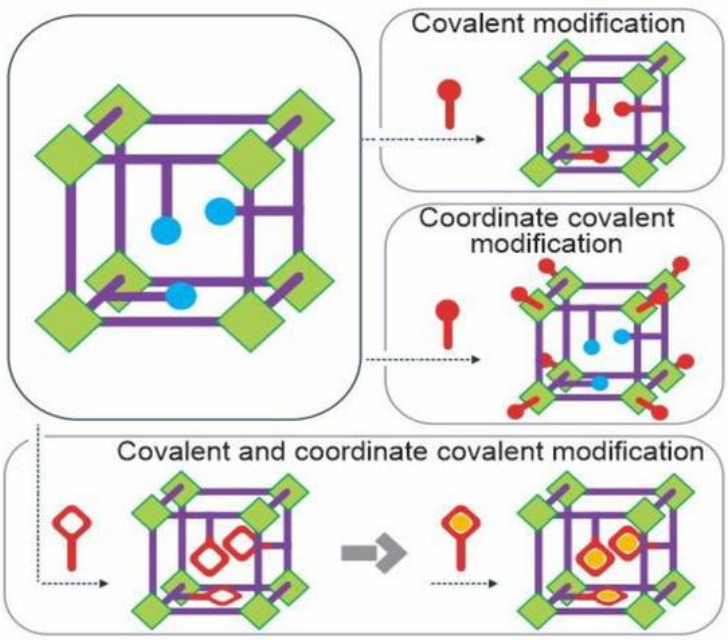

Figure 1.13 Schematic representation of different post-synthetic modification strategies. Reproduced with permission from ref. no. 127. Copyright 2023, MDPI.

In addition to covalent modification, dative modification via post-synthetic metalation has been developed. For instance, MOFs containing 2,2′-bipyridine (bpy) sites can be post-synthetically metalated with soft metals like Cu^{2+} and Pd^{2+}.[128] Additional ligands can also modify the coordinatively unsaturated metal sites in MOFs. For example, vacant coordination sites in Cr and Cu-based MOFs have been modified with alkane amines to enhance CO_2 uptake. Similarly, coordinatively unsaturated Zr_6 clusters can bind to carboxylates via simple acid/base reactions. The solvent-assisted ligand incorporation (SALI) method has been used to modify the Zr-cluster in NU-1000 MOF to enhance CO_2 uptake.[129] Post-synthetic ligand and metal ion exchange processes are also efficient methods for introducing new ligands and metal ions into MOFs. While the inert metal-ligand bonds in stable MOFs often hinder ligand and metal ion exchange, recent studies have shown that the robustness of these bonds may have been overestimated. Notably, coordinative PSM has been shown to preserve the porosity and crystallinity of MOF particles. In addition to covalent and coordinative PSM, several other techniques have been explored, such as metal exchange, metal incorporation, linker exchange, linker installation, guest incorporation into the MOF pores, and linker removal. Through PSM, MOFs can be functionalized with various substances, allowing for the modification of their properties, including hydrophobicity, hydrophilicity, porosity, luminescence, catalytic activity, and other functional attributes.[130] Exchange processes have been successfully applied to various stable MOFs, including ZIFs, MIL series, and UiO series, enabling the introduction of new functional properties. Overall, PSM has proven to be a powerful strategy for tailoring the properties of MOFs, expanding their functionality and applicability in various fields.

1.5 Parameters Controlling Synthesis of MOFs

The successful synthesis of a specific MOF structure requires careful control of various factors, to obtain the highly crystalline form of the MOF. These factors include reaction time, temperature, the molar ratio of metal ions and linkers, solvent choice, pressure, pH, and crystallization kinetics. The goal is to achieve proper nucleation and crystal growth with a defined shape and size. Ensuring the correct stoichiometric ratio of metal ion and linkers, selecting an appropriate solvent, and setting the optimal temperature are crucial steps for

obtaining the desired MOF structure. These factors can be categorized into two main groups: compositional parameters (e.g., solvent, molar ratio, pH, and concentration of counter ions) and process parameters (e.g., reaction time, temperature, and pressure).[131]

1.5.1 Effect of Solvent

Choosing the right solvent is essential in MOF synthesis. Solvents are selected based on their reactivity, basicity, solubility of reactants, and redox properties, all of which significantly impact the thermodynamics and activation energy of the reaction. High-boiling amide solvents such as DMF, DEF, and DMA are commonly used in solvothermal synthesis due to two advantages: (1) they have high boiling points, necessary for solvothermal reactions, and (2) they are converted into basic amines, which help deprotonate acidic hydrogen atoms, enhancing the coordination process. For example, in a study by Luo et al., three different MOF structures were obtained by reacting $Cd(NO_3)_2 \cdot 4H_2O$ with biphenyl tricarboxylic acid (H_3BPT) in DMF, DEF, and DMA.[132] The structures varied based on the solvent: in DMF, a 3D framework with Cd-O-Cd chains was formed; in DMA, metal-carboxylate chains were observed; and in DEF, a 2D honeycomb-type net was produced. These findings highlight the solvent's role in determining the final structure of the MOF.

1.5.2 Effect of Molar Ratio of Reacting Components

The molar ratio of metal ions to linkers is critical in determining the topological structure of a MOF. Luan et al. demonstrated this by synthesizing three Cu-based coordination polymers with varying linker-to-metal ratios, each with different structures and properties.[133] Similarly, Carlucci et al. synthesized two distinct Mn(II) complexes by adjusting the molar ratio of the linker 1,4-bis(imidazol-1-ylmethyl)benzene and $Mn(NO_3)_2 \cdot 4H_2O$, resulting in different structures and chemical compositions.[134] This emphasizes that controlling the molar ratio is key to achieving the desired MOF structure.

1.5.3 Effect of Reaction Temperature

Reaction temperature plays a significant role in MOF synthesis, particularly under solvothermal conditions. A temperature range of 80-200 °C is typically used.[108] At higher temperatures, the solvent's dielectric constant increases and its viscosity decreases, facilitating better solvation of the reactants and enhancing metal-ion and linker interactions.[108] For example, a study involving Ho(III) and succinic acid found two different complexes with distinct chemical compositions and properties formed at solvothermal and room temperatures.[135] Similarly, a Zn(II) MOF synthesized with 5-iodoisophthalic acid showed that high-temperature solvothermal conditions favor the formation of thermodynamically stable structures,[135] while low-temperature conditions lead to kinetically stable conformers.

1.5.4 Effect of pH of Reaction Medium

The pH of the reaction medium influences the crystallization and formation of MOFs by affecting the protonation or deprotonation of the organic linkers. A carboxylate group on a linker will more likely coordinate with a metal ion when it is deprotonated, depending on the pH of the medium.[135] For example, Hu et al. found that at pH 7.5, the carboxylate groups of oxalic acid were fully deprotonated, enabling coordination with a Cd(II) ion.[136] In contrast, no such coordination occurred at pH 5.5. Similarly, Luo et al. demonstrated how adjusting the pH affected the coordination environment and topology of Co-BTC-L MOFs, showing that pH can control the structure, color, and coordination of the resulting MOF.[137]

1.5.5 Effect of Modulator

In crystallography, we know that crystal formation is a slow process. Without slowing down the process, it is challenging to create well-ordered crystalline compounds. This is where modulator chemistry comes into play, especially for MOFs containing metal ions with high positive oxidation states (Zr(IV), Al(III), or Hf(IV)). These metal ions can react quickly with the carboxylate groups of the linker, which leads to rapid nucleation and often results in amorphous products. Before modulators were used, MOFs with these metal ions were often produced as gels.

A modulator helps control the speed of the MOF formation process, allowing the crystals to form properly. It plays a crucial role in determining the product's final texture, porosity, yield, crystallinity, and coordination structure. Typically, modulators are simple carboxylic acids attached to a carbon chain, such as acetic acid, benzoic acid, trifluoroacetic acid, or formic acid. These monocarboxylic acids bind to metal ions more quickly than dicarboxylate-based linkers, but this binding is reversible. Although the monocarboxylate groups form temporary bonds with the metal nodes, they can't form a stable crystal structure alone, as another carboxylate group is needed to complete the coordination from the opposite site. This helps slow the crystallization process, essential for proper crystal growth. However, using too much modulator can halt crystallization entirely.[138] Modulators are also important in the synthesis of M(IV)-based MOFs, where they help to form $M_6O_4(OH)_4$ structural building units (SBUs).[139] The concept of "coordination modulation" was introduced by the Kitagawa group in 2009 to describe how modulators can control the size and growth of crystals in materials like HKUST-1 and $[Cu_2(NDC)_2(dabco)]_n$.[140-141] Recently, De Vos and colleagues studied trifluoroacetic acid (TFA) as a modulator in synthesizing Zr(IV)-based UiO-66 MOF with terephthalic acid. Although the crystallinity and particle size did not change much with different amounts of TFA, the catalyst's reactivity in "ene"-type cyclization reactions increased as the concentration of TFA increased.[142]

Zhao et al. explored the role of different modulators, such as acetic acid, trifluoroacetic acid, and formic acid, in the synthesis of Zr(IV)/Hf(IV) MOFs with a fumarate linker. The study showed that the acidity of the modulator, rather than its specific type, significantly impacted the crystallinity and yield of the MOFs. Interestingly, both increasing and decreasing the acidity of the modulator led to similar effects on crystallinity.

1.5.6 Template Strategies

Template molecules are used in MOF synthesis to produce novel structures that might be challenging to form using traditional methods.[142] Templates such as organic amines, surfactants, and ionic liquids can influence the crystallization process in various ways. Organic amines, for instance, help regulate pH and facilitate the deprotonation of linkers, while surfactants can form micelles that capture specific ions, affecting the morphology of the resulting MOF. Template strategies are also used to create hierarchical porous materials with different pore sizes suitable for hosting large molecules like proteins and enzymes. Using linkers of varying lengths, the reticular chemistry approach is a popular method to create MOFs with the same topology but different pore sizes.[100]

1.6 Synthesis of Aqua-Stable MOFs via Linker Design

The development of MOFs over the past 30 years can be divided into three key stages. In the initial phase, research focused on MOFs' mechanical and thermal stability. The second phase centered on understanding the collapse of MOF frameworks when exposed to air. To address the above issues, various air- and water-stable MOFs were developed. The third phase involved synthesizing highly stable MOFs with excellent physicochemical properties, using advanced

crystal growth and structure determination techniques, which expanded their potential applications and commercialization.[143] Generally, the stability of MOFs depends on both thermodynamic and kinetic factors.[144] Thermodynamically, stability is influenced by the strength of the coordination bonds between the metal ion and the linker.[145] The hard-soft acid-base (HSAB) theory can help predict coordination bond strength. However, even if thermodynamic factors are similar, MOF stability can still vary significantly. For example, the stability of 'UiO' and SUMOF-7 series MOFs decreases with longer linkers and larger pores, which is mainly due to kinetic factors like the linker's rigidity, surface hydrophobicity, coordination number, and framework interpenetration.[146-147] Over the last two decades, researchers have developed several approaches to synthesize aqua-stable MOFs, outlined below.

1.6.1 Synthesis of MOFs with High Connectivity

In the early stages of MOF synthesis, soft divalent metal ions were used with hard carboxylate linkers, which led to low stability due to the violation of the HSAB theory. However, the stability of MOFs dramatically improved with the use of high-valent metals (e.g., Zr^{4+}, Al^{3+}, Cr^{3+}, Fe^{3+}) and hard O-donor linkers. The increased metal cluster connectivity and reduced structural defects are key factors in improving MOF stability.[148] From a kinetic perspective, when small nucleophiles (like water) replace coordinating groups, it often leads to the breakdown of MOFs. In defective structures, forming aqua complexes with the metal ion is more favorable, which causes the framework's collapse. On the other hand, frameworks with higher connectivity and a higher coordination number for metal ions slow down linker dissociation, enhancing stability. Using this concept, Ferey and his team synthesized Cr(III)-based MIL-101(Cr), a MOF with high stability, large surface area (~4000 m^2/g), and pore sizes (2.9 and 3.4 nm). This MOF resists both acid and alkali attacks and maintains its crystalline structure across a wide pH range (0-12) for two months.[33] Additionally, using rigid N-donor linkers with low-valent metals can also create stable frameworks, as seen in ZIF-8, which remains stable even in 8 M aqueous NaOH at 100 °C for one day.[149]

1.6.2 Use of Rigid Linkers in MOF Synthesis

The rigidity of the coordinating linker is crucial for the stability of the MOF framework. The stability tends to decrease as the linker becomes more flexible.[150] This is one reason why aromatic conjugated linkers are often preferred over flexible aliphatic linkers in MOF synthesis. Flexible linkers have more degrees of freedom, which increases their ability to bend and reduces the stability of the MOF. For example, while the UiO and SUMOF-7 series have similar coordination geometries, their stability decreases as the size of the coordinating linker increases.[146] MOFs with longer linkers tend to have lower activation energies for solvation, so shorter, more rigid linkers are usually preferred for creating aqua-stable frameworks.[150]

1.6.3 Synthesis of Mixed-Metal MOFs

The stability of MOFs can also be enhanced by using a mixture of metal ions instead of a single metal. This strategy is particularly effective for bivalent metal ions. For example, the stability of MOF-5 in water was improved by incorporating Ni^{2+} into the structure.[149] Similarly, the hydrolytic stability of STU-1 MOFs was enhanced by doping with Cd^{2+}, Fe^{2+}, and Cu^{2+}, all of which maintained their crystallinity and structure even after being soaked in boiling water for seven days.[151] This improved stability may be due to the formation of stronger coordination bonds, enhanced inertness of the metal cluster, or increased hydrophobicity of the metal-doped MOF.

1.6.4 Use of Hydrophobic Linkers in MOF Synthesis

Water can destabilize MOFs by forming hydroxides with metal ions. To prevent this, hydrophobic linkers are often used to protect the framework from nucleophilic attack by water. These linkers introduce water-repellent functional groups that shield the metal-linker coordination bonds. Hydrophobicity can also be achieved using PSM techniques. Long-chain alkyl or fluorine-containing groups, such as $-CF_3$, -F, $-CH_3$, $-C_2H_5$, or -Ph groups, are highly effective at making a MOF hydrophobic.[146] The use of pyrene linkers can also enhance hydrophobicity.[146] These hydrophobic modifications not only improve stability in water but also in highly acidic and basic pH environments. For example, the copper-based MOF USTC-6, which contains a hydrophobic fluorinated linker, shows remarkable resistance to water and remains stable in a pH range of 2-10, despite the Cu-O bonds being prone to hydrolysis.[139] The position of hydrophobic functional groups is also essential for stability; for instance, in bipyridine-based MOFs like MOF-508, the presence of methyl groups close to the metal cluster helps preserve porosity after exposure to humidity. Many other strategies have also been employed to synthesize aqua-stable MOFs.

1.7 Zr(IV) MOFs with Carboxylate Based Linkers

Zirconium, one of earth's most abundant transition metals, is primarily extracted from the mineral zircon.[152] Zr(IV) is a hard metal ion that strongly bonds with the hard oxygen atoms of carboxylate groups. In some cases, Zr-O coordination bonds are more stable than the carbon-carbon bonds in organic compounds.[153] This remarkable stability of Zr-O bonds enabled Lillerud et al. to synthesize the ultra-stable UiO-66 MOF in 2008 (UiO = University of Oslo). The UiO-66 structure includes an inorganic $Zr_6(\mu_3\text{-}O)_4(\mu_3\text{-}OH)_4(CO_2)_{12}$ building unit.[111] This unit features an inner $Zr_6O_4(OH)_4$ core, where the faces of the Zr_6 octahedron are alternately coordinated with μ_3-O and μ_3-OH groups. Carboxylate linkers interconnect the polyhedral edges to form a cluster, with each Zr atom occupying a square anti-prismatic coordination environment with a coordination number of 12. The framework has octahedral and tetrahedral cages. Two carboxylate groups form one square face, while the μ_3-O and μ_3-OH groups form the other.[146] Initially, the synthesis of Zr-MOF was carried out without using any modulators, which often resulted in an amorphous rather than a crystalline material.[138] Research then focused on converting this amorphous material into a crystalline form.

In 2011, Schaate et al. reported the first highly crystalline powdered Zr-UiO-66 MOF.[153] They achieved this by introducing a modulator during the synthesis process. Their work examined the effects of modulators (benzoic acid, acetic acid, and H_2O) on the synthesis of Zr-UiO-66. They found that increasing the concentration of the modulator controlled the synthesis process, leading to larger crystals. It was understood that modulators bind reversibly to the metal nodes, slowing crystallization and enabling controlled nucleation and crystal growth. These modulators, typically single carboxylic acids with the formula R-COOH (where R = -Ph, $-CH_3$, -H, or $-CF_3$), bind to the metal nodes but lack a second carboxylate group, preventing the crystal structure from propagating.[138] This slow crystallization process was crucial for good crystal formation, though excessive modulator concentration could inhibit crystal growth. Schaate et al. also reported the first single crystal of $-NH_2$ functionalized UiO-66 MOF using a similar strategy. The first UiO-66 MOF synthesized had a BET surface area of 1187 m^2/g.[138] Following this breakthrough, two isoreticular MOFs, Zr-UiO-67 (with H_2BPDC linker) and Zr-UiO-68 (with H_2TPDC linker), were developed. These MOFs, with 2400 and 3000 m^2/g surface areas, respectively, were produced by extending the number of benzene rings in the linkers (Figure 1.14).[138, 154]

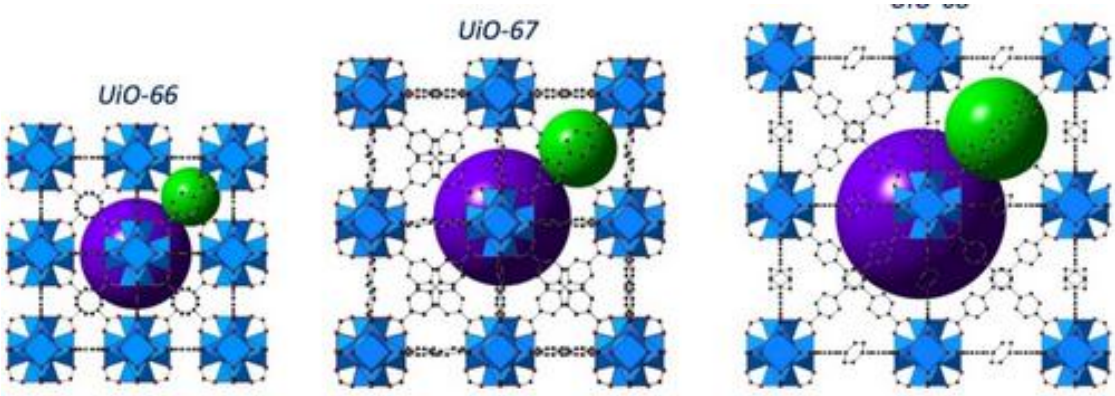

Figure 1.14 Illustrations of the structures of UiO-66, UiO-67 and UiO-68 and the ligands derived from BDC, BPDC and TPDC. Reproduced with permission from ref. 154. Copyright 2022, John Wiley and Sons.

In a short period, several Zr(IV) and Hf(IV)-based 'UiO' series MOFs were synthesized by various research groups and their diverse applications were explored. 2013 Kaskel et al. reported another single crystal of a 12-connected Zr(IV) MOF, DUT-52, using a 2,6-naphthalene dicarboxylic acid linker.[110] The structure of DUT-52 is similar to that of UiO series MOFs, with hexanuclear $[Zr_6O_4(OH)_4]^{12+}$ clusters as SBUs, interconnected by 12 dicarboxylate linker molecules. The development of different carboxylic acid linkers led to the synthesis of Zr-MOFs with various topologies and network connectivity (Table 1.1). For example, a ten-coordinated Zr-MOF (MOF-802) was synthesized using 1H-pyrazole-3,5-dicarboxylate linker,[155] and six-coordinated MOF-808 was made with a 1,3,5-benzene dicarboxylate linker.[110]

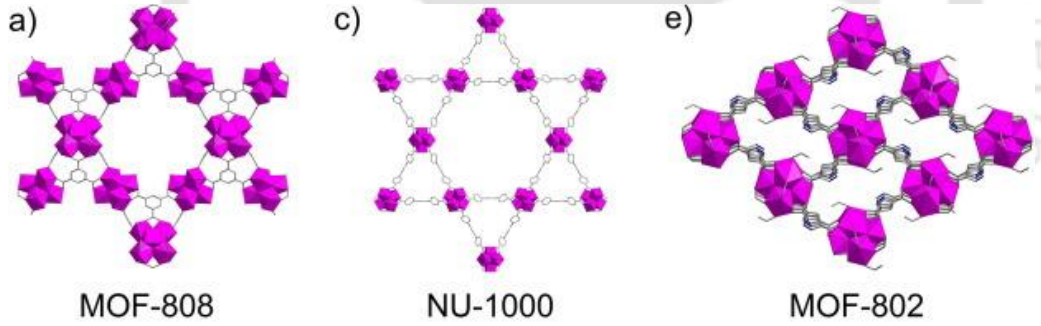

Figure 1.15 Crystal structures of (a) MOF-802, (b) MOF-808 and (c) NU-1000 (c) Colour code: ZrO_8 polyhedra: pink; O: red; C: grey; N: blue. H atoms are omitted. Reproduced with permission from ref. no. 156. Copyright 2016, Elsevier.

The NU-1000 MOF, based on a 1,3,6,8-tetrakis(p-benzoate)pyrene linker, features eight linked clusters (Figure 1.15). Other Zr-MOFs, such as DUT-84, PCN-94, and Zr-AP-2, exhibit framework connectivity of 3 or 4.[156] In a more recent development, Biswas and co-workers synthesized a 10-connected Zr-MOF using benzo[1,2-b:4,5-b′]dithiophene-2,6-dicarboxylate, which crystallized in a cubic space group.[157] Many Zr-MOFs, like those in the UiO series, contain the $[Zr_6O_4(OH)_4]^{12+}$ SBU. However, other Zr-MOFs, such as those in the MIL-140 series, feature polymeric double chains of ZrO_7 polyhedra linked by linear linkers.[158] MIL-153 and MIL-154 have ZrO_8 coordination and an 8-connected network.[159] Some Zr-MOFs, such as Zr-TPDC, incorporate $[Zr_{12}(\mu_3\text{-}O)_8(\mu_3\text{-}OH)_8(\mu_2\text{-}OH)_6(COO)_{18}]$ clusters, where six μ_2-OH groups connect two Zr_6 clusters in a face-to-face arrangement.[160] The combination of different linkers and metal ion coordination numbers is critical in shaping the crystal structure and

porosity of various Zr-MOFs. A summary of clusters, topologies, and network connectivity for several well-known, stable, and porous Zr-MOFs is presented in Table 1.1.

Table 1.1 Summary of clusters/cores, linker used, coordination number, topology, and surface area of some previously reported Zr(IV)-MOFs.

MOFs	Clusters	Linker[a]	Topology and Connectivity	BET Surface Area (m^2/g)	Ref.
UiO-66	$Zr_6(\mu_3\text{-}O)_4(\mu_3\text{-}OH)_4$	BDC	fcu, 12	1187	146
UiO-67	$Zr_6(\mu_3\text{-}O)_4(\mu_3\text{-}OH)_4$	BPDC	fcu, 12	3000	146
UiO-68	$Zr_6(\mu_3\text{-}O)_4(\mu_3\text{-}OH)_4$	TPDC	fcu, 12	4170	146
NU-1000	$Zr_6(\mu_3\text{-}OH)_8$	TBAPy	csq, 4,8	2320	161
NU-1100	$Zr_6(\mu_3\text{-}O)_4(\mu_3\text{-}OH)_4$	PTBA	ftw, 4,12	4020	162
MOF-801	$Zr_6(\mu_3\text{-}O)_4(\mu_3\text{-}OH)_4$	FUM	fcu, 12	990	163
MOF-802	$Zr_6(\mu_3\text{-}O)_4(\mu_3\text{-}OH)_4$	PZDC	bct, 10	<20	163
MOF-808	$Zr_6(\mu_3\text{-}O)_4(\mu_3\text{-}OH)_4$	BTC	spn, 3 and 6	2060	163
MOF-812	$Zr_6(\mu_3\text{-}O)_4(\mu_3\text{-}OH)_4$	MTB	ith, 4 and 12	2335	163
MOF-841	$Zr_6(\mu_3\text{-}O)_4(\mu_3\text{-}OH)_4$	MTB	flu, 4 and 8	1390	163
MOF-525	$Zr_6(\mu_3\text{-}O)_4(\mu_3\text{-}OH)_4$	TCPP	ftw, 4 and12	2620	163
MOF-545	$Zr_6(\mu_3\text{-}OH)_8$	TCPP	csq, 4 and 8	2260	163
DUT-51	$Zr_6(\mu_3\text{-}O)_6(\mu_3\text{-}OH)_2$	DTTDC	reo, 8	2335	164
DUT-52	$Zr_6(\mu_3\text{-}O)_4(\mu_3\text{-}OH)_4$	2,6-NDC	fcu,	1399	110
DUT-84	$Zr_6(\mu_3\text{-}OH)_8$	2,6-NDC	(4,4)IIb, 6	637	110
DUT-67	$Zr_6(\mu_3\text{-}O)_6(\mu_3\text{-}OH)_2$	TDC	reo, 8	1064	165
DUT-68	$Zr_6(\mu_3\text{-}O)_6(\mu_3\text{-}OH)_2$	TDC	8	891	165
PCN-221	$Zr_6(\mu_3\text{-}OH)_8$	TCPP	ftw, 4 and 12	1936	166
PCN-222	$Zr6(\mu_3\text{-}OH)_8$	TCPP	csq, 4 and 8	2223	167
PCN-223	$Zr_6(\mu_3\text{-}O)_4(\mu_3\text{-}OH)_4$	TCPP	shp, 4 and 6	1600	168
PCN-224	$Zr_6(\mu_3\text{-}O)_4(\mu_3\text{-}OH)_4$	TCPP	she, 4 and 6	2600	169
Zr-TPDC	$Zr_{12}(\mu_3\text{-}O)_8(\mu_3OH)_8$	TPDC	-	1967	169
IITG-5	$Zr_6(\mu_3\text{-}O)_4(\mu_3\text{-}OH)_4$	$C_{12}O_4H_4S_2$	10	1228	157
MIL-140A	$Zr(\mu_3\text{-}O)_3O_4$	BDC	-	415	158
MIL-140B	$Zr(\mu_3\text{-}O)_3O_4$	2,6-NDC	-	460	158
Zr-BTBA	$Zr_6(\mu_3\text{-}O)_4(\mu_3\text{-}OH)_4$	BTBA	ftw, 4 and 12	4342	170
MIL-153	ZrO_8	pgal	-	-	159
MIL-154	ZrO_8	Hgal, Hsal	-	-	159

[a]BDC = terephthalate; BPDC = biphenyl-4,4′-dicarboxylate; TPDC = [1,1′:4′,1″-terphenyl]-4,4″-dicarboxylate; TBAPy = 1,3,6,8-tetrakis(p-benzoate)pyrene; PTBA = 4-[2-[3,6,8-tris[2-(4-carboxylatephenyl)-ethynyl]-pyren-1-yl]ethynyl]-benzoate; FUM = fumarate; PZDC = 1H-pyrazole-3,5-dicarboxylate; BTC = benzene-1,3,5-tricarboxylate; MTB = 4,4′,4″,4‴-methanetetrayltetrabenzoate; TCPP = meso-tetrakis(4-carboxylate-phenyl)porphyrin; DTTDC = dithieno[3,2-b;20,30-d]-thiophene-2,6-dicarboxylate; 2,6-NDC = naphthalene-2,6-dicarboxylate; TDC = 2,5-thiophenedicarboxylate; TCPP = meso-tetrakis(4-carboxylate-phenyl)porphyrin; BTBA = 4,4′,4″,4‴-(biphenyl-3,30,5,50-tetrayltetrakis(ethyne-2,1-diyl))tetrabenzoate; $C_{12}O_4H_4S_2$ = benzo[1,2-*b*:4,5-*b*′]dithiophene-2,6-dicarboxylic acid; H_3Pgal = pyrogallol; gal = gallate; sal = salicylate.

1.8 Al(III) MOFs with Carboxylate Based Linkers

Ferey et al. introduced the Al-MOF with the formula [Al(OH)(BDC)], commonly referred to as MIL-53(Al) (MIL = Materials of Institute Lavoisier).[171] This structure consists of infinite linear zigzag chains of $AlO_4(OH)_2$ octahedra, forming 1D rhombic channels when linked with BDC ligands. A notable feature of MIL-53(Al) is the "breathing" phenomenon, where the framework's structure changes based on adsorbed guest molecules. This results in two distinct forms: narrow pore ("np") and large pore ("lp"), which are interconvertible through the reversible removal and incorporation of guest molecules (Figure 1.16).[172] Various MOFs with the MIL-53(Al) architecture have been synthesized using functionalized or extended linkers, including DUT-4 and DUT-5 (DUT stands for Dresden University of Technology).[173] Another isomer, MIL-68(Al), possesses a more rigid network,[174] and further elongation of the linker in MIL-68(Al) led to the creation of CYCU-3 (CYCU stands for Chung-Yuan Christian University).[175] The tritopic carboxylate ligand BTTB and $[Al(OH)(COO)_2]_n$ chains contributed to the formation of the highly stable 467-MOF.[176]

In addition to tritopic ligands, Al-MOFs incorporating $[Al(OH)(COO)_2]_n$ chains and tetratopic carboxylate ligands have also been explored, such as MIL-121, MIL-118, and MIL-120.[177-179] A notable Al-MOF, NOTT-300 (NOTT stands for University of Nottingham), is composed of $[Al(OH)(COO)_2]_n$ chains bridged by a four-connected BPTA linker.[180] Furthermore, a combination of $[Al(OH)(COO)_2]_n$ chains and a porphyrin linker (TCPP) resulted in the creation of Al-PMOF, which remains stable in aqueous media with pH values between 5 and 8.[181] MIL-96 represents the first example of an Al-MOF containing the $[Al_3(\mu_3\text{-}O)(COO)_6]$ cluster, comprising both isolated $[Al_3(\mu_3\text{-}O)(COO)_6]$ clusters and infinite chains with $AlO_4(OH)_2$ units, connected by the BTC ligand to form three types of cages.[182] The interaction of $[Al_3(\mu_3\text{-}O)(COO)_6]$ clusters with tricarboxylate linkers led to the formation of MIL-100(Al), which is composed of super-tetrahedral blocks based on $[Al_3(\mu_3\text{-}O)(COO)_6]$ SBUs and BTC linkers. An extended version of MIL-100,[183] PCN-333(Al),[184] incorporates TATB linkers and exhibits D_3h symmetry, showing excellent stability in aqueous environments with pH values ranging from 3 to 9.

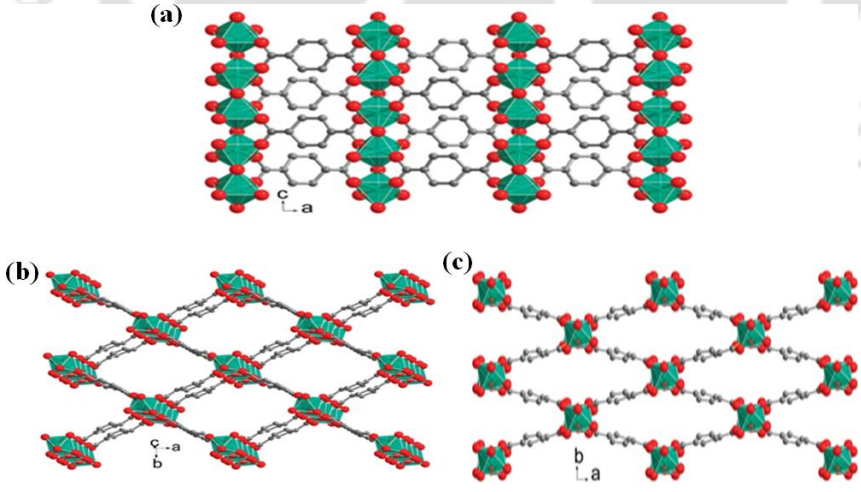

Figure 1.16 Ball-and-stick representations of the 3D framework structure of Al-MIL-53: (a) Infinite chains of corner-sharing octahedral $[AlO_4(OH)_2]$ units interconnected by the BDC linkers, (b) The large pore (lp) and (c) narrow pore (np) forms of the framework viewed along the crystallographic c-axis. Hydrogen atoms and guest molecules have been omitted from all structural plots for clarity. Color codes: Coordination environment of Al, green polyhedra; C, gray; O, red. Reproduced with permission from ref. 172. Copyright 2011, American Chemical Society.

Further extension of the tricarboxylate ligand in MIL-100 led to the formation of PCN-888, which features two hierarchical mesoporous cages.[185] The combination of a linear BDC-NH_2 linker and $[Al_3(\mu_3\text{-}O)(COO)_6]$ resulted in the formation of MIL-101-NH_2(Al), a structure known for its exceptional thermal and chemical stability.[186] Another Al-MOF, Al-soc-MOF, was synthesized by combining $[Al_3(\mu_3\text{-}O)(COO)_6]$ clusters and tetratomic TCPT ligands and is recognized for its high carbon dioxide uptake and oxygen deliverable uptake.[187] Stock et al. also reported CAU-10 (CAU stands for Christian-Albrechts-University), an Al-MOF made by combining $[Al(OH)(COO)_2]$ clusters with a V-shaped linker molecule, 1,3-benzene dicarboxylic acid.[188] The inorganic building unit of CAU-10 consists of a chain of cis-connected, corner-sharing AlO_6 polyhedra, which forms helices. This unique connectivity results in the formation of square-shaped 1D channels in the CAU-10-MOF (Figure 1.17). In CAU-1 MOF, 12-connected octanuclear wheels $[Al_8(OH)_4(OCH_3)_8(COO)_{12}]$ are linked by BDC, resulting in distorted octahedral and tetrahedral cages.[189] In CAU-3 MOF, 12-connected $Al_{12}(OCH_3)_{24}$ dodecanuclear wheels and BDC linkers form strongly distorted tetrahedral and octahedral cavities.[190] Extensive research has been devoted to designing and synthesizing Al-MOFs with unique topologies for various applications. Representative stable Al-MOFs discussed are summarized in Table 1.2.

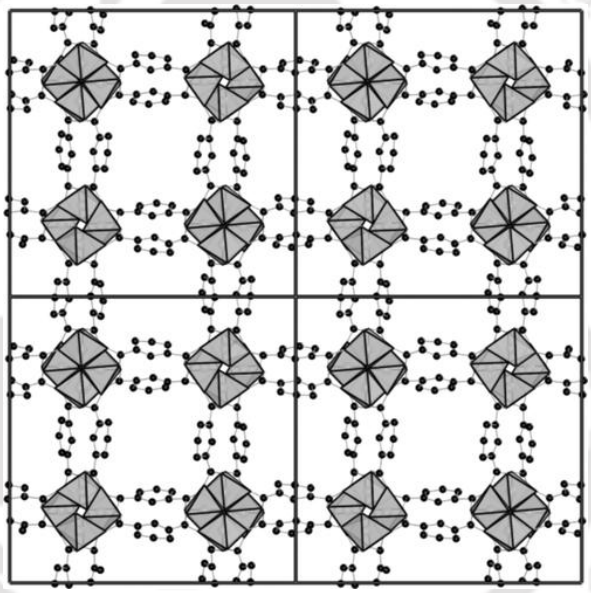

Figure 1.17 2×2 Supercell of the framework of CAU-10 showing 4-fold connectivity of the helices and square-shaped channels. Reproduced with permission from ref. 188. Copyright 2013, American Chemical Society.

Table 1.2 Summary of some representative Al(III) based MOFs reported in the literature.

MOFs	Cluster/Cores	Linkers[a]	Surface Area (m^2/g)	Ref.
MIL-53(Al)	$[Al(OH)(COO)_2]_n$	BDC	1181	171
DUT-5	$[Al(OH)(COO)_2]_n$	BPDC	1613	173
467-MOF	$[Al(OH)(COO)_2]_n$	BTTB	725	176
MIL-118	$[Al(OH)(COO)_2(COOH)_2]_n$	BTEC	-	178
MIL-120	$[Al(OH)(COO)_2]_n$	BTEC	308	179
MIL-121	$[Al(OH)(COO)_2]_n$	BTEC	162	177
NOTT-300	$[[Al(OH)(COO)_2]_n$	BPTA	1370	180
Al-PMOF	$[Al(OH)(COO)_2]_n$	TCPP	1400	181

MIL-96(Al)	$[Al_3(\mu_3\text{-}O)(COO)_6]$ $[Al(OH)(COO)_2]_n$	BTC	-	[182]
MIL100(Al)	$[Al_3(\mu_3\text{-}O)(COO)_6]$	BTC	2151	[183]
PCN-333(Al)	$[Al_3(\mu_3\text{-}O)(COO)_6]$	TATB	4000	[184]
MIL-101(Al)	$[Al_3(\mu_3\text{-}O)(COO)_6]$	BDC-NH_2	2100	[186]
Al-soc-MOF	$[Al_3(\mu_3\text{-}O)(COO)_6]$	TCPT	5585	[187]
CAU-10	$[Al(OH)(COO)_2]_n$	1,3-BDC	635	[188]
CAU-1	$[Al_8(OH)_4(OCH_3)_8(COO)_{12}]$	BDC-NH_2	1700	[189]
CAU-3-BDC	$[Al_{12}(OCH_3)_{24}(COO)_{12}]$	BDC	1550	[190]
CAU-3-BDC-NH_2	$[Al_{12}(OCH_3)_{24}(COO)_{12}]$	BDC-NH_2	1250	[190]
CAU-3-NDC	$[Al_{12}(OCH_3)_{24}(COO)_{12}]$	2,6-NDC	2320	[190]

[a] Linkers are abbreviated as: BDC = terephthalate, BPDC = biphenyl-4,4′-dicarboxylate, BTTB = 4,4′,4″-[benzene-1,3,5-triyl-tris(oxy)]tribenzoate, BTEC = 1,2,4,5-benzenetetracar-boxylate, BPTA = biphenyl-3,3′,5,5′-tetracarboxylate, TCPP = meso-tetrakis(4-carboxylatephenyl) porphyrin, BTC = benzene-1,3,5-tricarboxylate, TATB = 4,4′,4″-s-triazine-2,4,6-triyl-tribenzoate,, BDC-NH_2 = 2-aminoterephthalate, TCPT = 3,3″,5,5″-tetrakis(4-carboxyphenyl)-p-terphenyl, 1,3-BDC = isophthalate, 2,6-NDC = naphthalene-2,6-dicarboxylate.

1.9 Properties of MOFs

Due to their highly desirable properties, MOFs are regarded as superior materials in contemporary applications. High surface area, extensive porosity, tunable topology, optoelectronic properties, multiple affinities, and exceptional thermal and chemical stability distinguish them from other existing materials. Their functional tunability is one of the key reasons for their versatility, enabling the precise adjustment of their properties for a variety of applications. This tunability arises from the unique structural characteristics of MOFs, where the metal centers and organic linkers can be modified to control factors like porosity, surface area, stability, and selectivity in adsorption. MOFs can also be engineered for specific catalytic activity, optical properties such as fluorescence, and tunable proton or ion conductivity, making them ideal for use in energy storage, sensing, and catalysis. The functional tunability of MOFs is particularly beneficial for developing hydrophobic and fluorescence-based materials.

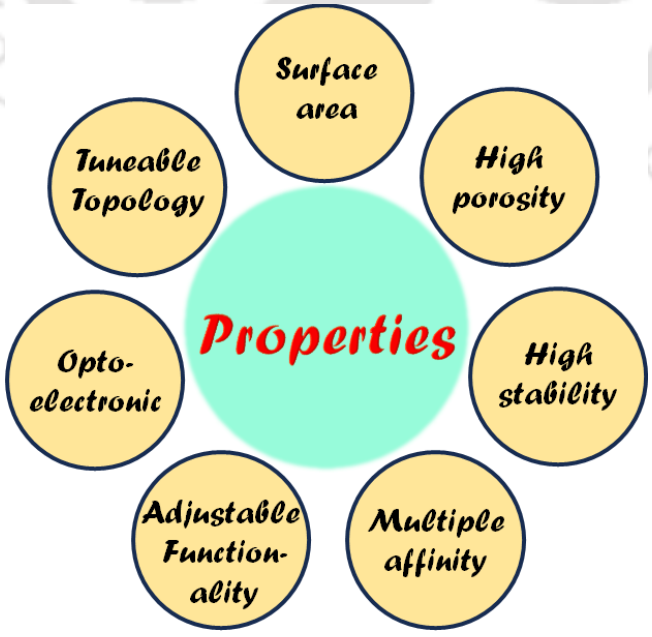

Figure 1.18 Various properties of MOFs.

1.9.1 Hydrophobic Properties of MOFs

Hydrophobic materials, which exhibit the ability to repel water, are typically characterized by a water contact angle (WCA) greater than 90º, with materials having a WCA above 150º categorized as superhydrophobic.[191] The hydrophobicity of these materials is significantly influenced by their surface structure and the chemical functional groups present. One of the key features that enhance hydrophobicity is the nano- or micro-structural arrangement of the surface.[191] This structural characteristic, as seen in materials like in lotus leave, creates micro- or nano-sized air pockets between the surface and the water droplet.[192] In such cases, the water droplet does not adhere to the surface but remains suspended on these air pockets, a phenomenon known as the Cassie-Baxter state.[193] According to the Cassie-Baxter model, when a water droplet rests on a textured surface, the contact area between the droplet and the surface is reduced as the droplet sits atop the air pockets. This reduces the interaction between the water and the surface, allowing the water to "roll off" without wetting the surface. The Cassie-Baxter state is crucial for achieving high levels of hydrophobicity, as it enables the surface to exhibit superhydrophobic behavior, characterized by water droplets that maintain a near-spherical shape due to their inability to wet the surface.[193]

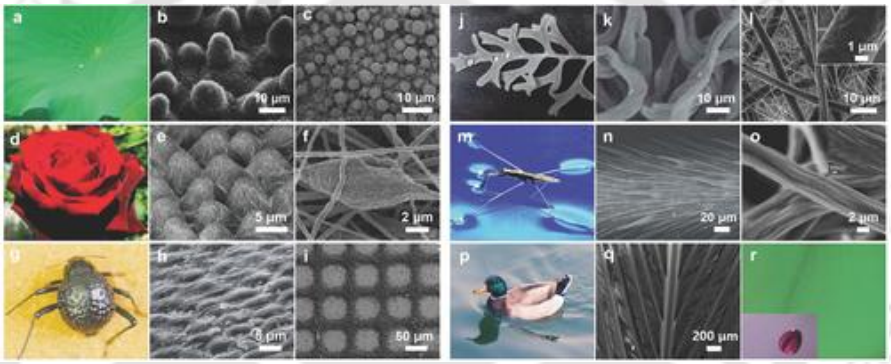

Figure 1.19 Nano-hierarchical structure of hydrophobic surfaces in nature. Reproduced with permission ref. 192, Copyright 2018, John Wiley and Sons.

In addition to surface texture, the chemical composition of the material, particularly the presence of fluorinated or alkynyl functional groups, plays a vital role in enhancing hydrophobicity.[194-195] Fluorinated groups are highly effective in repelling water due to the strong electronegativity of fluorine, which creates a repulsive force against the oxygen atoms in water molecules. This interaction between the electron cloud of fluorine and the lone pairs of oxygen in water molecules reduces the tendency of water to spread or wet the surface. Similarly, non-polar alkynyl groups also contribute to hydrophobic behavior by preventing interactions of the surface with water molecules, thereby keeping the surface dry. Nature itself provides abundant examples of hydrophobic surfaces, such as lotus leaves and bird feathers, where intricate hierarchical nano-structural designs have evolved to achieve water repellency (Figure 1.19).[192] These natural examples serve as inspiration for the development of synthetic hydrophobic materials. Hydrophobic and superhydrophobic materials, particularly MOFs, are of great interest due to their potential applications in areas like oil-water separation, anti-icing, self-cleaning, corrosion protection, and water harvesting.[196] The stability of hydrophobic MOFs in aqueous environments further enhances their applicability in various fields. While several hydrophobic materials, such as fluorinated polymers and gels, have been developed, only a select few MOFs have demonstrated effective superhydrophobic properties.[196] The hydrophobicity of MOFs can be tailored and controlled by adjusting their surface texture and incorporating hydrophobic functional groups, making them versatile materials for advanced applications.

1.9.2 Luminescence Properties of MOFs

Luminescence is the process in which a material absorbs photons, causing the transition of the electron to a higher energy level, then re-emit photons and returns to a lower energy state. This is a way of converting absorbed energy into light. Based on the time taken for this process and the energy states involved, luminescence can be classified into two types: fluorescence and phosphorescence. In fluorescence, the transition occurs between two electronic states with the same spin, while in phosphorescence, the transition happens between states with different spins. Fluorescence happens very quickly, typically in about 10 ns, whereas phosphorescence takes much longer, ranging from μs to s. While many MOFs have been studied for their fluorescent properties, fewer MOFs are known to exhibit phosphorescence. The fluorescence in MOFs can come from several factors, including the presence of π-conjugated organic linkers, which are highly fluorescent, the antenna effect of lanthanide metal ions, or the interaction between metal ions and organic linkers (like ligand-to-metal charge transfer (LMCT) and metal-to-ligand charge transfer (MLCT)).[197] Other factors contributing to fluorescence include aggregation-induced emission and the diffusion of guest molecules within the MOF framework (Figure 1.20).[22]

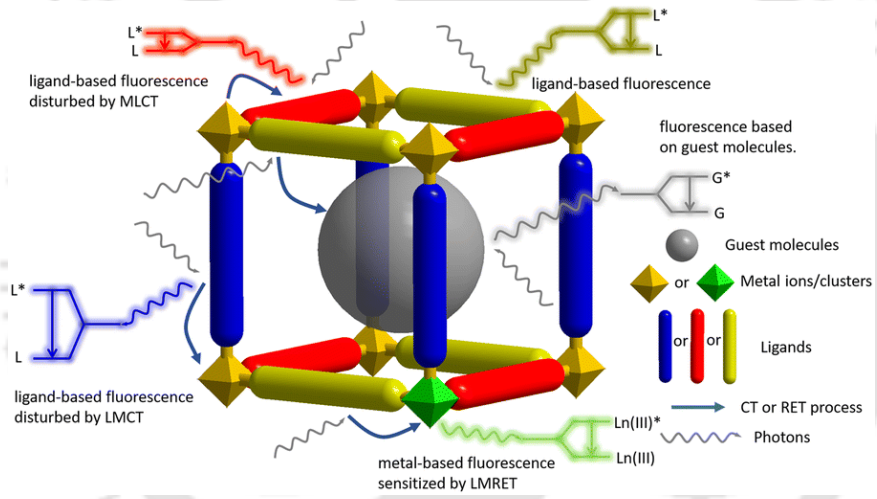

Figure 1.20 Schematic diagram showing the different sources of fluorescence signals in MOF-based fluorescence sensors. CT: charge transfer, RET: charge transfer, MLCT: metal-to-linker charge transfer, LMCT: metal-to-linker charge transfer, LMRET: linker-to-metal resonance energy transfer. Reproduced with permission from ref. no. 22. Copyright 2022, Royal Society of Chemistry.

1.9.2.1 Linker-Based Fluorescence

In most fluorescent MOFs, except those containing f-block metal ions, the fluorescence originates from the highly π-conjugated organic linkers. These linkers exhibit fluorescence due to the electronic circulation through their π-bonds. When these linkers form coordination complexes with metal ions, their fluorescence is further enhanced, primarily because the coordination bonds reduce unwanted relaxation of the linkers in the excited state. The coordination also affects the quantum efficiency and fluorescence lifetime of the linkers. For example, Li and colleagues synthesized a Cd-based MOF with an N-2-aryl-triazole (NAT) linker and showed that the fluorescence intensity of the MOF (Φ = 26%) was significantly higher than that of the free linker (Φ = 6.7%).[194] In another example, Zhou and his team developed a Zr-based MOF (PCN-94) using the H_4ETTC linker (4′,4‴,4⁗,4⁗′-(ethene-1,1,2,2-tetrayl)tetrakis(([1,1′-biphenyl]-3-carboxylic acid))). They found that by rigidifying the

fluorescent linker through MOF formation, both the fluorescence intensity and quantum yield of the linker improved.[198] The unique photoluminescent characteristics of the MOFs are attributed to the twisted linker conformation, the stiffness of the framework, and intramolecular hindrance. As a result, the spectral properties and the colors of the linker and the MOF differ significantly. For instance, the solid-state photoluminescence spectrum of the H_4ETTC linker shows a broad absorption profile with two distinct peaks, while the PCN-94 MOF displays a sharper absorption profile. Additionally, the H_4ETTC linker absorbs blue light and appears bright yellow, while PCN-94 absorbs UV light and reflects visible light, giving it a white color with slight decoloration.[198]

1.9.2.2 Metal-Based Fluorescence

Lanthanide-MOFs often show fluorescence due to transitions of electrons in the 4f orbitals of lanthanide ions. These transitions are responsible for the different colors emitted by the lanthanide ions, such as red from Eu^{3+}, orange from Sm^{3+}, green from Tb^{3+}, and blue from Tm^{3+}. However, these transitions are spectroscopically forbidden, meaning they naturally produce weak fluorescence. In MOFs, the "antenna effect" helps improve the fluorescence of lanthanide ions. This happens when organic linkers absorb light and transfer the energy to the lanthanide ions through their triplet state. The lanthanide ions need to be placed where energy does not flow back to make this energy transfer efficient. Therefore, the arrangement of energy states in both the lanthanide ions and the organic linkers is essential for achieving specific fluorescence colors. Although many fluorescent MOFs contain f-block metals, Eu(III) and Tb(III)-based MOFs are often used in sensing applications because their different fluorescence colors at various excitation wavelengths make them ideal for this purpose.[199]

1.9.2.3 Guest-Induced Fluorescence

The porous nature of MOFs allows for the incorporation of various fluorescent compounds within their cavities, such as precious metal complexes, organic and inorganic dyes, and lanthanide ions.[200-201] MOFs can enhance the stability of these guest molecules and prevent their aggregation through various interactions. Sometimes, the fluorescence of the MOF is enhanced by charge transfer or resonance energy transfer between the MOF and the guest molecules. By integrating multiple fluorescent molecules into a single MOF, multi-responsive MOF-based fluorescent sensors have been developed to detect various signals. A MOF's fluorescence spectrum can show two distinct signals from separate fluorescent linkers, making it possible to create sensors that respond to multiple stimuli without interfering with the fluorescence signals from the metal and linker. Partial sensitization can also be used to generate multiple fluorescence signals. For example, suppose the energy levels of the linkers and lanthanide ions do not align perfectly. In that case, the resulting "imperfect antenna effect" can lead to linker- and metal-based fluorescence signals.[202]

1.9.2.4 Aggregation-Induced Fluorescence

Aggregation-induced emission (AIE) has become a valuable property in luminescent MOFs for various sensing applications. Where aggregation refers to the process where molecules of a fluorescent material, typically organic luminophores, come together and form clusters or larger structures, either in solution or in the solid state. The challenge, however, lies in incorporating AIE-active molecules (AIEgens) into MOFs. It has been observed that when these AIEgens form coordination bonds with metal ions, the sites of AIEgen become rigid.[203] Some reported AIE-based MOFs, such as those containing tetraphenyl ethene, exhibit significant changes in electronic transitions. Normally, the rapid rotation of phenyl rings and twisting of the ethylene bond in tetraphenyl ethene would cause fluorescence quenching. However, this rotation and twisting are restricted in the aggregated state, leading to "turn-on"

fluorescence. For example, Omary and colleagues developed a Zr-based MOF using tetrakis(4-carboxyphenyl)ethylene as the linker. This MOF exhibited high fluorescence and quantum yield due to the linker's AIE effect. Similarly, Yang et al. synthesized an Hf-based 2D MOF that showed a 27.6% increase in electrochemiluminescence (ECL) efficiency, thanks to the AIE effect. This increase was due to the inhibition of the intramolecular motion of the linker, shortened diffusion distances of metal ions, and the increased electron density of the linker.[204]

1.9.2.5 Charge Transfer Fluorescence

In MOFs, two main types of charge transfer are typically observed: MLCT and LMCT. In MLCT, electrons are transferred from a metal ion's excited state to an organic linker's ground state.[205-207] In contrast, LMCT involves the opposite process, where electrons move from the linker to the metal ion. When there is no charge transfer or resonance energy transfer between the metal ion and the linker, the fluorescence emission spectrum of the MOF closely resembles that of the original linker. However, in the case of MLCT, the emission maxima are shifted to a higher wavelength, while in LMCT, they shift to a lower wavelength. In some cases, a linker-to-linker charge transfer (LLCT) can also occur between different linkers or parts of the same linker. Like MLCT and LMCT, LLCT results in changes in the emission intensity and wavelength of the MOF.

1.10 Mode of Fluorescence Response and its Causes

The fluorescence signal of a fluorophore can change due to alterations in the electronic transition pathway or changes in the excited state energy of the fluorophore. The four main types of fluorescence responses reported are: (i) increase in emission signal (turn-on), (ii) decrease in emission signal (turn-off), (iii) shift in emission signal, and (iv) a combination of the third type with either of the first two. Among these, fluorescence quenching (turn-off) caused by the presence of an external analyte is the most common. However, the turn-off response is not as user-friendly due to issues like poor recyclability, loss of signal, and vulnerability. In contrast, the turn-on response is more intuitive and responsive. The wavelength-shift type responses are less explored due to their short range of emission signal changes, poor linearity, and low sensitivity. However, the combined response, where both the wavelength and emission intensity change, has gained significant interest due to its potential in various applications. Several factors can lead to these changes in fluorescence, which are summarized below.

1.10.1 Structural Change of Fluorophore

The fluorescence signal can change when external molecules interact with the fluorophore through organic or inorganic reactions. These interactions can occur in the ground state, forming a ground state complex, or in the excited state, leading to the formation of an exciplex.[208-209] Such reaction-based changes in fluorescence can be either reversible or irreversible. In reversible cases, the fluorophore (or MOF) can regain its fluorescence once the external analyte is removed, but irreversible changes do not allow for recovery of the fluorescence.

1.10.2 Resonance Energy Transfer

Resonance energy transfer (RET) is a non-reaction-based process where excess energy is transferred from an excited molecule to an energy-deficient molecule. This transfer requires specific conditions, such as proper distance and orientation between the donor and acceptor molecules.[210] Fluorescence resonance energy transfer (FRET) is a widely studied energy transfer mechanism in MOF-based sensing. FRET is a long-range, dipole-dependent intermolecular process, with efficiency inversely proportional to the sixth power of the

intermolecular distance. The typical distance for effective FRET is between 10 and 100 Å. This energy transfer can occur from the MOF to the analyte or vice versa. For efficient FRET, there must be a significant overlap between the MOF's emission spectrum and the analyte's absorption spectrum. When energy is transferred from the MOF to the analyte, the fluorescence turns off, whereas the fluorescence turns on when the energy transfer occurs in the opposite direction.

1.10.3 Photo-Induced Electron Transfer (PET)

Photo-induced electron transfer (PET) is a redox process that occurs in the excited state of a molecule. During PET, electrons move from one molecule's excited state molecular orbital to a low-lying vacant orbital of another molecule. PET can also occur within the same molecule.[211] This process can lead to either an increase or decrease in the fluorescence emission intensity of the fluorophore. Suppose the excited state orbital energies of the sensor (MOF) are higher than those of the analyte. In that case, electrons can transfer from the MOF's lowest unoccupied molecular orbital (LUMO) to the LUMO of the analyte, causing a fluorescence turn-off. Conversely, when electrons transfer from the LUMO of the analyte to the LUMO of the MOF, fluorescence is turned on.[212-213]

1.10.4 Inner Filter Effect (IFE)

The inner filter effect (IFE) can lead to quenching of the fluorescence intensity when the excitation wavelength of the MOF is close to the absorption maximum of the analyte. In such cases, part of the excitation light may be absorbed by the analyte, reducing the excitation of the probe and resulting in weaker emission signals.[214] Additionally, IFE can occur when the analyte absorbs part of the emitted light from the probe. There are two types of IFE: competitive absorption and resonance energy transfer (RET). RET occurs when the analyte's UV-Vis absorption overlaps with the sensor's emission spectrum, while competitive absorption happens when the analyte's absorption spectrum overlaps with the sensor's excitation. Both RET and competitive absorption lead to fluorescence turn-off. Although IFE was once considered a flaw in fluorescence measurements, it has now been recognized as a non-radiative energy transformation process and has been applied in the development of several photoluminescent-based detection systems.[215-216]

1.11 Applications of MOFs

MOF-based materials are increasingly recognized as ideal candidates for a wide range of applications due to their distinctive chemical, physical, and structural properties (Figure 1.21). Unlike traditional materials such as zeolites and activated carbons, MOFs are preferred for various applications due to their high surface area, tunable functionality, suitable sites for guest molecule incorporation and precisely controlled pore characteristics, which make them particularly suitable for volume-specific tasks like separation, purification, sensing, adsorption and heterogeneous catalysis. This remarkable class of ultra-porous materials has been extensively studied for numerous industrial and technological uses, spanning areas such as proton conductivity, magnetic separation, nanofluids, gas separation, catalysis, bioimaging, drug delivery, water harvesting, oil-water separation, and chemical sensing. This thesis focuses primarily on the oil spill treatment and fluorescence sensing applications of MOFs.

Figure 1.21 Various applications of MOFs.

1.11.1 Adsorption of Oil Spills from Water

Oil spills in water are a significant form of environmental pollution, with their occurrence on the rise. These spills can result from the disposal of oily waste by industries, kitchen waste, or during the transportation of oils through water routes. Once oil mixes with water, it forms a layer on the surface, blocking sunlight from reaching the aquatic environment beneath.[216] This lack of sunlight disrupts the photosynthesis process in marine plants, negatively impacting the entire food chain. Aquatic life, especially organisms in coastal areas, fish nurseries, and seabirds, is highly vulnerable to the consequences of oil spills. Additionally, consuming contaminated seafood exposes humans to harmful and long-lasting components of oil, further exacerbating the issue. Moreover, oil spills can also affect global oil prices by increasing the demand for oil to replace the lost quantity.[217]

Various industrial methods, such as gravity separation, air flotation, centrifugation, and coagulation, have been developed to separate oil from water. However, these techniques tend to be ineffective, expensive, time-consuming, and often complex.[218] Alternative adsorbents like zeolites, linoleum, and cotton have been used to absorb oil from water. Despite their application, these materials often exhibit low adsorption capacity, poor selectivity, and limited reusability. They can also cause secondary contamination, making them less effective for large-scale operations.[219]

In recent years, material chemists have been exploring new materials to address the pollution caused by oil spills. Among these, hydrophobic MOFs have shown great promise as potential solutions. Due to their unique properties, these hydrophobic MOFs are highly suitable for the selective separation of oil from oil-water mixtures. Additionally, due to their robustness, MOF-based absorbents can be recycled up to many cycles.

Hydrophobic MOFs have become a major focus due to their effectiveness in oil spill adsorption. These MOFs are typically constructed using long-chain alkylated or highly fluorinated linkers because fluorides and alkyl groups tend to have low surface free energies, which enhances their hydrophobic characteristics. Since MOF powders cannot typically stand-alone, numerous hydrophobic MOF-based composites have been developed to make the oil-water separation process more efficient and practical (Figure 1.22).[220] For example, in 2016, Roy and colleagues developed a Zn(II)-MOF (NMOF-1) using a dialkoxyoctadecyl-oligo-(p-phenylene ethynylene)dicarboxylate (OPE-C_{18}) linker, which exhibited superhydrophobic

properties.[221] The water contact angle (WCA) of the MOF was measured to be 162°, and it was effectively used for oil-water separation and self-cleaning applications. That same year, Ghosh and co-workers developed a Cu(II)-containing ultra hydrophobic MOF with a WCA 176°. They used this MOF to separate oil from oil-water mixtures and water-in-oil emulsions. To improve the separation process further, they created a composite by spraying a cross-linked mixture of polydimethylsiloxane and the MOF (UHMOF-100) onto polypropylene fabric. This resulted in a membrane with an oil absorption capacity of 40-70 wt% and the ability to be reused up to 10 times.[222] Similarly, Du and colleagues synthesized four highly stable hydrophobic Zr/Hf-UiO-66 MOFs by introducing fluoroalkyl chains of varying lengths (C_6-C_{10}).[223] These MOFs were also employed for oil-water separation applications. In another study, Zhu et al. reported a long-chain hydrocarbon-containing Zr-UiO-67 MOF, which was also utilized for efficient oil separation.[224]

Moreover, Jayaramulu et al., developed a one-pot synthesis of a ZIF-8 MOF with highly fluorinated graphene oxide (HFGO), resulting in a superhydrophobic hybrid MOF composite with micro- and meso-porosity. The composite displayed a WCA of 162° and achieved remarkable oil and organic solvent absorption capacities ranging from 150-600 wt%.[225] Other notable studies have reported the development of superhydrophobic MOFs and their composites. For instance, Gu and his colleagues created a superhydrophobic ZIF-8@rGO@sponge composite. This composite exhibited a WCA of 158° and an outstanding oil absorption capacity of 1400-2900 wt%, with excellent recyclability (up to 100 times).[226] The key focus of these studies is to improve the absorption capacity, reusability, and stability of MOF-based composites to create more efficient and sustainable oil-water separation systems. With increasing attention from researchers, hydrophobic MOF composites have shown significant promise in addressing the challenges of oil spill management.

Table 1.3 Examples of some hydrophobic MOFs, functional groups responsible for hydrophobicity, their WCA, oil separation efficiency and flux of separation.

Sl. No.	MOF	Wettability Response Unit	WCA (°)	Separation Efficiency	Flux ($L\ m^{-2}\ h^{-1}$)	Ref.
1	ODPA-ZIF-8(n) @ZIF-8/PDMS	octadecylphosphonic acid	163	-	0.64	10
2	Ni_2(L-asp)$_2$ bipy@PDMS	polydimethylsiloxane	137.1	-	27.6	227
3	ZIF-8/PAN	surface roughness	153	99.9%	2550	228
4	MXene@UiO-66-(COOH)$_2$	hierarchical roughness & hydrophilicity of composite	>150	>99%	713.3	229
5	PAN@ZIF-8	surface roughness	155	>99.9%	>900	230
6	ZIF-90 membrane	fluorinated alkyls and the ZIF-90 layer	170	99.9%	1260	231
7	ZIF-8-DMBIM	hydrophobic 5,6-dimethyl-benzimidazole linker	141.7	>99.9%	1411.8-1643.1	232

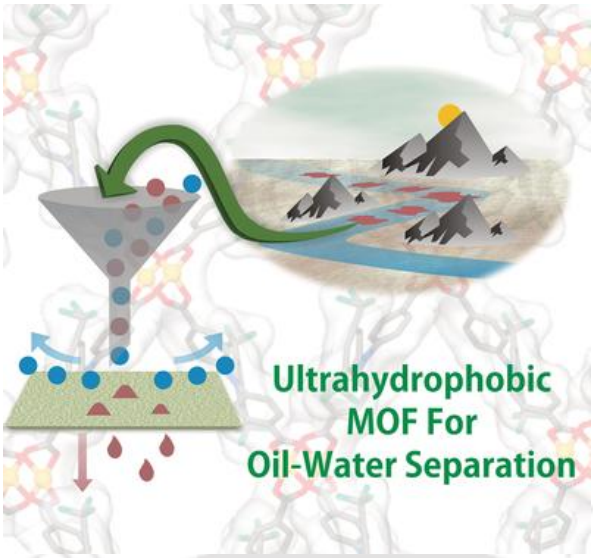

Figure 1.22 Selective separation of oil spills by superhydrophobic MOF. Reproduced with permission from ref. no. 220. Copyright 2016, John Wiley and Sons.

1.11.2 Fluorescence Sensing of Toxic Analytes

The rapid development of modern civilization, including socioeconomic growth, industrialization, urbanization, and the intensification of agricultural practices, has led to a significant rise in the production of chemical-related chemicals. This, in turn, has drastically increased environmental pollution, particularly due to toxic heavy metals, drugs, herbicides, antibiotics, pesticides, harmful anions, volatile organic compounds, inorganic pollutants and other emerging pollutants. Detecting and quantifying these pollutants in water bodies is one of the most effective and widely used methods to address pollution. Similarly, accurate measurement of biomolecule concentrations in body fluids is crucial for diagnosing diseases, conducting pharmacokinetic studies of various drugs, and supporting forensic science.

To address environmental pollution and accurately measure the concentrations of such pollutants, various quantification techniques have been developed. Among these, fluorescence-based sensing has emerged as one of the most accessible, cost-effective, and responsive methods for detecting pollutants in water and drugs in body fluids. The benefits of fluorescence-based sensing, including its simplicity, speed, and reliability, make it a more promising technique compared to traditional methods like HPLC, LC-MS, capillary electrophoresis, and atomic emission and absorption spectroscopy. The detection of target analytes can be enhanced by selecting appropriate fluorophore molecules. In this context, fluorescent MOFs can serve as effective fluorophores, addressing many of the challenges associated with other detection methods. This section of my thesis primarily focuses on developing functionalized MOFs for sensing a variety of pollutants (inorganic pollutants, heavy metal ions, drugs, and pesticides).

1.11.2.1 Inorganic Pollutant Sensing

The rapid, selective, sensitive, and cost-effective detection of toxic compounds has garnered significant attention due to the severe environmental and health risks posed by these species. The Environmental Protection Agency (EPA) has established threshold detection limits for harmful toxic compounds. A wide range of MOFs have been investigated for the detection of various toxic species, including volatile organic chemicals, toxic gases, heavy metals ions, organic and inorganic amines, pharmaceutical and agricultural wastes etc. Inorganic pollutants are a significant environmental concern due to their persistence and toxic effects on ecosystems

and human health. These pollutants include heavy metals such as lead, mercury, cadmium, arsenic and compounds like hydrazine, which can have devastating consequences when released into the environment. One of the most infamous examples is Japan's Minamata disease in 1956, which was caused by mercury contamination.[157, 233] In South Asia, particularly in India and Bangladesh, excessive arsenic levels in drinking water are a significant source of the water crisis.[233] Similarly, lead contamination in drinking water is linked to various health issues, including cardiovascular disease, hypertension, high blood pressure, and kidney dysfunction. On the other hand, cadmium contamination can lead to the development of Itai-Itai disease (Figure 1.23).[234]

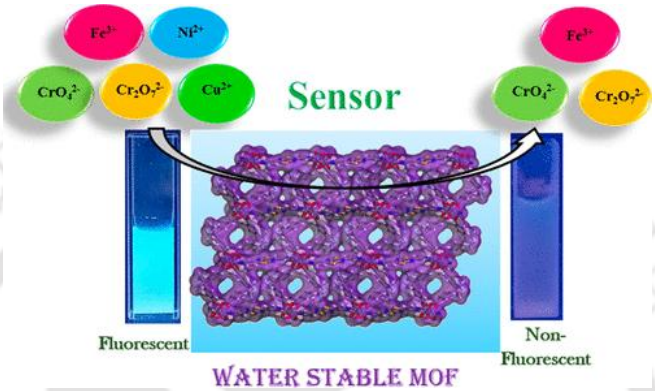

Figure 1.23 Schematic representation of fluorescence-based sensing of metal ions and oxyanions by luminescent water stable MOFs. Reproduced with permission ref. no. 234, Copyright 2022, American Chemical Society.

Given these alarming concerns, many MOF-based fluorescence sensors have been developed over the past decade to detect and quantify heavy metal ions. Mercury, being the softest of the heavy metals, poses a particularly significant environmental threat. In its inorganic form (Hg^{2+}), mercury readily transforms into the softer, more lipophilic methyl mercury in biological systems.[157] This transformation makes mercury pollution a critical concern. Even trace amounts of mercury can damage the immune and central nervous systems when it interacts with sulfur-containing amino acids. High mercury levels are associated with a range of health issues, including nephrotic syndrome, respiratory problems, cancer, motion disorders, kidney failure, and temporary blindness.[157] Numerous research groups have worked on developing MOF-based fluorescent sensors for detecting Hg^{2+}. For example, Li and his team created sulfone-functionalized, water-stable Zn-MOFs capable of detecting Hg^{2+} at parts per billion (ppb) levels.[235] Another group led by Mandal developed a Zn(II)-MOF for selective Hg^{2+} sensing.[24] Roy and colleagues developed a Ni(II)-based MOF, $[Ni(3\text{-bpd})_2(NCS)_2]_n$, for Hg^{2+} detection.[236] Safarifard and his team prepared a porphyrinic zirconium framework with exposed pyrrole Lewis basic sites for Hg^{2+} fluorescence sensing.[237] The Ghosh group synthesized a butyne-functionalized UiO-66 MOF that enables nanomolar-level detection of Hg^{2+} in water, with the triple bond interaction being key to its selective sensing capability.[238] Qian and his team developed a Tb(III)-based MOF that could quickly and selectively detect mercury, with a reported response time of just 3 s and a limit of detection (LOD) of 47.8 nM.[239] Recently, Biswas group introduced two sulfur-containing MOFs, IITG-5 and Hf-UiO-66-$NHCSNHCH_3$, for ultrafast and highly sensitive Hg^{2+} detection in environmental waters.[157] Furthermore Li et. al developed a functionalized luminescent UiO-66 MOF for the detection of Hg^{2+} in aqueous medium with ultralow LOD. These studies highlight the growing interest and progress in developing MOF-based sensors for detecting mercury contamination.

Hydrazine, a highly reactive inorganic compound, is primarily used in industrial applications, including as a rocket propellant, in producing plastics, and as a foaming agent. When hydrazine is released into the environment, it can contaminate water sources, soil, and air, leading to severe ecological damage.[240] The compound's toxicity is exacerbated by its ability to form highly reactive intermediates, which can further degrade environmental quality. The persistence of hydrazine in the environment is a major concern because conventional water treatment methods may not effectively eliminate it, requiring advanced technologies for detection and remediation. Recent advancements in sensing technologies, particularly fluorescence-based methods, have shown promising results for detecting hydrazine contamination in water and the environment. Due to their highly tunable structures and unique optical properties, MOFs have become one of the most promising materials for fluorescence sensing of hydrazine.[241] Luminescent MOFs can selectively detect hydrazine through changes in their fluorescence properties upon interaction with the compound. Studies have demonstrated the development of MOF-based sensors with high sensitivity and selectivity for hydrazine detection. For instance, research by Zhang et al. highlighted the use of a luminescent MOF to detect hydrazine, which rapidly achieves detection limits at nanomolar concentrations.[242] These MOF-based sensors offer advantages over traditional detection methods, such as ease of use, high sensitivity, and real-time monitoring capabilities, making them ideal tools for environmental monitoring and pollution control.[242-243] By utilizing these advanced sensing techniques, the detection and removal of hydrazine from contaminated water sources can be more efficient, reducing the harmful environmental and health impacts of this toxic pollutant.

H_2S is a well-known toxic gas, and dysregulation of its endogenous concentration can lead to several serious health conditions, such as Down syndrome, Alzheimer's disease, Parkinson's disease, and cancer.[244-245] Therefore, real-time monitoring of H_2S levels remains a challenging task. Ghosh and co-workers first reported a post-synthetically modified azide-functionalized Zr-UiO-66 MOF for the selective "turn-on" detection of H_2S under physiological conditions.[246] This material utilizes the reduction of the azide group to an auxochromic amine group, which accounts for the "turn-on" fluorescence response in the presence of H_2S. Subsequent work by Ghosh and colleagues involved the development of a nitro-functionalized Zr-UiO-66 framework, wherein the nitro group is reduced to an amine upon exposure to H_2S.[247] Biswas group also reported both azide- and nitro-functionalized Ce-UiO-66 MOFs that demonstrate the ability to detect H_2S in biological conditions.[248] Formaldehyde, a carcinogenic compound associated with sick building syndrome (SBS), is commonly found in household goods like adhesives, cosmetics, and paints.[249] The World Health Organization (WHO) has set a permissible exposure limit of 0.08 ppm for 30 min. In 2014, Dong et al. reported a porous Cu(I) MOF (MOF-2) constructed with Cu_2I_2 SBUs and ligands, capable of fluorescent and colorimetric detection of formaldehyde in the vapor phase through a single-crystal-to-single-crystal transition.[250] Zhao and colleagues developed a ZIF-8-based platform for the sensitive detection of formaldehyde vapor, with a detection limit of 0.057 ppm.[251] Vellingiri et al. discovered that Zr-UiO-66-NH_2 could detect formaldehyde directly in trizma buffer without the need for post-synthetic modifications, demonstrating selectivity over other aldehydes like propionaldehyde, butyraldehyde, and valeraldehyde, with a detection limit of 4 ppm.[252]

Cyanide is a highly toxic contaminant, and the WHO has recommended a maximum cyanide concentration of 2 μM in drinking water. Ghosh et al. developed a post-synthetically modified ZIF-90 MOF with dicyanovinyl functionalization for selective cyanide sensing, achieving a detection limit of 2 μM in DMSO/H_2O.[253] The same group later reported a bio-MOF-1 loaded with a cationic dye (3,6-diaminoacridinium cation) for cyanide anion detection in pure aqueous medium, with a detection limit of 5.2 ppb.[254] Biswas and co-workers developed carbazole-

functionalized Zr(IV)-MOF[255] and CAU-10-N_2H_3 [256] MOFs for selective cyanide detection in pure aqueous media, with detection limits of 0.14 and 0.48 µM, respectively.

Phosphate (PO_4^{3-}) is a major water pollutant that causes eutrophication, which poses a severe threat to aquatic life. Qian et al. used a Tb(III)-based framework with a nitrilotriacetate ligand for phosphate detection in aqueous media.[257] Zhao et al. developed ZnO QDs and MOF-5 for PO_4^{3-} recognition, with a detection limit of 53 nM.[258]

Table 1.4 Examples of some literature reported fluorescent MOFs and their response time, detection limit, and sensing media used for the sensing of inorganic pollutants.

Sensor Type	Sensor Material	Sensing Medium	Detection Limit	Response Time	Ref
Hg^{2+}	$[Ni(3\text{-}bpd)_2(NCS)_2]_n$	water	-	120	236
	[PCN-221]	water	10 nM	1	237
	[Cu(Dcbb)(Bpe)]	HEPES buffer	3.3 nM	30	259
	UiO-66@ Butyne	water	10.9 nM	3	260
	$Ln(TATAB)\cdot(DMF)_4(H_2O)(MeOH)_{0.5}$	water	4.4 nM	-	261
	Eu^{3+}/CDs@MOF-253	water	47.88 nM	3	262
	$[Cu(Cdcbp)(H_2O)_2\cdot 2H_2O]_n$	water	2.3 nM	2	263
	Al-MOF (TAM)	water	2.94 nM	0.5	264
	$[Cu(Cbdcp)(Dps)(H_2O)_3]_6$	HEPES buffer	2.6 nM	10	265
	Cd−EDDA	water	2 nM	0.25	266
	Hf-UiO-66-NHCSNHMe	H_2O	4.0 nM	-	267
hydrazine	Zr-UiO-66-$(OSO_2\text{-}Ph\text{-}NO_2)$	water	52.6 nM	2	243
	Zr-UiO-66-$(OCOCH_3)_2$	water	78.8 nM	-	268
	UiO-66-phmd	HEPES buffer	0.87 µM	20	269
	Hf-UiO-66-$NHCSNHCH_3$	H_2O	1.9 nM	50 s	267
H_2S	Zr-UiO-66-N_3	HEPES buffer	118 µM	-	246
	Zr-UiO-66-NO_2	HEPES buffer	188 µM		247
	Ce-UiO-66-N_3	HEPES buffer	12.2 µM	60 s	248
	Ce-UiO-66-NO_2	HEPES buffer	34.84 µM	60 s	248
HCHO	Cu-MOF	water	666 µM	-	250
	ZIF-8	solid state	1.89 µM	-	251
	Zr-UiO-66-NH_2	base buffer	133 µM	-	252
CN^-	M-ZIF-90	DMSO/H_2O	2 µM	-	253
	bio-MOF-1⊃DAAC	HEPES buffer	0.11 nM	-	254
	Zr-UiO-67-carbazole	water	0.14 µM	-	255
	CAU-10-N_2H_3	water	0.48 µM	60 s	256
PO_4^{3-}	TbNTA1	water	-		257
	ZnO QDs & MOF	water	53 nM		258

1.11.2.2 Agricultural Pollutant Sensing

Pesticide contamination are major concerns for both environmental and human health. Pesticides used in agriculture to control pests, diseases, and weeds. Pesticides can persist in the environment, affecting non-target organisms like pollinators, aquatic life, and soil microbes.[258] These chemicals may contaminate water, soil, air, and food, posing long-term risks to biodiversity and human health, including cancer, neurotoxicity, and endocrine disruption.[270] Monitoring both pesticide residues is essential to ensure contamination stays within safe limits,

support compliance with regulatory standards like maximum residue limits, and promote sustainable agricultural practices. This proactive approach is key to reducing environmental risks and safeguarding public health (Figure 1.24).[271]

To address the above issue due various scientific group developed luminescent MOF based sensors for the selective sensing of different pesticides. A La(III)/Ta(III) mixed-metal fluorescent MOF was developed by Zhang et al. for selective detection of nitenpyram, but this probe has a relatively high detection limit of 0.63 μM.[272] In contrast, Yang et al. created a functional Zr-MOF (FMOF) that can detect nitenpyram with a lower detection limit of 0.11 μM.[273] Rana et al. developed a 2-hydroxy naphthalene-functionalized Al-MIL-53 MOF for the selective detection of nitenpyram, achieving a detection limit in the nanomolar range and an ultrafast response time of just 5 s.[274] Similarly, Mehta et al. designed an -NH_2 functionalized Zr-UiO-66 MOF for the selective detection of methyl parathion in aqueous media, with a detection limit of 38 nM.[275] In another study, Yang et al. synthesized a 2D-Cd-MOF for the detection of methyl parathion, demonstrating a sensitivity of up to 3 nM.[276] Xu et al. utilized a luminescent Zn-MOF for methyl parathion sensing, achieving an impressive detection limit of 0.46 nM.[277] Wang et al. developed a Zn-MOF sensor for parathion detection with a detection limit of 1.95 nM.[278] The same research group also synthesized a Zn-MOF sensor for detecting 2,4-dichloro-4-nitroaniline (DCN), with a detection limit of 0.27 μM.[279] In another study, Guo et al. developed a Zn-MOF sensor for DCN detection, achieving a detection limit of 1.9 μM,[280] while Di et al. utilized a different Zn-MOF sensor for the same purpose, with a detection limit of 14.2 μM.[281] Wiwiasuku et al. developed a MOF sensor for glyphosate, with a detection limit of 25 nM and a response time of 30 s.[282] Additionally, Eskandari et al. prepared a polymer composite of luminescent MOFs for the detection of chlorpyrifos, exhibiting nanomolar sensitivity (9.38 nM).[283]

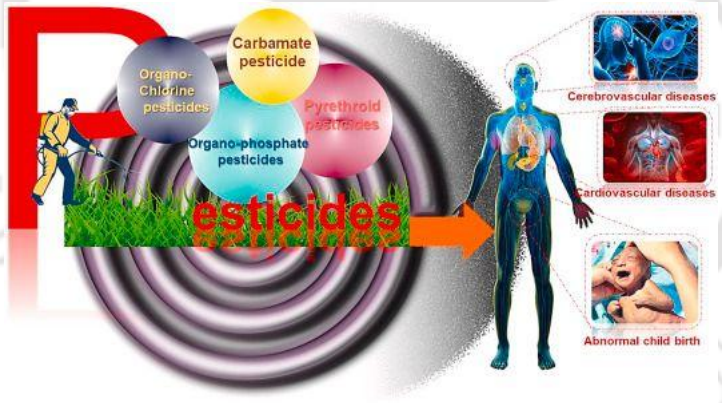

Figure 1.24 Schematic representation of fluorescence-based sensing of pesticides. Reproduced with permission ref. no. 271, Copyright 2023, Elsvier.

Table 1.6 Examples of some literature reported fluorescent MOFs and their response time, detection limit and sensing media used for the sensing of pesticides.

Sensor Type	Sensor Material	Sensing Medium	LOD	Response Time	Ref.
nitenpyram	In-Tb@MOF	water	0.63 μM	-	272
	FMOF	water	0.11 μM	-	273
	Dye@MOFs	water	0.27 μM	-	284
	EY@Zr-MOF	water	1.18 μM	-	285
	[Al(OH)(L)]·0.5H_2O	water	13.8 nM	5 s	274

parathion-methyl	ZnPO-MOFs	water	0.46 nM	-	[277]
	UiO-66-NH_2	water	38 nM	60 min	[275]
	Cd-MOF	water	3 nM	-	[276]
parathion	Zn-MOF	water	1.95 µM	-	[278]
DCN	Zn-MOF-1	water	1.90 µM	-	[280]
	Zn-MOF	water	0.27 µM	-	[279]
	ABW-type MOF	water	14.2 µM	-	[281]
glyphosate	Cd-MOF-NH_2	water	25 nM	30 s	[282]
chlorpyrifos	Tb-MOF-76	water	9.38 nM	-	[283]

1.11.2.3 Active Pharmaceutical Chemical Sensing

Recent studies have highlighted a concerning rise in the use of pharmaceutical drugs and antibiotics, with consumption increasing by 10-15 times since the COVID-19 pandemic. This surge has led to a significant increase in pharmaceutical waste, particularly in urban wastewater, where the concentration of these drugs and their metabolites has risen by over 70% in the past 2-3 years due to misuse and improper disposal.[286-287] This rapid increase in pharmaceutical contamination in the environment is a growing global issue, making it crucial to develop selective and sensitive sensor systems to continuously monitor synthetic drug residues in our surroundings. Addressing this issue is vital to mitigate the adverse effects on human health and the environment.

Various research group explored detection of pharmaceutical drugs by luminescent MOFs. Rana et al. designed a functional luminescent Al-MIL-53 MOF for the nanomolar level detection of rifampicin from biofluids with an ultrafast detection time (5 s). Recently, Ding et al. synthesized a dual-emissive post-modified Eu(III)@Zn(II) MOF for the selective, ratiometric sensing of procaterol in an aqueous medium, achieving a detection limit of 46.1 nM.[288] In a separate study, Gao et al. designed a Tb(III)-based fluorescent MOF, reporting that its photoluminescence intensity was rapidly suppressed within 40 s after adding lamotrigine to the MOF suspension in water, with a limit of detection (LOD) of 1.66 µM.[289] Yan and his team developed the first MOF-based photoluminescent sensor for aspirin, which exhibited an impressive LOD of 0.02 µM.[290] Additionally, Yan et al. synthesized an Eu-MOF and modified it with Cu(II) to create a Cu-Eu-MOF, enabling selective detection of 6-mercaptopurine and 6-thioguanine with LODs of 14 µM and 2.8 µM, respectively, and a detection time of 30 s.[291] Furthermore, Liu et al. designed a 2D Zn(II)-based MOF for selective sensing of ceftriaxone via a quenching mechanism.[292] This Zn(II)-MOF demonstrated excellent selectivity, rapid response time, and an ultra-low sensitivity with a LOD of 5.89 nM for detecting targeted antibiotics.

Table 1.7. Examples of some literature reported fluorescent MOFs and their response time, detection limit and sensing media used for the sensing of active pharmaceutical ingredients.

Sensor Type	Sensor Material	Sensing Medium	LOD (nM)	Response Time	Ref.
rifampicin	[Al(OH)(L)]·0.5H_2O	water	11.7 nM	5 s	[274]
procaterol	Eu(III)@Zn(II) MOF	water	46.1 nM	-	[288]
lamotrigine	Tb-MOF	water	1.66 µM	-	[289]
aspirin	UiO-66-NH_2	water	0.02 µM	-	[290]
6-thioguanine	Cu-Eu-MOF	water	2.8 µM	30 s	[291]
ceftriaxone	Zn-MOF	serum	5.89 nM	-	[292]
6-mercaptopurin	Cu-Eu-MOF	water	14 µM	30 s	[291]

1.12 Conclusions and Outlook

In conclusion, this chapter has comprehensively explored the historical development and diverse applications of highly physicochemically stable porous MOFs, with a particular emphasis on Zr(IV) and Al(III)-based frameworks. It has outlined various synthesis methods, delved into the origins of their fluorescence and hydrophobic properties, and examined the mechanistic aspects of their sensing capabilities. The chapter highlights the promising potential of fluorescent MOFs for detecting and quantifying inorganic pollutants, agricultural chemicals, and pharmaceutically active compounds. Additionally, it has explored the design of hydrophobic MOFs tailored for efficient oil spill adsorption, emphasizing their environmental significance and potential for sustainable development.

While fluorescent MOFs present significant advantages for pollutant detection, several challenges must be addressed for their practical implementation. Issues such as stability under different environmental conditions (acidic, alkaline, or aqueous media) and selectivity for specific analytes have been identified as key limitations. To overcome these, strategies such as utilizing hard Lewis acids and bases for improved stability, designing MOF-based composites, and introducing pre-functionalized linkers or guest molecules to enhance selectivity have been discussed. Furthermore, the development of chiral luminescent MOFs offers exciting possibilities for precisely detecting enantiomers in pharmaceutical applications.

The research presented in this thesis contributes to advancing the field of MOF-based sensing, offering insights into the design of selective, reusable, and cost-effective sensors. By addressing stability, selectivity, and practicality challenges, this work paves the way for the future development of more efficient MOF-based solutions for environmental monitoring, pollutant detection, and sustainable resource management. The ideas presented here will undoubtedly be valuable to researchers in materials science, environmental chemistry, pharmaceutical chemistry, oil spill treatment, fluorescence sensing, and related fields.

1.13 References

1. F. Basolo, R. C. Johnson and R. Carl, *Coordination chemistry*, Science reviews Northwood, 1986.
2. E. C. Constable, *Chemistry*, 2019, **1**, 126-163.
3. R. E. Schöllhorn, J. Atwood, J. Davies and D. MacNicol, *Inclusion compounds structural aspect of inclusion compounds formed by inorganic and organometallic host lattices*, Academic Press, 1984.
4. H. Buser, D. Schwarzenbach, W. Petter and A. Ludi, *Inorg. Chem.*, 1977, **16**, 2704-2710.
5. T. Iwamoto, T. Nakano, M. Morita, T. Miyoshi, T. Miyamoto and Y. Sasaki, *Inorg. Chim. Acta*, 1968, **2**, 313-316.
6. T. R. Cook, Y.-R. Zheng and P. J. Stang, *Chem. Rev.*, 2013, **113**, 734-777.
7. J. M. Lehn, *Vch, Weinheim*, 1995, **1**.
8. K. Margeta and A. Farkaš, *Zeolites-New Challenges*, 2020, 1-10.
9. B. F. Hoskins and R. Robson, *J. Am. Chem. Soc.*, 1990, **112**, 1546-1554.
10. Y. Pan, T. Zhu, Q. Xia, X. Yu and Y. Wang, *J. Environ. Chem. Eng.*, 2021, **9**, 104977.
11. K. Biradha, A. Ramanan and J. J. Vittal, *Cryst. Growth Des.*, 2009, **9**, 2969-2970.
12. R. B. S, N. R. Champness, X.-M. Chen, J. G. -Martinez, S. Kitagawa, L. Öhrström, M. O'Keeffe, M. P. Suh and J. Reedijk, *Pure Appl. Chem.*, 2013, **85**, 1715-1724.
13. J. L. Rowsell and O. M. Yaghi, *Microporous Mesoporous Mater.*, 2004, **73**, 3-14.
14. P. G. -García, M. Müller and A. Corma, *Chem. Sci.*, 2014, **5**, 2979-3007.

15. A. Kirchon, L. Feng, H. F. Drake, E. A. Joseph and H.-C. Zhou, *Chem. Soc. Rev.*, 2018, **47**, 8611-8638.
16. V. Pascanu, G. G. Miera, A. K. Inge and B. M.-Matute, *J. Am. Chem. Soc.*, 2019, **141**, 7223–7234.
17. B. Li, H.-M. Wen, W. Zhou and B. Chen, *J. Phys. Chem. Lett.*, 2014, **5**, 3468–3479.
18. J. Cao, X. Li and H. Tian, *Curr. Med. Chem.*, 2020, **27**, 5949-5969.
19. J.-R. Li, J. Sculley and H.-C. Zhou, *Chem. Rev.*, 2012, **112**, 869-932.
20. P. Horcajada, C. Serre, M. Vallet-Regí, M. Sebban, F. Taulelle and G. Férey, *Angew. Chem.*, 2006, **118**, 6120-6124.
21. P. Kumar, A. Deep and K.-H. Kim, *Trends Anal. Chem.*, 2015, **73**, 39-53.
22. T. Wu, X.-j. Gao, F. Ge and H.-g. Zheng, *CrystEngComm*, 2022, **24**, 7881-7901.
23. X.-D. Zhu, K. Zhang, Y. Wang, W.-W. Long, R.-J. Sa, T.-F. Liu and J. Lü, *Inorg. Chem.*, 2018, **57**, 1060-1065.
24. A. Pankajakshan, D. Kuznetsov and S. Mandal, *Inorg. Chem.*, 2019, **58**, 1377-1381.
25. S. Nandi and S. Biswas, *Dalton Trans.*, 2020, **48**, 17612-17620.
26. A. Das, M. Alam, C. Gogoi, R. Dalapati and S. Biswas, *Dalton Trans.*, 2020, **49**, 16928-16934.
27. H.-Y. Li, S.-N. Zhao, S.-Q. Zang and J. Li, *Chem. Soc. Rev.*, 2020, **49**, 6364-6401.
28. S. Ghosh, A. Das and S. Biswas, *Microporous Mesoporous Mater.*, 2021, **323**, 111251.
29. O. K. Farha, I. Eryazici, N. C. Jeong, B. G. Hauser, C. E. Wilmer, A. A. Sarjeant, R. Q. Snurr, S. T. Nguyen, A. Ö. Yazaydın and J. T. Hupp, *J. Am. Chem. Soc.*, 2012, **134**, 15016-15021.
30. J. Lyu, X. Zhang, K.-I. Otake, X. Wang, P. Li, Z. Li, Z. Chen, Y. Zhang, M. C. Wasson, Y. Yang, P. Bai, X. Guo, T. Islamoglu and O. K. Farha, *Chem. Sci.*, 2019, **10**, 1186-1192.
31. R. Dalapati, S. Nandi and S. Biswas, *Dalton Trans.*, 2020, **49**, 8684-8692.
32. J. Krautwurst, D. Smets, R. Lamann and U. Ruschewitz, *Inorg. Chem.*, 2019, **58**, 8622-8632.
33. G. Férey, C. M. -Draznieks, C. Serre, F. Millange, J. Dutour, S. Surblé and I. Margiolaki, 2005, **309**, 2040-2042.
34. H. Chevreau, T. Devic, F. Salles, G. Maurin, N. Stock and C. Serre, *Angew. Chem. Int. Ed.*, 2013, **52**, 5056-5060.
35. K. Wu, X. Xu, F. Ma and C. Du, *ACS Omega*, 2022, **7**, 35970-35980.
36. H. L. Nguyen, *New J. Chem.*, 2017, **41**, 14030-14043.
37. B. Wang, Y. Ma, W. Xu and K. Tang, *Langmuir*, 2022, **38**, 8954-8963.
38. R. A. -Baah and H. Liu, *Materials*, 2018, **11**, 2250-2271.
39. Y. Sun, Q. Sun, H. Huang, B. Aguila, Z. Niu, J. A. Perman and S. Ma, *J. Mater. Chem. A*, 2017, **5**, 18770-18776.
40. X. Chen, P. Qian, T. Zhang, Z. Xu, C. Fang, X. Xu, W. Chen, P. Wu, Y. Shen, S. Li, J. Wu, B. Zheng, W. Zhang and F. Huo, *Chem. Commun.*, 2018, **54**, 3936-3939.
41. W. Gong, M. Kazem-Rostami, F. A. Son, S. Su, K. M. Fahy, H. Xie, T. Islamoglu, Y. Liu, J. F. Stoddart and Y. Cui, *J. Am. Chem. Soc.*, 2022, **144**, 22574-22581.
42. S. Leubner, R. Siegel, J. Franke, M. T. Wharmby, C. Krebs, H. Reinsch, J. r. Senker and N. Stock, *Inorg. Chem.*, 2020, **59**, 15250-15261.
43. S. Mollick, S. Saurabh, Y. D. More, S. Fajal, M. M. Shirolkar, W. Mandal and S. K. Ghosh, *Energy Environ. Sci.*, 2022, **15**, 3462-3469.
44. M. Zhang, B. Guo, Y. Feng, C. Xie, X. Han, X. Kong, B. Xu and L. Zhang, *Inorg. Chem.*, 2019, **58**, 5384-5387.
45. J. Gu, H. Fan, L. U. Hannover, C. Li and J. Caro, *Angew. Chem. Int.*, 2019, **16**, 58.
46. D. M. DeChellis, C. M. Ngule and D. T. Genna, *J. Mater. Chem. A*, 2020, **8**, 5848-5852.

47. C. Kumunda, A. S. Adekunle, B. B. Mamba, N. W. Hlongwa and T. T. Nkambule, *Front. Mater.*, 2021, **7**, 616787.
48. X. Ma, Y. Chai, P. Li and B. Wang, *Acc. Chem. Res.*, 2019, **52**, 1461-1470.
49. L. Lin, H. Yang and X. Xu, *Front. Environ. Sci.*, 2022, 975.
50. J. N. Halder and M. N. Islam, *J. Hum. Environ. Stud.*, 2015, **2**, 36-46.
51. G. Delin, H. Essaid, I. Cozzarelli, M. Lahvis and B. Bekins, *Ground Water Contamination By Crude Oil*, 1998.
52. S. Ismail and A. Dadrasnia, *PLoS One*, 2015, **10**, e0120931.
53. P. N. Wassenaar and E. M. Verbruggen, *Chemosphere*, 2021, **276**, 130113.
54. N. Andrews, N. J. Bennett, P. L. Billon, S. J. Green, A. M. C. Montemayor, S. Amongin, N. J. Gray and U. R. Sumaila, *Energy Res. Soc. Sci.*, 2021, **75**, 102009.
55. A. P. Onyena and K. Sam, *Proc. Genet. Evol. Comput. Conf. Companion*, 2020, **22**, e00961.
56. S. E. Chang, J. Stone, K. Demes and M. Piscitelli, *Ecol. Soc.*, 2014, **19**.
57. O. Hettithanthri, T. B. T. Nguyen, T. Fiedler, C. Phan, M. Vithanage, S. Pallewatta, T. M. L. Nguyen, P. Q. A. Nguyen and N. Bolan, *Asia-Pac. J. Chem. Eng.*, 2024, **19**, e3128.
58. G. Troisi, S. Barton and S. Bexton, *Int. J. Hydrogen Energy*, 2016, **41**, 16549-16555.
59. B. M. Jenssen, *Environ. Pollut.*, 1994, **86**, 207-215.
60. J. C. Cirer-Costa, *Mar. Pollut. Bull.*, 2015, **91**, 65-72.
61. A. Knap, T. Sleeter, R. E. Dodge, S. Wyers, H. Frith and S. Smith, *Oil Petrochem. Pollut.*, 1983, **1**, 157-169.
62. T. A. Birkland and R. G. Lawrence, *SS&T Bulletin*, 2002, **7**, 17-22.
63. D. A. Gill, L. A. Ritchie and J. S. Picou, *Extr. Ind. Soc.* , 2016, **3**, 1105-1116.
64. R. L. Eklund, L. C. Knapp, P. A. Sandifer and R. C. Colwell, *GeoHealth*, 2019, **3**, 391-406.
65. J. Beyer, H. C. Trannum, T. Bakke, P. V. Hodson and T. K. Collier, *Mar. Pollut. Bull.*, 2016, **110**, 28-51.
66. G. E. Challenger, S. Gmur and E. Taylor, *Mar. Pollut. Bull.*, 2021, **164**, 111983.
67. A. Dhaka and P. Chattopadhyay, *J. Environ. Manag.*, 2021, **288**, 112428.
68. B. Purohit, S. Tewari, K. Prasad, V. K. Talari, N. Pandey, P. Choudhury and S. S. Panda, *Reg. Stud. Mar. Sci.*, 2024, 103876.
69. N. Bhardwaj and A. N. Bhaskarwar, *Environ. Pollut.*, 2018, **243**, 1758-1771.
70. S. ben Hammouda, Z. Chen, C. An and K. Lee, *J. Clean. Prod.*, 2021, **311**, 127630.
71. Y. Shin, K. S. Han, B. W. Arey and G. T. Bonheyo, *ACS Omega*, 2020, **5**, 13894-13901.
72. J.-F. Meng, B.-Y. Song, F. Li and T.-H. Li, *Mater. Today Chem.*, 2023, **28**, 101371.
73. F. Zadehahmadi, N. T. Eden, H. Mahdavi, K. Konstas, J. I. Mardel, M. Shaibani, P. C. Banerjee and M. R. Hill, *Environ. Sci. Water Res.* , 2023, **9**, 1305-1330.
74. X. Liu, Y. Shan, S. Zhang, Q. Kong and H. Pang, *Green Energy Environ.*, 2022, **8**, 2468-0257.
75. E. Zhang, L. Wu, L. Jiang, K. Guo, Z. Su and P. Ju, *J. Mol. Struct.*, 2022, **1264**, 133314.
76. Y. Zhao, Q. Wang, H. Wang, H. Zhangsun, X. Sun, T. Bu, Y. Liu, W. Wang, Z. Xu and L. Wang, *Sensor. Actuator. B Chem.*, 2021, **334**, 129610.
77. X.-J. Zhang, F.-Z. Su, D.-M. Chen, Y. Peng, W.-Y. Guo, C.-S. Liu and M. Du, *Dalton Trans.*, 2019, **48**, 1843-1849.
78. A. Das, S. Ghosh, L. Bourda, S. Mostakim, K. Banerjee, K. Van Hecke and S. Biswas, *CrystEngComm*, 2022, **24**, 4723-4730.
79. Y. Yang, G. Ren, W. Yang, X. Qin, D. Gu, Z. Liang, D.-Y. Guo and Q. Pan, *Polyhedron*, 2021, **194**, 114923-114928.
80. X. Fang, B. Zong and S. Mao, *Nano-Micro Lett.*, 2018, **10**, 1-19.

81. H. Liu, T. Fu and Y. Mao, *ACS Omega*, 2022, **7**, 14430-14456.
82. W. Cheng, X. Tang, Y. Zhang, D. Wu and W. Yang, *Trends Food Sci. Technol.*, 2021, **112**, 268-282.
83. L. E. Kreno, K. Leong, O. K. Farha, M. Allendorf, R. P. Van Duyne and J. T. Hupp, *Chem. Rev.*, 2012, **112**, 1105-1125.
84. A. Karmakar, P. Samanta, S. Dutta and S. K. Ghosh, *Chem. Asian J.*, 2019, **14**, 4506-4519.
85. S. Kitagawa, R. Kitaura and S. i. Noro, *Angew. Chem. Int. Ed.*, 2004, **43**, 2334-2375.
86. V. F. Yusuf, N. I. Malek and S. K. Kailasa, *ACS Omega*, 2022, **7**, 44507-44531.
87. K. O. Kirlikovali, S. L. Hanna, F. A. Son and O. K. Farha, *ACS Nanosci. Au*, 2022, **3**, 37-45.
88. S. A. A. Razavi and A. Morsali, *Coord. Chem. Rev.*, 2019, **399**, 213023.
89. W. Lu, Z. Wei, Z.-Y. Gu, T.-F. Liu, J. Park, J. Park, J. Tian, M. Zhang, Q. Zhang and T. Gentle III, *Chem. Soc. Rev.*, 2014, **43**, 5561-5593.
90. H. Li, L. Li, R.-B. Lin, W. Zhou, Z. Zhang, S. Xiang and B. Chen, *EnergyChem*, 2019, **1**, 100006.
91. H. Wang, X. Dong, J. Lin, S. J. Teat, S. Jensen, J. Cure, E. V. Alexandrov, Q. Xia, K. Tan and Q. Wang, *Nat. Commun.*, 2018, **9**, 1745.
92. P. Rocío-Bautista, I. Taima-Mancera, J. Pasán and V. Pino, *Separations*, 2019, **6**, 33.
93. G. Férey, *Chem. Soc. Rev.*, 2008, **37**, 191-214.
94. D. Wang, Y. Zhang, J. Gao, G. Ge and C. Li, *Cryst. Growth Des.*, 2019, **19**, 4571-4578.
95. R. J. Kuppler, D. J. Timmons, Q.-R. Fang, J.-R. Li, T. A. Makal, M. D. Young, D. Yuan, D. Zhao, W. Zhuang and H.-C. Zhou, *Coord. Chem. Rev.*, 2009, **253**, 3042-3066.
96. O. M. Yaghi, M. O'Keeffe, N. W. Ockwig, H. K. Chae, M. Eddaoudi and J. Kim, *Nature*, 2003, **423**, 705-714.
97. P. V. Dau, K. K. Tanabe and S. M. Cohen, *Chem. Commun.*, 2012, **48**, 9370-9372.
98. D. J. Collins and H.-C. Zhou, *J. Mater. Chem.*, 2007, **17**, 3154-3160.
99. B. Chen, C. Liang, J. Yang, D. S. Contreras, Y. L. Clancy, E. B. Lobkovsky, O. M. Yaghi and S. Dai, *Angew. Chem. Int. Ed.*, 2006, **45**, 1390-1393.
100. C. P. Raptopoulou, *Materials*, 2021, **14**, 310.
101. S. R. Halper, L. Do, J. R. Stork and S. M. Cohen, *J. Am. Chem. Soc.*, 2006, **128**, 15255-15268.
102. K. N. Lazarou, V. Psycharis, A. Terzis and C. P. Raptopoulou, *Polyhedron*, 2011, **30**, 963-970.
103. J. Klinowski, F. A. A. Paz, P. Silva and J. Rocha, *Dalton Trans.*, 2011, **40**, 321-330.
104. Z. Ni and R. I. Masel, *J. Am. Chem. Soc.* , 2006, **128**, 12394-12395.
105. R. M. Barrer, *J. Chem. Soc.*, 1948, 127-132.
106. R. Lalawmpuia, M. Lalhruaitluangi and D. Tiwari, *Environ. Eng. Res.*, 2024, **29**.
107. E. Biemmi, S. Christian, N. Stock and T. Bein, *Microporous Mesoporous Mater.*, 2009, **117**, 111-117.
108. X.-X. Zhao, J.-P. Ma, Y.-B. Dong, R.-Q. Huang and T. Lai, *Cryst. Growth Des.*, 2007, **7**, 1058-1068.
109. M. Lammert, M. T. Wharmby, S. Smolders, B. Bueken, A. Lieb, K. A. Lomachenko, D. De Vos and N. Stock, *Chem comm*, 2015, **51**, 12578-12581.
110. V. Bon, I. Senkovska, M. S. Weiss and S. Kaskel, *CrystEngComm*, 2013, **15**, 9572-9577.
111. X. -LiangL, M. Tong, H. Huang, B. Wang, L. Gan, Q. Yang, C. Zhong and J.-R. Li, *J. Solid State Chem.*, 2015, **223**, 104-108.
112. A. Imtiyaz and A. Singh, *J. Inorg. Organomet. Polym. Mater.*, 2023, **33**, 3027-3048.

113. A. M. Araújo-Cordero, F. Caddeo, B. Mahmoudi, M. Bron and A. Wouter Maijenburg, *ChemPlusChem*, 2024, **89**, e202300378.
114. Z. Han, Y. Yang, J. Rushlow, J. Huo, Z. Liu, Y.-C. Hsu, R. Yin, M. Wang, R. Liang and K.-Y. Wang, *Chem. Soc. Rev.*, 2025, **54**, 367-395.
115. T. Friščić, I. Halasz, P. J. Beldon, A. M. Belenguer, F. Adams, S. A. Kimber, V. Honkimäki and R. E. Dinnebier, *Nat. Chem.*, 2013, **5**, 66-73.
116. A. L. Garay, A. Pichon and S. L. James, *Chem. Soc. Rev.*, 2007, **36**, 846-855.
117. P. A. Julien, K. Užarević, A. D. Katsenis, S. A. Kimber, T. Wang, O. K. Farha, Y. Zhang, J. Casaban, L. S. Germann and M. Etter, *J. Am. Chem. Soc.*, 2016, **138**, 2929-2932.
118. A. Pichon and S. L. James, *CrystEngComm*, 2008, **10**, 1839-1847.
119. T.-H. Wei, S.-H. Wu, Y.-D. Huang, W.-S. Lo, B. P. Williams, S.-Y. Chen, H.-C. Yang, Y.-S. Hsu, Z.-Y. Lin and X.-H. Chen, *Nat. Commun.*, 2019, **10**, 5002.
120. V. Snowlin, H. J. Prabu, A. F. Sahayaraj, I. Johnson, E. Thaninayagam, R. Gopi, J. Salamon and A. Simi, *J. Inorg. Organomet. Polym. Mater.*, 2024, **34**, 251-265.
121. N. Ahmad, H. A. Younus, Z. Gaoke, K. Van Hecke and F. Verpoort, *Adv. Mater.*, 2019, **31**, 1801399.
122. Z.-Y. Yao, J.-H. Guo, P. Wang, Y. Liu, F. Guo and W.-Y. Sun, *Mater. Lett.*, 2018, **223**, 174-177.
123. A. Aslani and A. Morsali, *Inorg. Chim. Acta*, 2009, **362**, 5012-5016.
124. J. Kim, S.-T. Yang, S. B. Choi, J. Sim, J. Kim and W.-S. Ahn, *J. Mater. Chem.*, 2011, **21**, 3070-3076.
125. W.-J. Son, J. Kim, J. Kim and W.-S. Ahn, *Chem. Commun.* , 2008, 6336-6338.
126. B. F. Hoskins and R. Robson, *J. Am. Chem. Soc.*, 1990, **112**, 1546-1554.
127. C. Păun, L. Motelică, D. Ficai, A. Ficai and E. Andronescu, *Materials*, 2023, **16**, 6143.
128. E. D. Bloch, D. Britt, C. Lee, C. J. Doonan, F. J. Uribe-Romo, H. Furukawa, J. R. Long and O. M. Yaghi, *J. Am. Chem. Soc.*, 2010, **132**, 14382-14384.
129. C. Paun, L. Motelica, D. Ficai, A. Ficai and E. Andronescu, *Materials*, 2023, **16**.
130. M. Kalaj and S. M. Cohen, *ACS Cent. Sci.*, 2020, **6**, 1046-1057.
131. R. Seetharaj, P. Vandana, P. Arya and S. Mathew, *Arab. J. Chem.*, 2019, **12**, 295-315.
132. L. Li, S. Wang, T. Chen, Z. Sun, J. Luo and M. Hong, *Cryst. Growth Des.*, 2012, **12**, 4109-4115.
133. X. J. Luan, X. H. Cai, Y. Y. Wang, D. S. Li, C. J. Wang, P. Liu, H. M. Hu, Q. Z. Shi and S. M. Peng, *Chem. Eur. J.*, 2006, **12**, 6281-6289.
134. L. Carlucci, G. Ciani, S. Maggini and D. M. Proserpio, *Cryst. Growth Des.*, 2008, **8**, 162-165.
135. C. Livage, C. Egger and G. Ferey, *Chem. Mater.*, 2001, **13**, 410-414.
136. F. Yuan, J. Xie, H.-M. Hu, C.-M. Yuan, B. Xu, M.-L. Yang, F.-X. Dong and G.-L. Xue, *CrystEngComm*, 2013, **15**, 1460-1467.
137. L. Luo, G.-C. Lv, P. Wang, Q. Liu, K. Chen and W.-Y. Sun, *CrystEngComm*, 2013, **15**, 9537-9543.
138. J. Winarta, B. Shan, S. M. Mcintyre, L. Ye, C. Wang, J. Liu and B. Mu, *Cryst. Growth Des.*, 2019, **20**, 1347-1362.
139. Z.-R. Jiang, J. Ge, Y.-X. Zhou, Z. U. Wang, D. Chen, S.-H. Yu and H.-L. Jiang, *NPG Asia Mater.*, 2016, **8**, e253-e253.
140. T. Tsuruoka, S. Furukawa, Y. Takashima, K. Yoshida, S. Isoda and S. Kitagawa, *Angew. Chem. Int. Ed.*, 2009, **121**, 4833-4837.
141. S. Diring, S. Furukawa, Y. Takashima, T. Tsuruoka and S. Kitagawa, *Chem. Mater.*, 2010, **22**, 4531-4538.

142. F. Vermoortele, B. Bueken, G. Le Bars, B. Van de Voorde, M. Vandichel, K. Houthoofd, A. Vimont, M. Daturi, M. Waroquier and V. Van Speybroeck, *J. Am. Chem. Soc.*, 2013, **135**, 11465-11468.
143. M. Ding, X. Cai and H.-L. Jiang, *Chem. Sci.*, 2019, **10**, 10209-10230.
144. S. Yuan, L. Feng, K. Wang, J. Pang, M. Bosch, C. Lollar, Y. Sun, J. Qin, X. Yang and P. Zhang, *Adv. Mater.*, 2018, **30**, 1704303.
145. N. C. Burtch, H. Jasuja and K. S. Walton, *Chem. Rev.*, 2014, **114**, 10575-10612.
146. J. H. Cavka, S. Jakobsen, U. Olsbye, N. Guillou, C. Lamberti, S. Bordiga and K. P. Lillerud, *J. Am. Chem. Soc.*, 2008, **130**, 13850-13851.
147. Q. Yao, A. Bermejo Gómez, J. Su, V. Pascanu, Y. Yun, H. Zheng, H. Chen, L. Liu, H. N. Abdelhamid and B. n. Martín-Matute, *Chem. Mater.*, 2015, **27**, 5332-5339.
148. T.-F. Liu, D. Feng, Y.-P. Chen, L. Zou, M. Bosch, S. Yuan, Z. Wei, S. Fordham, K. Wang and H.-C. Zhou, *J. Am. Chem. Soc.*, 2015, **137**, 413-419.
149. X. C. Huang, Y. Y. Lin, J. P. Zhang and X. M. Chen, *Angew. Chem. Int. Ed.*, 2006, **45**, 1557-1559.
150. N. M. Padial, E. Quartapelle Procopio, C. Montoro, E. López, J. E. Oltra, V. Colombo, A. Maspero, N. Masciocchi, S. Galli and I. Senkovska, *Angew. Chem. Int. Ed.*, 2013, **125**, 8448-8452.
151. X.-W. Zhu, X.-P. Zhou and D. Li, *Chem. Commun.*, 2016, **52**, 6513-6516.
152. L. Xu, Y. Xiao, A. Van Sandwijk, Q. Xu and Y. Yang, *J. Nucl. Mater.*, 2015, **466**, 21-28.
153. J. Winarta, B. Shan, S. M. Mcintyre, L. Ye, C. Wang, J. Liu and B. Mu, *Cryst. Growth Des.*, 2020, **20**, 1347−1362.
154. M. Leloire, C. Walshe, P. Devaux, R. Giovine, S. Duval, T. Bousquet, S. Chibani, J. F. Paul, A. Moissette and H. Vezin, *Chem. Eur. J.*, 2022, **28**, e202104437.
155. M. Taddei, *Coord. Chem. Rev.*, 2017, **343**, 1-24.
156. Y. Bai, Y. Dou, L.-H. Xie, W. Rutledge, J.-R. Li and H.-C. Zhou, *Chem. Soc. Rev.*, 2016, **45**, 2327-2367.
157. S. Ghosh, F. Steinke, A. Rana and S. Biswas, *Inorg. Chem. Front.*, 2022, **9**, 859-869.
158. V. Guillerm, F. Ragon, M. Dan-Hardi, T. Devic, M. Vishnuvarthan, B. Campo, A. Vimont, G. Clet, Q. Yang and G. Maurin, *Angew. Chem. Int. Ed.*, 2012, **51**, 9267-9271.
159. L. Cooper, N. Guillou, C. Martineau, E. Elkaim, F. Taulelle, C. Serre and T. Devic, *Eur. J. Inorg. Chem.*, 2014, **2014**, 6281-6289.
160. P. Ji, K. Manna, Z. Lin, X. Feng, A. Urban, Y. Song and W. Lin, *J. Am. Chem. Soc.*, 2017, **139**, 7004-7011.
161. J. E. Mondloch, W. Bury, D. Fairen-Jimenez, S. Kwon, E. J. DeMarco, M. H. Weston, A. A. Sarjeant, S. T. Nguyen, P. C. Stair and R. Q. Snurr, *J. Am. Chem. Soc.*, 2013, **135**, 10294-10297.
162. O. V. Gutov, W. Bury, D. A. Gomez-Gualdron, V. Krungleviciute, D. Fairen-Jimenez, J. E. Mondloch, A. A. Sarjeant, S. S. Al-Juaid, R. Q. Snurr and J. T. Hupp, *Chem. Eur. J.*, 2014, **20**, 12389-12393.
163. H. Furukawa, F. Gandara, Y.-B. Zhang, J. Jiang, W. L. Queen, M. R. Hudson and O. M. Yaghi, *J. Am. Chem. Soc.*, 2014, **136**, 4369-4381.
164. V. Bon, V. Senkovskyy, I. Senkovska and S. Kaskel, *Chem. Commun.*, 2012, **48**, 8407-8409.
165. V. Bon, *Cryst. Growth Des*, 2013, **13**, 1231-1237.
166. D. Feng, H.-L. Jiang, Y.-P. Chen, Z.-Y. Gu, Z. Wei and H.-C. Zhou, *Inorg. Chem.*, 2013, **52**, 12661-12667.
167. D. Feng, Z. Y. Gu, J. R. Li, H. L. Jiang, Z. Wei and H. C. Zhou, *Angew. Chem. Int. Ed*, 2012, **124**, 10453-10456.

168. D. Feng, Z.-Y. Gu, Y.-P. Chen, J. Park, Z. Wei, Y. Sun, M. Bosch, S. Yuan and H.-C. Zhou, *J. Am. Chem. Soc.*, 2014, **136**, 17714-17717.
169. H.-L. Jiang, D. Feng, K. Wang, Z.-Y. Gu, Z. Wei, Y.-P. Chen and H.-C. Zhou, *J. Am. Chem. Soc.*, 2013, **135**, 13934-13938.
170. S. B. Kalidindi, S. Nayak, M. E. Briggs, S. Jansat, A. P. Katsoulidis, G. J. Miller, J. E. Warren, D. Antypov, F. Corà and B. Slater, *Angew. Chem. Int. Ed.*, 2015, **54**, 221-226.
171. C. S. T. Loiseau, C. Huguenard, G. Fink, F. Taulelle, M. Henry, T. Bataille and G. Férey,, *Chem. Eur. J.*, 2004, **10**, 1373-1382.
172. S. Biswas, T. Ahnfeldt and N. Stock, *Inorg. Chem.*, 2011, **50**, 9518-9526.
173. I. Senkovska, F. Hoffmann, M. Fröba, J. Getzschmann, W. Böhlmann and S. Kaskel, *Microporous Mesoporous Mater.*, 2009, **122**, 93-98.
174. Q. Yang, S. Vaesen, M. Vishnuvarthan, F. Ragon, C. Serre, A. Vimont, M. Daturi, G. De Weireld and G. Maurin, *J. Mater. Chem.*, 2012, **22**, 10210-10220.
175. S.-H. Lo, C.-H. Chien, Y.-L. Lai, C.-C. Yang, J. J. Lee, D. S. Raja and C.-H. Lin, *J. Mater. Chem. A*, 2013, **1**, 324-329.
176. Z. W. Wang, M. Chen, C. S. Liu, X. Wang, H. Zhao and M. Du, *Chem. Eur. J.*, 2015, **21**, 17215-17219.
177. C. Volkringer, T. Loiseau, N. Guillou, G. Férey, M. Haouas, F. Taulelle, E. Elkaim and N. Stock, *Inorg. Chem.*, 2010, **49**, 9852-9862.
178. C. Volkringer, T. Loiseau, N. Guillou, G. Férey, M. Haouas, F. Taulelle, N. Audebrand, I. Margiolaki, D. Popov and M. Burghammer, *Growth Des.*, 2009, **9**, 2927-2936.
179. C. Volkringer, T. Loiseau, M. Haouas, F. Taulelle, D. Popov, M. Burghammer, C. Riekel, C. Zlotea, F. Cuevas and M. Latroche, *Chem. Mater.*, 2009, **21**, 5783-5791.
180. S. Yang, J. Sun, A. J. Ramirez-Cuesta, S. K. Callear, W. I. David, D. P. Anderson, R. Newby, A. J. Blake, J. E. Parker and C. C. Tang, *Nat. Chem.*, 2012, **4**, 887-894.
181. A. Fateeva, P. A. Chater, C. P. Ireland, A. A. Tahir, Y. Z. Khimyak, P. V. Wiper, J. R. Darwent and M. J. Rosseinsky, *Angew. Chem., Int. Ed.*, 2012, **124**, 7558.
182. T. Loiseau, L. Lecroq, C. Volkringer, J. Marrot, G. Férey, M. Haouas, F. Taulelle, S. Bourrelly, P. L. Llewellyn and M. Latroche, *J. Am. Chem. Soc.*, 2006, **128**, 10223-10230.
183. C. Volkringer, D. Popov, T. Loiseau, G. Férey, M. Burghammer, C. Riekel, M. Haouas and F. Taulelle, *Chem. Mater.*, 2009, **21**, 5695-5697.
184. D. Feng, T.-F. Liu, J. Su, M. Bosch, Z. Wei, W. Wan, D. Yuan, Y.-P. Chen, X. Wang and K. Wang, *Nat. Commun.*, 2015, **6**, 5979.
185. X. Lian, Y.-P. Chen, T.-F. Liu and H.-C. Zhou, *Chem. Sci.*, 2016, **7**, 6969-6973.
186. P. Serra-Crespo, E. V. Ramos-Fernandez, J. Gascon and F. Kapteijn, *Chem. Mater.*, 2011, **23**, 2565-2572.
187. D. Alezi, Y. Belmabkhout, M. Suyetin, P. M. Bhatt, Ł. J. Weseliński, V. Solovyeva, K. Adil, I. Spanopoulos, P. N. Trikalitis and A.-H. Emwas, *J. Am. Chem. Soc.*, 2015, **137**, 13308-13318.
188. H. Reinsch, M. A. van der Veen, B. Gil, B. Marszalek, T. Verbiest, D. De Vos and N. Stock, *Chem. Mater.*, 2013, **25**, 17-26.
189. T. Ahnfeldt, N. Guillou, D. Gunzelmann, I. Margiolaki, T. Loiseau, G. Férey, J. Senker and N. Stock, *Angew. Chem., Int. Ed.*, 2009, **48**, 5163-5166.
190. H. Reinsch, M. Feyand, T. Ahnfeldt and N. Stock, *Dalton Trans.*, 2012, **41**, 4164-4171.
191. K.-Y. Law, *J. Phys. Chem. Lett.*, 2014, **5**, 686-688.
192. L. Hou, N. Wang, J. Wu, Z. Cui, L. Jiang and Y. Zhao, *Adv. Funct. Mater.*, 2018, **28**, 1801114.
193. M. T. Rauter, S. K. Schnell and S. Kjelstrup, *J. Phys. Chem. B*, 2021, **125**, 12730-12740.

194. D. Wang, Q. Sun, M. J. Hokkanen, C. Zhang, F.-Y. Lin, Q. Liu, S.-P. Zhu, T. Zhou, Q. Chang and B. He, *Nature*, 2020, **582**, 55-59.
195. M. Shi, R. Huang, W. Qi, R. Su and Z. He, *Colloids Surf. A*, 2020, **602**, 125102.
196. L. H. Xie, M. M. Xu, X. M. Liu, M. J. Zhao and J. R. Li, *Adv. Sci.*, 2020, **7**, 1901758.
197. T. Wu, X.-j. Gao, F. Ge and H.-g. Zheng, *CrystEngComm*, 2022, **24**, 7881-7901.
198. Z. Wei, Z.-Y. Gu, R. K. Arvapally, Y.-P. Chen, R. N. McDougald Jr, J. F. Ivy, A. A. Yakovenko, D. Feng, M. A. Omary and H.-C. Zhou, *J. Am. Chem. Soc.*, 2014, **136**, 8269-8276.
199. S. Petoud, S. M. Cohen, J.-C. G. Bünzli and K. N. Raymond, *J. Am. Chem. Soc.*, 2003, **125**, 13324-13325.
200. H. Li, Y. Han, Z. Shao, N. Li, C. Huang and H. Hou, *Dalton Trans.*, 2017, **46**, 12201-12208.
201. Z. Zhang, Z. Wei, F. Meng, J. Su, D. Chen, Z. Guo and H. Xing, *Chem. Eur. J.*, 2020, **26**, 1661-1667.
202. M. Lei, F. Ge, S. Ren, X. Gao and H. Zheng, *Sep. Purif. Technol.*, 2022, **286**, 120433.
203. M. Asad, M. I. Anwar, A. Abbas, A. Younas, S. Hussain, R. Gao, L.-K. Li, M. Shahid and S. Khan, *Coord. Chem. Rev.*, 2022, **463**, 214539.
204. Y. Yang, G.-B. Hu, W.-B. Liang, L.-Y. Yao, W. Huang, Y.-J. Zhang, J.-L. Zhang, J.-M. Wang, R. Yuan and D.-R. Xiao, *Nanoscale*, 2020, **12**, 5932-5941.
205. X. Li, J. Yu, D. J. Gosztola, H. C. Fry and P. Deria, *J. Am. Chem. Soc.*, 2019, **141**, 16849-16857.
206. Y. Zhou, D. Zhang, W. Xing, J. Cuan, Y. Hu, Y. Cao and N. Gan, *Anal. Chem.*, 2019, **91**, 4845-4851.
207. M.-X. Li, H. Wang, S.-W. Liang, M. Shao, X. He, Z.-X. Wang and S.-R. Zhu, *Cryst. Growth Des.*, 2009, **9**, 4626-4633.
208. S. K. Panda, S. Mishra and A. K. Singh, *Dalton Trans.*, 2021, **50**, 7139-7155.
209. S.-L. Yao, S.-J. Liu, X.-M. Tian, T.-F. Zheng, C. Cao, C.-Y. Niu, Y.-Q. Chen, J.-L. Chen, H. Huang and H.-R. Wen, *Inorg. Chem.*, 2019, **58**, 3578-3581.
210. R. B. Sekar and A. Periasamy, *J. Cell Biol.*, 2003, **160**, 629.
211. D. Escudero, *Acc. Chem. Res.*, 2016, **49**, 1816-1824.
212. V. Ramamurthy, *Organic and inorganic photochemistry*, CRC Press, 1998.
213. X. Zhang, Y. Wu, S. Ji, H. Guo, P. Song, K. Han, W. Wu, W. Wu, T. D. James and J. Zhao, *J. Org. Chem.*, 2010, **75**, 2578-2588.
214. S. C. Chen, C. Y. Lin, T. L. Cheng and W. L. Tseng, *Adv. Funct. Mater.*, 2017, **27**, 1702452.
215. S. Ghosh, J. Krishnan, V. Karthik, A. Dhakshinamoorthy and S. Biswas, *Inorg. Chem.*, 2023.
216. L. Han, S. G. Liu, J. Y. Liang, Y. J. Ju, N. B. Li and H. Q. Luo, *J. Hazard. Mater.*, 2019, **362**, 45-52.
217. A. Riaz, L. Xingong, Z. Jiao and M. Shahbaz, *Energy Rep.*, 2023, **9**, 3493-3507.
218. R. K. Gupta, G. J. Dunderdale, M. W. England and A. Hozumi, *J. Mater. Chem. A*, 2017, **5**, 16025-16058.
219. H. Saini, E. Otyepková, A. Schneemann, R. Zbořil, M. Otyepka, R. A. Fischer and K. Jayaramulu, *J. Mater. Chem. A*, 2022, **10**, 2751-2785.
220. S. Mukherjee, A. M. Kansara, D. Saha, R. Gonnade, D. Mullangi, B. Manna, A. V. Desai, S. H. Thorat, P. S. Singh and A. Mukherjee, *Chem. Eur. J.*, 2016, **22**, 10937-10943.
221. S. Roy, V. M. Suresh and T. K. Maji, *Chem. Sci.*, 2016, **7**, 2251-2256.

222. S. Mukherjee, A. M. Kansara, D. Saha, R. Gonnade, D. Mullangi, B. Manna, A. V. Desai, S. H. Thorat, P. S. Singh and A. Mukherjee, *Chem. Eur. J.*, 2016, **22**, 10937-10943.
223. J. Du, L. Chen, X. Zeng, S. Yu, W. Zhou, L. Tan, L. Dong, C. Zhou and J. Cheng, *ACS Appl. Mater. Interfaces.*, 2020, **12**, 28576-28585.
224. N. X. Zhu, Z. W. Wei, C. X. Chen, D. Wang, C. C. Cao, Q. F. Qiu, J. J. Jiang, H. P. Wang and C. Y. Su, *Angew. Chem. Int. Ed.*, 2019, **131**, 17189-17196.
225. K. Jayaramulu, K. K. R. Datta, C. Rösler, M. Petr, M. Otyepka, R. Zboril and R. A. Fischer, *Angew. Chem., Int. Ed.*, 2016, **55**, 1178-1182.
226. J. Gu, H. Fan, C. Li, J. Caro and H. Meng, *Angew. Chem. Int. Ed.*, 2019, **131**, 5351-5355.
227. S. Wang, Z. Kang, B. Xu, L. Fan, G. Li, L. Wen, X. Xin, Z. Xiao, J. Pang and X. Du, *Inorg. Chem. Commun.*, 2017, **82**, 64-67.
228. H. Li, P. Mu, J. Li and Q. Wang, *J. Mater. Chem. A*, 2021, **9**, 4167-4175.
229. S. He, Y. Zhan, J. Hu, G. Zhang, S. Zhao, Q. Feng and W. Yang, *Composites Part B: Engineering*, 2020, **197**, 108188.
230. Y. Cai, D. Chen, N. Li, Q. Xu, H. Li, J. He and J. Lu, *J. Membr. Sci.*, 2017, **543**, 10-17.
231. R. Qu, W. Zhang, N. Liu, Q. Zhang, Y. Liu, X. Li, Y. Wei and L. Feng, *ACS Sustainable Chem. Eng.*, 2018, **6**, 8019-8028.
232. H. You, G. Y. Shangkum, P. Chammingkwan and T. Taniike, *Colloids Surf. A*, 2021, **614**, 126204.
233. Y. Peng, H. Huang, Y. Zhang, C. Kang, S. Chen, L. Song, D. Liu and C. Zhong, *Nat. Commun*, 2018, **9**, 187.
234. S. C. Pal, D. Mukherjee and M. C. Das, *Inorg. Chem.*, 2022, **61**, 12396-12405.
235. N. D. Rudd, H. Wang, E. M. Fuentes-Fernandez, S. J. Teat, F. Chen, G. Hall, Y. J. Chabal and J. Li, *ACS Appl. Mater. Interfaces.* , 2016, **8**, 30294-30303.
236. S. Halder, J. Mondal, J. Ortega-Castro, A. Frontera and P. Roy, *Dalton Trans.*, 2017, **46**, 1943-1950.
237. E. Moradi, R. Rahimi and V. Safarifard, *J. Solid State Chem.*, 2020, **286**, 121277.
238. P. Samanta, A. V. Desai, S. Sharma, P. Chandra and S. K. Ghosh, *Inorg. Chem.*, 2018, **57**, 2360-2364.
239. P. Soleimani Abhari, B. Habibi and A. Morsali, *Cryst. Growth Des.*, 2024, **24**, 3491-3500.
240. G. Choudhary and H. Hansen, *Chemosphere*, 1998, **37**, 801-843.
241. Z. Wen, Y. Leng, Q. Li, X. Cai, X. Li, Y. Zhang and J. Zhang, *Tetrahedron Lett.*, 2023, **117**, 154371.
242. M. Gutiérrez, Y. Zhang and J.-C. Tan, *Chem. Rev.*, 2022, **122**, 10438-10483.
243. S. Ghosh and S. Biswas, *Microporous Mesoporous Mater.*, 2022, **329**, 111552.
244. S. Fiorucci, E. Antonelli, A. Mencarelli, S. Orlandi, B. Renga, G. Rizzo, E. Distrutti, V. Shah and A. Morelli, *Hepatology*, 2005, **42**, 539-548.
245. S. Nandi, H. Reinsch and S. Biswas, *Microporus Mesoporous Mater.*, 2020, **293**, 109790.
246. S. S. Nagarkar, T. Saha, A. V. Desai, P. Talukdar and S. K. Ghosh, *Sci. Rep.*, 2014, **4**, 7053-7058.
247. S. S. Nagarkar, A. V. Desai and S. K. Ghosh, *Chem. Eur. J.*, 2015, **21**, 9994-9997.
248. A. Buragohain and S. Biswas, *CrystEngComm*, 2016, **18**, 4374-4381.
249. W. Kim, N. Terada, T. Nomura, R. Takahashi, S. Lee, J. Park and A. Konno, *Clin. Exp. Allergy*, 2002, **32**, 287-295.
250. Y. Yu, X.-M. Zhang, J.-P. Ma, Q.-K. Liu, P. Wang and Y.-B. Dong, *Chem. Commun.*, 2014, **50**, 1444-1446.

251. H. Zhao, X. Li, W. Li, P. Wang, S. Chen and X. Quan, *RSC Adv.*, 2014, **4**, 36444-36450.
252. K. Vellingiri, A. Deep, K.-H. Kim, D. W. Boukhvalov, P. Kumar and Q. Yao, *Sens. Actuators B*, 2017, **241**, 938-948.
253. A. Karmakar, N. Kumar, P. Samanta, A. V. Desai and S. K. Ghosh, *Chem. Eur. J.*, 2016, **22**, 864-868.
254. A. Karmakar, B. Joarder, A. Mallick, P. Samanta, A. V. Desai, S. Basu and S. K. Ghosh, *Chem. Commun.*, 2017, **53**, 1253-1256.
255. A. Das and S. Biswas, *Sens. Actuators B.*, 2017, **250**, 121-131.
256. R. Dalapati, S. Nandi, H. Reinsch, B. K. Bhunia, B. B. Mandal, N. Stock and S. Biswas, *CrystEngComm*, 2018, **20**, 4194-4201.
257. H. Xu, Y. Xiao, X. Rao, Z. Dou, W. Li, Y. Cui, Z. Wang and G. Qian, *J. Alloys Compd.*, 2011, **509**, 2552-2554.
258. D. Zhao, X. Wan, H. Song, L. Hao, Y. Su and Y. Lv, *Sens. Actuators B*, 2014, **197**, 50-57.
259. P.-P. Hu, N. Liu, K.-Y. Wu, L.-Y. Zhai, B.-P. Xie, B. Sun, W.-J. Duan, W.-H. Zhang and J.-X. Chen, *Inorg. Chem.*, 2018, **57**, 8382–8389.
260. P. Samant, A. V. Desai, S. Sharma, P. Chandra and S. K. Ghosh, *Inorg. Chem.*, 2018, **57**, 2360−2364.
261. T. Xia, T. Song, G. Zhang, Y. Cui, Y. Yang, Z. Wang and G. Qian, *Chem. Eur. J.*, 2016, **22**, 18429-18434.
262. X.-Y. Xu and B. Yan, *J. Mater. Chem. C*, 2016, **4**, 1543-1549.
263. N.-H. Huang, R.-T. Li, C. Fan, K.-Y. Wu, Z. Zhang and J.-X. Chen, *J. Inorg. Biochem.*, 2019, **197**, 110690-110697.
264. A. Radwan, I. M. E. -Sewify, A. Shahat, H. M. E. Azzazy, M. M. H. Khalil and M. F. E. -Shahat, *ACS Sustainable Chem. Eng.*, 2020, **8**, 15097–15107.
265. N.-H. Huang, Y. Liu, R.-T. Li, J. Chen, P.-P. Hu, D. J. Young, J.-X. Chen and W.-H. Zhang, *Analyst*, 2020, **145**, 2779-2788.
266. P. Wu, Y. Liu, Y. Liu, J. Wang, Y. Li, W. Liu and J. Wang, *Inorg. Chem.*, 2015, **54**, 11046−11048.
267. A. Rana and S. Biswas, *Inorg. Chem. Front.*, 2023, **10**, 2742-2753.
268. S. Nandi, S. Mostakim and S. Biswas, *Dalton Trans.* , 2020, **49**, 12565-12573.
269. S. Mostakim, M. R. U. Z. Khan, A. Das, S. Nandi, V. Trivedi and S. Biswas, *Dalton Trans.*, 2019, **48**, 12615-12621.
270. M. F. Ahmad, F. A. Ahmad, A. A. Alsayegh, M. Zeyaullah, A. M. AlShahrani, K. Muzammil, A. A. Saati, S. Wahab, E. Y. Elbendary and N. Kambal, *Heliyon*, 2024.
271. R. Yousefi, S. Asgari, A. B. Dehkordi, G. M. Ziarani, A. Badiei, F. Mohajer, R. S. Varma and S. Iravani, *Environ. Res.*, 2023, **226**, 115664.
272. A. Li, Q. Chu, H. Zhou, Z. Yang, B. Liu and J. Zhang, *Inorg. Chem. Front.*, 2021, **8**, 2341-2348.
273. J. Liu, W. H. Xiong, L. Y. Ye, W. S. Zhang and H. Yang, *J. Agric. Food Chem.*, 2020, **68**, 5572-5578.
274. A. Rana, N. U. D. Mir, A. Banik, A. Hazra and S. Biswas, *J. Mater. Chem. C.*, 2024, **12**, 1030-1039.
275. J. Mehta, S. Dhaka, A. K. Paul, S. Dayananda and A. Deep, *Environ. Res.*, 2019, **174**, 46-53.
276. L. Yang, Y.-L. Liu, C.-G. Liu, F. Ye and Y. Fu, *Inorg. Chem. Commun.*, 2020, **122**, 108272.
277. X. Xu, Y. Guo, X. Wang, W. Li, P. Qi, Z. Wang, X. Wang, S. Gunasekaran and Q. Wang, *Sensor. Actuator. B Chem.*, 2018, **260**, 339-345.

278. L. Wang, K. He, H. Quan, X. Wang, Q. Wang and X. Xu, *Microchem. J.*, 2020, **153**, 104441.
279. X.-Q. Wang, D.-D. Feng, J. Tang, Y.-D. Zhao, J. Li, J. Yang, C. K. Kim and F. Su, *Dalton Trans.*, 2019, **48**, 16776-16785.
280. X.-Y. Guo, Z.-P. Dong, F. Zhao, Z.-L. Liu and Y.-Q. Wang, *New J. Chem.*, 2019, **43**, 2353-2361.
281. L. Di, Z. Xia, J. Li, Z. Geng, C. Li, Y. Xing and Z. Yang, *RSC adv.*, 2019, **9**, 38469-38476.
282. T. Wiwasuku, J. Boonmak, R. Burakham, S. Hadsadee, S. Jungsuttiwong, S. Bureekaew, V. Promarak and S. Youngme, *Inorg. Chem. Front.*, 2021, **8**, 977-988.
283. H. Eskandari, M. Amirzehni, J. Hassanzadeh and B. Vahid, *Microchim. Acta*, 2020, **187**, 1-10.
284. L. Yang, Y.-L. Liu, C.-G. Liu, F. Ye and Y. Fu, *J. Hazard. Mater.*, 2020, **381**, 120966.
285. Z. Wei, D. Chen, Z. Guo, P. Jia and H. Xing, *Inorg. Chem.*, 2020, **59**, 5386-5393.
286. S. Saadat, D. Rawtani and C. M. Hussain, *Sci. Total Environ.*, 2020, **728**, 138870.
287. H.-B. Zhu, Y. Shen, Z.-Z. Fu, Y.-Y. Yu, Y.-F. Jiang and Y. Zhao, *Inorg. Chem. Commun.*, 2019, **103**, 21-24.
288. X. Z. Wang, Y. F. Shi, Y. P. Jiang, Y. Y. Liu, J. Z. Huo, L. Fei, J. LaCoste, X. R. Wang and B. Ding, *Sens. Actuators B: Chem.*, 2021, **344**, 130199.
289. Y. Ma, Z. Zhao, M. Zhu, Y. Zhang, M. Kosinova, V. P. Fedin, S. Wu and E. Gao, *Polyhedron*, 2022, **220**, 115803.
290. X.-Y. Xu and B. Yan, *Sens. Actuators B Chem.*, 2016, **230**, 463-469.
291. Y. Zhang, X. Xu and B. Yan, *J. Mater. Chem. C.*, 2022, **10**, 3576-3584.
292. W. Liu, X. Qu, C. Zhu, Y. Gao, C. Mao, J. Song and H. Niu, *Microchim. Acta*, 2020, **187**, 1-12.

Superhydrophobic Self-Cleaning Composite of a Metal–Organic Framework with Polypropylene Fabric for Efficient Removal of Oils from Oil–Water Mixtures and Emulsions

This chapter represents the synthesis, characterization and application of -CF_3 group functionalized hydrophobic MOF (**1**), [**1**: $Hf_6O_4(OH)_4(L^1)_6]\cdot 6H_2O\cdot 2DMF$ MOF, H_2L^1 = 1-(2,2,2-trifluoroacetamido)naphthalene-3,7-dicarboxylate), which possesses excellent chemical and thermal stability along with the remarkable hydrophobic character. The activated MOF (**1'**) was used for the *in-situ* coating on the polypropylene (PP) fabric to make a superhydrophobic **1'@PP** fabric composite. The immobilization of nanocrystalline particles of **1'** creates a nanoscale hierarchy that enhances the hydrophobicity of the material (nanoscale hierarchy: smoothness of surface in nanoscale). The superhydrophobic **1'@PP** composite showed a water contact angle (WCA) of 160°. The successful integration of MOF compound with PP fabric was confirmed using field emission scanning electron microscopy (FE-SEM), Powder X-ray diffraction spectroscopy (PXRD), Fourier transform infrared spectroscopy (FT-IR) and electron dispersive X-ray analysis (EDX) experiments. Superhydrophobic **1'@PP** displayed high separation efficiency (95-99 %) for separating light, heavy and crude oils from oil-water mixtures. The flux for oil-water separation was found to be 13-18 k $Lm^{-2}h^{-1}$. Importantly, **1'@PP** composite can be used repetitively up to a minimum of 20 times for oil-water separation. The recyclability was also maintained in high acidic and alkaline medium. Moreover, superhydrophobic **1'@PP** showed excellent oil absorption capacity (29-39 g/g) for heavy and light oils at ambient temperature. A gravity-driven active-filtration process and separation against the gravity process were also performed to examine the flexibility of the composite for separation. We demonstrate that **1'@PP** composite has the merit of very high separation efficiency, absorption capacity, good recyclability and exceptional robustness, showing high potential for versatile oil-water separation. Additionally, the material displayed noticeable self-cleaning and antifouling properties. The **1'@PP** composite also exhibited good efficiency (95-99%) and flux (1845-1899 $Lm^{-2}h^{-1}$) for the separation of water-in-oil emulsions.

ACS APPLIED NANO MATERIALS

Abhijeet Rana, Chiranjib Gogoi, Subhrajyoti Ghosh, Rushikesh Fopase, Lalit M. Pandey and Shyam Biswas

2.1 Introduction

Pollution due to oil-water spills is one of the first-row pollution events for many decades. A large volume of oil is released to the marine system every year due to offshore platforms, and crude oil tankers during transportation and refilling events.[293] In January 1991, during the gulf war, 2 to 4 million barrels of crude oil were dumped into the Persian Gulf, the largest oil spill in history.[294] The water used in oil industries became contaminated with oil that needed pre-treatment or separation of the oil part before releasing it into the environment as described by Saleh et. al.[295-298] Even from the kitchen on an everyday basis, some amount of oil-water emulsion causes contamination of water or soil. The presence of an oil layer on the surface of water inhibits the spontaneous mixing of oxygen to water, causing a decreased level of Dissolved Oxygen (DO) which is a threat to marine ecosystems.[299] Oil spill causes direct death to sea birds as well as badly affects the eggs and habitats, causing a severe threat to their population.[300] According to research reports, more than thirty thousand birds of ninety species have died after the 1989 Exxon Valdez oil spill in Alaska.[301] The bioaccumulative and long-lasting components of crude oil are absorbed into the tissues of aquatic life and thereby cause serious health hazards to aquatic life.[302-304] By taking seafood, the human body indirectly accumulates those oil components and can have serious health issues.[305] Soil contamination causes the unavailability of nutrients to plants and causes their ultimate death.[306] Another example of oil-water separation includes the machine engines, wherein the presence of water in diesel can cause damage to the mechanical part of an engine. Because of that, every diesel engine has an oil-water separator. The above stated severe and long-term effects of oil spills attract environmental scientists to actively participate and bring out a cost-effective, easy solution. Even a small oil spill cleaning requires billions of dollars. The traditional way of cleaning oil spills are in-situ burning and mechanic extraction. Mechanical extraction is not that much efficient and it requires time and energy.[307] In-situ burning causes serious air pollution.[308] Scientific community is in a search of cost-effective, eco-friendly and less time consuming solution to settle this significant environmental issues as described by Saleh et al.[309-311]

In a marine oil spill, the medium is water. Thus, separating oil from a larger amount of water is a less time-consuming and easy task with superhydrophobic materials over superhydrophilic materials to separate a large amount of water from less amount of oil.[312] Water contact angle measurement is usually used to characterize superhydrophobic materials. The static water contact angle of a superhydrophobic material should be above 150°. Low surface energy and rough surface nanoscale hierarchy of feathers of birds and lotus leave inspired us to synthesize a nanoscale superhydrophobic metal-organic framework (MOF) for oil-water separation.[313] The absorbent of oil, like polymers did not have any nanoscale hierarchy because of which these materials could not achieve the Cassie-Baxter state. In contrast, the MOF on the surface of composite can bring the Cassie-Baxter state and the hydrophobicity can be achieved due to the presence of fluorine atoms on the organic backbone of MOF. The hydrophilic absorbents used for the separation of oil-water mixtures are not suitable in case of marine system and they have drawbacks for real field application as they will also absorb the water.[314-315]

MOFs are a new class of highly porous organic-inorganic composite materials known for their versatile application in the field of sensing, drug delivery, catalysis, gas adsorption, separation, etc.[316-321] The interesting chemical and physical properties of MOF materials are variable pore size, large surface area, chemical stability in a wide range of pH and solvents, high thermal stability, etc.[322-324] The gas adsorption and separation is one of the unique applications of MOFs due to their highly porous nature as well as variability in pore size, which can be achieved by fine tuning of structures.[325] Like gas adsorption/separation, MOF materials can also be used for the separation of a mixture of liquids, particularly a mixture of oil and water.[326] For oil-

water separation, a material with low surface energy (i.e., less surface wettability and hydrophobic nature) is highly favourable. As reported by Rabalo et al., the replacement of a -CH_3 group by a -CF_3 group leads to a great increase in hydration energy which makes the modified material hydrophobic in comparison to the unmodified one.[327] Other reported fluorinated materials and few MOF materials with fluorinated functionality, including one from our group inspired us to develop a hydrophobic MOF for oil-water separation purposes.[328-331]

MOFs are polycrystalline powders. Therefore, the application of a MOF for oil-water separation is not possible without binding it with a substrate. In this regard, a cotton composite of MOF was prepared in a previous study by our group.[328] Cellulose, being the primary building unit of cotton, provides enormous free -OH groups on the surface of cotton to bind the MOF nanoparticles and gives rise to a highly superhydrophobic surface with a hierarchical nanoscale structure suitable for oil-water separation. Here, we chose 2 × 2 cm^2 sized polypropylene (PP) fabric (obtained from an N95 mask) as support to anchor MOF nanocrystals. Herein, a dicarboxylic acid linker functionalized with a trifluoroacetamido group was used as the hydrophobic linker. The pre-functionalized hydrophobic linker and Hf-metal salt underwent a single-step solvothermal reaction. The resulting powder Hf-MOF compound (**1**) showed excellent chemical and thermal stability and also exhibited hydrophobic in nature (water contact angle of 131°). The coating of PP fabric with the MOF in a single-step in-situ procedure resulted in a composite named as **1'@PP**. This single-step procedure is advantageous over the recently developed composites for oil-water separation by Lin et. al. and Maity et. al., which require multiple steps and tedious processes.[332-333] **1'@PP** was examined for separation of both lights floating oil and heavy sedimentary oils from water. The separation efficiency, absorption capacity and stability after repeated experiments of oil-water separation of the developed **1'@PP** composite were investigated. Because of single-step easy preparation, zero energy consumption during separation and eco-friendly separation process (that is not causing any pollution in the separation step), the composite can be used for an industrial scale oil-water separation.

Furthermore, the self-cleaning property of the composite was also investigated. In nature, there are many plants and animals which possess hydrophobic properties like lotus leave, pitcher plant, butterfly wings, shark skin and gecko feet. The hydrophobic nature helps them to maintain hygiene and cleanness even in a dirty environment.[334] The hydrophobic nature inhibits the growth of fungus and bacteria on them. The above phenomena inspired us to investigate the self-cleaning and antifouling nature of our material.

The material was also utilized for the separation of oil from water-in-oil emulsion. The formation of emulsion due to the presence of a small amount of water in a large amount of oil causes surface corrosion of oil pipes. The presence of water also causes high pressure in oil pipes used for the transportation of oils. The above-mentioned problems could be overcome by separating the water part from the oil. The flux for emulsion separation for **1'@PP** was found to be between 1845 and 1899 $Lm^{-2}h^{-1}$, which is comparable with the previously reported literature.[335]

2.1.1 Reasons Behind Selective Oil-Water Separation

The **1'@PP** has embedded nanocrystalline **1'** particles on the PP fibres which provided nano hierarchy to the material. The presence of fluorine atoms in the organic backbone of **1'** converted the standard PP fabric into a low surface energy material. Both the hydrophobicity and nano hierarchy on **1'@PP** led to selective separation of oil.[336] As shown in Figure 2.21, the water droplet remained on the surface due to the formation of air pockets between the surface

nanostructure and the water droplet, whereas the low surface energy of the **1'@PP** attracts the oil droplets to pass through the material.

2.2 Experimental Section

2.2.1 Synthesis of H_2L^1 Linker

The characterization of the ligand was carried out by mass spectrometry, ^{1}H NMR, ^{13}C NMR and ^{19}F NMR spectroscopy. The ^{1}H NMR spectrum (Figure 2.1) confirmed the presence of six types of protons in H_2L^1 ligand. The naphthalene moiety contains five types of protons, and one proton is present in the nitrogen atom of acetamido functionality. The chemical shift values are observed at 11.79 (s, ^{1}H, -NH), 8.70 (s, ^{1}H, Ar-H), 8.12 (d, ^{1}H, Ar-H), 8.33 (d, ^{1}H, Ar-H), 8.58 (s, ^{1}H, Ar-H) and 8.10 (s, ^{1}H, Ar-H) ppm, respectively. Since there are no additional protons in the ^{1}H NMR spectrum, the formation of by-products is ruled out. The ^{13}C NMR spectrum (Figure 2.2) revealed that there are fourteen types of carbon atoms present in the ligand. The observed chemical shift values are 115.13, 117.99, 124.37, 125.32, 126.90, 130.36, 130.95, 131.07, 132.77, 135.47, 156.48, 156.85, 166.98 and 167.42 ppm. The ^{19}F NMR spectrum (Figure 2.3) showed an intense peak at -73.70 ppm due to the same type of fluorine atoms present in trifluoroacetamido moiety. In the mass spectrum of the ligand (Figure 2.4), the most intense peak was found at m/z = 326.004 (measured in negative ion mode), which corresponds to (M-H)- ion (M is the mass of H_2NDC-NHCOCF3 ligand). The theoretically calculated mass of the ligand is 327.22 g mol^{-1}. Therefore, it can be concluded that the desired H_2L^1 ligand has been synthesized.

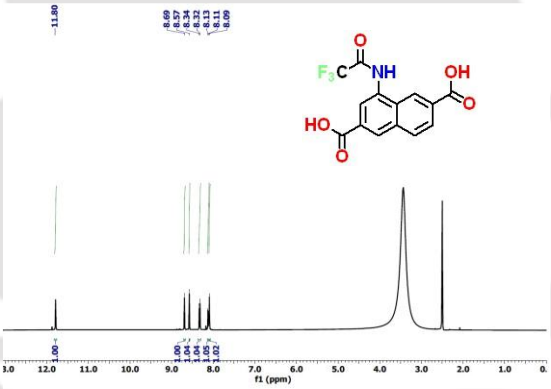

Figure 2.1 ^{1}H NMR spectrum of H_2L^1 ligand measured in DMSO-d_6.

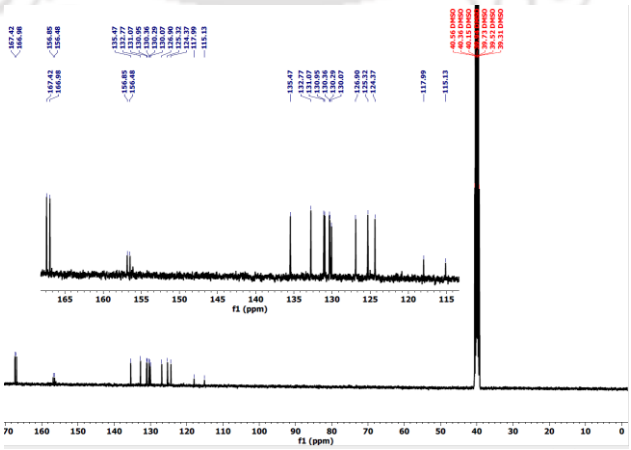

Figure 2.2 ^{13}C NMR spectrum of H_2L^1 ligand measured in DMSO-d_6.

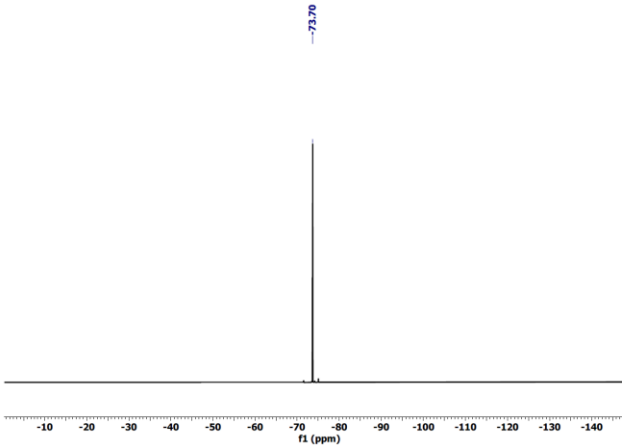

Figure 2.3 ^{19}F NMR spectrum of H_2L^1 ligand measured in DMSO-d_6.

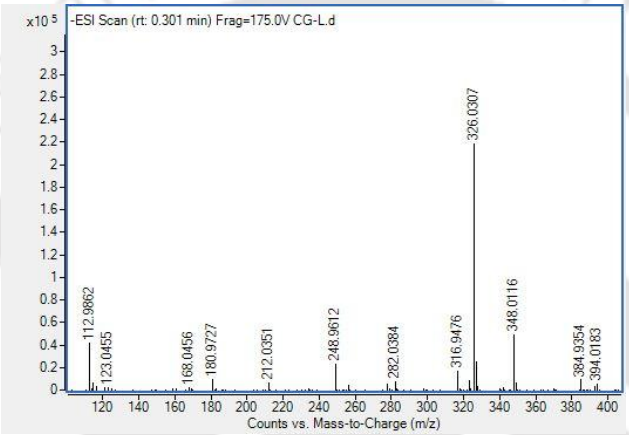

Figure 2.4 HR-MS spectrum of H_2L^1 ligand measured in methanol.

2.2.2 Preparation of $[Hf_6O_4(OH)_4(L^1)_6]\cdot 6H_2O\cdot 2DMF$ (1)

Solvothermal synthesis of **1** was executed by taking hafnium tetrachloride ($HfCl_4$) (0.02 g, 0.06 mmol) and H_2L^1 (H_2L^1 = 1-(2,2,2-trifluoroacetamido)naphthalene-3,7-dicarboxylic acid) linker (0.02 g, 0.06 mmol) in 1:1 molar ratio in a sealed glass tube containing 30 equivalents (0.22 g) of benzoic acid as modulator with respect to the metal salt and 3 mL of *N,N*-dimethyl formamide (DMF). The molar ratio between modulator benzoic acid and metal salt was 30:1 during the solvothermal synthesis, where DMF was chosen as the medium to carry out the reaction. The above-mentioned sealed glass tube was sonicated for 0.5 h and placed in a preheated block heater at 120 °C for 24 h to get good crystallinity and yield of the product. The obtained material after 24 h was brought to room temperature slowly and washed several times with acetone. After drying in an oven for 12 h at 65 °C, the crystalline material was obtained with a yield of 0.026 g (0.01 mmol, 76 %) with respect to the metal salt. The obtained product was named **1**. FT-IR (KBr, cm^{-1}): 3246 (br), 1726 (s), 1650 (w), 1627 (sh), 1590 (sh), 1425 (vs), 1161 (s), 935 (w), 787 (s), 677 (s), 450 (s).

2.2.3 Activation of 1

During synthesis, DMF (used as a solvent) was absorbed in the pores of **1**. The DMF molecules need to be removed before further characterization. To eliminate the absorbed DMF molecules from **1**, 150 mg of **1** was taken in a round bottom flask having 30 mL of methanol and the mixture was stirred at 400 rpm for 18 h. The process was carried out in order to replace the high boiling point DMF by a low boiling point solvent, i.e., methanol. Then, the mixture was

filtered and kept in a vacuum for 24 h at 120 °C. The obtained activated material after performing above mentioned processes was referred as **1'**.

2.2.4 In-Situ Synthesis of 1'@PP Composite

A PP fabric sheet from a N95 surgical respirator was cut into small squares of (2 × 2) cm^2 area (Figure 2.14) and the pieces were taken in a beaker containing acetone. The small squares of PP fabric in acetone were sonicated for 0.5 h in order to remove any absorbed unwanted substance and dried in an oven at 60 °C. In order to prepare hydrophobic MOF-PP composite, four pieces of previously cleaned PP fabric were taken in a 40 mL Teflon lined autoclave containing a combination of 0.1 g of $HfCl_4$ and 0.1 g of H_2TFNDC linker in a 1:1 molar ratio. 30 mL of DMF and 1.1 g of benzoic acid modulator were added to the same autoclave and put at 120 °C in an oven (Scheme 1). After a day, the obtained **1'@PP** composite was brought to room temperature and washed properly using acetone and dried in an oven at 70 °C. During in-situ synthesis, the **1'** particles are strongly adsorbed on the surface of PP fibers to give a robust superhydrophobic composite. The dried composite was stirred in methanol in order to remove DMF and excess amount of MOF. The dried composite was used for further characterization and application. The obtained superhydrophobic **1'@PP** was stored in an air atmosphere for further use. The prepared composite was named **1'@PP**.

Scheme 2.1. Scheme for the single-step in-situ synthesis of **1'@PP** in a solvothermal process.

The percentage of loading of **1'** on PP fabric was estimated using the following equation: percentage of loading = $(W_2\text{-}W_1)/W_1$ where, W_1 and W_2 are the oven-dry weights of PP fabric and **1'** composite, respectively.

2.2.5 Absorption Capacities for Various Oils By 1'@PP Fabric Composite

For the oil absorption test, fully dry pre-weighed (~20 mg) **1'@PP** fabric composite was placed in various heavy oils (dichloromethane, chloroform and carbon tetrachloride) and light oils (ethyl acetate, toluene, hexane, motor oil and kerosene) for 1 min to reach absorption equilibrium and then removed and weighed. All the experiments were performed at room temperature and the absorption capacity was measured using the following equation.

Absorption capacity (wt%) = $(W_2\text{-}W_1)/W_1 \times 100\%$

Absorption capacity (g/g) = $(W_2\text{-}W_1)/W_1$, where, W_1 is the weight of native **1'@PP** and W_2 is the weight of oil-absorbed **1'@PP**. At least five measurements were carried out for each oil sample and average value was plotted.

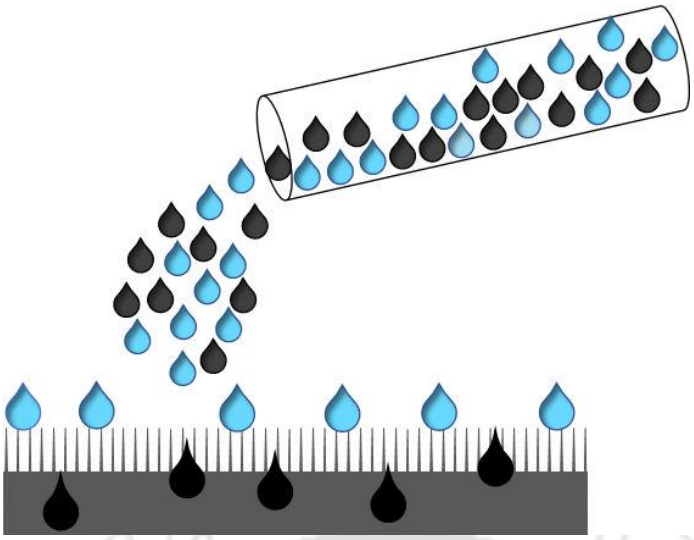

Figure 2.5 Schematic representation of Cassie-Baxter state of a water droplet on the nanoscale hierarchical surface of **1'@PP** allowing selective separation of oil (water droplets: blue, oil droplets: black).

2.3 Results and Discussion

2.3.1 FE-SEM and EDX Analysis

Homogeneous octahedral nanocrystals were obtained after completion of the reaction as shown in FE-SEM image (Figure 2.5). The uniform sized crystalline particles, as shown in the FE-SEM images, confirmed that the material is free from impurities.[337] The EDX spectrum (Figure 2.6a) and EDX elemental mapping (Figure 2.6b) data revealed the presence of Hf, C, O, N and F atoms in **1**. The presence of only the desired elements is another evidence for the purity of the synthesized material.

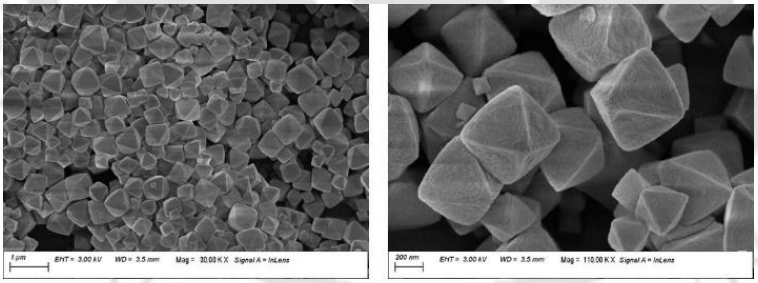

Figure 2.5. The FE-SEM images of **1'** displaying its nanoscale octahedral structure.

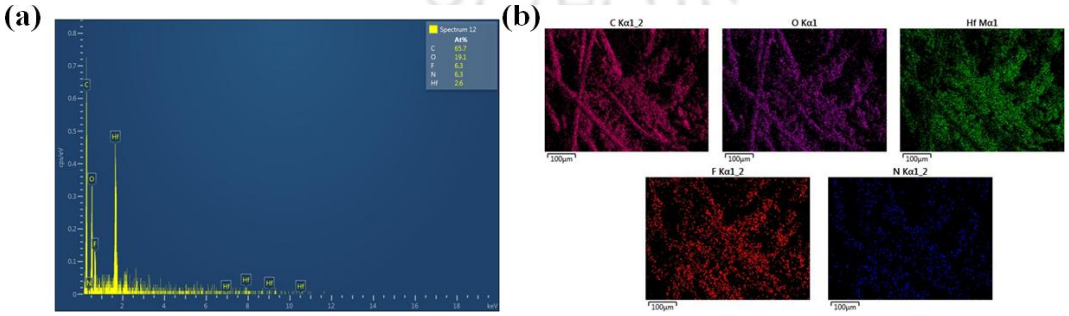

Fig. 2.6. (a) EDX spectrum of **1'** showing the distribution of the desired elements in atomic percentage and (b) EDX elemental mapping.

2.3.2 PXRD Analysis of 1

To investigate the phase purity and structural resemblance of 1 with the parent DUT-52 MOF, PXRD analysis was carried out. The obtained result showed almost the same PXRD pattern of the presented material with parent DUT-52 MOF material (Figure 2.7). The Pawley refinement was carried out, which showed **1** has almost exact peak patterns with the parent DUT-52 (Figure 2.7b). Additionally, the lattice parameters of our as-synthesized material were determined by indexing the slow-scan PXRD data of **1**. The obtained (h, k, l) values of important peaks are shown above the respective peaks in Figure 2.7a.[338] The obtained results highly support that the synthesized MOF material possesses DUT-52 structure (Table 1).

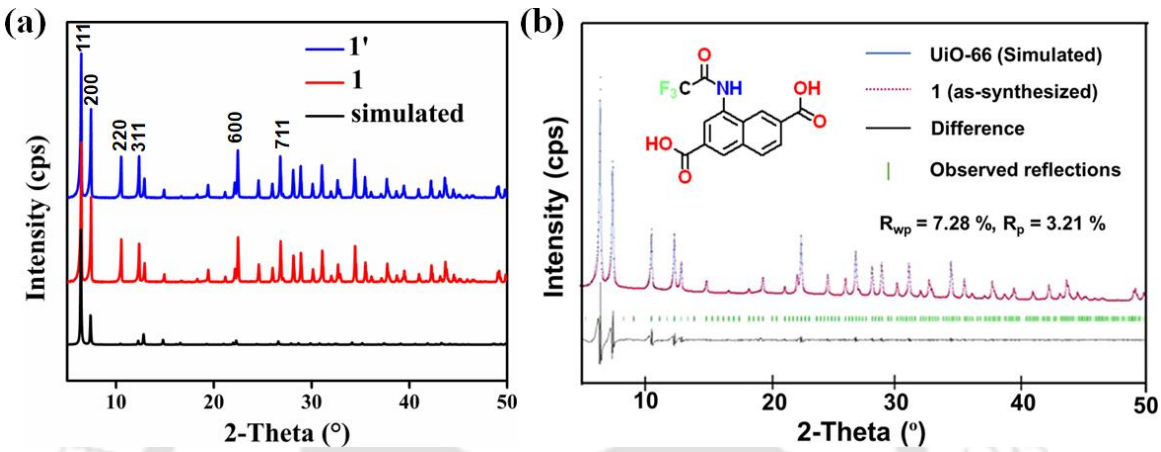

Figure 2.7 (a) PXRD patterns of DUT-52 simulated, as-synthesized MOF (**1**) and activated MOF (**1′**). (b) Pawley fit for the PXRD pattern of as-synthesized **1** (R_p = 7.28, R_{wp} = 3.81). Structure of H_2L^1 ligand is shown in inset of (b).

Table 2.1 Unit cell parameters of **1'** obtained by indexing its PXRD data. The obtained values have been compared with parent DUT-52 MOF.

Compound Name	**1'**	DUT-52
Crystal System	cubic	cubic
a = b = c (Å)	23.675(23)	23.910(3)
V (Å3)	13269(22)	13669(9)

2.3.3 ATR-IR Analysis

The FT-IR spectra of **1** and **1'** were measured in order to confirm the presence of functionality. The sharp peak at 1726 cm^{-1} in **1** and **1'** was attributed to the carbonyl group of trifluoroacetamido functionality (Figure 2.8), which confirmed that the trifluoroacetamido functionality was intact in the organic backbone after the synthesis of MOF.[339-341] The asymmetric and symmetric stretching frequencies of Hf bound carboxylate were present at 1590 and 1425 cm^{-1}, respectively. The position of carboxyl peak at lower frequency region was due to the coordination between the carboxylate and metal centre, which confirmed the formation of MOF. The peak at 1175 cm^{-1} was because of the C-F bond stretching frequency. The peak at 1656 cm^{-1} only for **1** was due to the carbonyl group of DMF molecules absorbed in the pores of MOF material. The absence of this particular peak in the activated MOF material confirmed the elimination of DMF from **1**.[342]

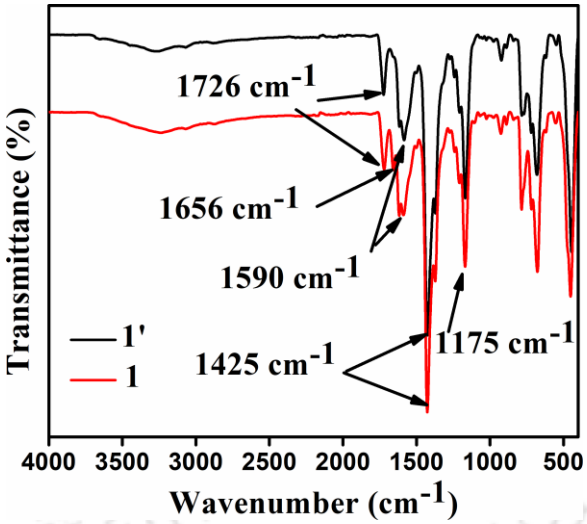

Figure 2.8 ATR-IR spectra of as-synthesized MOF (**1**) in red and activated MOF (**1′**) in black.

2.3.4 Thermal Stability Analysis

Thermogravimetric analysis (TGA) was conducted from 25-700 °C in an air atmosphere at a heating rate of 10 °C per min to know the behaviour of the prepared material at a high temperature (Figure 2.9). There was an initial weight loss of 3.1% from 25-120 °C due to the removal of six molecules of H_2O per unit formula (cal. 3.2%). The next loss of weight 4.7% occurred from 120-310 °C owing to the removal of two DMF molecules per unit formula of **1** (cal. 4.5%). The final weight loss after 310 °C was due to the decomposition of linkers from the MOF material. From the obtained results from TGA data, we can conclude that **1** and **1'** are stable nearly up to 310 °C.

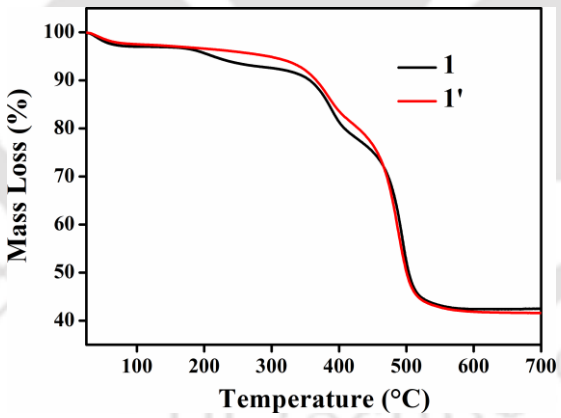

Figure 2.9 Thermogravimetric analysis curve of **1** (black) and activated MOF **1′** (red).

2.3.5 Structure Description

The synthesis of **1** was executed with the help of benzoic acid modulator. Therefore, when benzoic acid was added to a DMF solution of $HfCl_4$, $[Hf_6O_4(OH)_4(C_7H_6O_2)_{12}]$ units were formed. The reaction was carried out for 24 h where TFNDC linkers slowly replaced all the monocarboxylic benzoate anions to give rise to the $[Hf_6O_4(OH)_4(L^1)_6]$ unit. The first report on the synthesis of DUT-52 MOF was by Kaskel *et al.*, where they used naphthalene-2,6-dicarboxylic acid (H_2NDC) linker to prepare both Zr(IV) and Hf(IV) MOFs.[338] In this report, we present a Hf(IV) MOF with trifluoroacetamido functionalized NDC linker. Since the coordination sites and linker type are almost the same, we expect our synthesized MOF to have DUT-52 structure. According to the reported literature, the DUT-52 structure is similar to UiO-

n series of MOFs. The only difference in both type of structures arises due to the straight linker in the case of UiO-n series whereas the NDC linker is slightly twisted in the case of DUT-52. Like UiO-n series of MOFs, the SBUs of DUT-52 are made up by the coordination of six central metal atoms with eight μ_3-OH and μ_3-O sites.[338] The SBU in **1** is $Hf_6O_4(OH)_4$, where Hf(IV) is the central metal atom coordinated with four μ_3-OH and four μ_3-O sites.[343] The $Hf_6O_4(OH)_4$ SBUs are joined to twelve H_2L^1 linkers to give rise to the final $[Hf_6O_4(OH)_4(L^1)_{12}]$ MOF material with DUT-52 structure (Figure 2.10).[344] Similar to UiO-n series of MOFs, there are two types of voids: one type is larger octahedral voids and the other type is smaller tetrahedral voids. Both these two types of voids are linked by triangular windows.[345]

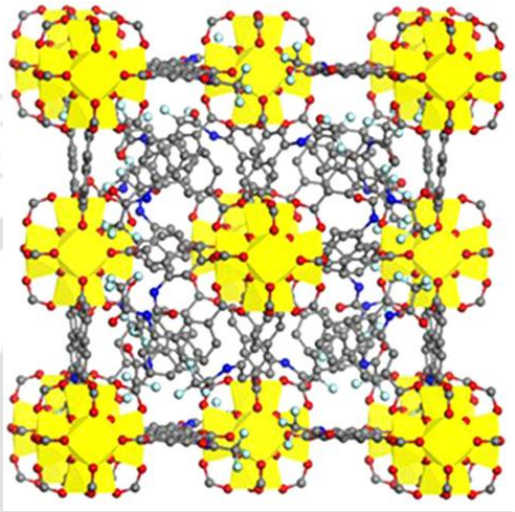

Figure 2.10 Simulated crystal structure of **1** (Hf polyhedron, C, O, N and F are shown in yellow, grey, red, blue respectively.

2.3.6 Surface Area Study

To find the BET surface area and microporous volume, we carried out N_2 gas sorption analysis (Figure 2.11). A type-I N_2 sorption isotherm was found for **1'** and the specific BET surface area and microporous volume were 884 $m^2\ g^{-1}$ and 0.50 $cm^3\ g^{-1}$ at $p/p_0 = 0.5$, respectively. The data revealed that the activated form of the compound was sufficiently porous as other MOF materials for any application.

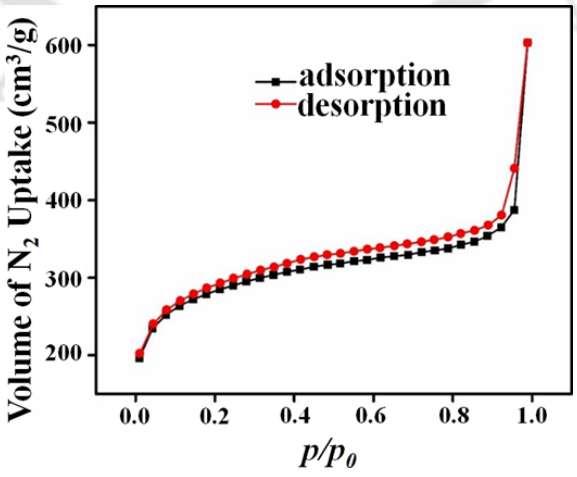

Figure 2.11 Nitrogen adsorption and desorption isotherms of **1'** recorded at –196 °C.

2.3.7 Chemical Stability

We studied the chemical stability of **1'** in different organic solvents like MeOH, EtOH, DMF, acetone, DMA, THF, acetonitrile and water as well as in model oils like hexane, CCl_4, $CHCl_3$, DCM. The obtained PXRD data showed no change in PXRD pattern after treatment with solvents for 24 h (Figure 2.12a). We also examined the chemical stability in a variable range of pH (Figure 2.12b). The PXRD data showed the robustness of **1'** in a wide pH range for real field application. The chemical stability of **1'** in different organic solvents and oils as well as in different pH systems was sufficient enough for the application of oil-water separation.

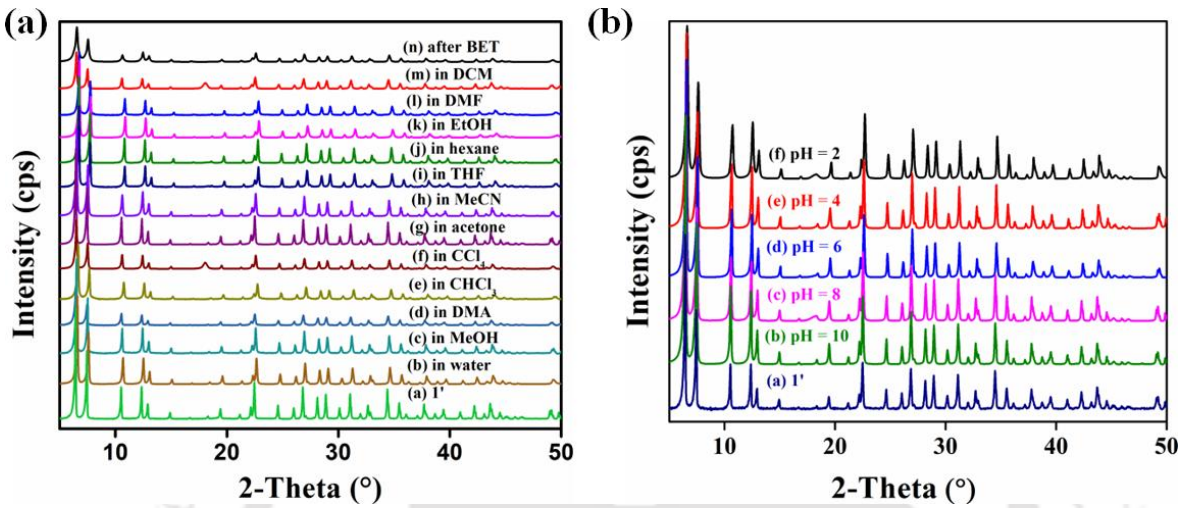

Figure 2.12 PXRD patterns of **1'** before and after stiring various organic solvents (a) and diffrerent pH media (b).

2.3.8 Hydrophobic Nature of 1'

The self-floating ability of **1'** was revealed when the powder sample was put on water. But the powder was immediately immersed when it was placed in hexane (Figure 2.13a). The above property simply demonstrates the hydrophobic property of **1'**. The hydrophobic property of **1'** is expected due to the presence of $-CF_3$ group in the material. To prove the hydrophobic nature of **1'**, we carried out the water contact angle (WCA) measurement. The WCA for **1'** was found to be 131° (Figure 2.13b). The WCA measurement data revealed that **1'** is hydrophobic in nature.[336]

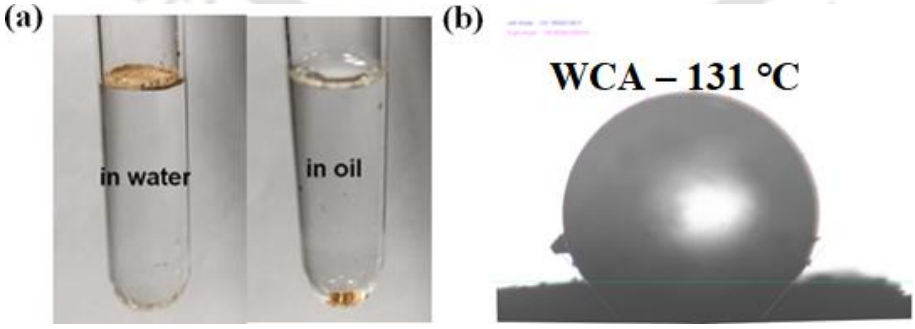

Figure 2.13 (a) Digital image of self-floating ability of **1'** in water and in oil (hexane). (b) Water contact angle image of beaded water droplets on the surface of **1'** powder.

2.3.9 Characterization of Superhydrophobic 1'@PP Composite

The WCA measurement mentioned above revealed that the synthesized MOF, i.e., **1'** is hydrophobic. Hydrophobic materials have many applications like corrosion protection,[346] oil-

water separation,[328] hydrophobic paints, hydrophobic coatings,[347] etc. Among them, oil-water separation is a challenging environmental issue. Thus, inspired from the above facts, we dedicated this work to oil-water separation. Since **1'** was prepared in powder form, it did not have the free-standing ability. Hence, its direct application in oil-water separation is time-consuming and tedious. To overcome this drawback, we prepared a superhydrophobic composite with the help of PP fabric of an N95 mask and **1'**. The immobilisation of **1'** on the surface of PP fabric not only gave a superhydrophobic surface but also provided a rough nanoscale hierarchical surface which was ideal for oil-water separation. As observed from Figure 2.14, the native PP fabric is white in colour. But after surface modification, its colour changed to tan.

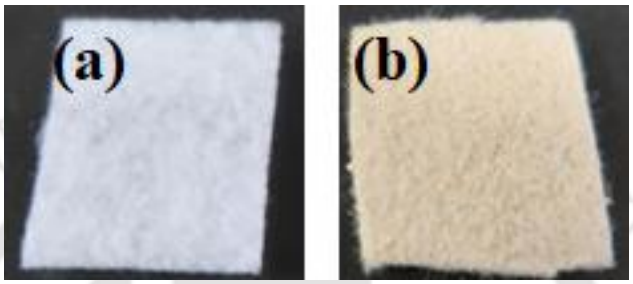

Figure 2.14. Digital images of PP fabric before (a) and after (b) surface modification with **1'**.

The successful integration of MOF compound with PP fabric during in-situ synthesis was firstly confirmed by PXRD analysis. The PXRD patterns of **1'@PP** composite showed good similarity with **1'** (Figure 2.15a). The characteristic peaks of **1'** were absent in untreated PP fabric. Therefore, the combination of peaks of PP fabric and **1'** in **1'@PP** composite indicated the immobilization of **1'** on the surface of PP fabric. Next, the deposition of **1'** on PP fabric was established by FT-IR data (Figure 2.15b). The asymmetric and symmetric stretching frequency of the metal coordinated –COO group appeared at 1590 and 1425 cm^{-1} in **1'@PP** as well as all the peaks of FT-IR spectra of **1'**. The presence of metal coordinated carboxylate group peak and the other desired peaks in FT-IR data confirmed the binding of **1'** to the PP fabric. Thus, looking at the FT-IR spectra of **1'@PP** composite, one can unambiguously confirm the presence of **1'** on the surface of PP fabric. The calculated percentage of loading of **1'** on the fabric surface was found to be 40%.

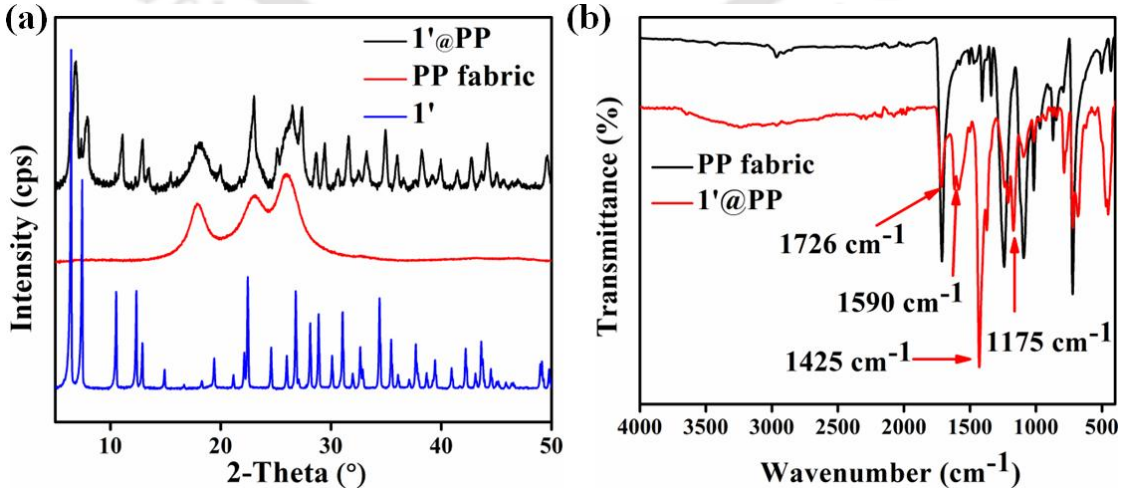

Figure 2.15 (a) PXRD patterns of **1'**, only PP fabric and **1'@PP** fabric. (b) ATR-IR spectra of PP fabric and **1'@PP** fabric composite.

The loading of **1'** onto the surface of PP fabric was again confirmed by EDX spectrum and EDX elemental mapping (Figure 2.16a). The EDX elemental spectrum the PP fabric after surface immobilization with **1'** showed the presence of C, O, N, F and Hf. The obtained results clearly indicated the surface coating of PP fabric by **1'**. Further EDX mapping showed the homogenous distribution of elements on **1'@PP** composite (Figure 2.16b).

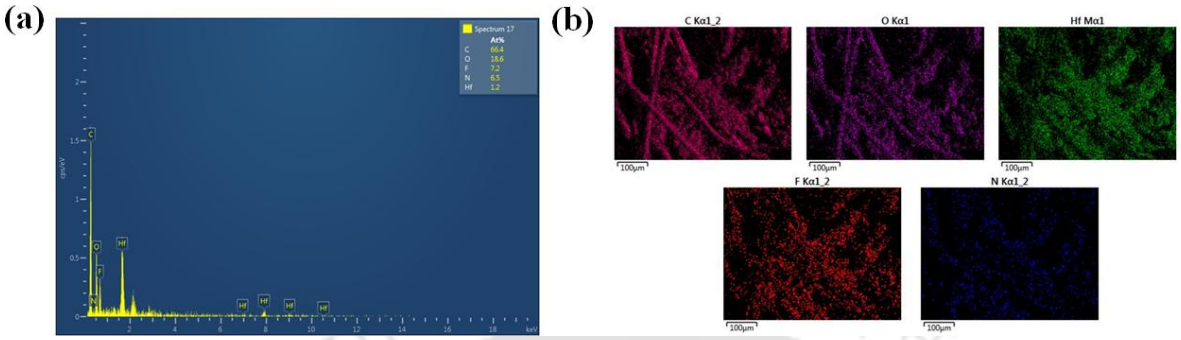

Figure 2.16 (a) EDX spectrum of **1'@PP** fabric composite showing the presence of desired elements in atom%. (b) EDX elemental mapping of **1'@PP** fabric composite showing the homogenous distribution of desired elements (C: pink, O: violet, Hf: green, F: red and N: blue).

The final proof for successful surface immobilization was obtained from FE-SEM images of PP fabric before and after surface modification. The FE-SEM image of PP fabric before surface modification displayed a smooth surface (Figure 2.17). But, after surface modification, the PP fabric exhibited a rough surface with clearly visible octahedral MOF nanocrystals (Figure 2.18).[341, 348-349] This fact demonstrated the surface immobilization of **1'** onto the surface of PP fabric. The appearance of roughness caused the water droplet not to be adsorbed on the surface but rather created a Cassie-Baxter situation. The presence of the Cassie-Baxter state increased the hydrophobicity of the composite after the modifications.

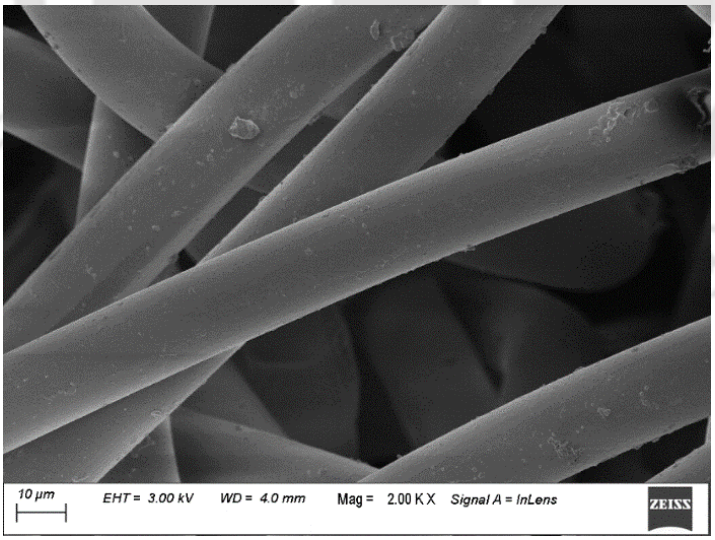

Figure 2.17 High resolution FE-SEM images of PP fabric.

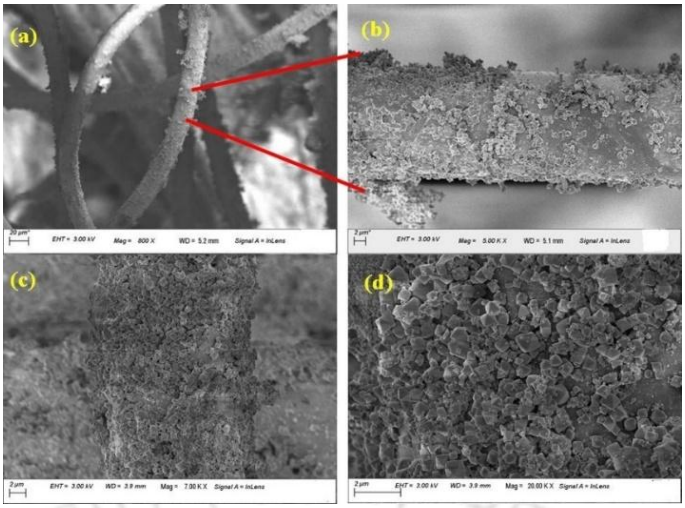

Figure 2.18 (a) High-resolution FE-SEM images of **1'@PP** composite. The magnified images are shown in (b-d) showing the nanoscale hierarchy due to surface immobilization on PP fabric.

In the case of the surface of lotus leaves, the nanoscale architecture generates an ideal situation for the water droplets to roll over the leaves without wetting them. The surface immobilization of the nano-sized particles of **1'** produced nanoscale hierarchical roughness to the PP fabric surface, which is similar to lotus leaves. Therefore, with few MOF materials, a large composite can be fabricated to reach the industrial level of oil-water separation. Additionally, we measured the BET surface area of PP fabric before and after surface modification (Figures 2.19a and 2.19b). The obtained surface area of PP fabric before surface modification was negligible. But, after surface modification, the surface area of PP fabric increased to 257 m^2/g. The substantial increase in specific BET surface area after surface modification supported the fact that a successful surface immobilization of MOF particles onto the surface of PP fabric occurred.

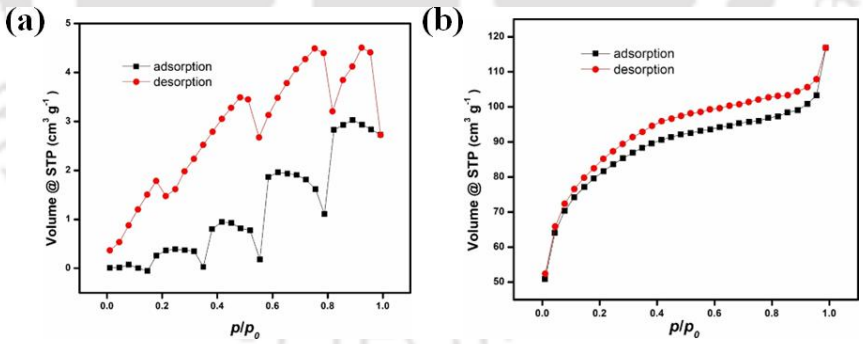

Figure 2.19 (a) Nitrogen adsorption and desorption isotherms of PP fabric. (b) Nitrogen adsorption and desorption isotherms of **1'@PP** fabric recorded at -196 °C.

2.3.10 Superhydrophobic Nature of 1'@PP

The in-situ surface immobilisation of PP fabric was carried out in order to get an effective composite for oil-water separation. Initially, we checked the self-floating property of **1'@PP** in water. As we observe from Figure 2.20a, the pieces of white coloured native PP fabric dip immediately into water but tan coloured **1'@PP** composite floats on the surface of water. If water droplets are put on the native PP fabric surface, they are immediately soaked into the fabric. But, in the case of **1'@PP** composite, the water droplets remain on the surface for longer periods of time (Figure 2.21).

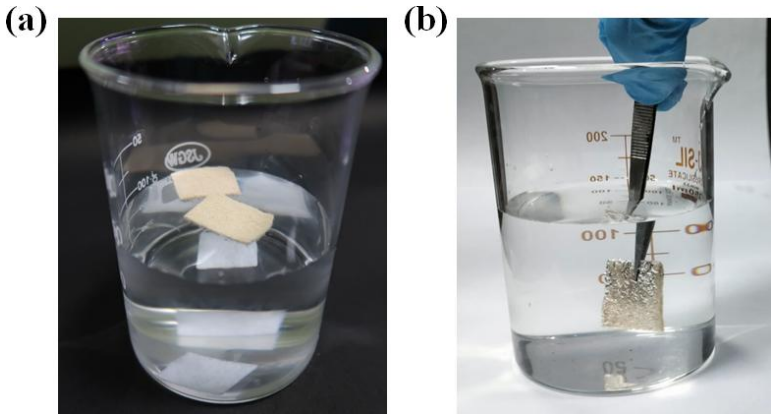

Figure 2.20 (a) Digital images of floating **1'@PP** fabric composite on water and immersion of native PP fabric in water. (b) Digital image of forcefully submerged **1'@PP** fabric composite under water showing the formation of air pocket due to a Cassie-Baxter state.

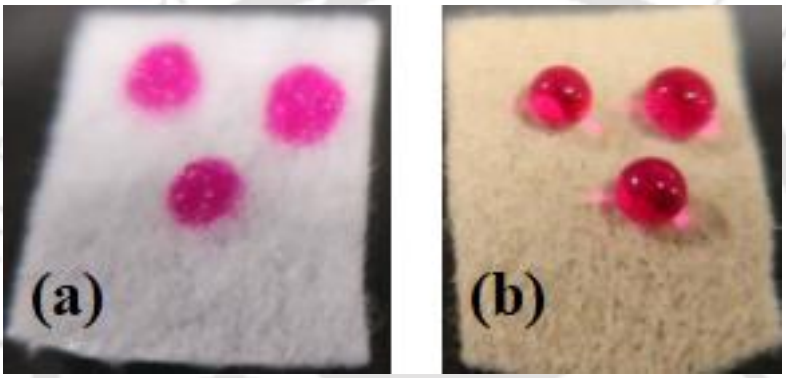

Figure 2.21 (a) Visual images of water droplets (red colour helps visual inspection) suspended on native PP fabric absorbing water droplets. (b) **1'@PP** composite forming Cassie-Baxter state of red water droplets on the surface of superhydrophobic **1'@PP** composite.

Next, we carried out WCA measurement. The WCA measurement was executed at the ambient temperature where, 10 µL of deionized water was beaded with the surface of the composite and the image was captured. The obtained contact angle for native PP fabric was 106° but for **1'@PP** composite, it was 160±1° (Figure 2.22). The PP fabric endowed increased hydrophobicity to **1'@PP** in comparison to only **1**. The increased value of contact angle for **1'@PP** composite as compared to **1'** (WCA = 131°) was due the spatial arrangements of **1'** on the surface of the PP fabric. The hydrophobic **1'** exhibited a superhydrophobic character after combining with the PP fabric. The superhydrophobic nature of **1'@PP** arose due to the presence of hydrophobic MOF particles, which gave a nano roughness to the surface similar to the lotus leaf effect.[350] It was reported that the presence of small hydrophobic epidermis on the surface of lotus leaves creates a nano hierarchal structure on their surface. When the lotus leaves are forcefully immersed into water, one can notice a silver-coloured shining surface which is due to the air pockets created on their surface. The created air pockets decrease the contact area between water and surface of lotus leaves and also decrease the surface energy.[351] Therefore, the adhesion of water on the leaf surface became weak.[352] The superhydrophobic **1'@PP** composite also featured a mirror-like appearance upon forceful immersion into water (Figure 2.20b).

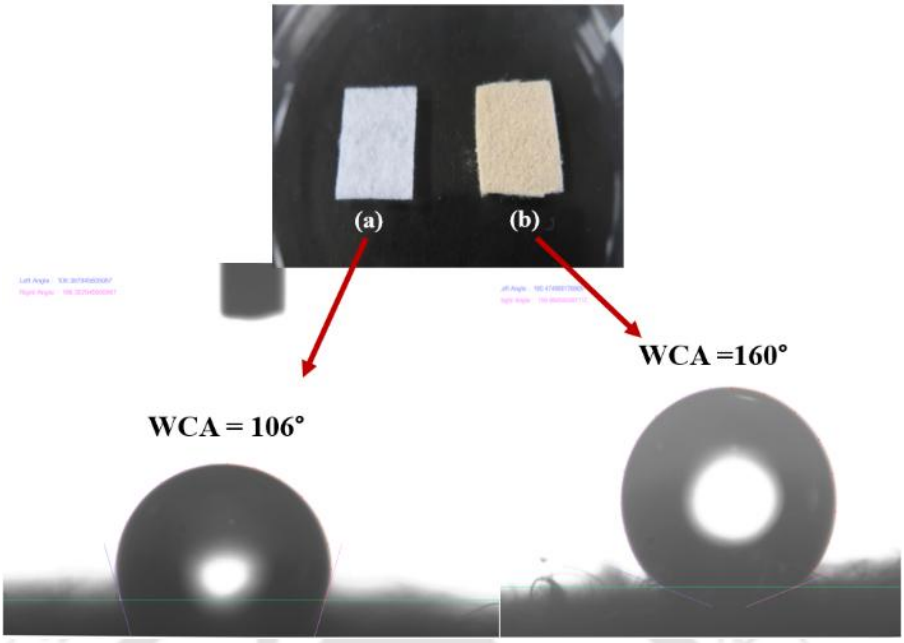

Figure 2.22. WCA value of (a) native PP fabric and (b) **1'@PP** composite showing the increased hydrophobicity of **1'@PP** with respect to native PP fabric due to immobilization of **1'** onto PP fabric.

2.3.11 Durability of 1'@PP in Different Water and Oil Samples

The native PP fabric is little hydrophobic. But, after surface modification, **1'@PP** became extremely water repellent. To check the durability of **1'@PP** in different types of water specimens, we forcefully kept the composite inside different types of water samples like artificial sea water, lake water, river water, cold water and hot water. After 30 min, the composite was taken out of the medium and WCA measurement was carried out. As notice from Figure 2.23, the WCA remained almost the same for all water specimens. These experiments showed that composite retained its superhydrophobicity in different types of water environments.

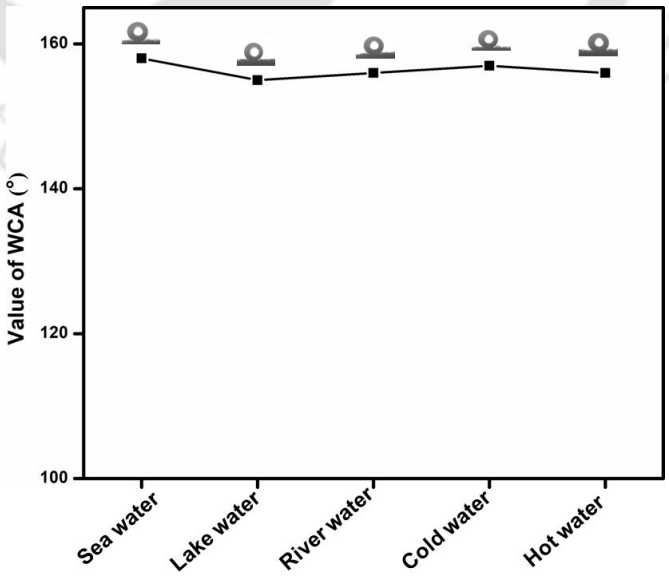

Fig. 2.23 Water Contact angle (WCA) of **1'@PP** fabric after treatment with different types of water specimens.

Again, for the application purpose the composite should be stable and durable enough. The samples of **1'@PP** composite were stirred in different oils and pH solutions like dichloromethane, chloroform, carbon tetrachloride, ethyl acetate, hexane, toluene, kerosene, petrol, diesel, pH 2 and pH 12 solutions for 1 day. Afterward, it was recovered and PXRD measurements were performed. Similar PXRD patterns of the composite were obtained before and after the stability experiments (Figure 23a and 23b). The mass of all the composite samples before and after stirring were measured. There were negligible mass changes for the composite samples, which confirmed that the **1'** MOF particles did not come out from the **1'@PP** composite during the stirring experiments. The WCA and FT-IR experiments were also performed, which showed similar properties with the as-prepared **1'@PP** composite (Figures 24a-b and Table 2.2). The above results showed that the material was stable enough in various chemical environments. The stability of the composite was checked in a simulated seawater sample in order to be suitable to tackle marine oil spillage.

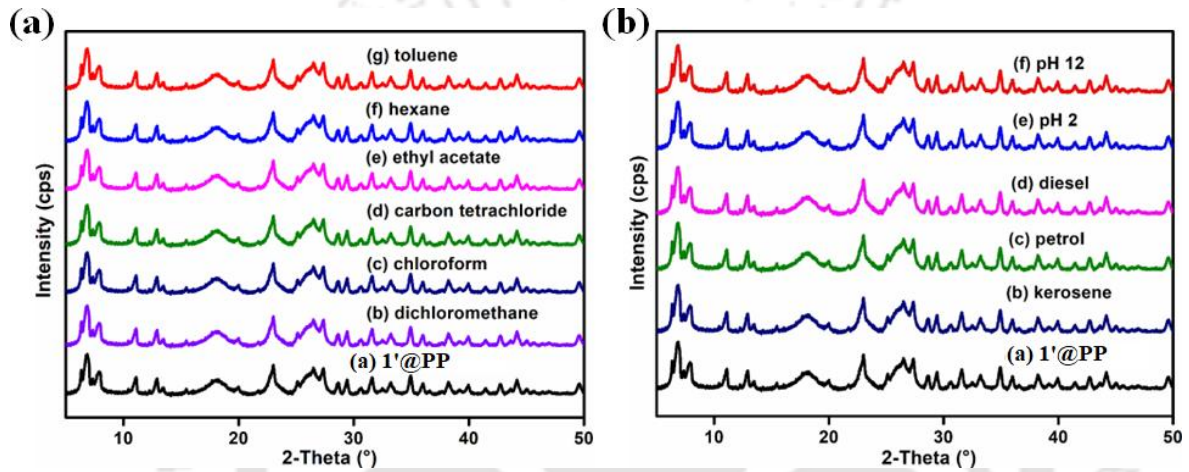

Figure 2.24 (a) PXRD patterns of **1@PP** composite before and after stirring in different organic solvents, and (b) pH media.

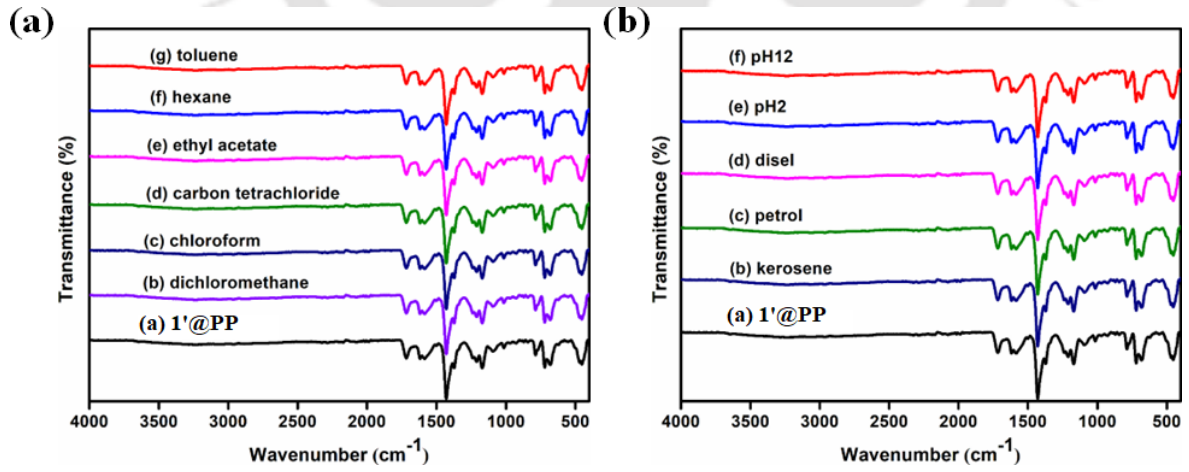

Figure 2.25 (a) ATR-IR spectra of **1@PP** composite before and after stirring in different organic solvents and (b) pH media.

The **1'@PP** composite was put in the simulated seawater sample for 7 days. Afterward, PXRD, FT-IR and WCA measurements were carried out with the recovered sample. The recovered sample showed similar PXRD, FT-IR and WCA results like as-prepared **1'@PP**

(Figures 2.26a-2.26b and Table 2.2). The as-prepared **1'@PP** composite was stored in open air for 180 days. Afterward, PXRD, FT-IR and WCA experiments were carried out. The material displayed similar PXRD, FT-IR and WCA data with the as-prepared **1'@PP** composite (Figures 2.27a-2.27b and Table 2.2). To examine the mechanical stability of the composite, it was scratched with sandpaper and then PXRD and FT-IR data were collected. Similar peak patterns were found in the PXRD profile and FT-IR spectra as the as-synthesized **1'@PP** composite (Figure 2.28a-2.18b). Since the surface of the **1'@PP** composite became rough after scratching, we were unable to measure the WCA. However, the water droplets rolled over the scratched composite when manually drop-casted. These results confirmed that the material possessed the functionality as well as the superhydrophobicity after scratching with sandpaper. The durability of the material in harsh chemical and mechanical conditions made it more favourable for environmental applications over the recently developed composite by Lin et. al.[332-333]

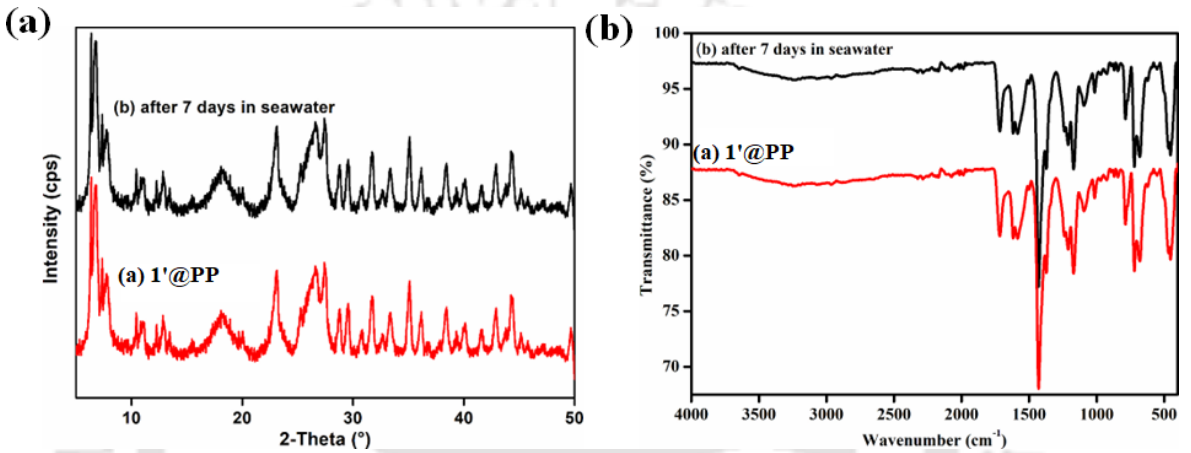

Figure 2.26 (a) PXRD patterns and (b) ATR-IR spectra of **1'@PP** before and after treatment with seawater for 7 days.

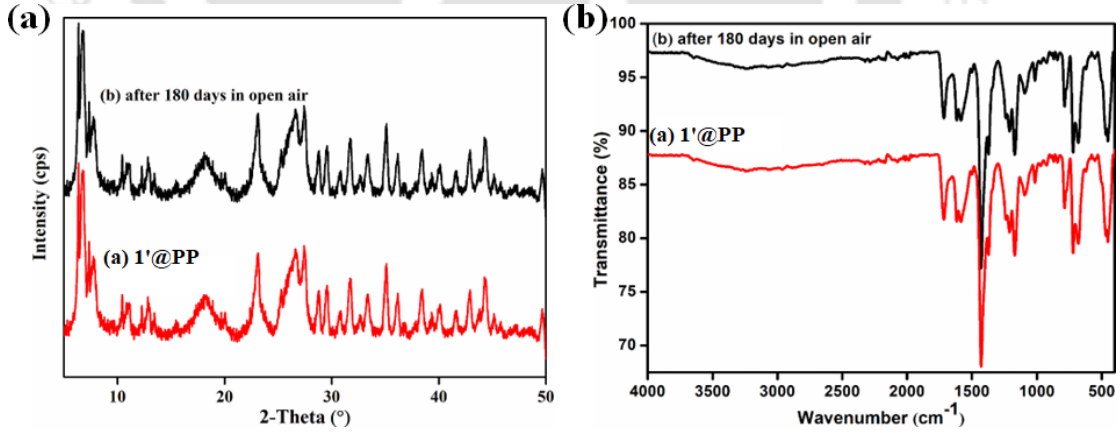

Figure 2.27 (a) PXRD patterns and (b) ATR-IR spectra of **1'@PP** before and after staying 6 months in open air condition.

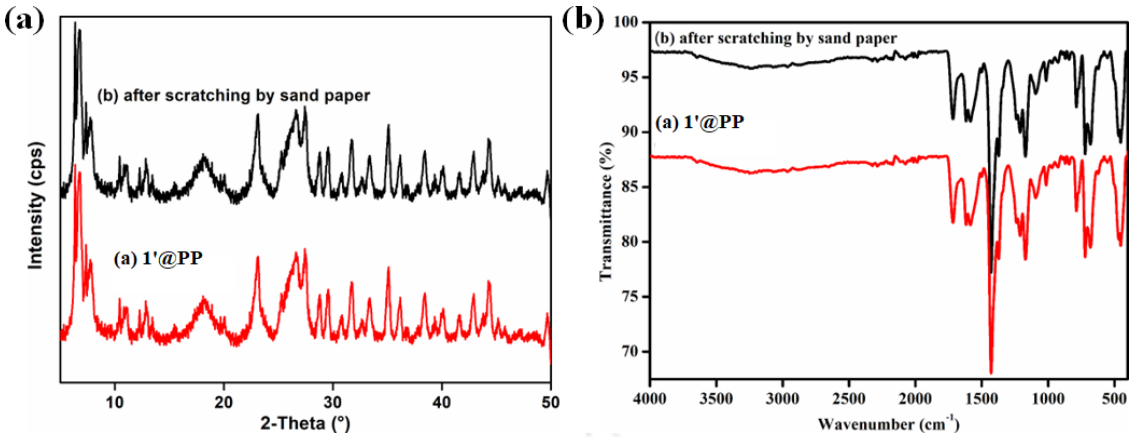

Figure 2.28 (a) PXRD patterns and (b) ATR-IR spectra of **1'@PP** before and after scrtching with sand paper.

Table 2.2 Water contact angle after stability experiments.

Experiments	WCA
Fresh **1'@PP**	160±1°
1'@PP after stirring in toluene for 1 day	159±1°
1'@PP after stirring in hexane for 1 day	158±2°
1'@PP after stirring in ethyl acetate for 1 day	159±2°
1'@PP after stirring in CCl_4 for 1 day	160±1°
1'@PP after stirring in CH_3Cl for 1 day	161±1°
1'@PP after stirring in CH_2Cl_2 for 1 day	158±1°
1'@PP after stirring in pH 12 for 1 day	156±1°
1'@PP after stirring in pH 2 for 1 day	159±2°
1'@PP after stirring in diesel for 1 day	158±3°
1'@PP after stirring in petrol for 1 day	158±1°
1'@PP after stirring in kerosene for 1 day	161±1°
1'@PP after stirring in seawater for 7 days	157±2°
1'@PP after stay in in air atmosphere for 180 days	157±2°
1'@PP after antifouling experiment	158±1°

2.3.12 Discriminative Oil Separation from Oil-Water Mixture by Superhydrophobic 1'@PP Composite

The structural robustness and hydrophobic behaviour of **1'@PP** composite inspired us to study its efficiency for the removal of oils from oil-water mixtures. To check the oil-water separation property, we chose one light oil (toluene) and one heavy oil (chloroform). To distinguish between the layers of water and oil, we prepared coloured solutions of toluene and chloroform by adding a pinch of neutral red and Rhodamine B, respectively. 5 mL of light model oil (toluene) was added to approximately 50 mL of water. Toluene layer floated on the surface of the water (Figure 6a) since its density is lower than water. When **1'@PP** composite was brought into contact with the upper oil layer of the mixture, the composite immediately soaked all the volume of oil selectively (Figure 2.29a). Similarly, 5 mL of heavy model oil (chloroform) was added to approximately 50 mL of distilled water in a 250 mL beaker. When we immersed **1'@PP** composite into the mixture forcefully, it immediately soaked all the volume of oil

selectively (Figure 2.29b). These results strongly suggested that **1'@PP** can be very useful for the separation of light oils as well as heavy oils from water.

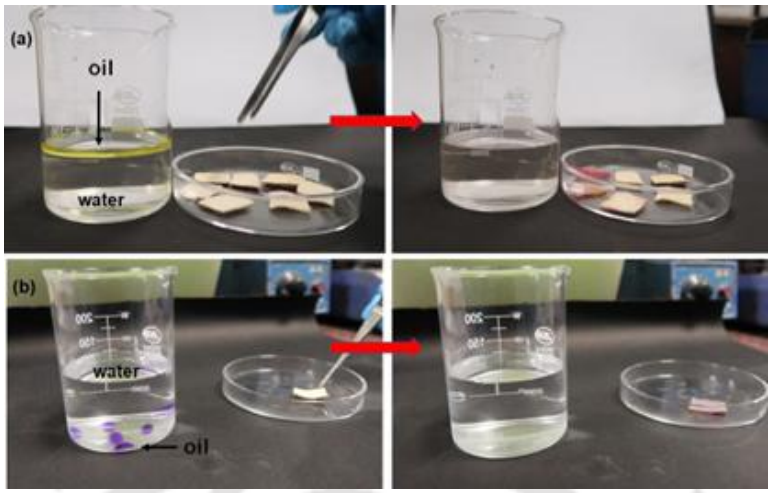

Figure 2.29 Digital photographs of the discriminative absorption-based separation of floating oil (a) and underwater oil (b) by **1'@PP** composite. Light and heavy oils were coloured with yellow and red for better visualization effect.

We evaluated the separation efficiency (%) for different light oils like ethyl acetate, hexane, toluene, kerosene, petrol and diesel, and heavy oils like carbon tetrachloride, dichloromethane and chloroform. The separation efficiency (%) was calculated using formula: separation efficiency (%) = $V_2/V_1 \times 100$ where, V_1 is the volume of oil (mL) used and V_2 is the absorbed volume of oil (mL) by **1'@PP** Five measurements were carried out for each oil sample and the mean value was plotted. After every experiment, the oil was collected by squeezing the composite manually. Figure 2.30a suggested that the separation efficiency (%) varied in between 95% and 99% for different oils. The separation efficiency of our composite quite better than the recent literatures.[332] We also checked the separation efficiency (%) in different types of water like tap water, river water, artificial sea water and water at pH 1 and pH 12 by taking chloroform as a model oil. It was found that the separation efficiency of **1'@PP** composite was not affected by different aqueous systems (Figure 2.30b). For all the above experiments, a mixture of 5 mL of oil in 20 mL of water and a piece of composite having a mass of 0.1 g was used. The mean values of the volume of oil after separation for ethyl acetate, hexane, toluene, kerosene, petrol, diesel, carbon tetrachloride, dichloromethane and chloroform were 4.78, 4.78, 4.95, 4.82, 4.78, 4.78, 4.96, 4.84 and 4.76 mL, respectively.

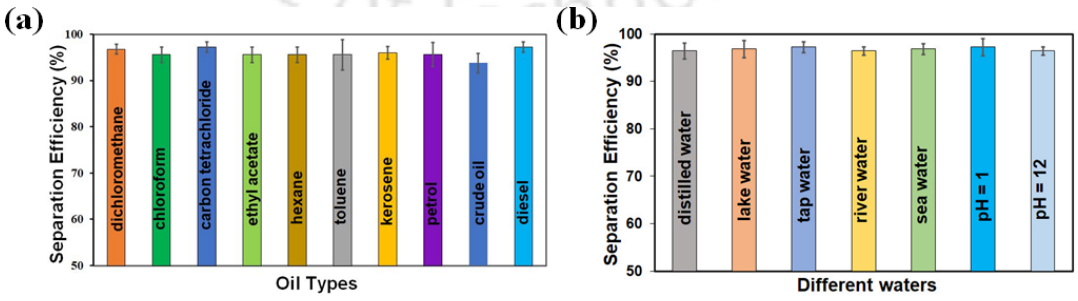

Figure 2.30 (a) Separation efficiency (%) of **1'@PP** towards various oils from oil-water mixtures presented by error bar plot and (b) Separation efficiency (%) of **1'@PP** towards chloroform from different real water samples to show its applicability in various environmental water bodies.

The removal of oil from the mixtures of oil-water in an easy, fast and less consuming way is a prime requirement for a material to be applicable for this purpose. In this work, we used the process of absorption technique and mechanical squeezing to remove oils from the composite. The absorption of oil by the composite was observed within seconds. Therefore, our material fulfils all the criteria of potential material for oil-water separation. Another prime requirement for a material to be ideal for oil-water separation is recyclability. We performed recyclability experiments up to 20th cycle and the loss of separation efficiency after 20th cycle was found to be only 9% (Figure 2.31) which is better than the previous study of cotton-based composite from our group. EDX spectrum and elemental mapping of **1'@PP** were carried out after 20th cycle of the separation experiment. The obtained results showed the presence of the desired elements in the composite (Figure 2.32a-2.32b). The FE-SEM image of **1'@PP** revealed the homogenous distribution of octahedral micro-crystals after 20th cycle of separation (Figure 2.33a). The presence of similar octahedral shaped nanocrystals confirmed durability of the composite even after 20 cycles of oil-water separation studies.[348] It can be noticed from the PXRD plot in Figure 2.33b that the characteristic peaks of **1'** were present in reused **1'@PP.** All the results indicated the effective applicability of our probe up to 20th cycle of oil-water separation.

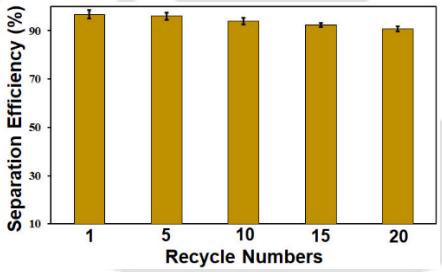

Figure 2.31 Reusabiity of **1'@PP** fabric composite for oil/water separation experiment (model oil: $CHCl_3$).

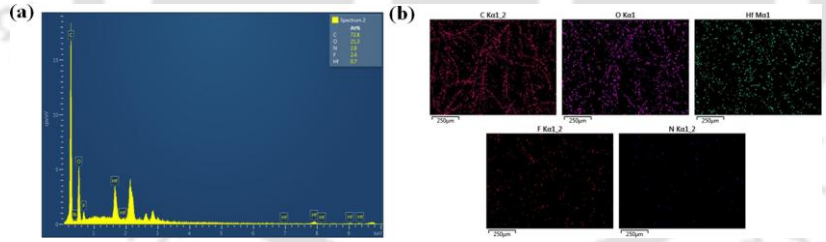

Figure 2.32 (a) EDX spectrum and (b) mapping of **1'@PP** fabric composite after 20th cycle of separation experiment.

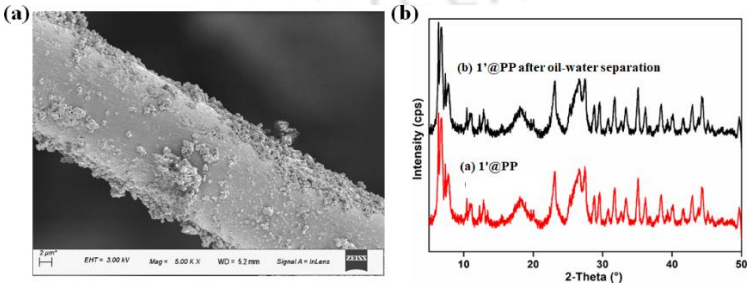

Figure 2.34 (a) High resolution FE-SEM images of **1'@PP** fabric composite after 20th cycle of separation experiment. (b) PXRD patterns of **1'@PP** fabric composite before and after oil-water separation experiments (model oil: $CHCl_3$).

The recyclability of the material in highly alkaline (pH 12) and acidic media (pH 2) was checked. The loss of separation efficiency of **1'@PP** in pH 2 media after the 20th cycle is only 12.3% (Figure 2.35a). **1'@PP** lost its separation efficiency by 10.6% due to slow leaching of **1'** from PP fabric after the 10th cycle in case of pH 12 (Figure 2.35b). The above results suggested that the **1'@PP** could be used in acidic media but its application in alkaline media is limited up to only few cycles due to leaching. The recyclability and durability in harsh conditions make this material applicable for the industrial purposes.

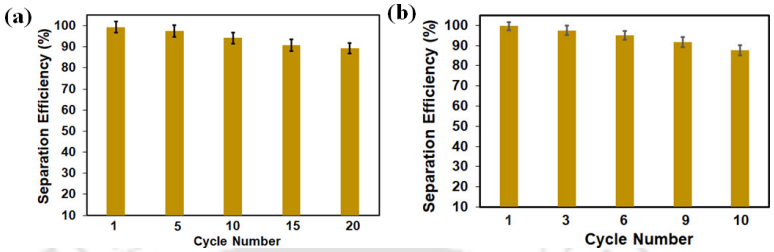

Figure 2.35 (a) Recyclability of **1'@PP** in alkaline (pH 12) and (b) acidic (pH 2) for oil-water separation.

2.3.13 Oil Absorption Capacity of 1'@PP

The selectivity of **1'@PP** toward separation of oil from oil-water mixture inspired us to study the absorption capacity of **1'@PP** towards different oils. The **1'@PP** material showed an almost negligible water absorption capacity but a very high oil absorption capacity (Figure 2.36a). We also measured the absorption capacity in g/g unit, that is, absorption of mass of oil in gram per gram of composite (Figure 2.36b). The absorption capacities for different oils were found to be: carbon tetrachloride: 38.93 ± 2.34 g/g, chloroform: 35.34 ± 1.90 g/g, dichloromethane: 34.44 ± 0.68 g/g, ethyl acetate: 30.39 ± 1.36 g/g, kerosene: 28.54 ± 2.26 g/g, toluene: 29.48 ± 1.29 g/g, petrol: 30.64 ± 1.36 g/g, diesel: 29.68 ± 2.23 g/g, crude oil: 34.21 ± 2.32 and hexane: 28.24 ± 2.92 g/g. The obtained results of oil absorption capacity are comparable with previously reported materials for oil-water separation (Table 2.3).[328, 353-354]

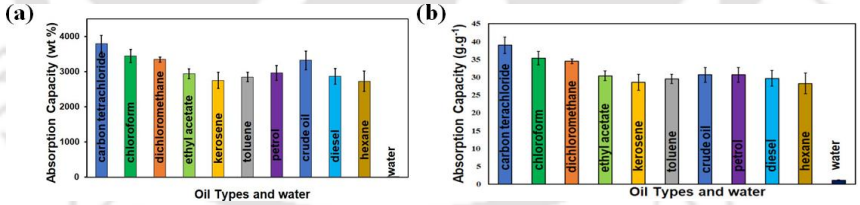

Figure 2.36 (a) Absorption capacity of **1'@PP** towards different oils in weight% and (b) in g/g of oil with respect to weight of **1'@PP**.

Gravity Driven Selective Oil-Water Separation by 1'@PP.

The oil-water separation using the principle of absorption-based environmentally friendly method as discussed above has great utility in a real-field application. Again, we used another very simple and efficient method of oil-water separation, that is gravity-driven separation of oil from oil-water mixture. We papered a mixture containing 5 mL of water and 5 mL of chloroform. Then, it was poured in a glass syringe containing a piece of **1'@PP** as shown in Figure 2.37. it is clearly understandable that the red-coloured chloroform having a higher density than water was separated or filtered through **1'@PP** But the water remained over **1'@PP**. The superhydrophobic nature of **1'@PP** opposes the water layer to pass below. The principle of gravity-driven separation neither requires energy nor any complicated set-up. The oil-water separation can be executed in a simple, fast and eco-friendly way. The flux of oil

separation was also calculated using the equation: flux = V/A × T (V = volume of oil in L, A = area of cross section in m^2, T = time in h). The flux of oil varied from 15783 to 18263 $Lm^{-2}h^{-1}$ for pure oils. But, for crude oil, it was 13203 $Lm^{-2}h^{-1}$ due to the higher viscosity and sticky nature of crude oil (Figure 2.38). The flux of oil separation was almost double as compared to the recent report on oil-water separation by Lin et. al. and Li et. al.[332, 355]

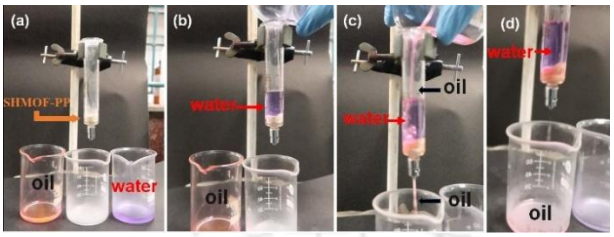

Figure 2.37 Digital photographs of selective separation of heavy oil by gravity driven method of separation by **1'@PP** (chloroform: red, water: violet).

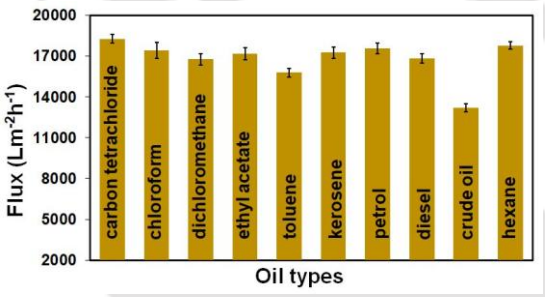

Figure 2.38 Flux for oil-water separation by **1'@PP** composite for different oils in $Lm^{-2}\,h^{-1}$.

2.3.14 Separation of Oil Opposite to Gravity by 1'@PP

The separation of sedimentary oil from oil-water mixture in the opposite direction of gravity was already explored by our group before. Here, we used the same method for the separation of sedimentary oil by **1'@PP**. For the separation of sedimentary oil, we used a Pasteur pipette which was plugged with **1'@PP**. Again, a mixture of chloroform and water was prepared where chloroform is highlighted with red colour for better visualization. When the Pasteur pipette plugged with **1'@PP** was dipped into the beaker containing the mixture of chloroform and water, it did not absorb water. But, when it reached the chloroform layer, it immediately absorbed chloroform. After absorption, the opposite end of the pipette was capped to avoid the escape of oil by the attraction of gravity. The pipette was removed in capped state and uncapped in another beaker to remove the oil. The pipette was ready for the next round sedimentary oil separation (Figure 2.39).

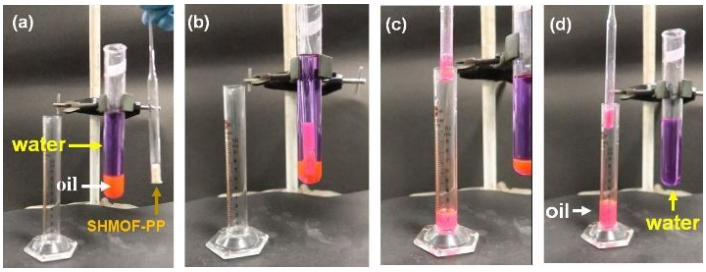

Figure 2.39 Digital photographs of separation of sedimentary oil by antigravity method of separation by **1'@PP**. Oil and water were coloured with red and violet for better visualisation.

Although some hydrophobic MOF composites were employed for oil-water separation, there is no report so far on superhydrophobic MOF composite prepared with N95 mask fabric as support and applied for oil-water separation. The unique composition and high efficiency of **1@PP** towards oil-water separation indicate its importance for real field applications over the traditional methods, i.e., vacuum filtration,[356] distillation,[357] solvent extraction[358] and burning.[359] The separation of oils from oil-water mixtures in an eco-friendly, cheap and easy way is highly required, which could be easily achieved with the presented material.

2.3.15 Self-Cleaning Property

The hydrophobic nature of our synthesized material promoted us to examine its self-cleaning nature.[360] To evaluate the self-cleaning nature the composite, a MOF coated glass slide was first prepared and then dry grass powder was added on its surface. The water droplets when rolled over the MOF-coated glass slide carrying out the grass particles. (Figure 2.40a). The water contact angle hysteresis (WCAH) was measured with a 3° interval from 0° to 12° following the procedure of Hak et. al.[361] We found that the WCAH increased with increase in tilting angle and the WCAH remained in between 0° to 4.87° which confirmed the superhydrophobic nature of **1'**-coated glass slide. The water droplet was rolled over from the surface at 12° (Figure 2.41). To demonstrate the self-cleaning and anti-fouling nature of **1'@PP** composite, it was dipped into a suspension of soil in water coloured with rhodamine-B. The weight of composite before and after dipping in soil-rhodamine-B suspension was almost the same. When the experiment was repeated with only PP-fabric, the mass of 65 mg of PP-fabric increased to 662 mg due absorption of soil-rhodamine-B suspension (Figure 2.40b).[362] The above experiments showed that the **1'@PP** composite has both self-cleaning as well as anti-fouling nature. The microorganism present in water body requires water for their growth. Since the composite is superhydrophobic, it will hinder the absorption of water and inhibit the growth of any colony of microorganism.

Figure 2.40 Digital image of **1'@PP** coated glass slide displaying self-cleaning nature and (b) digital images of **1'@PP** composite and PP-fabric before and after antifouling experiment.

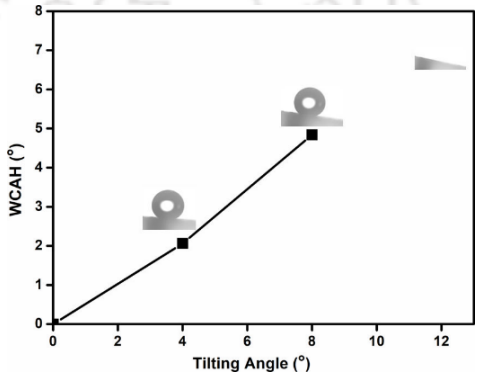

Figure 2.41 Plot for contact angle hysteresis versus tilting angle for **1'@PP** coated glass surface from 0 to 12°.

2.3.16 Emulsion Separation

The presence of water in large amount of oil causes the formation of emulsion. The formation of emulsion inside the pipeline of oil transporting systems can cause the corrosion of the metal pipes. The emulsion inside the pipe causes unusual high pressure and increases the risk towards the leakage of pipes. Therefore, the separation of water from water-in-oil emulsion is very much required. The results of emulsion separation by **1'@PP** are shown in Figure 2.42. The separation efficiency for emulsions of different oils ranges from 95-99 % (Figure 2.43a). The flux of emulsion separation was from 1845-1899 $LM^{-2}h^{-1}$ for emulsions of different oils (Figure 2.43b). The obtained flux for emulsion separation by **1'@PP** was comparable with the previously reported literature.[335, 363]

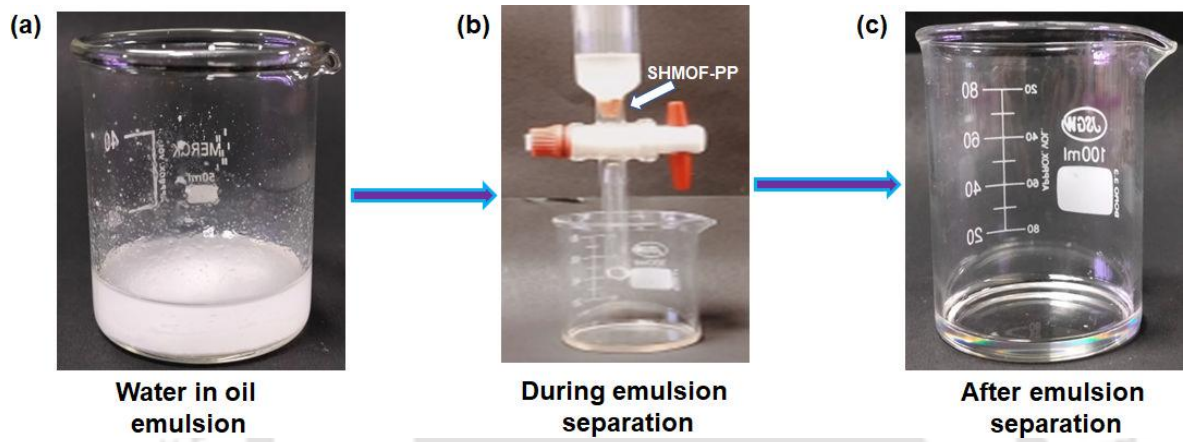

Figure 2.42 Digital photographs of emulsion separation: (a) image of emulsion in beaker, (b) image during emulsion separation by **1'@PP**, and (c) image of only oil separated from the emulsion.

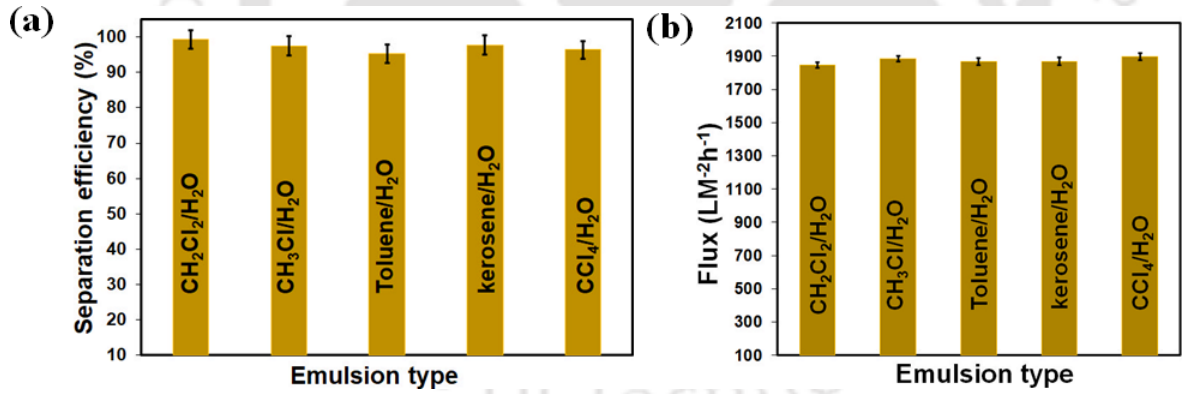

Figure 2.43 (a) Bar plot showing the separation of efficiency of **1'@PP** for emulsions of different oils. (b) Bar plot showing the flux for separation of emulsions of different oils.

Table 2.3 Comparisons of absorption capacities (in g/g) and separation efficiency (%) of some absorbents with **1'@PP**.

S. No.	Absorbents	Absorption Substances	Absorption Capacity (g/g)	Separation Efficiency (%)	Ref.
1	**1'@PP**	**diesel oil, petrol oil, kerosene, crude oil, dichloromethane, chloroform, carbon tetrachloride, ethyl acetate, hexane, toluene**	**28.24-38.93**	**95-99**	**this work**
2	PDMS-TiO2-PU sponge	diesel oil, pump oil, silicone oil, edible oil, kerosene, dichloromethane, chloroform	16.7-43.57	-	[364]
3	SH-UiO-66@CFs	motor oil, silicone oil, gasoline, kerosene, toluene, hexane, ethyl acetate, carbon tetrachloride, chloroform, dichlomrthane	27.14-49.27	95-98	[365]
4	superhydrophobic/superoleophilic sawdust	crude oil, n-hexane, gasoline, diesel oil, engine oil	10.00-17.50	-	[366]
5	cotton fiber modified via the sol-gel method	diesel oil, lubrication oil, crude oil, peanut oil	25.61-57.01	98.5	[367]
6	modified jute fiber via the sol-gel method	crude oil, diesel oil, lubricatiom oil, peanut oil	7.41-10.29	-	[368]
7	mesoporous silica aerogel	petrol oil, diesel oil, toluene	19.10-18.60	-	[369]
8	ultralight cellulose-based aerogel	pump oil, diesel oil, chloroform, dodecane, hexane, soybean oil, pump oil, diseal oil, motor oil, heptane, tolune, DMSO, isopropanol	18.00-41.80	-	[370]
9	cellulose-based aerogel	crude oil, diesel oil, lubrication oil silicone oil, soyabean oil, toluene, n-hexane, trichloromethane, acetone, ethanol	60.44-152.3	-	[371]
10	polystyrene branched 9-octadecenoic acid grafted graphene	hexane, heptane, nonane, decane, hexadecane	11.00-27.00	-	[372]
11	MOF-PU sponge	n-hexane, paraffin, ethanol, edible oil, DMF, carbon tetrachloride	29.00-56.00	>96	[353]
12	UiO-66-F4@rGO/MS	n-hexane, isooctane, dichloromethane, 1,3,5-trimethylbenzene, silicone oil diesel oil light diesel oil crude oil	26.00-61.00	99.73	[373]
13	MOF@Rgo composites	chloroform, n-hexane, silicone oil, bump oil, bean oil, toluene, acetone, butanone	14.00-37.00	50-80	[374]
14	MOFs-copper foam	soybean oil, n-hexane, isooctane, gasoline, dichloromethane, chloroform	1.50-3.50	>96	[375]
15	FGO@MOG	crude oil, decane, heptane, hexane, octadecane, octane, petrolether, pentane, toluene, veg oil, carbon tetrachloride	2.00-5.00	-	[376]
16	Macroporous silicone sponges	crude oil, sunflower oil, kerosene, diesel, alcohol, acetic acid, chloroform, acetone, diethyl ether, n-hexane, isooctane, dichloromethane	9.70-27.00	>99	[377]

17	GO/PDA coated fabric	formamide, engine oil, ethylene glycol, liquide paraffin, propylene carbonate, rapeseed oil	-	>99.50	[378]
18	CBM-CuO-SA	n-hexane, toluene, trichloromethane	-	>97	[379]

2.4 Conclusions

The current research presents a novel, easy and inexpensive strategy to design **1'@PP** composite for oil separation. Initially, we synthesized and characterized a stable trifluoroacetamido-functionalized Hf-based MOF having formula $[Hf_6O_4(OH)_4(TFNDC)_6]\cdot 6H_2O\cdot 2DMF$ (**1**). Next, we synthesized a superhydrophobic composite coded as **1'@PP** *via* an *in-situ* growth of **1'** on the surface of PP fabric. The superhydrophobic **1'@PP** material exhibited excellent chemical and mechanical stability and was resistant to extreme acidic and alkaline conditions. Superhydrophobic **1'@PP** was highly efficient (separation efficiency: 95-99%) for the separation of light, heavy and crude oil from water. The separation process can be repeated for at least 20 times with almost equal separation efficiency. The recyclability was maintained in high acidic as well as alkaline conditions. Furthermore, the **1'@PP** composite is capable of selectively absorbing oil from water. The material exhibited a very good oil absorption capacity (29-39 g/g) for different kinds of oil specimens. The flux of oil separation was found to be between 13k to 18k $Lm^{-2}h^{-1}$ which is much higher compared to other reported materials. It shows great potential for designing a cost-effective and environmentally friendly strategy for the separation of oil from oil-water mixture. In future, we can use it for industrial applications for the separation of oil from seawater. Finally, we could demonstrate the interesting self-cleaning property of the composite. **1'@PP** was also utilised for water-in-oil emulsion separation with a high flux of 1845-1899 $Lm^{-2}h^{-1}$ for emulsion of different oils.

2.5 References

1. A. Carpenter, *Hydrobiologia*, 2019, **845**, 109–127.
2. H. Khordagui and D. Al-Ajmi, *Environ. Manage*, 1993, **17**, 557-562.
3. F. I. Alghunaimi, D. J. Alsaeed, A. M. Harith and T. A. Salehc, *J. Clean. Prod*, 2019, **233**, 946-953.
4. B. O. Abdullahi, E. Ahmed, H. A. Abdulgader, F. Alghunaimi and T. A. Saleh, *J. Mol. Liq.*, 2021, **325**, 115057.
5. T. A. Saleh, M. Mustaqeem and M. Khaled, *Environ. Nanotechnol. Monit. Manag.*, 2022, **17**, 100617.
6. T. A. Saleh, *Trends Environ. Anal. Chem.*, 2020, **25**, 00080.
7. M. G. Barron, D. N. Vivian, R. A. Heintz and U. H. Yim, *Environ. Sci. Technol.*, 2020, **54**, 6456–6467.
8. G. Troisi, S. Barton and S. Bextonc, *Int. J. Hydrog. Energy*, 2016, **41**, 16549-16555.
9. J. F. Piatt, C. J. Lensink, W. Butler, M. Kendziorek and D. R. Nysewander, *Auk*, 1990, **107**, 387–397.
10. R. Almeda, Z. Wambaugh, C. Chai, Z. Wang, Z. Liu. and E. J. Buskey, *PLoS One*, 2013, **8**, 74476.
11. Ø.Langangen, E. Olsen, L. C. Stige, J. Ohlberger, N. A. Yaragina, F. B. Vikeb, B. Bogstad, N. C. Stenseth and D. Ø. Hjermann, *Mar. Pollut. Bull.*, 2017, **119**, 102-109.
12. Q. Karam and Z. Al-Wazzan, *J. Mar. Biolog. Assoc. U.K.*, 2021, 1-16.
13. H. Wang, X. Xia, R. Liu, Z. Wang, Y. Zhai, H. Lin, W. Wen, Y. Li, D. Wang, Z. Yang, D. C. G. Muir and J. C. Crittenden, *Environ. Sci. Technol.*, 2019, **53**, 4274–4284.

14. M. Rusin, J. Gospodarek and A. Nadgórska-Socha, *Pol. J. Environ. Stud.*, 2015, **24**, 2157–2166.
15. S. A. Shedid, J. H. Abou-Kassem and A. Y. Zekri, *Energy Sources*, 2005, **27**, 1257-1268.
16. D. D. Evans, G. W. Mulholland, H. R. Baum, W. D. Walton and K. B. McGrattan, *J Res Natl Inst Stand Technol.*, 2001, **106**, 231–278.
17. F. AlGhunaimi, D. Alsaeed, A. Harith and T. Saleh, *Abu Dhabi International Petroleum Exhibition & Conference*, 2018, 12-15.
18. T. A. Saleh, *Environ. Technol. Innov.*, 2021, **24**, 101821.
19. T. A. Saleh, *Environ. Technol. Innov.*, 2020, **20**, 101067.
20. G. Rena, Y. Songa, X. Li, Y. Zhou, Z. Zhang and X. Zhua, *Appl. Surf. Sci.*, 2018, **428**, 520-525.
21. E. Bormashenko, O. Gendelman and G. Whyman, *Langmuir*, 2012, **28**, 14992–14997.
22. J. Lu, Z. Gao, T. Xu, X. Zhu, X. Miao, Y. Song, G. Ren and X. Li, *ACS Appl. Mater. Interfaces*, 2020, **12**, 49138–49145.
23. J. Lu, X. Zhu, B. Wang, L. Liu, Y. Song, X. Miao, G. Ren and X. Li, *Cellulose*, 2020, **27**, 2817–2827.
24. M. Safaei, M. M. Foroughi, N. Ebrahimpoor, S. Jahani, A. Omidi and M. Khatam, *Trends Anal. Chem.*, 2019, **118**, 401-425.
25. c. Gogoi and S. Biswas, *Cryst. Growth Des.*, 2021, **21**, 2680–2689.
26. H. D. Lawson, S. P. Walton and C. Chan, *ACS Appl. Mater. Interfaces*, 2021, **13**, 7004–7020.
27. L. Dandan, X. Hai-Qun, J. Long and J. Hai-Long, *EnergyChem*, 2019, **1**, 100005.
28. R. Ma, Y. J. Colón and T. Luo, *ACS Appl. Mater. Interfaces*, 2020, **12**, 34041–34048.
29. C. Altintas, O. F. Altundal, S. Keskin and R. Yildirim, *J. Chem. Inf. Model.*, 2021, **61**, 2131–2146.
30. H. M. Wen, C. Liao, L. Li, A. Alsalme, Z. Alothman, R. Krishna, H. Wu, W. Zhou, J. Hu and B. Chen, *J. Mater. Chem. A*, 2019, **7**, 3128-3134.
31. O. K. Farha, I. Eryazici, N. C. Jeong, B. G. Hauser, C. E. Wilmer, A. A. Sarjeant, R. Q. Snurr, S. T. Nguyen, A. Ö. Yazaydın and J. T. Hupp, *J. Am. Chem. Soc.*, 2012, **134**, 15016–15021.
32. C. Gogoi, A. Kumar, M. SK and S. Biswas, *Microporous Mesoporous Mater.*, 2021, **311**, 110725.
33. H. Li, K. Wang, Y. Sun, C. T. Lollar, J. Li and H. C. Zhou, *Mater. Today*, 2018, **21**, 108-121.
34. M. L. Gao, S. Y. Zhao, Z. Y. Chen, L. Liu and Z. B. Han, *Inorg. Chem.*, 2019, **58**, 2261–2264.
35. J. R. Robalo, S. Huhmann, B. Koksch and A. V. Verde, *Chem*, 2017, **3**, 881-897.
36. R. Dalapati, S. Nandi, C. Gogoi, A. Shome and S. Biswas, *ACS Appl. Mater. Interfaces*, 2021, **13**, 8563–8573.
37. C. Yang, U. Kaipa, Q. Z. Mather, X. Wang, V. Nesterov, A. F. Venero and M. A. Omary, *J. Am. Chem. Soc.*, 2011, **133**, 18094–18097.
38. M. M. Bashar, H. Zhu, S. Yamamoto and M. Mitsuishi, *RSC Adv.*, 2017, **7**, 37168-37174.
39. S. Mukherjee, A. M. Kansara, D. Saha, R. Gonnade, D. Mullangi, B. Manna, A. V. Desai, S. H. Thorat, P. S. Singh, A. Mukherjee and S. K. Ghosh, *Chem. Eur. J.*, 2016, **22**, 10937-10943.
40. H. Liu, L. Yang, Y. Zhan, J. Lan, J. Shang, M. Zhou and S. Lin, *Cellulose*, 2021, **28**, 1715–1729.

41. S. Pala, S. Mondal, P. Pal, A. Das, S. Pramanik and J. Maity, *Colloids Interface Sci. Commun.*, 2021, , **44**, 100469.
42. Q. Xu, W. Zhang, C. Dong, T. S. Sreeprasad and Z. Xia, *J. R. Soc. Interface*, 2016, **13**, 1742-5662.
43. H. J. Kwon, M. Lee, S. K. Hong, C. Park, S. J. Cho and G. Lim, *ACS Nano*, 2021, **15**, 15815–15823.
44. S. Parvate, P. Dixit and S. Chattopadhyay, *J. Phys. Chem. B*, 2020, **124**, 1323–1360.
45. T. A. Saleh, *Environ. Sci. Pollut. Res*, 2015, **22**, 16721–16731.
46. V. Bon, I. Senkovska, M. S. Weissb and S. Kaskela, *CrystEngComm*, 2013, **15**, 9572-9577.
47. M. R. Shaaban, *Arab. J. Chem.*, 2017, **10**, 2796-S2805.
48. T. A. Saleh, *J. Clean. Prod*, 2018, **172**, 2123-2132.
49. T. A. Saleh, *Desalination Water Treat.*, 2016, **57**, 10730-10744.
50. S. Ghosh, F. Steinke, A. Rana, M. Alam and S. Biswas, *Eur. J. Inorg. Chem.*, 2021, 1–7.
51. S. Yuan, J. S. Qin, C. T. Lollar and H. C. Zhou, *ACS Cent. Sci.*, 2018, **4**, 440−450.
52. C. Gogoi, N. Nagarjun, S. Roy, S. K. Mostakim, D. Volkmer, A. Dhakshinamoorthy and S. Biswas, *Inorg. Chem.*, 2021, **60**, 4539–4550.
53. J. Winarta, B. Shan, S. M. Mcintyre, L. Ye, C. Wang, J. Liu and B. Mu, *Cryst. Growth Des.*, 2020, **20**, 1347–1362.
54. H. Chen, F. Wang, H. Fan, R. Hong and W. Li, *Chem. Eng. J.*, 2021, **408**, 127343.
55. D. R. Bassett, *J. Coat. Technol.*, 2001, **73**, 43–55.
56. T. A. Saleh, *Appl. Surf. Sci.*, 2011, **257**, 7746-7751.
57. T. A. Saleh, *J. Water Supply Res. T.*, 2015, **64**, 892–903.
58. S. S. Latthe, C. Terashima, K. Nakata and A. Fujishima, *Molecules*, 2014, **19**, 4256-4283.
59. V. S. Yadav, M. R. Sankar and L. M. Pandey, *J. Magnes*, 2020, **8**, 999-1015.
60. Y. Liu, J. Tang, R. Wang, H. Lu, L. Li, Y. Kong, K. Qi and J. H. Xin, *J. Mater. Chem.*, 2007, **17**, 1071-1078.
61. Z. He, H. Wu, Z. Shi, X. Duan, S. Ma, J. Chen, Z. Kong, A. Chen, Y. Sun and X. Liu, *Colloids Surf. A Physicochem. Eng. Asp.*, 2022, **648**, 129142.
62. J. Gu, H. Fan, C. Li, J. Caro and H. Meng, *Angew. Chem. Int. Ed.*, 2019, **58**, 5297-5301.
63. T. Xu, Z. Gao, Y. Jia, X. Miao, X. Zhu, J. Lu, B. Wang, Y. Song, G. Ren and X. Li, *Cellulose*, 2021, **28**, 4835–4846.
64. Y. Huang, H. Li, L. Wang, Y.Qiao, C. Tang, C. Jung, Y. Yoon, S. Li and M. Yu, *Adv. Mater. Interfaces*, 2015, **2**, 1400433.
65. Y. Q. Li, Y. A. Samad, K. Polychronopoulou, S. M. Alhassan and K. Liao, *ACS Sustainable Chem. Eng.*, 2014, **2**, 1492–1497.
66. Z. Zhang, G. Sèbe, D. Rentsch, T. Zimmermann and P. Tingaut, *Chem. Mater.*, 2014, **26**, 2659–2668.
67. A. O. Ekperusi, A. P. Onyena, M. Y. Akpudo, C. C. Peter, C. O. Akpoduado and O. H. Ekperusi, 2019.
68. S. Nishimoto and B. Bhushan, *RSC Adv.*, 2013, **3**, 671-690.
69. M. A. Samaha, H. V. Tafreshi and M. G. Hak, *Langmuir*, 2012, **28**, 9759–9766.
70. Y. Li, S. Yang, Y. Chen and D. Zhang, *Int. J. Environ. Res. Public Health*, 2020, **17**, 644.
71. Y. Cai, D. Chen and Q. X. N. Li, Hua Li, Jinghui He, and Jianmei Lu, *ACS Sustain. Chem. Eng.*, 2019, **7**, 2709–2717.
72. Q. Shuai, X. Yang, Y. Luo, H. Tang, X. Luo, Y. Tan and M. Ma, *Mater. Chem. Phys.*, 2015, **162**, 94-99.

73. R. Dalapati, S. Nandi, C. Gogoi, A. Shome and S. Biswas, *ACS Appl. Mater. Interfaces*, 2021, **13**, 8563-8573.
74. D. Zang, F. Liu, M. Zhang, Z. Gao and C. Wang, *Chem. Eng. Res. Des.* , 2015, **102**, 34-41.
75. N. Lv, X. Wang, S. Peng, L. Luo and R. Zhou, *RSC Adv.*, 2018, **8**, 30257-30264.
76. N. Lv, X. Wang, S. Peng, H. Zhang and L. Luo, *Int. J. Environ. Res. Public Health*, 2018, **15**, 969.
77. C. Zhang, C. Dai, H. Zhang, S. Peng, X. Wei and Y. Hu, *Mar. Pollut. Bull.*, 2017, **122**, 129-138.
78. H. Zhang, Y. Li, Y. Xu, Z. Lu, L. Chen, L. Huang and M. Fan, *Phys. Chem. Chem. Phys.* , 2016, **18**, 28297-28306.
79. T. Yin, X. Zhang, X. Liu and C. Wang, *Mar. Pollut. Bull.*, 2017, **118**, 267-274.
80. F. I. Alghunaimi, D. J. Alsaeed, A. M. Harith and T. A. Saleh, *J. Clean. Prod.*, 2019, **233**, 946-953.
81. Y. Zhan, S. He, J. Hu, S. Zhao, G. Zeng, M. Zhou, G. Zhang and A. Sengupta, *J. Hazard. Mater.*, 2020, **388**, 121752.
82. J. Gu, H. Fan, C. Li, J. Caro and H. Meng, *Angew. Chem. Int. Ed.*, 2019, **58**, 5297-5301.
83. J. Du, C. Zhang, H. Pu, Y. Li, S. Jin, L. Tan, C. Zhou and L. Dong, *Colloids Surf. A Physicochem. Eng. Asp.*, 2019, **573**, 222-229.
84. K. Jayaramulu, F. Geyer, M. Petr, R. Zboril, D. Vollmer and R. A. Fischer, *Adv. Mater.*, 2017, **29**, 1605307.
85. J. Cao, D. Wang, P. An, J. Zhang and S. Feng, *J. Mater. Chem. A*, 2018, **6**, 18025-18030.
86. X. Zhu, Z. Gao, F. Li, G. Miao, T. Xu, X. Miao, Y. Song, X. Li and G. Ren, *Carbon*, 2022, **190**, 329-336.
87. Z. Yin, F. Yuan, M. Xue, Y. Xue, Y. Xie, J. Ou, Y. Luo, Z. Hong and C. Xie, *J. Colloid Interface Sci.*, 2022, **611**, 93-104.

An Eco-Friendly Approach by Nonfluorous Self-Cleaning Metal-Organic Framework Composite and Membrane for Oil-Water Separation

Here, we report a first-ever superhydrophobic fluorine metal-organic framework (MOF) material that is prepared from a pre-synthesized long-chain hydrocarbon-based linker. The fluorine free MOF was synthesized using palmitamidoterephthalic acid (H_2L^2, H_2L^2: BDC-4-NH-CO-$(CH_2)_{14}$-CH_3) linker and zirconium salt. The material was systematically characterized by PXRD, FT-IR, EDX and FE-SEM experiments in order to confirm its crystallinity, functionality, elemental purity and particle nature. Further, the material's superhydrophobicity was proved by water contact angle (WCA) measurement. The MOF material was further utilized to design superhydophobic melamine sponge composite and silk membrane. Both the composite and membrane were applied for the selective separation of oil from the oil-water mixture. The separation efficiency in both the absorption and filtration-based method was higher than 99%. The absorption capacity of the composite ranged between 43.8 and 97.2 $g \cdot g^{-1}$. The flux of oil-water separation was as high as 58263-47416 $Lm^{-2}h^{-1}$. Both the membrane and composite displayed remarkable self-cleaning property. The long-chain hydrocarbon-based linker is the reason behind the superhydrophobic nature of MOF. The tiny nanostructure of MOF on the surface of composite and membrane causes the arrival of the Cassie-Baxter state when they come in contact with water. The nonpolar-nonpolar interaction between MOF and different oil is the reason behind the selective oil-water separation. Since water is polar in nature, the superhydrophobic composite and membrane inhibit the permeation of water through them. The mechanism of nonpolar-nonpolar interaction was supported by the ESP diagram of the linker, water and all the organic molecules present in crude oil.

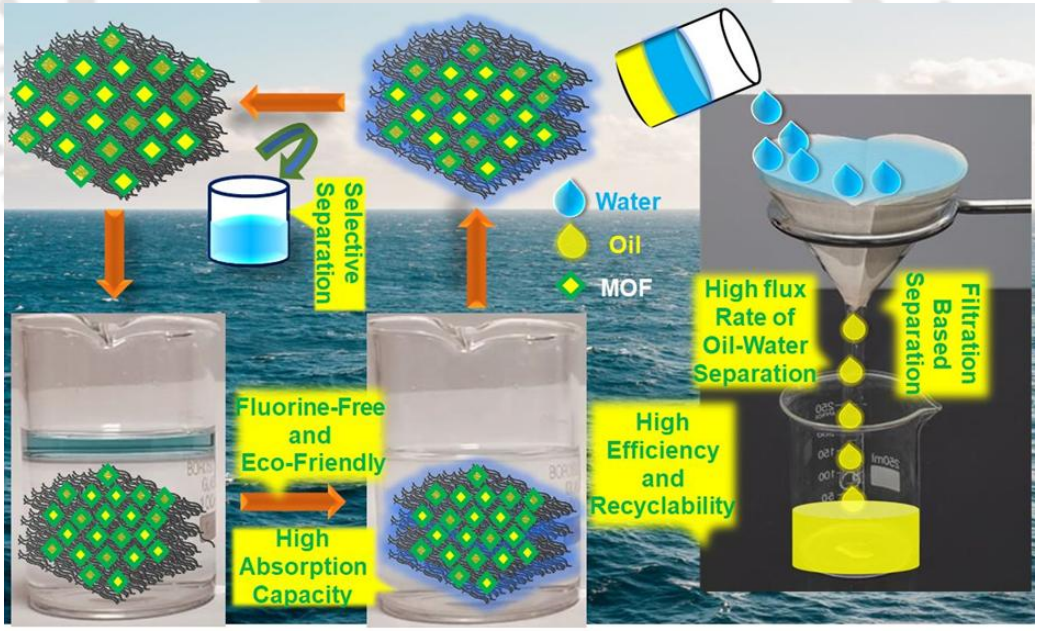

INORGANIC CHEMISTRY FRONTIERS

Abhijeet Rana, Subhrajyoti Ghosh and Shyam Biswas

1 Introduction

Water pollution is one of the prime concerns of an environmental scientist. Among the contaminants of water, oil is one of the major candidates. Therefore, separating oil from the oil-water mixture is a prime challenge for everyone working in this field. To work out one easy and ecologically sound solution, numerous materials have been developed to separate the oil-water mixtures employing superhydrophobic and superhydrophilic materials.[380] The superhydrophobic absorbent or membrane materials used for oil-water separation are metal mesh-based membranes,[381] sponge-based composites of fluorinated linkers,[382] fluorinated polymers, and aerogel materials.[383] The metal-based membrane has the threat of corrosion. The organic compound-based membranes or sponge composites are not very stable in organic solvent media and have the disadvantage of leaching from the composite. The fluorinated compound-based absorbent or membranes are not environmentally friendly due to the fluorine content. The fluorinated metal-organic framework-based materials dominate other materials due to stability and porosity and hydrophobic character.[384] The superhydrophobic-based MOFs reported up to the present time are made up of fluorinated linkers. The polyfluorinated compounds (PFCs) are highly persistent due to the strong bond between carbon and fluorine (the large electronegativity difference between fluorine and carbon).[385] The considerable exposure of PFCs to the human body has life risks. It was explained by Vieira et al. that exposure to perfluorooctanoic acid causes kidney, testicular, ovarian and prostate cancer and non-Hodgkin lymphoma.[386] The fluorinated materials are efficient and cheap but not environmentally sound. Although the superhydrophobic-based aerogel materials have good absorption capacity, these materials could not be used for filtration-based oil-water separation.[383]

The above-mentioned drawbacks of fluorinated materials insisted us to find a solution with equal efficiency and in an environmentally friendly manner. Having been concerned with the above facts and using the concept of nonpolar-nonpolar interaction, we replaced fluorine with a long-chain hydrocarbon. Oils are hydrocarbons and they are hydrophobic. Therefore, the material with a long-chain hydrocarbon could serve equally as a fluorinated material. Consequently, we synthesized palmitamidoterephthalic acid linker-based (BDC-NH-R, (R: -NH-CO-$(CH_2)_{14}$-CH_3)) Zr(IV)-UiO-66 MOF (Scheme 1). The polycrystalline MOF powder was utilized to make melamine and polymer-based (crosslinked PDMS-PHDMS) superhydrophobic sponge composite (**2′@sponge**). The WCA of the MOF powder was 168 °. The superhydrophobic crystalline MOF powder was inserted and adhered to the melamine sponge with the help of the PDMS-PHDMS crosslinked polymer to get one superhydrophobic and robust composite with an average WCA of 169 ± 1°. The adsorption capacity of the **2′@sponge** composite was better than the previously reported superhydrophobic composites, as shown in Table 3.4.

Additionally, we developed one superhydrophobic membrane (**2′@silk**) with the help of the above polymeric mixture of MOF and silk cloth. The separation efficiency was explored with the help of **2′@silk** membrane and **2′@sponge** composite by filtration-based and absorption-based separation. The separation efficiency was found to be more than 99% in both methods. The separation efficiency was better than previously reported oil-water separation materials (Table 3.4). The absorption capacity of the composite ranged between 43.8-97.2 $g \cdot g^{-1}$. The flux of oil-water separation varied between 58263 and 47416 $Lm^{-2}h^{-1}$ for filtration-based oil-water separation by **2′@silk**. The reusability of the melamine composite for oil-water separation was verified up to 70 times. At the same time, the **2′@silk** membrane was reusable at least up to 60 times for filtration-based oil-water separation. The **2′@sponge** composite and **2′@silk** membrane were designed strategically for environmental purposes. The composite and membrane are superior to the other hydrophobic materials based on absorption capacity,

separation efficiency and flux of oil separation from the oil-water mixture. The membrane and composite also showed good self-cleaning and antifouling nature.

3.2 Experimental Section

3.2.1 Synthesis of H_2L^2 Linker

The organic linker was synthesized using tetrahydrofuran (THF) as a solvent and pyridine as a base. 1 g (5.52 mmol) of 2-amino benzene-1,4-dicarboxylic acid and 1.75 mL (5.52 mmol) of palmitoyl chloride were taken in a round bottom flask containing 3.5 equivalents of pyridine. The mixture was refluxed for 24 h and then THF was evaporated. The resulting white powder was washed thoroughly with slightly acidic water to remove the excess pyridine. Further, it was washed with chloroform to remove any unreacted palmitoyl chloride to obtain the pure product. The ^{1}H NMR, ^{13C} NMR and HR-MS spectra are given below as Figure 3.1-3.3.

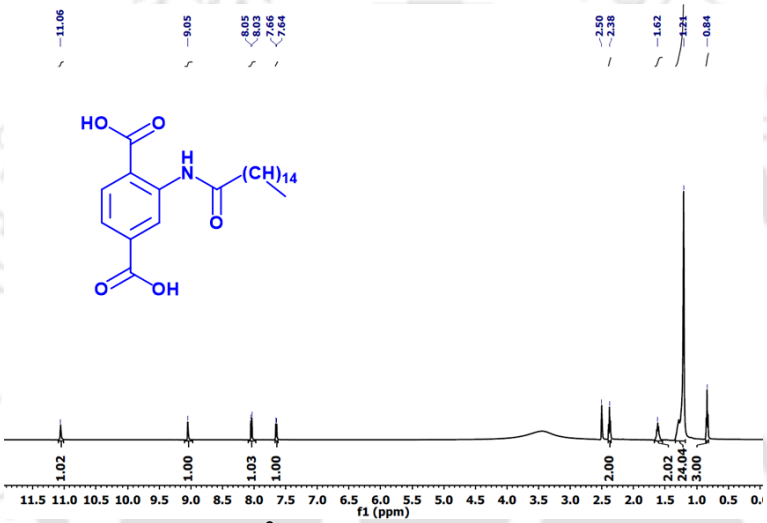

Figure 3.1 ^{1}H NMR spectrum of H_2L^2 linker in DMSO-d_6.

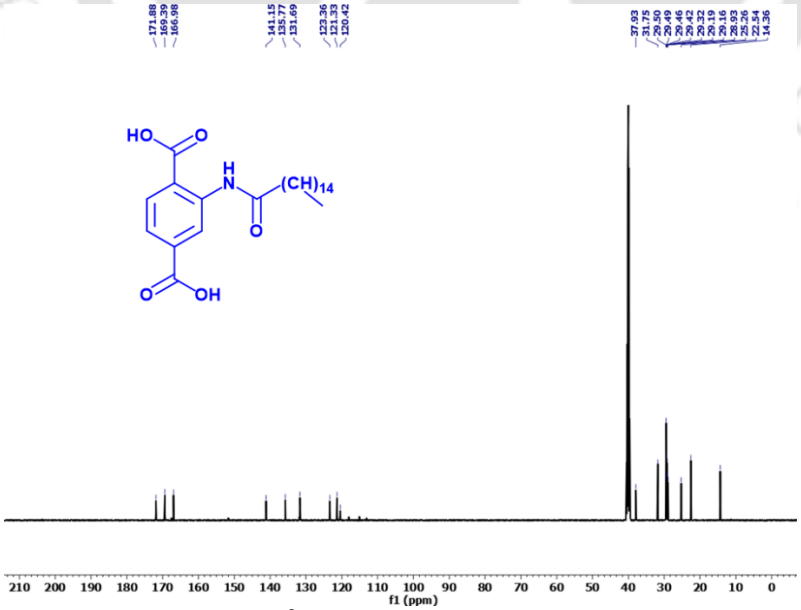

Figure 3.2 ^{13}C NMR spectrum of H_2L^2 linker in DMSO-d_6.

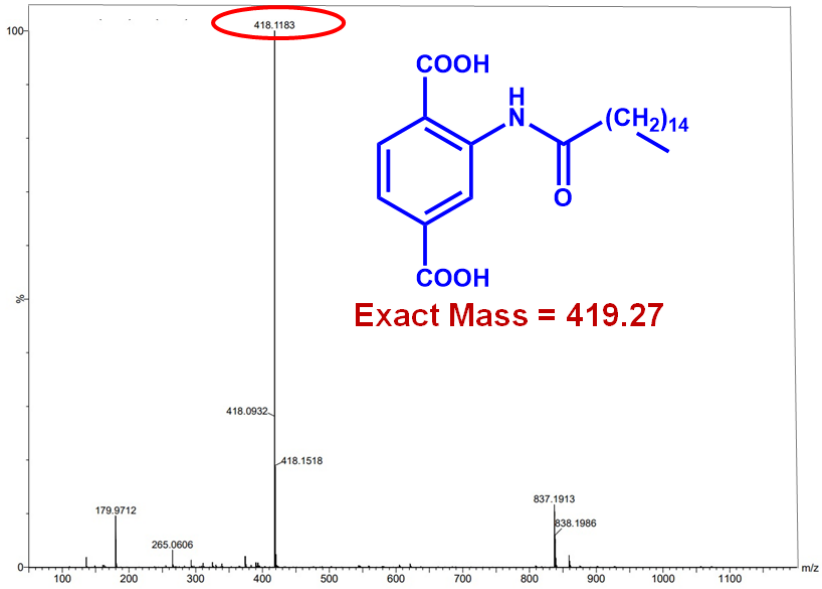

Figure 3.3 ESI-MS spectrum of H_2L^2 linker measured in methanol. The spectrum shows m/z peak at 418.1183, which corresponds to $(M-H)^-$ ion (M = mass of H_2L^2 linker).

3.2.2 Synthesis and Activation of $[Zr_6O_4OH_4(L^2)_6]\cdot 4H_2O\cdot 4DMF$ (2)

The superhydrophobic Zr(IV) MOF of UiO-66 topology was synthesized using a palmitamdoterephthalic acid. During synthesis optimization, in order to get good crystalline MOF material, $ZrOCl_2\cdot 8H_2O$, $ZrCl_4$, and $ZrN_2O_7\cdot xH_2O$ were used as metal salts. The monocarboxylic acids like trifluoroacetic acid (TFA), formic acid, acetic acid and benzoic acid were employed as modulators. *N,N*-dimethyl formamide (DMF), *N,N*-diethyl formamide (DEF) and *N,N*-dimethyl acetamide were utilised as solvents. After a systematic approach of solvothermal reactions for MOF synthesis, we received an optimized reaction condition using TFA as a modulator, $ZrOCl_2\cdot 8H_2O$ as metal salt and DMF as solvent at 140 °C for 24 h. **2** was synthesized using $ZrOCl_2\cdot 8H_2O$ (68 mg), H_2L^2 (100 mg) and TFA (1750 µL) in DMF (15 mL) at 140 °C (Scheme 3.1). The above mixture of metal salt, modulator, organic linker and solvent was sonicated for 15 min to get a clear solution. The transparent mixture was put into a 50 mL Teflon-lined autoclave and heated at 140 °C for 24 h to get a crystalline form of **2**. After 24 h, the obtained white powder was filtered, cleaned properly with DMF, then with acetone and dried. Yield: 101 mg (81%). ATR-IR data (cm^{-1}): 2924 (w), 2853 (w), 1656 (s), 1575 (s), 1425 (vs), 1264 (w), 770 (sh), 658 (sh), 475 (s). The material was named as **2**. The observed elemental analysis data: C 54.40 %, N 2.61 %, 6.69 % (calculated: C 54.44 %, N 2.65 %, 6.74 %).

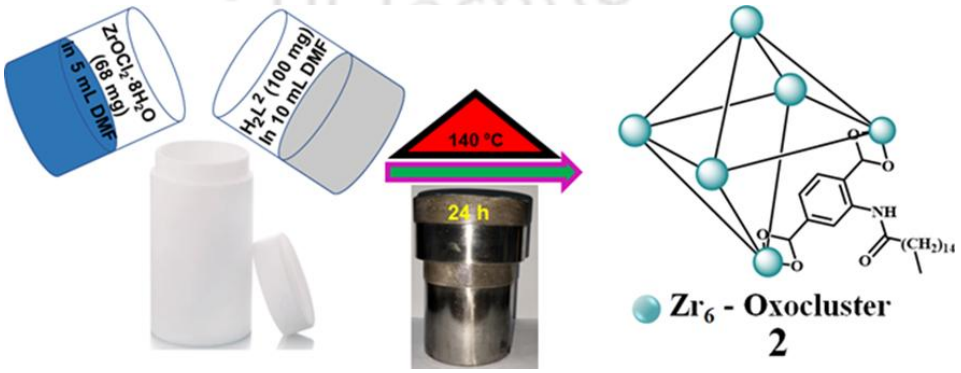

Scheme 3.1 Detailed synthesis route of **2**.

The obtained as-synthesized form of the material was stirred in methanol for 24 h. It was then filtered and vacuum dried at 100 °C for one day to get one solvent-free activated material named **2′**.

3.2.3 Synthesis of Superhydrophobic 2′@Sponge Composite and 2′@Silk Membrane

A superhydrophobic polymer-MOF composite and a membrane were synthesized following the previous work from our group with slight modifications.[387] In the first step (2 × 2 × 2 cm^3) size melamine sponges were cleaned by sonicating in a mixture of ethanol and acetone. Afterward a, 160 mg of dopamine was taken in an 80 mL solution of a 1:1 mixture of ethanol and water. Then 80 mL of 8.5 pH tris-buffer solution was added to the above dopamine hydrochloride solution. Thereafter ten pieces of clean and dried melamine were added and stirred for 24 h to obtain a black color dopamine coated sponge. In the next step, a crossed-linked polymer solution was prepared by mixing PDMS and PHMS in a 10:1 ratio and a 3 % dibutyltin dilaurate has added as a catalyst. Then PHMS and PDMS polymeric solutions were diluted 40 times instead of 25 times as in the case of prior work. Thereafter 50 gm of MOF powder was added per mL of polymeric solution and the mixed suspension was sonicated and heated at 40 °C for 1 h to cross-polymerise. The concentrated solution of the polymer causes the blockage of the pores of the dopamine-treated sponge in our previous work.[387] But after diluting the polymeric solution, the sponge's pores are more available to absorb the oils. The same polymeric solution was also utilized to synthesize a polymer-MOF-coated silk membrane. 10 cm^2 silk clothes were dipped into the PHMS and PDMS polymer-MOF suspension and then dried in a 130 °C oven (Scheme 3.2). The amount of MOF powder varied from 30-80 mg per mL of polymer solution, but the highest separation efficiency was obtained with the composite and membrane prepared from 50 mg/mL of polymer suspension. With lower MOF content, the filtration-based separation efficiency by the membrane is lower, and at very higher MOF content, the pores of the sponge and silk became blocked, which resulted in a less absorption capacity of **2′@sponge** and in the case of **2′@silk** membrane the flux of filtration-based oil-water separation was decreased due to pore blockage.

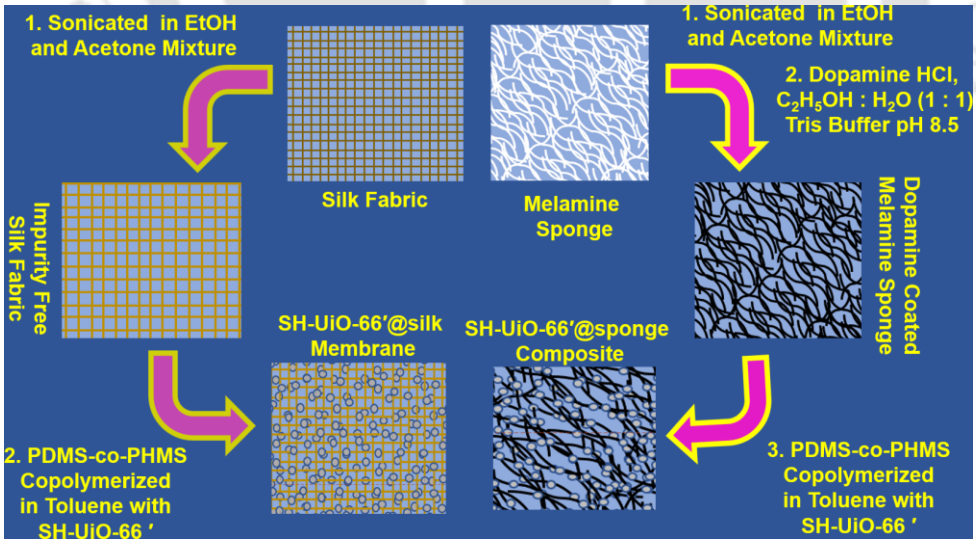

Scheme 3.2 Synthesis route of **2′@sponge** composite and **2′@silk** membrane.

3.2.4 Measurement of Absorption Capacities for Various Oils by 2′@Sponge Composite

For the absorption of various heavy and light oils, fully dry pre-weighed (~250-300 mg) **1′@sponge** composite was placed in various heavy oils ($CHCl_3$, CH_2Cl_2 and CCl_4) and light oils (hexane, ethyl acetate, petrol, diesel, crude oil, toluene, cyclohexane and kerosene). The

composites were kept in oil for 1 min to reach absorption equilibrium and then removed and weighed. All the experiments were performed at room temperature. Absorption capacities for various oils were calculated using the following formula:

Absorption capacity (g/g) = $(W_f-W_i)/W_i$, where W_i is the initial weight of **2′@sponge** and W_f is the weight of oil-absorbed **2′@sponge**. Five measurements were performed for each oil sample and the average value was plotted.

3.2.5 Absorption-Based Separation of Oil and Water by 2′@Sponge Composite

A single piece of dry pre-weighed **2′@sponge** composite (~250-300 mg) was placed in several oil/water combinations containing 3 mL of oil and 20 mL of water to separate the light oils (hexane, EtOAc, toluene, motor oil, gasoline and kerosene) from the surface of the water. For heavy oils (CH_2Cl_2, $CHCl_3$ and CCl_4), a piece of **2′@sponge** composite was brought into contact with the sediment oil for the separation of heavy oils from the oil/water combination from the bottom of the water. For each case, the **2′@sponge** composite selectively soaked the oils when it came into contact and the separated oil was recovered by physically squeezing the material. All the tests were performed at room temperature. Separation efficiency (%) for various oils was calculated using the following formula:

separation efficiency (%) = $V_f/V_i \times 100\%$, where V_i was the amount of oil used (mL) and V_f was the absorbed volume of water (mL). Five measurements were performed for each oil sample and the average value was plotted.

3.2.6 Filtration-Based Separation of Oils from the Oil-Water Mixture by 2′@Silk Membrane

To separate different oils using the filtration-based method of separation, a round shaped piece of **2′@silk** was bound with a round shaped solid circle and a mixture of different oils and water was allowed to pass through the membrane. The time needed for each step of the separation process was noted for each water-oil mixture.

The fluxes for the oil-water separation were determined using the formula: flux = $V/(A \times T)$ (where V = volume of separated oil, A = area of the membrane and T = time required for the separation of oil from the oil-water mixture).

3.2.7 Separation of Emulsions Using 2′@Silk Membrane

All the water-in-oil emulsions were prepared (water/$CHCl_3$, water/toluene, water/ kerosene and water/gasoline) by sonicating the water-oil mixtures for 60 min. To make the emulsion stable, 50 µL of surfactant **(**Triton X-100) was added to the oil-water mixture before sonication. Then, 4 mL (3.5 mL of oils in 0.5 mL of water) of different water-in-oil emulsions were allowed to pass through the **2′@silk** membrane. The time required for all the separation processes were recorded.

3.3 Results and Discussion

3.3.1 Characterization of 2

After the successful synthesis of **2** it was systematically characterized through various experiments. The PXRD data completely agreed that the synthesized material was of UiO-66 topology (Figure 3.4). The FE-SEM image of **2** showed homogenous crystalline particles (Figure 3.5). The EDX spectrum showed the presence of expected elements such as Zr, C, N, and O (Figure 3.6). The Pawley fit of the as-prepared material disclosed similar peak patterns with UiO-66 type MOF materials with very low R_p and R_{wp} values of 2.30 % and 3.60 %, respectively (Figure 3.7). The indexing of the slow scan PXRD data showed comparable lattice

parameters with UiO-66 topology (Table 3.1). The above-obtained results from various experiments confirmed that the synthesized material belongs to the UiO-66 family.

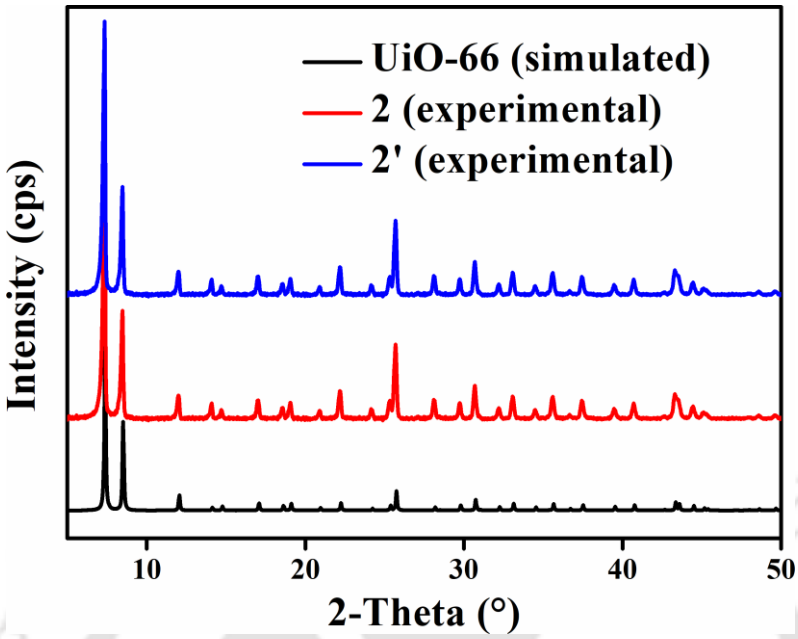

Figure 3.4. PXRD patterns of (a) UiO-66 (simulated), (b) **2** and (c) **2′**.

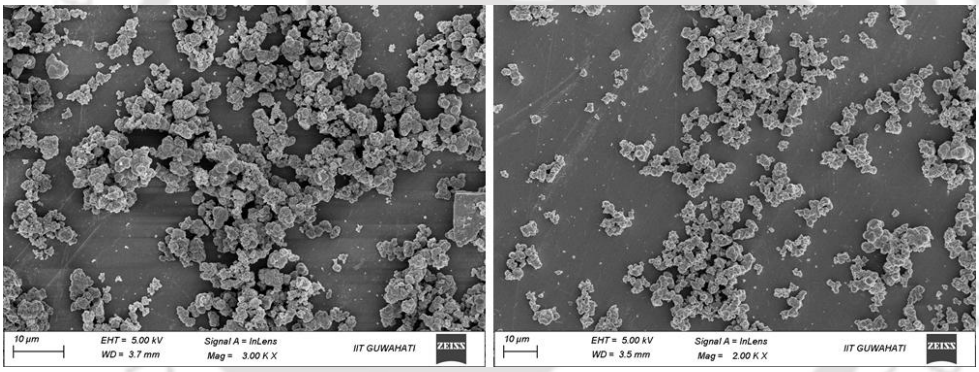

Figure 3.5 FE-SEM images of **2**.

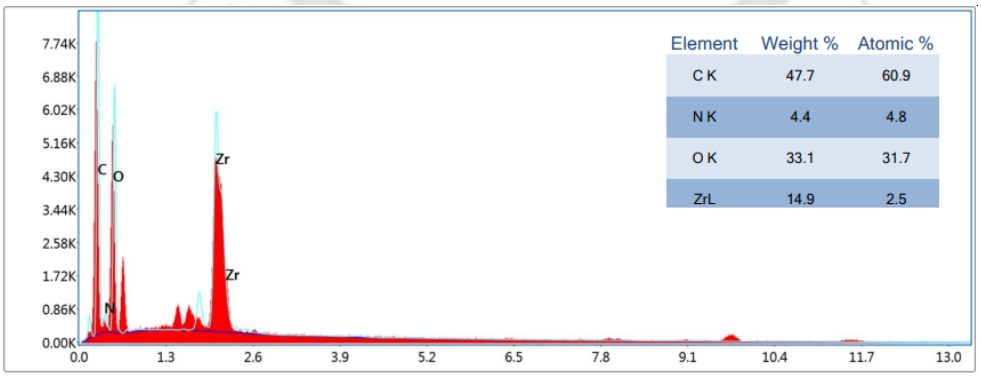

Figure 3.6 EDX spectrum of **2**.

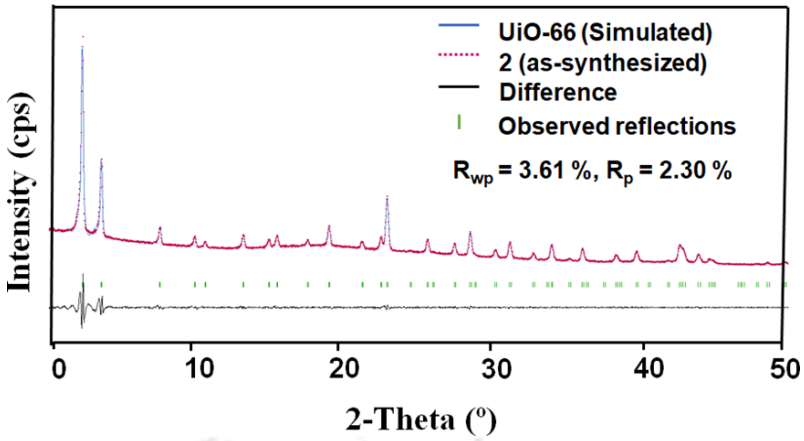

Figure 3.7 Pawley fit for the PXRD pattern of **2**.

Table S1. Unit cell parameters of **2** obtained by indexing its PXRD data. The obtained values have been compared with parent UiO-66 MOF.

Compound Name	**2**	UiO-66
Crystal System	cubic	cubic
a = b = c (Å)	20.753 (4)	20.790(3)
V (Å3)	8938.3 (29)	8985.9(9)

The FT-IR experiments were executed to confirm the existence of functional groups. The peaks at 1657 and 1425 cm^{-1} were due to the asymmetric and symmetric stretching frequency of the -COOH group of the linker (Figure 3.8). The peak of the $-COO^-$ group after synthesis of MOF was shifted to 1571 and 1378 cm^{-1} which confirmed the coordination between the carboxylate group of the linker and Zr(IV) metal center.[388] The carbonyl group of adsorbed DMF in **2** was at 1656 cm^{-1},[389] which decreased after the activation process.

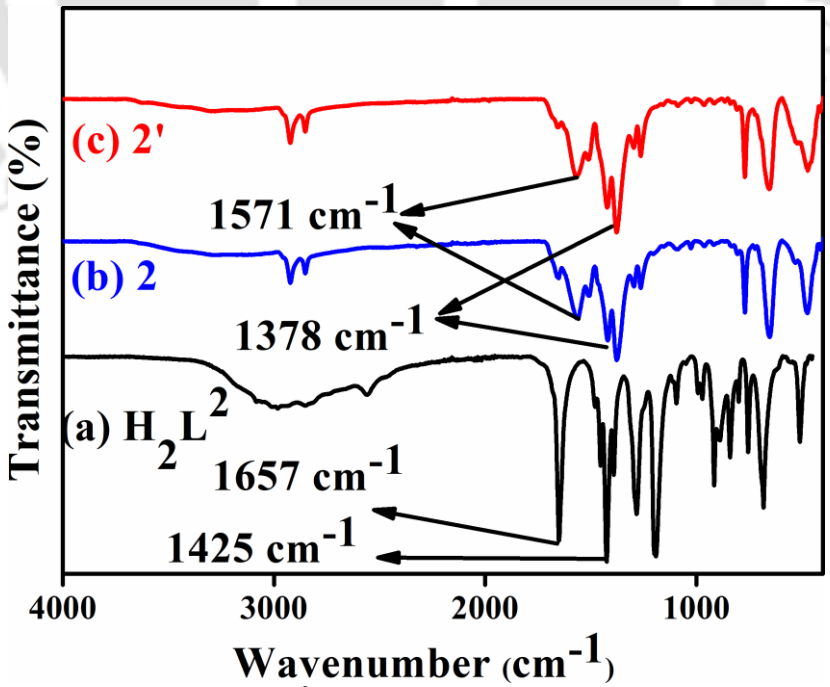

Figure 3.8 ATR-IR spectra of (a) H_2L^2 linker, (b) **2** and (c) **2′.**

The WCA measurement of **2′** was performed to know the hydrophobic nature of the material. The average WCA for **2′** was found to be 168°. The material with WCA above 90° is in the class of hydrophobic material and the material with WCA above 150° is under the category of superhydrophobic material.[390-391] The synthesized material is under the superhydrophobic class due to a WCA of 168° (Figure 3.9). The self-floating nature of **2′** in water and sinking nature in hexane supported the superhydrophobic and lipophilic nature of **2′** (Figure 3.10).

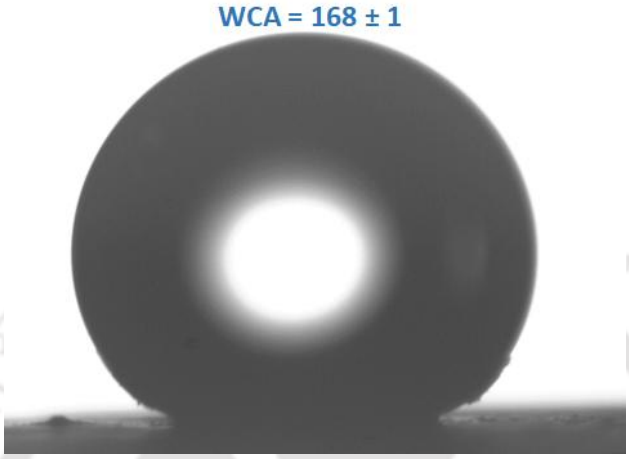

Figure 3.9 WCA measurement image of **2′.**

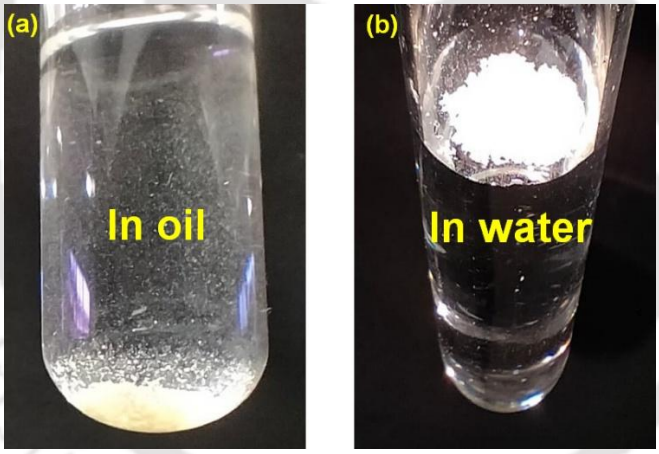

Figure 3.10 (a) Self-floating ability of **2′** in water and (b) oil (hexane).

The material was exposed to high temperature by thermogravimetric (TG) experiment at a rate of 4 °C per minute from 30 °C to 700 °C. We found a breakpoint at 105 °C in the TG curve of as-synthesized material due to the removal of 4 water molecules (2.4 % weight loss). Finally, the second breakpoint arose at 320 °C due to the removal of linkers from the secondary building units. The experimental weight loss between 105 and 320 °C was 8.7% (loss of 4 DMF molecules). The calculated weight loss due to water and DMF were 2.5% and 8.2% which were in good agreement with the experimental data. In the case of activated material, the TG trace displayed an almost straight line before decomposition due to the solvent exchange and vacuum drying to remove occluded solvent molecules from the pores (Figure 3.11). The thermogravimetric analysis confirmed that the material is stable up to 310 °C.

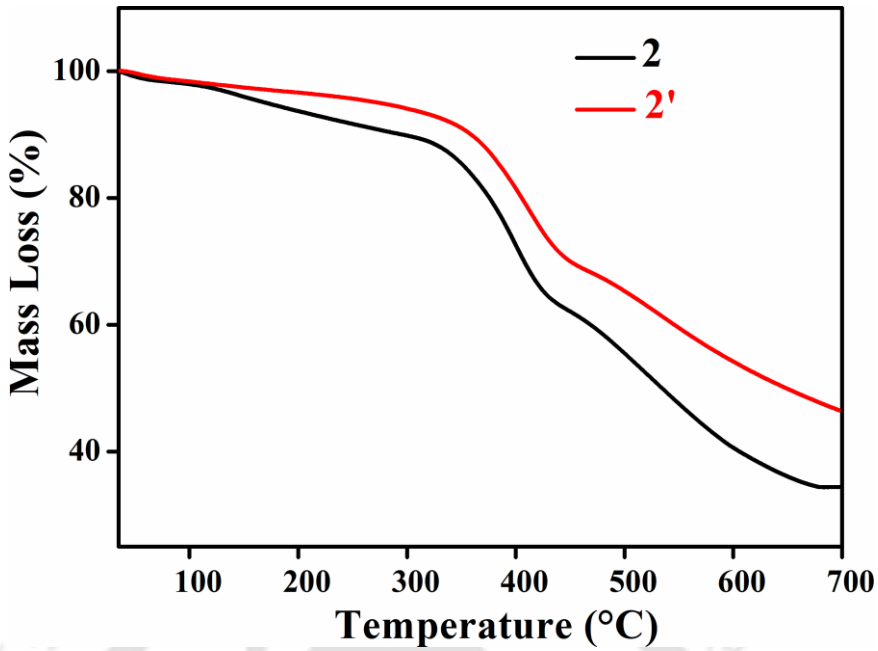

Figure 3.11 TGA curves of as-synthesized **2** (black) and activated **2′ (red)** recorded in N_2 atmosphere in temperature range of 30-700 °C at a heating rate of 4 °C min^{-1}.

The N_2 sorption analysis was performed for the activated form to find the porosity and surface area of the MOF. The specific BET surface area and pore volumes were 418 $m^{-2}g^{-1}$ and 0.21 $cm^{-3}g^{-1}$, respectively (Figure 3.12). The BET surface area of the material is high even after attaching such a bulky long-chain functional group. Therefore, there is a doubt that the long-chain functional group might detached from the original linker during the synthesis condition to produce a mixed linker based MOF. Therefore, we have taken the digested ^{1}H NMR spectra of **2′** in DMSO-D_6 digested with the help of HF. The ^{1}H NMR spectra attached in the supporting information section Figure 3.13 confirmed that form 18 % of the original linker the long-chain palmitoyl part was detached to provide a mixed MOF material with formula $Zr(OH)_4O_4(C_{24}H_{35}NO_5)_{4.92}(C_8H_5NO_4)_{1.08}$. Therefore, the mixed MOF material shows both the property of porosity and superhydrophobicity.

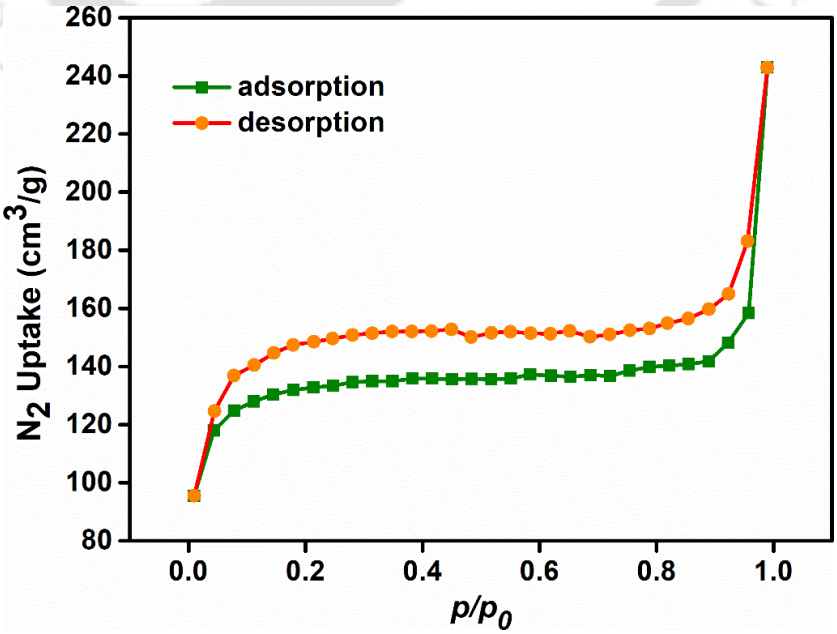

Figure 3.12 Nitrogen adsorption and desorption isotherms of **2′** recorded at –196 °C.

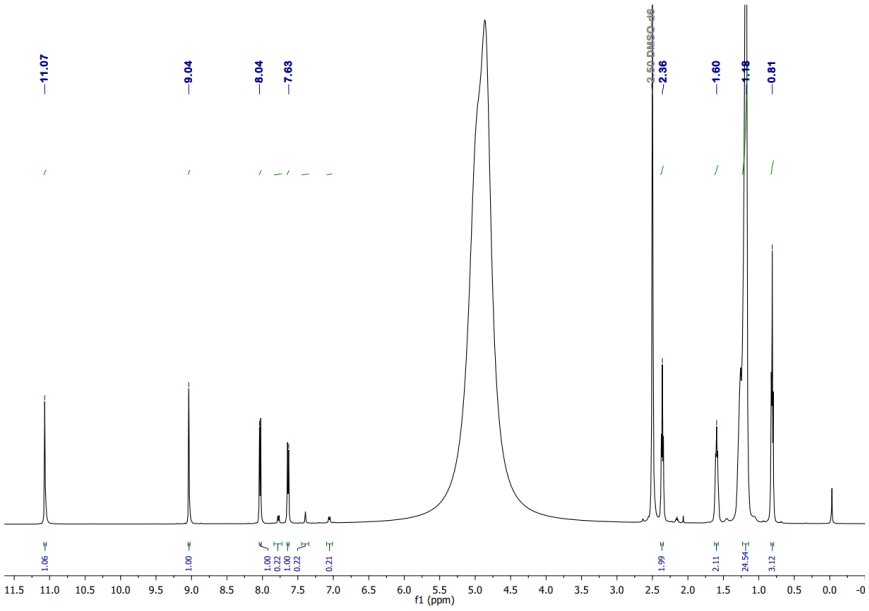

Figure 3.13 ^{1}H NMR spectra of **2′** in DMSO-d_6 after digestion by HF.

The chemical stability of the material was checked in different organic solvents, oils, pH solutions and seawater. The MOF powder was suspended in the above liquids for 24 hours and in seawater for four weeks. The PXRD and contact angle data were collected using the recovered samples (Figure 3.14-3.16, Table 3.2). The material retained its crystallinity after the chemical stability experiments and the contact angle was also comparable to **2′**. The obtained results confirmed that the synthesized material is chemically robust enough to be used for environmental applications.

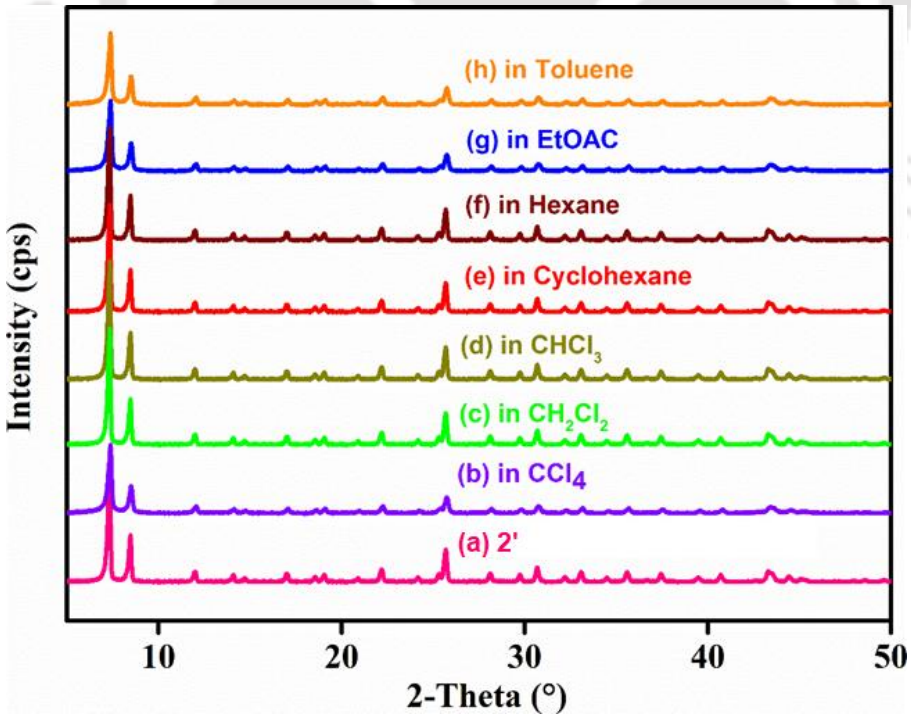

Figure 2.14 PXRD patterns of (a) **2′**and **2′** after stirring in (b) CCl_4, (c) CH_2Cl_2, (d) $CHCl_3$, (e) cyclohexane, (f) hexane, (g) EtOAc and (h) toluene.

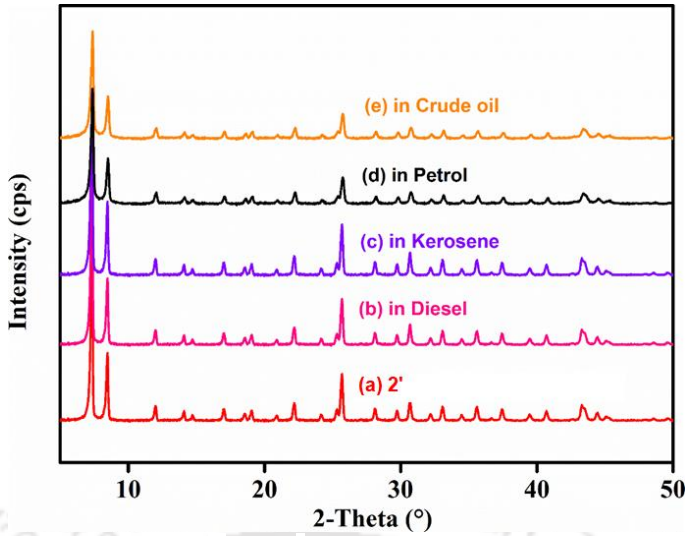

Figure 2.15 PXRD patterns of (a) **2′** and **2′** after stirring in (b) diesel, (c) kerosene, (d) petrol and (g) crude oil for 24 h.

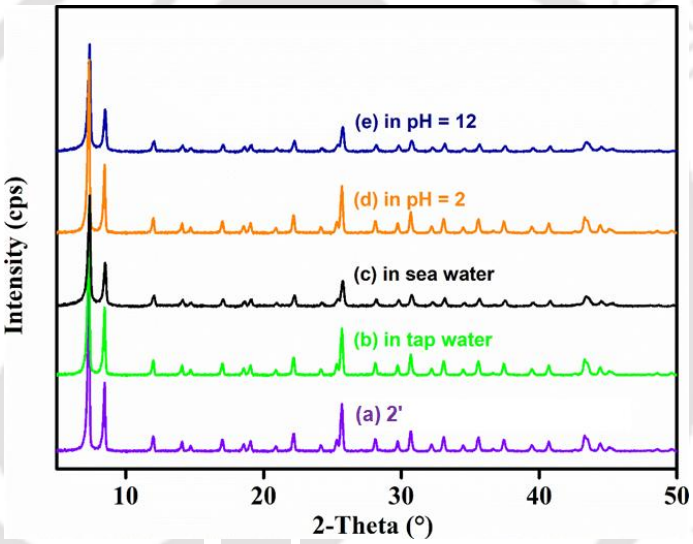

Figure 2.16 PXRD patterns of (a) **2′** and **2′** after stirring in (b) tap water, (c) sea water, (d) pH = 2 and (e) pH = 12 for 24 h.

Table 3.2 WCA of **2′** after treatment with different types of water and oil specimens.

Liquids	Average WCA of **2′** (°)
Fresh **2′**	168 ± 1
CCl_4	169 ± 2
$CHCl_3$	167 ± 2
CH_2Cl_2	168 ± 1
Hexane	167 ± 1
Cyclohexane	168 ± 2
EtOAc	166 ± 2
Toluene	168 ± 3
kerosene	167 ± 1
Diesel	167 ± 2
Petrol	166 ± 1

Crude oil	165 ± 3
Tap water	168 ± 1
pH = 2	167 ± 1
pH = 12	165 ± 2
Sea water	166 ± 1

3.3.2 Structural Description

Among the different classes of MOFs, UiO-66 (University of Oslo) is one of the chemically and thermally robust categories of materials. Generally, the UiO-66 topology-based MOFs are comprised of Zr(IV) or Hf(IV) metal centers and benzene-1,4-dicarboxylic acid (BDC) linkers. The BDC linker is bound to the metal oxo-cluster by the oxygen atom of the carboxylate linker. The metal oxo cluster is formed by the 4-μ_3-OH and 4-μ_3-O bridges.[392] The metal oxo cluster is made up of a metal center, oxygen and hydroxide groups without any organic moiety. The oxo-cluster without any organic moiety is also known as an inorganic secondary building subunit (SBUs) with the formula $M_6(OH)_4O_4$(M: Hf, Zr).[345] The metal in the +4 oxidation state behaves as a hard acid and carboxylate oxygen as a hard base to give strong bonding between them. The strong binding between the BDC linker and metal oxo cluster resulted in the formation of a face-centered cubic 3D structure.[393] The 3D framework possesses small tetrahedral voids and large octahedral voids. In this work, we synthesized a zirconium MOF using H_2L^2 as an organic ligand. The PXRD pattern of the as-synthesized material **2** wholly matched with the UiO-66 simulated pattern and additional support to the UiO-66 was found from the Pawley plot and indexing data. The obtained parameters from indexing closely agreed with the UiO-66 MOFs and the Pawley fit pattern almost precisely matched with the simulated UiO-66 MOFs.

3.3.3 Characterization of Superhydrophobic 2′@Sponge Composite and 2′@Silk Membrane

The digital images of both the **2′@sponge** composite and **2′@silk** membrane are displayed in Figure 3.17. Both superhydrophobic composite and membrane were characterized by PXRD, FT-IR, FE-SEM and EDX analyses. The PXRD patterns of both **2′@sponge** composite and **2′@silk** membrane have similar peaks as the MOF material itself (Figure 3.18). The FT-IR peaks of the **2′@sponge** and **2′@silk** membrane confirmed the successful immobilization of MOF particles to the silk fiber and dopamine-coated sponge (Figure 3.19). The elemental analysis also supported the successful integration of MOF particles onto the melamine sponge and silk fibers (Figure 3.20-3.21). The FE-SEM image of the **2′@sponge** and **2′@silk** membrane showed the adhesion of MOF particles to the threads of silk and melamine sponge (Figure 3.23a-3.23b) when compared with the FE-SEM image of only polymer-coated sponge and polymer coated silk (Figure 3.22a-3.22b). The digital images of water droplets on the surface of the **2′@sponge** and **2′@silk** membrane are exhibited in Figure 3.24.

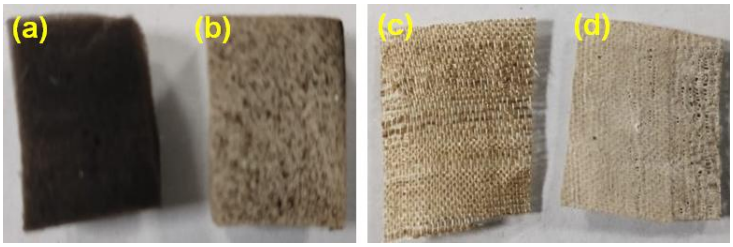

Figure 3.17 Digital images of (a) polymer-coated sponge, (b) **2′@sponge composite**, (c) polymer-coated silk membrane and (d) **2′@silk** membrane.

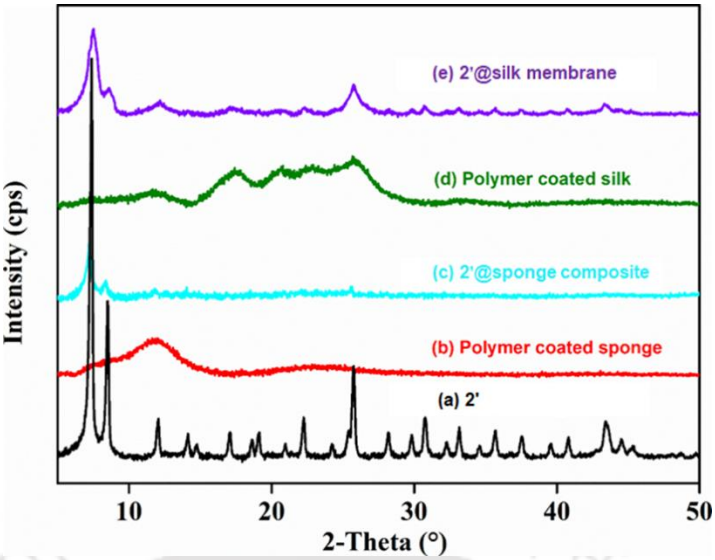

Figure 3.18 PXRD patterns of (a) activated **2′** (b) **2′** polymer-coated sponge (c) **2′@sponge** composite and (d) polymer-coated silk membrane and (e) **2′@silk** membrane.

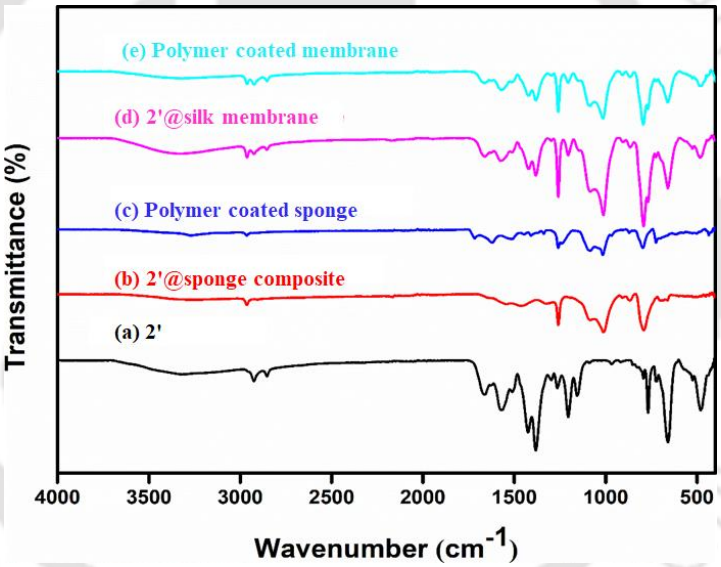

Figure 3.19 ATR-IR spectra of (a) activated **2′**, (b) polymer-coated sponge, (c) polymer-coated membrane, (d) **2′@sponge** composite and (e) **2′@silk** membrane.

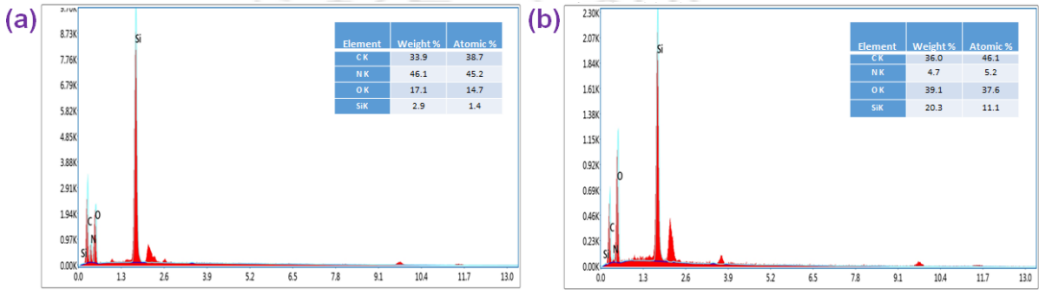

Figure 3.20 EDX spectrum of (a) melamine sponge and (b) sheet of silk.

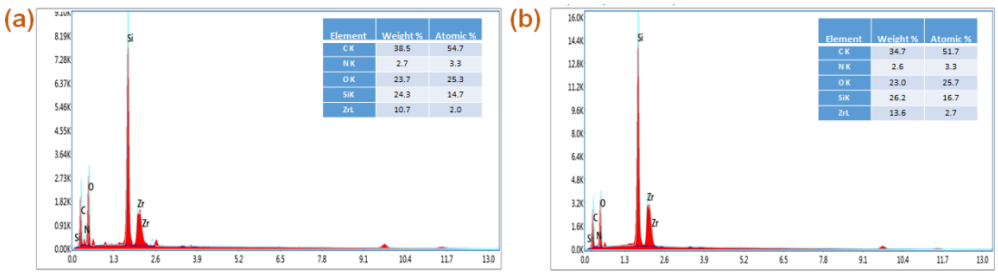

Figure 3.21 EDX spectrum of (a) **2′@sponge** composite and (b) **2′@silk** membrane.

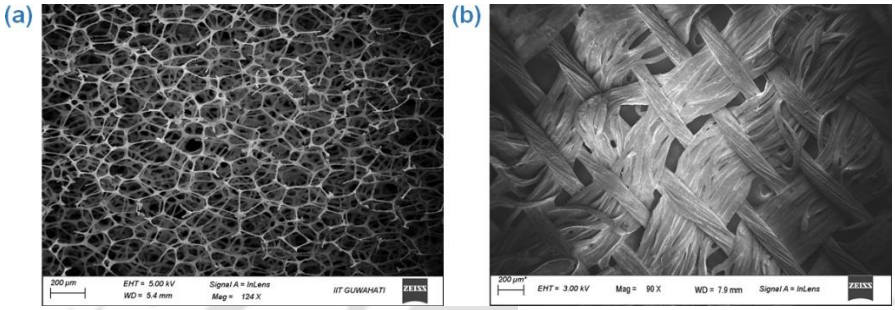

Figure 3.22 High-resolution FE-SEM images of (a) melamine sponge and (b) silk sheet.

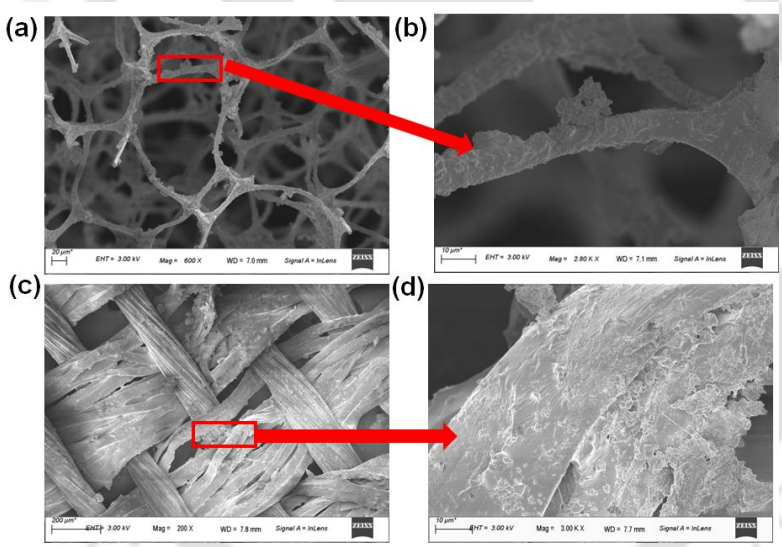

Figure 3.23 FE-SEM image of **2′@sponge** (a, b) and **2′@silk** (c, d).

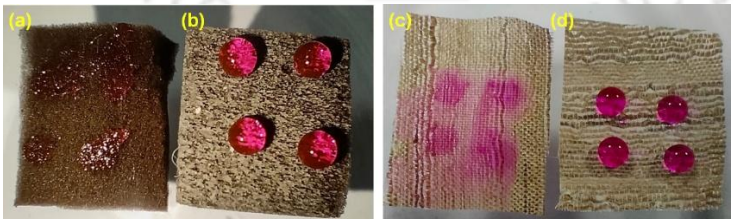

Figure 3.24 Digital image of beaded water droplets on the surface of (a) polymer-coated sponge, (b) **2′@sponge** composite, (c) polymer-coated membrane and (c) **2′@silk** membrane.

The WCA of the **2′@sponge** and **2′@silk** membrane was found to be 169 ± 1° (Figure 3.25) respectively. As the value of WCA is more than 150°, both the **2′@sponge** and **2′@silk** membrane belong to the class of superhydrophobic materials. The WCA of the polymer-coated sponge and silk membrane without MOF was only 106 ± 1° and 109 ± 1° which proved that

the arrival of superhydrophobicity was only due to the superhydrophobic MOF powder. The hydrophobicity of the **2′@sponge** and **2′@silk** membrane was also confirmed by their self-floating nature. In sharp contrast, the polymer-coated sponge and silk membrane without MOF were unable to float on the surface of the water as they do not possess any hydrophobic nature (Figure 3.26). Again, the BET surface area of both the **2′@sponge** and **2′@silk** membrane were examined which prove that the porosity of the composite and sponge arose due to the successful immobilization of porous MOF on the surface of sponge and silk (Figure 3.27), the porosity of composite were calculated with respect to wight of composite.

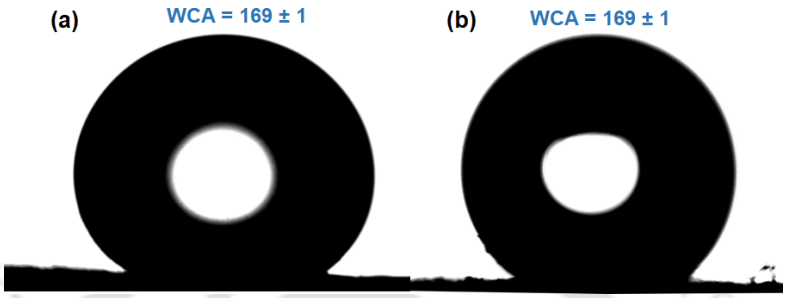

Figure 3.25 The contact angle image of beaded water droplets on the surface of (a) **2′,** (b) **2′@sponge** composite and (b) **2′@silk** membrane.

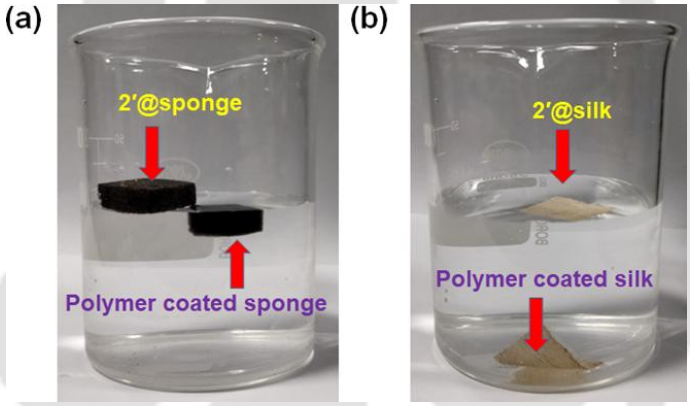

Figure 3.26 (a) Digital images of floating **2′@sponge** composite and immersion of polymer-coated melamine sponge. (b) Digital images of floating **2′@silk** membrane on water and immersion of polymer-coated silk fabric in water.

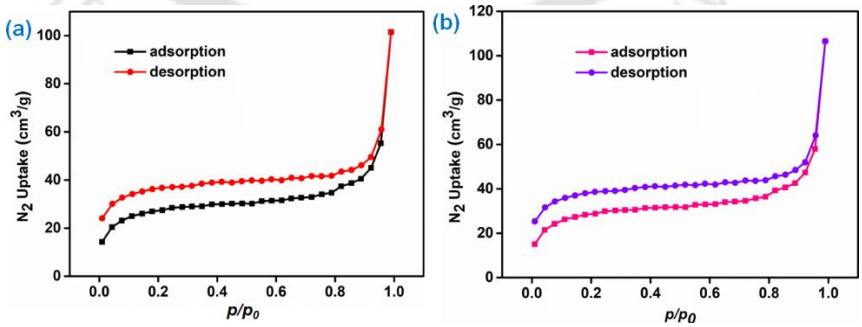

Figure 3.27 Nitrogen adsorption and desorption isotherms of (a) **2′@sponge** and (b) **2′@silk** recorded at –196 °C.

After the successful design of the **2′@sponge** and **2′@silk** membrane, the durability of the composite and membrane in a different chemical environment was demonstrated in order to be applicable for real-field purposes. The chemical stability of the composite and membrane was

shown by putting the composite and membrane in different oils, organic solvents, pH solutions and seawater. The PXRD, FT-IR and contact angle measurements were performed after the chemical stability tests (Figure 3.28 to 3.31 and Table 3.3). The crystallinity, functionality and superhydrophobicity were retained for both **2′@sponge** and **2′@silk** membrane after the stability experiments, which confirmed that the material is stable enough to be applicable for environmental applications.

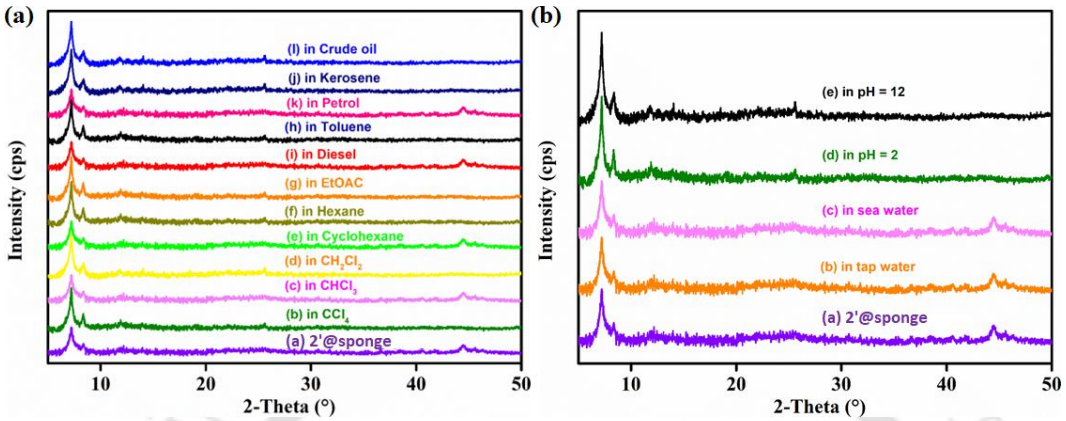

Figure 3.28 (a) PXRD patterns of **2′@sponge** composite after treatment with different types of oil and (b) after stirring in different water specimens.

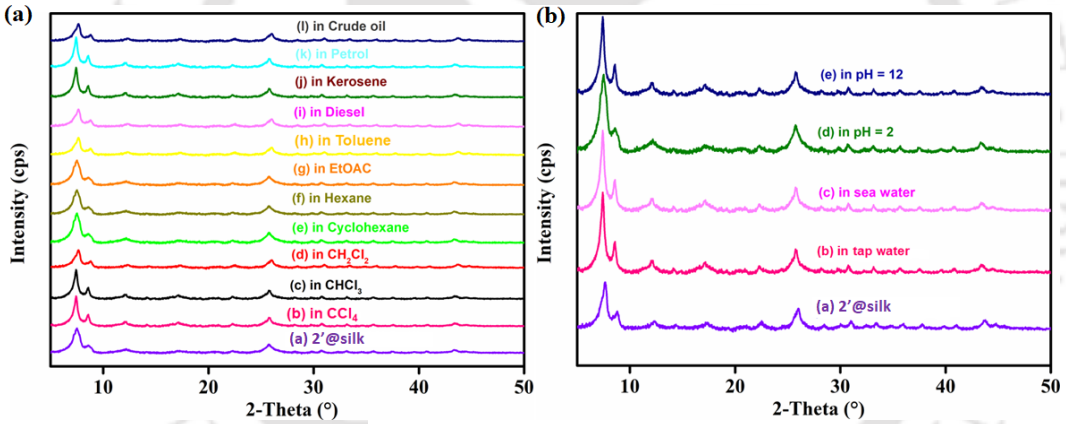

Figure 3.29 (a) PXRD patterns of **2′@silk** composite after treatment with different types of oil and (b) after stirring in different water specimens.

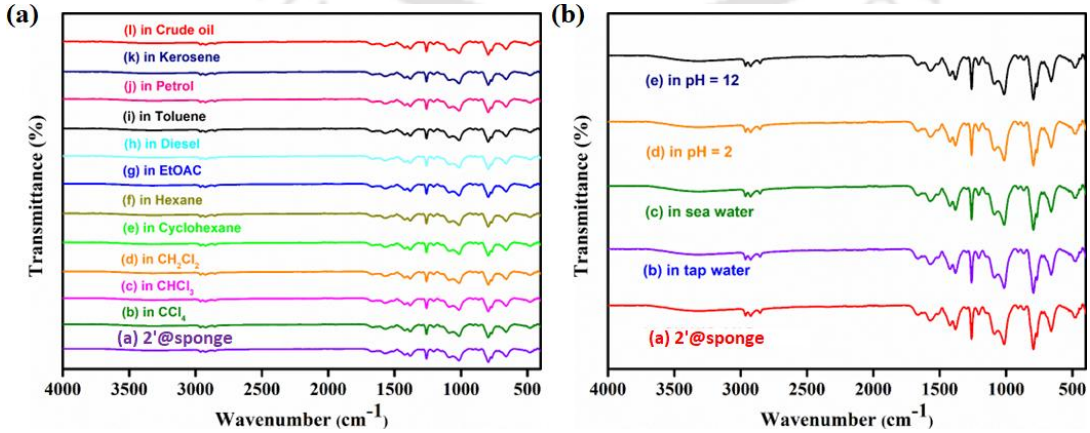

Figure 3.30 (a) ATR-IR spectra of **2′@sponge** composite after treatment with different types of oil and (b) after stirring in different water specimens

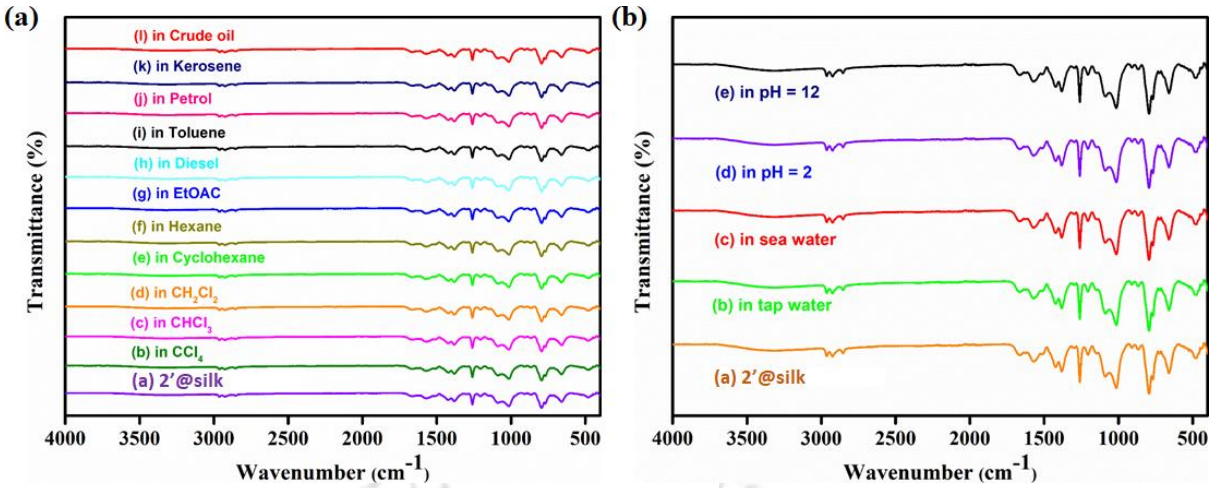

Figure 3.31 (a) ATR-IR spectra of **2′@silk** composite after treatment with different types of oil and (b) after stirring in different water specimens.

Table 3.3 WCA of **2′@sponge** and **2′@silk** after treatment with different types of water and oil specimens.

Liquids	Average WCA of **2′@sponge** and **2′@silk** (°) after stirring in different liquids
Fresh **2′@sponge** and **2′@silk** (°)	169 ± 1 and 169 ± 1
CCl_4	167 ± 1 and 168 ± 2
$CHCl_3$	169 ± 2 and 168 ± 1
CH_2Cl_2	167 ± 2 and 168 ± 1
Hexane	167 ± 2 and 167 ± 2
Cyclohexane	166 ± 2 and 168 ± 1
EtOAc	167 ± 1 and 168 ± 2
Toluene	169 ± 2 and 167 ± 2
kerosene	167 ± 2 and 167 ± 1
Diesel	167 ± 2 and 168 ± 1
Petrol	167 ± 1 and 169 ± 2
Crude oil	169 ± 2 and 167 ± 2
Tap water	169 ± 2 and 169 ± 1
pH = 2	166 ± 1 and 167 ± 2
pH = 12	166 ± 2 and 165 ± 3
Sea water	165 ± 2 and 167 ± 2

3.3.4 Absorption and Filtration-Based Oil-Water Separation by 2′@Sponge Composite and 2′@ Silk Membrane

The absorption-based oil-water separation was explored for the **2′@sponge** composite. A mixture of 5 mL of water and 5 mL of $CHCl_3$ was prepared. For visualization purposes, $CHCl_3$ was colored with Rhodamine B. The composite was dipped into the mixture to absorb the heavy underwater $CHCl_3$ selectively. A similar process was repeated, taking hexane and water for the absorption-based separation of light oil from the oil-water mixture. The absorption capacity of the composite in $g \cdot g^{-1}$ was calculated using the formula W_1-W_0/W_0 (W_0 is the weight of the composite before the absorption of oil and W_1 is the weight of the composite after absorption of the oil). The absorption capacity of the **2′@sponge** composite ranged between 43.8 and 97.2

$g \cdot g^{-1}$ (Figure 3.32a). It is comparable with other sponge-based fluorinated absorbents and higher than the fluorine-free absorbent documented to date (Table 3.4). The **2′@sponge** composite displayed a higher absorption capacity due to the use of dilute polymeric solution, which helped in availing the pores of the sponge to absorb oil. The separation efficiency of the composite was calculated using the formula $1-((V_1-V_0)/V_0)$ (V_0 is the volume of oil taken and V_1 is the recovered volume of oil by the composite). The separation efficiency of the composite was higher than 99% for oils (Figure 3.32b). The material was also recyclable up to 70 cycles due to the strong binding of superhydrophobic MOF particles to the sponge with the help of the cross polymerized PHMS-PDMS. The loss of separation efficiency after the 70th cycle was only 7.6% taking petrol as the model oil (Figure 3.33a).

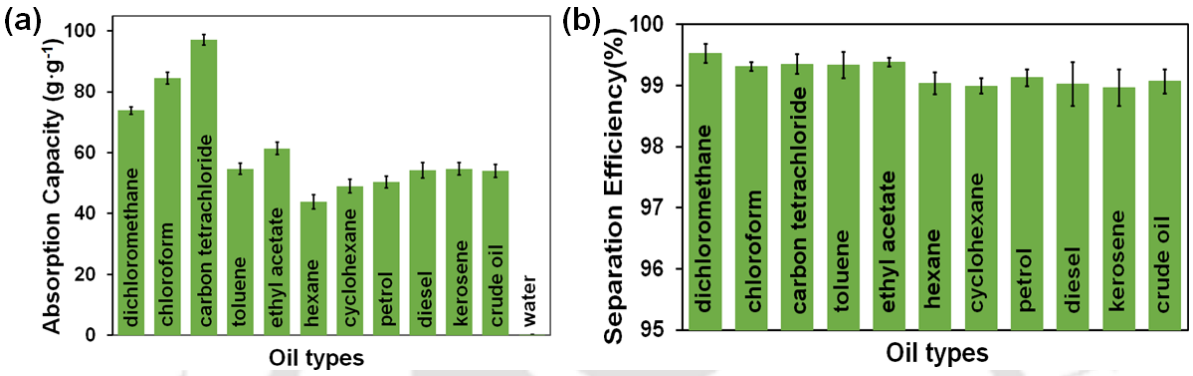

Figure 3.32 (a) Absorption capacity of **2′@sponge** composite in $g \cdot g^{-1}$. (b) Separation efficiency of **2′@sponge** composite in percentage.

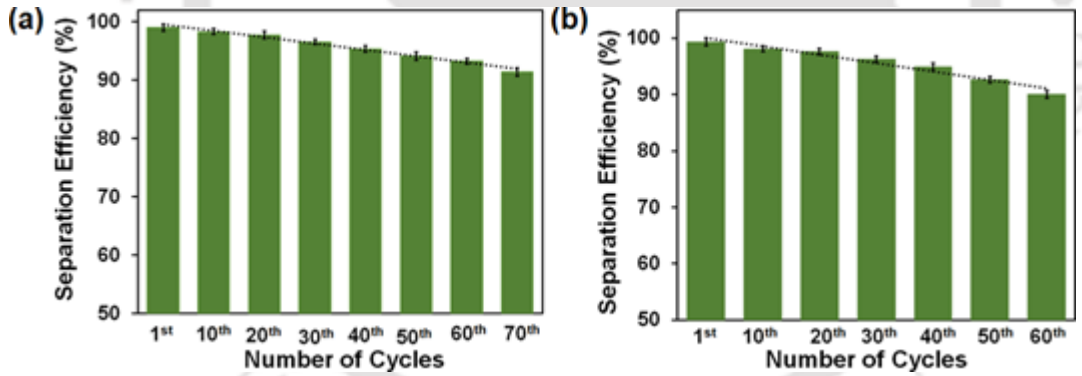

Figure 3.33 Reusability of **2′@sponge (a) and 2′@silk (b) composite** for oil/water separation experiments (model oil: petrol).

The thinness of **2′@silk** the membrane allows the speedy separation of oil through the **2′@silk** membrane. The filtration-based oil-water separation was carried out through the use of membrane **2′@silk**. The separation efficiency of the membrane was also calculated as using the above formula mentioned above for adsorption-based oil-water separation by **2′@sponge** composite. The separation efficiency for filtration-based oil-water separation by **2′@silk** is near about 99% for different oils and organic solvents (Figure 3.34a). The flux of oil separation was 58263-47416 $Lm^{-2}h^{-1}$ (Figure 3.34b), which is much higher than recent literature reports (Table 3.4). Hence, the fluorine-free superhydrophobic **2′@silk** membrane is environmentally friendly and advantageous over the other reported material. Furthermore, the reusability of the **2′@silk** composite was verified, the **2′@silk** composite is found to be reusable up to 6oth cycle without losing its separation efficiency to a significant extent (Figure 3.33b).

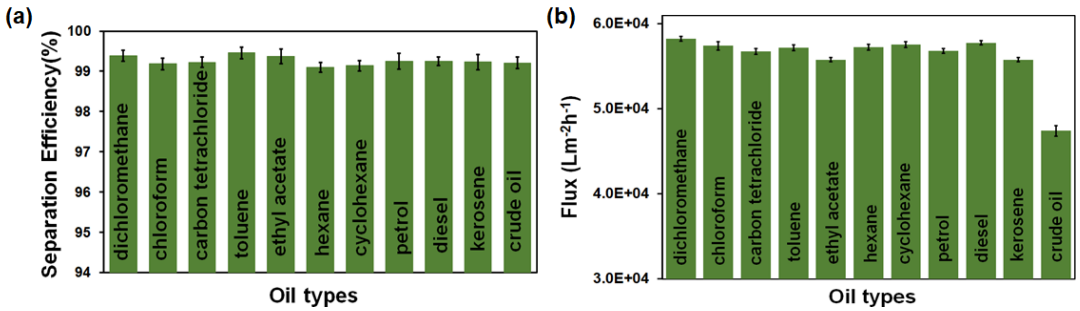

Figure 3.34 (a) Separation efficiency of **2′@silk** membrane towards various oils in percentage. (b) Flux of oil-water separation by different oils in $Lm^{-2}h^{-1}$.

The cross-polymer inhibits the leaching of MOF particles from the sponge composite and silk membrane. The FE-SEM, EDX, FT-IR, PXRD and contact angle of **2′@silk** membrane and **2′@sponge** composite were measured after the 70th cycle. All the above experimental data proved that the MOF material is stable and it was also present on the surface of the sponge (Figure 3.35 to 3.39,). This work is the first-ever report of fluorine-free superhydrophobic MOF composite to date. The separation efficiency of the **2′@sponge** composite and **2′@silk** membrane after the 70th cycle in seawater, lake water, tap water, pH 12 and pH 2 did not decrease to a considerable amount (Figure 3.40). The fluorine-free composite is environmentally friendly and efficient over the other fluorinated composites. The fluorine free long chain hydrocarbon functionalized superhydrophobic MOFs developed by various research groups for oil-water separation are synthesized by post-synthetic modifications.[394-396] The post-synthetic modification always suffers from less functional conversion which leads to the poor recyclability and absorption capacity of the materials, as shown in Table 3.4.

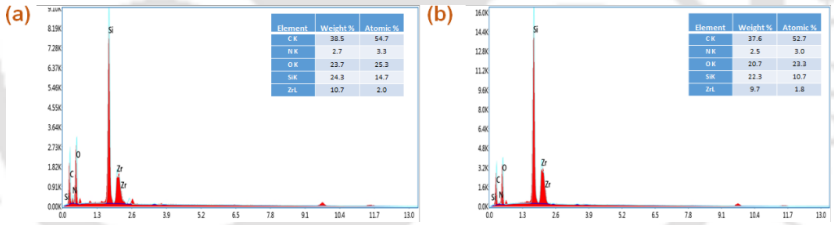

Figure 3.35 (a) EDX spectrum of **2′@sponge composite and (b) 2′@silk** after 70th and 60th cycle of oil-water separation experiments, respectively.

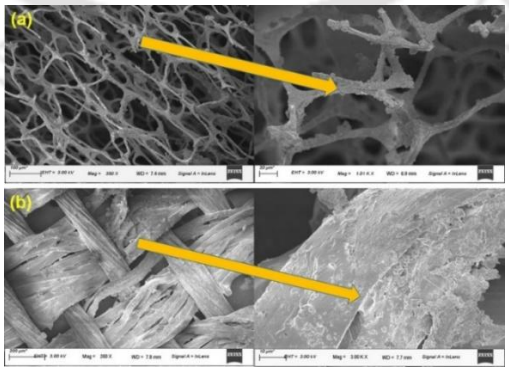

Figure 3.36 (a) High-resolution FE-SEM images of **2′@sponge composite and (b) 2′@silk** after 70th and 60th cycle of oil-water separation experiments, respectively.

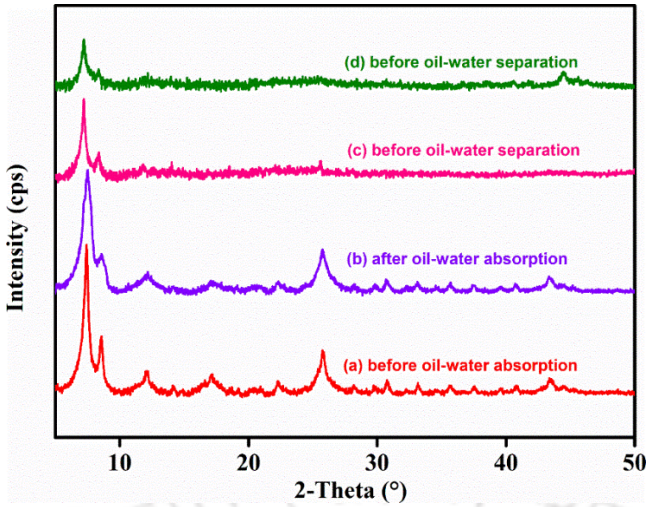

Figure 3.37 PXRD patterns of **2′@sponge composite (a) before and** (b) after oil absorption experiments and **2′@silk** membrane (c) before and (d) after oil-water separation experiments.

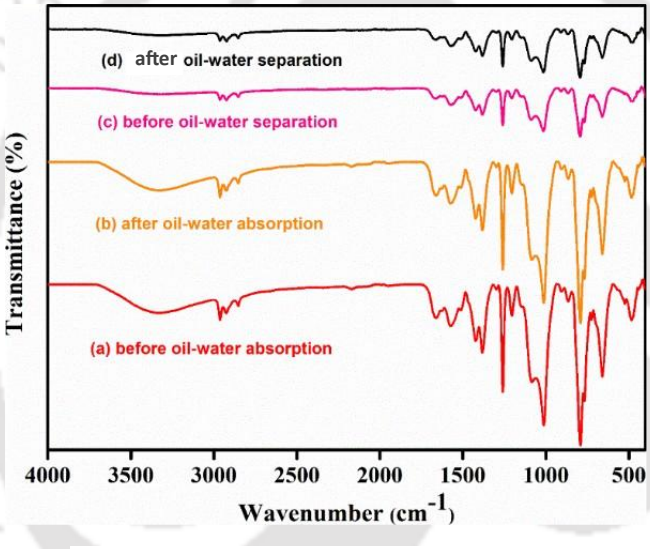

Figure 3.38 ART-IR of **2′@sponge** composite (a) before and (b) after oil absorption experiments and **2′@silk** membrane (c) before and (d) after oil-water separation experiments.

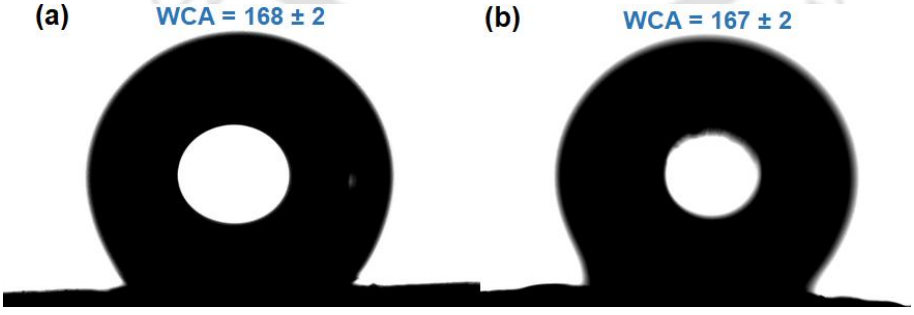

Figure 3.39 WCA of **2′@sponge** composite (a) after oil absorption experiments and **2′@silk** membrane (b) after oil-water separation experiments.

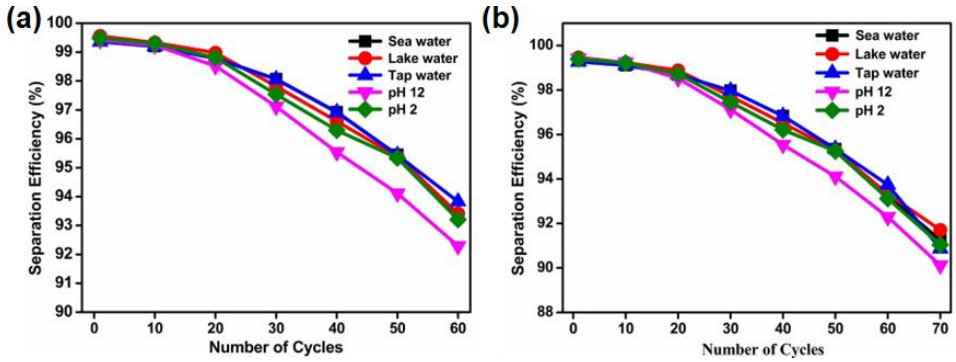

Figure 3.40 Change of absorption-based separation efficiency of oil-water by (a) **2′@silk** membrane and (b) **2′@sponge** composite up to 60th cycle and 70th in various hazardous conditions respectively.

3.3.5 Self-cleaning and Antifouling Nature of 2′@sponge Composite and 2′@silk Membrane

The self-cleaning nature has mostly been explored by many research groups by cleaning the sand or dry grass particles from the surface of the material by adding water droplets. But, the above way of exploration of self-cleaning nature has no link between the oil-water separation materials for environmental applications. The materials should keep themselves clean in dirty environments in order to be applicable in the marine system. Therefore, we prepared a mixture of clay and Rhodamine B. The membrane and composite were dipped into the above mixture. It was observed that the solution did not adhere to the surface of the **2′@sponge** composite and **2′@silk** membrane, as shown in Figure 3.41. When applied, the polymer-coated sponge composite and membrane were unable to maintain the self-cleaning nature. The self-cleaning nature of the above composite and membrane avoids the adhesion of any nutrient or soil material that could help them develop fouling. The above result confirmed the self-cleaning and antifouling nature of composite and membrane. The PXRD, FT-IR, FE-SEM, EDX and WCA measurements confirmed that material possesses the similar properties before and after the self-cleaning experiment (Figures 3.42-3.46).

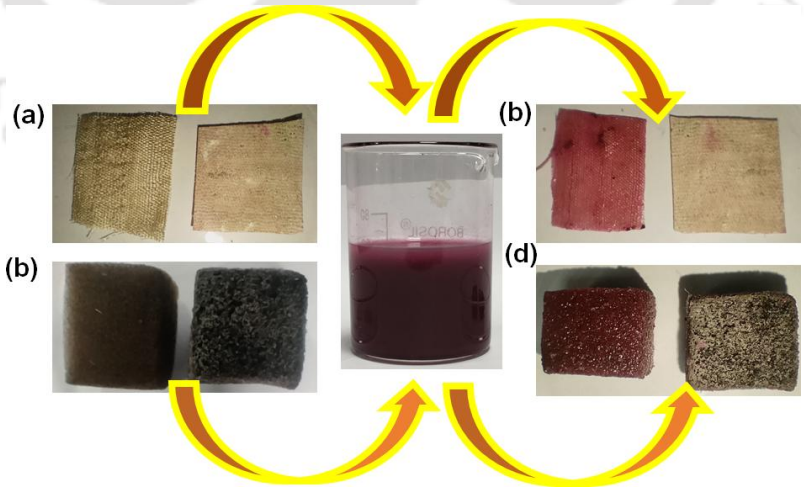

Figure 3.41 Digital image of **2′@silk** membrane and polymer-coated silk (a) before and (b) after self-cleaning and **2′@sponge** composite (c) before and (d) after self-cleaning.

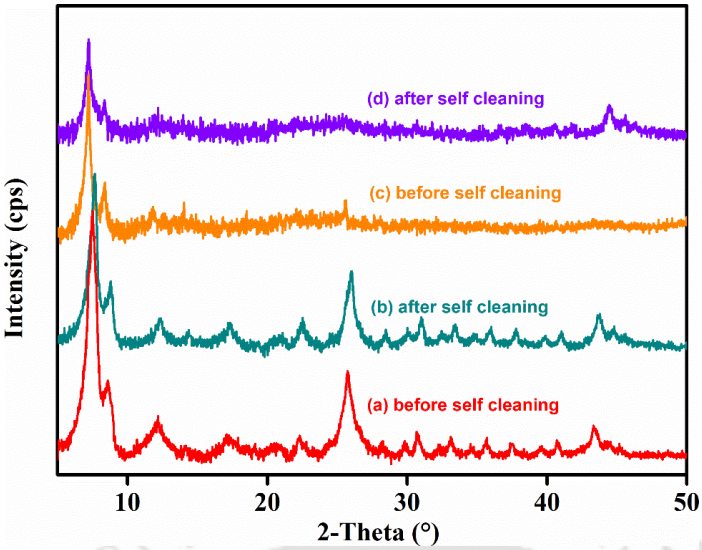

Figure 3.42 PXRD patterns of **2′@sponge** (a) before and (b) after self-cleaning and **2′@silk** (c) before and (d) after self-cleaning.

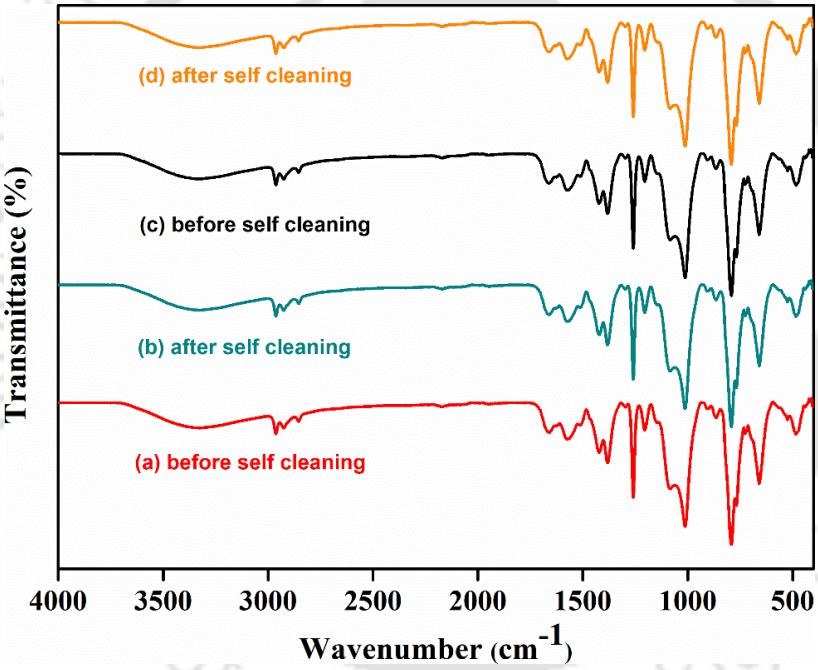

Figure 3.43 ART-IR spectra of **2′@sponge** (a) before and (b) after self-cleaning and **2′@silk** (c) before and (d) after self-cleaning.

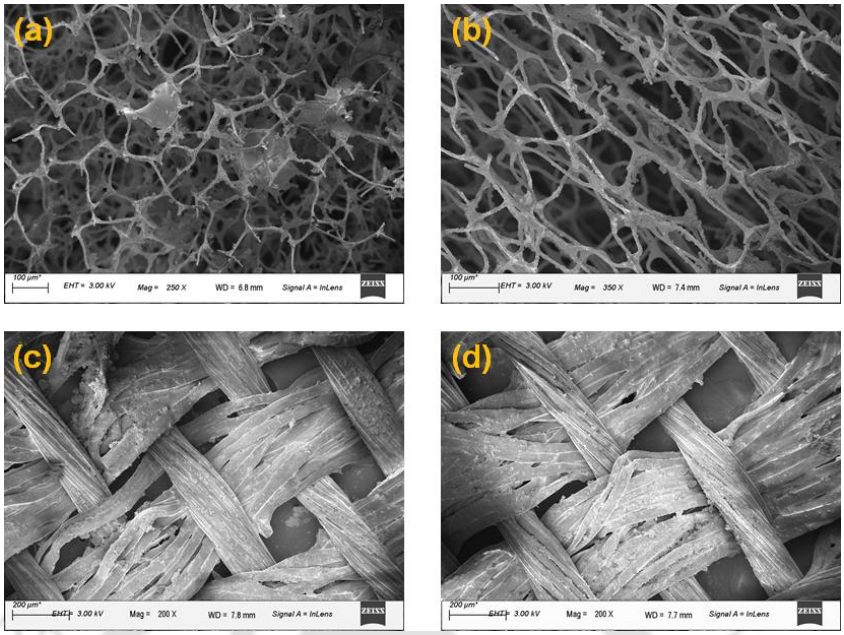

Figure 3.44 High-resolution FE-SEM images of **2′@sponge** (a) before and (b) after self-cleaning and **2′@silk** (c) before and (d) after self-cleaning.

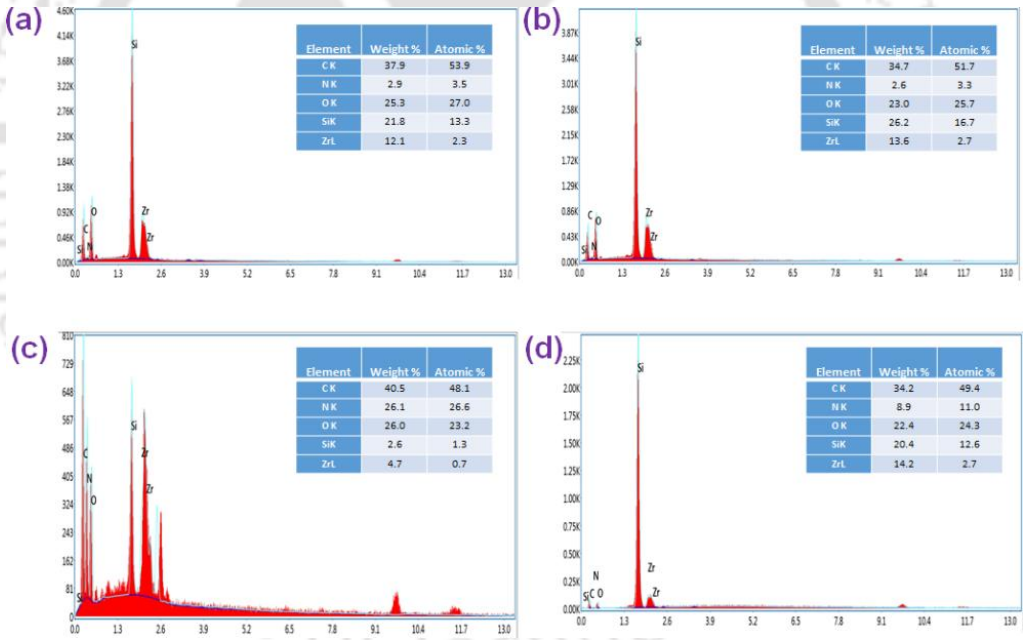

Figure 3.45 EDX spectrum of **2′@sponge** (a) before and (b) after self-cleaning and **2′@silk** (c) before and (d) after self-cleaning.

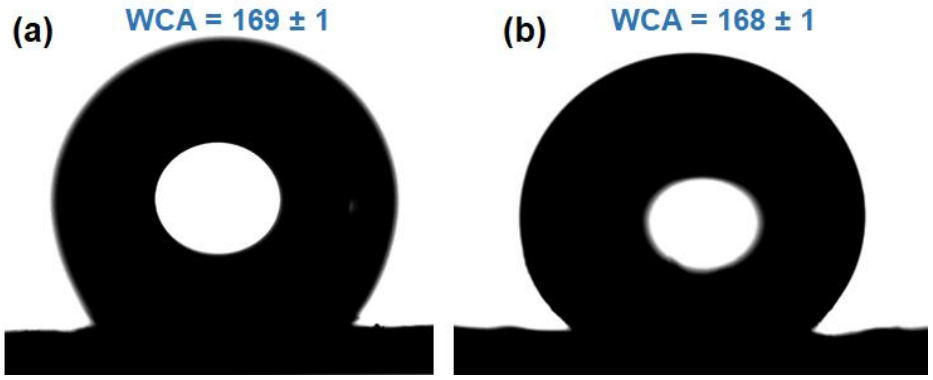

Figure 3.46 WCA of **2′@sponge** (a) after self-cleaning and **2′@silk** (b) after self-cleaning.

Table 3.4. Comparison of important parameters of superhydrophobic absorbents or membranes materials for oil water separation.

Sl. No.	Absorbents	Absorption Substances	Absorption Capacity (g/g)	Oil-water Separation Efficiency (%)	Flux of Oil-Water Separation ($Lm^{-2}h^{-1}$)	Ref.
1	**2′@sponge and 2′@silk**	**diesel oil, petrol oil, kerosene, crude oil, dichloromethane, chloroform, carbon tetrachloride, ethyl acetate, hexane, toluene**	**43.8-97.2**	**≥ 99**	**58263-47416**	**this work**
2	PDMS-TiO_2-PU sponge	diesel oil, pump oil, silicone oil, edible oil, kerosene, dichloromethane, chloroform	16.7-43.5	NA	NA	[364]
3	SH-UiO-66@CFs	motor oil, silicone oil, gasoline, kerosene, toluene, hexane, ethyl acetate, carbon tetrachloride, chloroform, dichlomrthane	27.1-49.2	95-98	NA	[365]
4	superhydrophobic/superoleophilic sawdust	crude oil, n-hexane, gasoline, diesel oil, engine oil	10.0-17.5	NA	NA	[366]
5	cotton fiber modified via the sol-gel method	diesel oil, lubrication oil, crude oil, peanut oil	25.6-57.0	98.5	NA	[367]
6	modified jute fiber via the sol-gel method	crude oil, diesel oil, lubricatiom oil, peanut oil	7.4-10.2	NA	NA	[368]
7	mesoporous silica aerogel	petrol oil, diesel oil, toluene	19.1-18.6	NA	NA	[397]
8	ultralight cellulose-based aerogel	pump oil, diesel oil, chloroform, dodecane, hexane, soybean oil, pump oil, diseal oil, motor oil, heptane, tolune, DMSO, isopropanol	18.0-41.8	NA	NA	[370]
9	cellulose-based aerogel	crude oil, diesel oil, lubrication oil	60.4-152.3	NA	NA	[371]

		silicone oil, soyabean oil, toluene, n-hexane, trichloromethane, acetone, ethanol				
10	polystyrene branched 9-octadecenoic acid grafted graphene	hexane, heptane, nonane, decane, hexadecane	11.0-27.0	NA	NA	[372]
11	MOF-PU sponge	n-hexane, paraffin, ethanol, edible oil, DMF, carbon tetrachloride	29.0-56.0	>96	NA	[353]
12	UiO-66-F_4@rGO/MS	n-hexane, isooctane, dichloromethane, 1,3,5-trimethylbenzene, silicone oil diesel oil light diesel oil crude oil	26.0-61.0	99.73	NA	[373]
13	MOF@rgo composites	chloroform, n-hexane, silicone oil, bump oil, bean oil, toluene, acetone, butanone	14.0-37.0	>98	NA	[374]
14	MOFs-copper foam	soybean oil, n-hexane, isooctane, gasoline, dichloromethane, chloroform	1.5-3.5	>96	NA	[375]
15	FGO@MOG	crude oil, decane, heptane, hexane, octadecane, octane, petrolether, pentane, toluene, veg oil, carbon tetrachloride	2.0-5.0	NA	NA	[398]
16	Macroporous silicone sponges	crude oil, sunflower oil, kerosene, diesel, alcohol, acetic acid, chloroform, acetone, diethyl ether, n-hexane, isooctane, dichloromethane	9.7-27.0	>99	NA	[377]
17	GO/PDA coated fabric	formamide, engine oil, ethylene glycol, liquide paraffin, propylene carbonate, rapeseed oil	NA	>99.50	1452 - 308	[378]
18	CBM-CuO-SA	n-hexane, toluene, trichloromethane	NA	>96	141	[379]
19	PVDF membrane	water-in-petroleum ether, water-in-toluene, water-in-isooctane, and water-in-dichloromethane	NA	NA	NA	[399]
20	Cu(OH)2@ZIF-8 membrane	heptane, cychlohexane, toluene, trichloromethane diesel, dichloromethane, petroleum	NA	>97	90 000	[400]
21	UiO-66-NH-C_{18}-PSM	diesel, hexane, ethyl acetate, acetone, toluene, decane, dichloromethane	32.3 -66.1	>99	NA	[394]
22	SMIL-101(Cr)-PSM	petrol, chloroform, hexane, toluene	1.18-2.81	>99	NA	[401]

23	OctA/rGA composite	DCM, chloroform, toluene, benzene, chloroform, dichloromethane, hexadecane, p-xylene, ethylbenzene	4.70-16.12	NA	Very less	[402]

3.3.6 Mechanism of Selective Separation of Oil from Oil-Water Mixture

As we already know that the hydrophobic nanostructure of any material causes the formation of air pockets between water and the material surface when the material come in contact of water.[403-404] Most of the work reported in the field of oil-water separation was designed by fluorinated compounds. The electronegativity of fluorine causes the accumulation of electron density on its surface and repels the electron cloud on the oxygen of water and thereby, hydrophobicity arrives into the materials.[336, 400] Here, we report a first-ever superhydrophobic MOF material that is prepared from a pre-synthesized long-chain hydrocarbon-based linker. The long-chain hydrocarbon has no charge on its surface. Therefore, the nonpolar nature of the material did not give any chance to water molecules for any type of polar interaction. At the same time, the nonpolar nature of the oils or organic solvents passes through the nonpolar sponge or membrane very easily. The above fact was again supported by the electrostatic potential (ESP) diagram of our material, oils and water. The ESP diagram confirmed that our material and all type of molecules present in crude oil are nonpolar in nature, whereas the distribution of red and blue colors in water molecules confirmed its polar nature (Figure 3.47).[405-406] Therefore both lipophilic as well as hydrophobic nature and nanostructure of **2′**on the surface of sponge and silk membrane caused the selective permeation of oil from oil-water mixture.

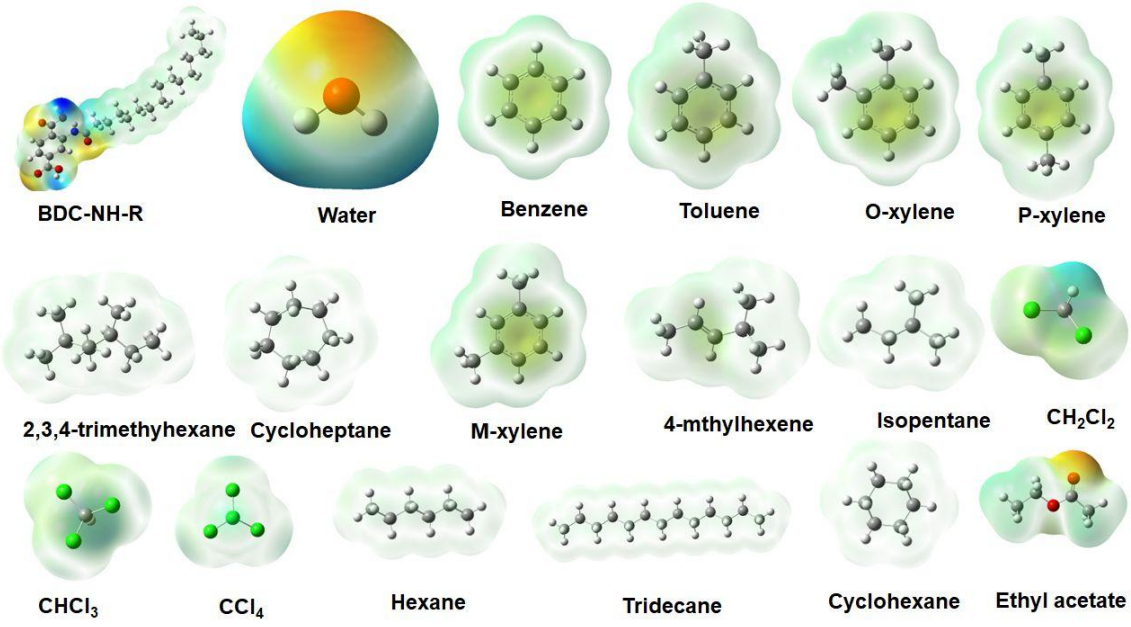

Figure 3.47. ESP diagram of H_2L^2 linker and organic molecules present in crude oil and non-polar solvents.

3.4 Conclusion

This present work is the first-ever report on long-chain hydrocarbon functionalized MOF prepared from a pre-synthesized linker for oil-water separation. Both the **2′@sponge** composite and **2′@silk** membrane are superior over other reported superhydrophobic

absorbents and membranes in terms of recyclability (up to 70 and 60 cycles, respectively). The **2′@silk** membrane has a superior flux of oil-water separation over the other superhydrophobic membranes. The absorption capacity of the **2′@sponge** composite was quite better than the reported materials for oil-water separation purposes. The separation efficiency of the **2′@sponge** composite and **2′@silk** membrane was also very high and it is above 99% for all the types of oils and organic solvents. The fluorine free nature of **2′** made the membrane and composite environmentally friendly. The selective separation of oil was due to the nanostructure of MOF material on the surface of the membrane and composite and the selectivity over the permeation of water was achieved by nonpolar-nonpolar interaction. This interaction between the MOF and oils was further supported by the ESP diagram. This is the first ever material reported to date with eco-friendly, superior oil absorption and flux of oil-water separation.

3.5 References

1. N. Zhang, Y. Qi, Y. Zhang, J. Luo, P. Cui and W. Jiang, *Ind. Eng. Chem. Res.*, 2020, **59**, 14546–14568.
2. E. S. Dmitrieva, T. S. Anokhina, E. G. Novitsky, V. V. Volkov, I. L. Borisov and A. V. Volkov, *Polymers*, 2022, **14**, 980.
3. C. Gogoi, A. Rana, S. Ghosh, R. Fopase, L. M. Pandey and S. Biswas, *ACS Appl. Nano Mater.*, 2022, DOI: doi.org/10.1021/acsanm.2c02418.
4. W. Li, J. Shi, Y. Zhao, Q. Huo, Y. Sun, Y. Wu, Y. Tian and Z. Jiang, *ACS Sustain. Chem. Eng.*, 2020, **8**, 1831–1839.
5. A. Rana, C. Gogoi, S. Ghosh, S. Nandi, S. Kumar, U. Manna and S. Biswas, *New J. Chem.*, 2021, **45**, 20193-20200.
6. I. T. Cousins, J. C. DeWitt, J. Glüge, G. Goldenman, D. Herzke, R. Lohmann, C. A. Ng, M. Scheringer and Z. Wang, *Environ. Sci.: Process. Impacts*, 2022, **22**.
7. V. M. Vieira, K. Hoffman, H. M. Shin, J. M. Weinberg, T. F. Webster and T. Fletcher, *Environ Health Perspect.*, 2013, **121**, 318-323.
8. S. Ghosh, A. Rana, S. Kumar, C. Gogoi, S. Mukherjee, U. Manna and S. Biswas, *Mater. Chem. Front.*, 2022, **6**, 2051-2060.
9. A. Rana, S. Nandi and S. Biswas, *New J. Chem.*, 2022, **46**, 10477-10483.
10. S. Ghosh, F. Steinke, A. Rana and S. Biswas, *Inorg. Chem. Front.*, 2022, **9**, 859-869.
11. A. K. Kota, G. Kwon and A. Tuteja, *NPG Asia Mater.*, 2014, **6**, 109.
12. Z. Xu, *Micro Nano Lett.*, 2014, **9**, 6-10.
13. J. Hajek, C. Caratelli, R. Demuynck, K. D. Wispelaere, L. Vanduyfhuys, M. Waroquiera and V. V. Speybroeck, *Chem. Sci.*, 2018, **9**, 2723-2732.
14. J. Winarta, B. Shan, S. M. Mcintyre, L. Ye, C. Wang, J. Liu and B. Mu, *Cryst. Growth Des.*, 2020, **20**, 1347–1362.
15. Q. Gu, H. Y. Ng, D. Zhao and J. Wang, *APL Materials.*, 2020, **8**, 040902.
16. M. Shi, R. Huang, W. Qi, R. Su and Z. He, *Colloids Surf. A Physicochem. Eng.*, 2020, **602**, 125102.
17. M. Gao, S. Zhao, Z. Chen, L. Liu and Z. Han, *Inorg. Chem.*, 2019, **58**, 2261–2264.
18. S. Eom, D. W. Kang, M. Kang, J. H. Choe, H. Kim, D. W. Kim and C. S. Hong, *Chem. Sci.*, 2019, **10**, 2663-2669.
19. Q. Shuai, X. Yang, Y. Luo, H. Tang, X. Luo, Y. Tan and M. Ma, *Mater. Chem. Phys.*, 2015, **162**, 94-99.
20. R. Dalapati, S. Nandi, C. Gogoi, A. Shome and S. Biswas, *ACS Appl. Mater. Interfaces*, 2021, **13**, 8563-8573.

21. D. Zang, F. Liu, M. Zhang, Z. Gao and C. Wang, *Chem. Eng. Res. Des.* , 2015, **102**, 34-41.
22. N. Lv, X. Wang, S. Peng, L. Luo and R. Zhou, *RSC Adv.*, 2018, **8**, 30257-30264.
23. N. Lv, X. Wang, S. Peng, H. Zhang and L. Luo, *Int. J. Environ. Res. Public Health*, 2018, **15**, 969.
24. C. Zhang, C. Dai, H. Zhang, S. Peng, X. Wei and Y. Hu, *Mar. Pollut. Bull.* , 2017, **122**, 129-138.
25. H. Zhang, Y. Li, Y. Xu, Z. Lu, L. Chen, L. Huang and M. Fan, *Phys. Chem. Chem. Phys.* , 2016, **18**, 28297-28306.
26. T. Yin, X. Zhang, X. Liu and C. Wang, *Mar. Pollut. Bull.*, 2017, **118**, 267-274.
27. F. I. Alghunaimi, D. J. Alsaeed, A. M. Harith and T. A. Saleh, *J. Clean. Prod.*, 2019, **233**, 946-953.
28. Z. He, H. Wu, Z. Shi, X. Duan, S. Ma, J. Chen, Z. Kong, A. Chen, Y. Sun and X. Liu, *Colloids Surf. A Physicochem. Eng. Asp.*, 2022, **648**, 129142.
29. Y. Zhan, S. He, J. Hu, S. Zhao, G. Zeng, M. Zhou, G. Zhang and A. Sengupta, *J. Hazard. Mater.*, 2020, **388**, 121752.
30. J. Gu, H. Fan, C. Li, J. Caro and H. Meng, *Angew. Chem. Int. Ed.*, 2019, **58**, 5297-5301.
31. J. Du, C. Zhang, H. Pu, Y. Li, S. Jin, L. Tan, C. Zhou and L. Dong, *Colloids Surf. A Physicochem. Eng. Asp.*, 2019, **573**, 222-229.
32. K. Jayaramulu, F. Geyer, M. Petr, R. Zboril, D. Vollmer and R. A. Fische, *Adv. Mater.*, 2017, **29**, 1605307.
33. J. Cao, D. Wang, P. An, J. Zhang and S. Feng, *J. Mater. Chem. A*, 2018, **6**, 18025-18030.
34. X. Zhu, Z. Gao, F. Li, G. Miao, T. Xu, X. Miao, Y. Song, X. Li and G. Ren, *Carbon*, 2022, **190**, 329-336.
35. Z. Yin, F. Yuan, M. Xue, Y. Xue, Y. Xie, J. Ou, Y. Luo, Z. Hong and C. Xie, *J. Colloid Interface Sci.*, 2022, **611**, 93-104.
36. W.Zhang, Z. Shi, F. Zhang, X. Liu, J. Jin and L. Jiang, *Adv. Mater.*, 2013, **25**, 2071-2076.
37. H. Lei, M. Xiong, J. Xiao, L. Zheng, Y. Zhu, X. Li, Q. Zhuang and Z. Han, *Prog. Org. Coat.*, 2018, **103**, 182-192.
38. M. Gao, S. Zhao, Z. Chen, L. Liu and Z. Han, *Inorg. Chem.*, 2019, **58**, 2261–2264.
39. D. W. Kang, M. Kang, J. H. Choe, H. Kim, D. W. Kim and C. S. Hong, *Chem. Sci.*, 2019, **10**, 2663-2669.
40. T. Stegmaier, V. V. Arnim, A. Scherrieble and H. Planck, *Biologically Inspired Textiles*, 2008, 137-149.
41. M. Sun, J. Zhang, G. S. Watson, J. A. Watson, D. Han and A. Liang, *J. Appl. Biomech.*, 2018, **2018**.
42. S. Parvate, P. Dixit and S. Chattopadhyay, *J. Phys. Chem. B*, 2020, **124**, 1323–1360.
43. A. Fabrizio, A. Grisafi, B. Meyer, M. Ceriotti and C. Corminboeuf, *Chem. Sci.*, 2019, **10**, 9424-9432.
44. S. R. Gadre, C. H. Suresh and N. Mohan, *Molecules*, 2021, **26**, 3289.

Electrophilicity Modulated Targeted Luminescence of MOF-Coated Cotton Composite for Dual Analyte Detection in Aqueous Medium

Sulfur is a soft Lewis base and thiocarbonyl has moderate electrophilicity. Our probe's properties are adjusted in such a way that it could simultaneously detect a Lewis acid (Hg^{2+}) and a strong nucleophile (NH_2–NH_2). Considering the above fact, a thioureido-functionalized robust MOF material was prepared, which was utilized for the selective fluorometric detection of environmentally significant toxic pollutants (Hg^{2+} and NH_2–NH_2) in an aqueous medium. The probe detected mercury by quenching the fluorescence emission intensity in a static pathway by soft-soft interaction with the S-atom of the probe. In contrast, the detection of hydrazine was furnished by a reaction-based pathway by the attack of hydrazine to the moderate electrophilic (thiocarbonyl) part of the probe, which resulted in an enhancement in the fluorescence emission intensity of the probe. A MOF-coated cotton composite was developed for the naked-eye detection of Hg^{2+} and hydrazine for real-life applicability. The MOF was highly sensitive towards detecting Hg^{2+} and hydrazine with very low detection times, *i.e.*, 10 s and 50 s, respectively. The probe's sensitivity also remained unaltered under a significantly lower concentration of the targeted analytes, *i.e.*, the detection limits for hydrazine and Hg^{2+} were 1.9 nM and 4.0 nM, respectively. Our probe's response time and LOD are much lower than the other previously reported probes for Hg^{2+} and hydrazine to date. A 92% fluorescence quenching and 28-fold fluorescence enhancement of the MOF were observed after the interaction of the probe with Hg^{2+} and hydrazine, respectively. The probe has excellent selectivity over the competitive analytes of Hg^{2+} and hydrazine. The MOF could also sense hydrazine in various environmental water specimens. Systematic mechanistic investigations were conducted to know the phenomena behind the fluorescence quenching and enhancement processes.

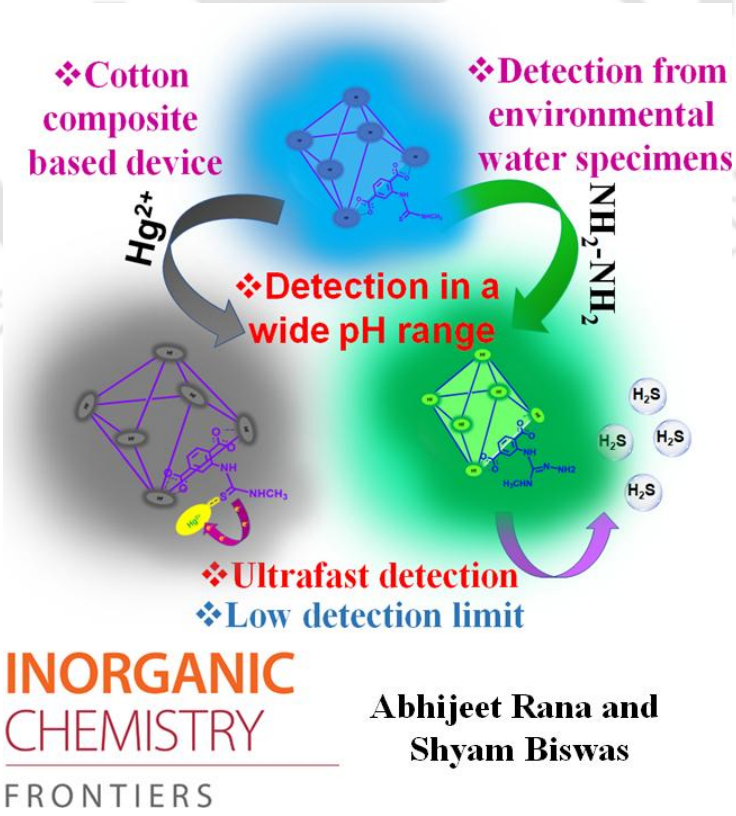

4.1 Introduction

Mercury is a toxic soft Lewis acid present in many forms in the environment.[407] Various natural and anthropogenic sources are the major contributor of mercury toward the environment.[408] Once the mercury comes into the environment, ocean help to redistribute it into marine and terrestrial ecosystems.[409] Once the inorganic mercury, i.e., Hg(II) or Hg(0), comes into the environment, immediately these species are converted to methylmercury, a bioaccumulative neurotoxicant.[410] The organic methylmercury is easily absorbed into the tissues of fishes and thereby, methylmercury comes to the human body due to the consumption of sea foods.[408] Exposure to methylmercury causes Minamata disease. The hyper-concentration of mercury directly affects the human heart, kidney, nervous system, and immune system and causes cancer and liver dysfunction.[389, 411] Therefore, USA environmental protection agency (USA EPA) and Canadian drinking water quality (CDWQ) have set the highest concentration limit of mercury in water as 2 ppb and 1 ppb respectively. Therefore, the selective detection of mercury below the limits set by the USA EPA and CDWQ is highly required. Here, the presented MOF can detect mercury below the safe limit set by EPA and CDWQ.

Hydrazine has both nucleophilic and reductant properties. Therefore, it is used as a catalyst,[412] fuel (propellant for spacecraft),[413-414] blowing agent,[415], etc. The enormous application of hydrazine as an industrial raw material and its environmental adaptation can not be avoided. However, at the same time, the toxic effect of hydrazine should not be overlooked. The carcinogenic impacts of hydrazine on humans make it a hazardous material. Hydrazine has been included in the hazardous chemical group and the threshold concentration of hydrazine in drinking water has been set as 10 ppb.[416] Therefore, the detection of hydrazine below the safe limit is highly required and in this work, we can detect this pollutant below the safe limit. Our probe can detect hydrazine with the ultra-low detection limit of 1.9 nM in aqueous medium.

Looking into the detrimental effects of mercury and hydrazine in drinking water, many environmental scientists working in the field of sensing hazardous materials have put forward their contribution by varieties of methods. The selective sensing of hazardous materials has been reported by enormous research groups with the help of ion-exchange chromatography, electrochemical,[417] spectrometry,[418] voltammetry[419] and fluorescence-based methods.[388, 420-421] Among the above-mentioned techniques, fluorescence-based method has several advantages over other techniques due to easy handling and simple observation process.[422] There are many class of materials utilized for the sensing of hazardous materials including quantum dots,[423-424] graphene oxide-based materials,[425] carbon nanotubes[426] and organic probes.[427] Metal-organic frameworks (MOFs) are porous with very high surface areas and their active sites for sensing could be easily tuneable. Therefore, MOF-based materials are advantageous over other classes of materials.

The above-mentioned toxic properties of hydrazine and mercury and the easy handling fluorescence method inspired us to develop a fluorescence-based selective probe to detect mercury and hydrazine. The soft nature of Hg^{2+} pushed us to design a soft centre-based probe with sulfur-containing functionality. In contrast, the nucleophilic nature of hydrazine having alpha-effect inspired us to design a probe with moderate electrophilic centre. The moderate electrophilic nature guides the probe to selectively react with hydrazine even in the presence of other nucleophilic congeners. The above idea was incorporated by designing a thioureido functionalized robust Hf-MOF named **3′**. The soft sulfur atom and moderate electrophilic thiocarbonyl group was the active centres for the selective interaction of Hg^{2+} and hydrazine with the probe. A 28-fold increment in fluorescence intensity of **3′** was observed after the addition of hydrazine solution and a fluorescence quenching efficiency of 92% was observed

after adding Hg^{2+} solution in aqueous medium. The probe can detect Hg^{2+} and hydrazine below the permissible limit in drinking water. A thorough study of the mechanistic pathway was explored via various analytical techniques to present the work systematically and be applicable in future endeavours. The selectivity and applicability for real field purposes, the ultralow detection limit and the relevance of dual sensing purpose make our material one unique sensor of mercury and hydrazine.

4.2 Experimental Section

4.2.1 Synthesis of $[Hf_6O_4(OH)_4(C_{10}H_8N_2O_4S)_{3.3}(C_8H_5NO_4)_2]\cdot 1H_2O$ (3)

The synthesis of probe **3** was initiated from a solvothermal synthesis of Hf(IV) metal salt and BDC-NH_2 linker-based MOF. The UiO-66 topology-based Hf(IV) MOF bearing BDC-NH_2 (BDC-NH_2: 2-amino 1,4-benzenedicarboxylic acid) ligand, i.e., Hf-UiO-66-NH_2 was synthesized by a systematic solvothermal approach. A mixture of $HfCl_4$ (0.54 mM) and H_2BDC-NH_2 linker (0.75 mM) in 15 mL DMF using 1 mL of HCl was heated at 80 °C for 24 h. The precipitate was collected after 24 h and was appropriately washed with water and then with acetone. The obtained material was solvent exchanged with methanol for 24 h and then was vacuum dried at 100 °C for 24 h to get the activated form of Hf-UiO-66-NH_2. In the second step, a post-synthetic modification approach was taken forward by utilizing a mixture of 60 mg of Hf-UiO-66-NH_2 and 20 mg of methyl isothiocyanate in a mixture of solvent ($CHCl_3$:CH_3OH = 9:1) and was heated at 55 °C for 3 days as shown in Scheme 1.

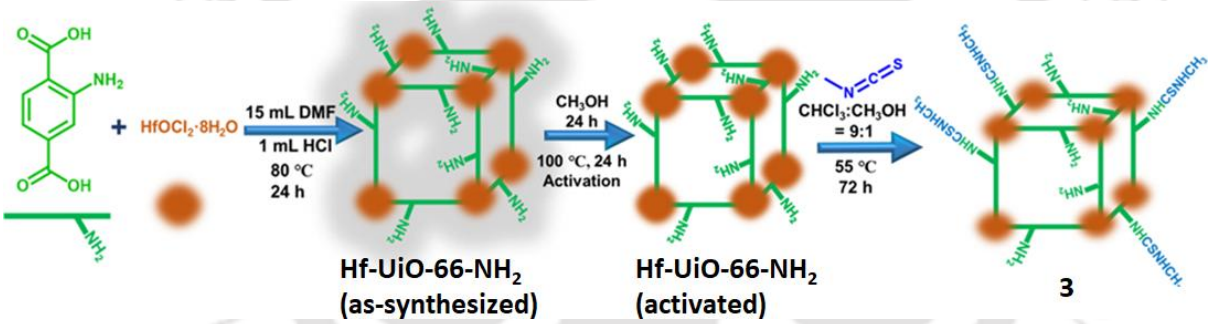

Scheme 1 Detailed stepwise synthesis of **3**.

4.3 Results and Discussion

4.3.1 Characterization of 3

During post-synthetic modification of Hf-UiO-66-NH_2 with methyl isothiocyanate, -NH_2 group of **3** was expected to react with $H_3CN{=}C{=}S$ functionality to provide –NH(C=S)$NHCH_3$ group. When the post-synthetically modified MOF named **3** was digested with 40% HF solution, 46% conversion of the -NH_2 group to –NH(C=S)$NHCH_3$ functionality could be noticed by comparing the digested ^{1}H NMR spectra of **3** and Hf-UiO-66-NH_2 (Figure 4.1 and 4.2). The ^{1}H NMR spectra of **3** showed the presence of two doublets and one singlet due to three aromatic protons at 7.76 (d, 1H), 7.37 (S, 1H) and at 7.03 (D, 1H). The ^{1}H NMR spectra of **3** showed three additional peaks at 8.05 (d, 1H), 7.95 (S, 1H) and 7.78 (D, 1H) and a singlet at 3.65 (S, 3H) due to three methyl protons. A downfield chemical shift was observed after post-synthetic modification as the binding of methyl isothiocyanate to the free amine group causes a decreased electron density in the benzene ring. The presence of six aromatic protons proved that some amount of BDC-NH_2 linker gets reacted with the methyl isothiocyanate group to afford 46% post-synthetic modification. Again, the arrival of the peak due to the methyl group is a direct evidence of the successful post-synthetic modification. The percentage of post-

synthetic modification that occurred was calculated by comparing the area under each proton. Again, the ^{13}C NMR spectra of Hf-UiO-66-NH_2 (^{13}C NMR: 169.3, 167.5, 150.5, 135.7, 132.0, 118.5, 116.1, 114.1) (Figure 4.3) and **3** (^{13}C NMR: 175.9, 169.2, 167.3, 166.3, 163.3, 159.5, 151.0, 139.2, 136.8, 135.4, 131.7, 128.8, 124.45, 118.3, 116.9, 115.2, 113.1) (Figure 4.4) were compared. The additional peak at 175 ppm due to the thiocarbonyl group in the ^{13}C NMR spectrum of **3** also supported the successful bonding between amine of Hf-UiO-66-NH_2 with the methyl isothiocyanate moiety.[428] The mass spectrometry of the digested MOF Hf-UiO-66-NH_2 showed the presence of a strong peak at 180 m/z which is due to the linker from the digested MOF (Figure 4.5) and the mass spectrum of **3** displayed m/z peaks at 180 as well as 253 due the presence of both the linkers BDC-NH_2 and BDC-$NHCSNHCH_3$ (Figure 4.6). The above result is a strong evidence of the successful post-synthetic modification.

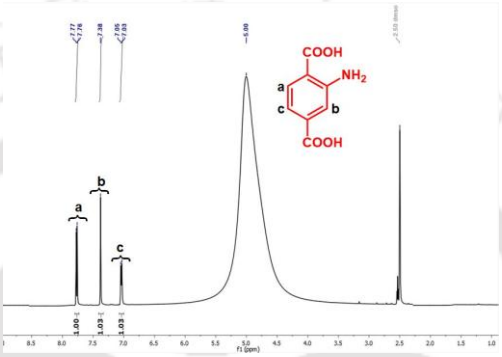

Figure 4.1 Digested ^{1}H NMR spectrum of Hf-UiO-66-NH_2 (digested using 10 µL of 40% HF in 500 µL of DMSO-D_6 and 20 mg of MOF).

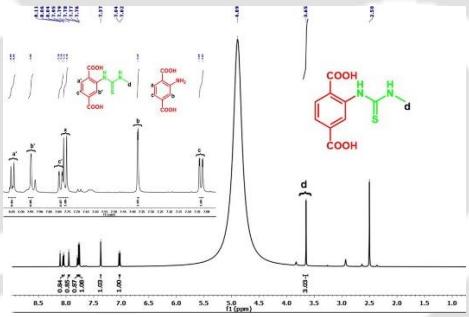

Figure 4.2 Digested ^{1}H NMR spectrum of **3** MOF (digested using 10 µL of 40% HF in 500 µL of DMSO-D_6 and 20 mg of MOF).

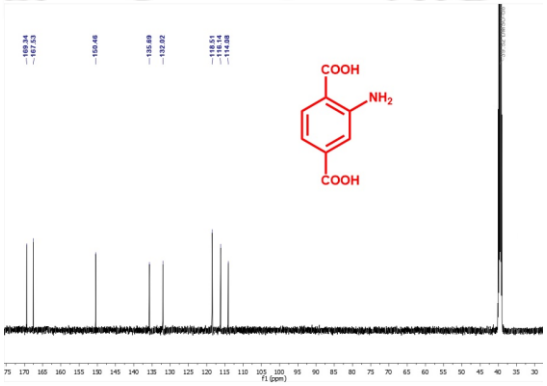

Figure 4.3 Digested ^{13}C NMR spectrum of Hf-UiO-66-NH_2 (digested using 10 µL of 40% HF in 500 µL of DMSO-D_6 and 20 mg of MOF).

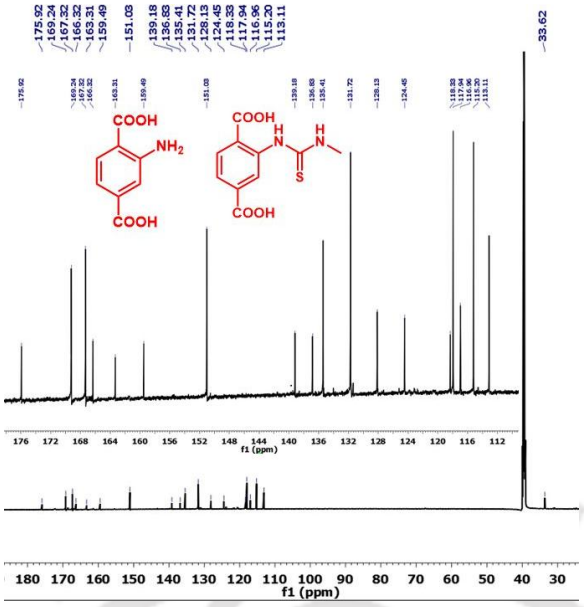

Figure 4.4 Digested ^{13}C NMR spectrum of **3** MOF (digested using 10 µL of 40% HF in 500 µL of DMSO-D_6 and 20 mg of MOF).

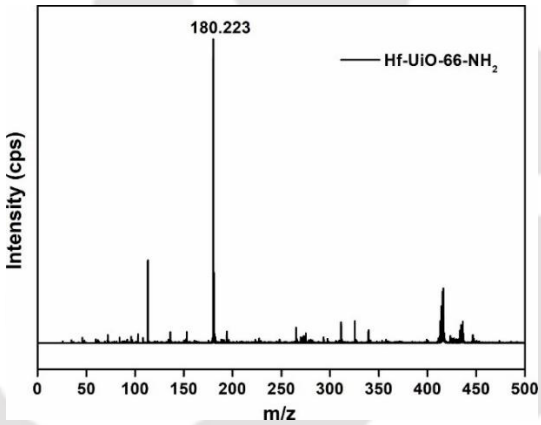

Figure 4.5. Mass spectrum of Hf-UiO-66-NH_2 after digestion by HF in methanol/water mixture.

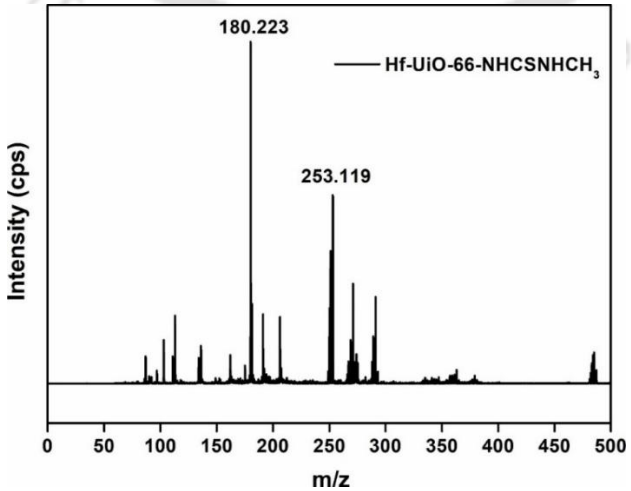

Figure 4.6 Mass spectrum of **3** after digestion by HF in methanol/water mixture.

The FT-IR spectra of Hf-UiO-66-NH_2 possesses two peaks (at 1575 and 1385 cm^{-1}) due to the asymmetric and symmetric stretching frequency of the carboxylic group of Hf-UiO-66-NH_2. These two carboxyl frequencies are present in **3** MOF, which proves that there is no structural detachment of carboxylate from the metal centre during post-synthetic modification. The FT-IR spectra showed additional peaks at 1280, 1085 and 798 cm^{-1} due to the -C=S bond of **3′** MOF,[429] which confirmed the successful post-synthetic modification (Figure 3.7).

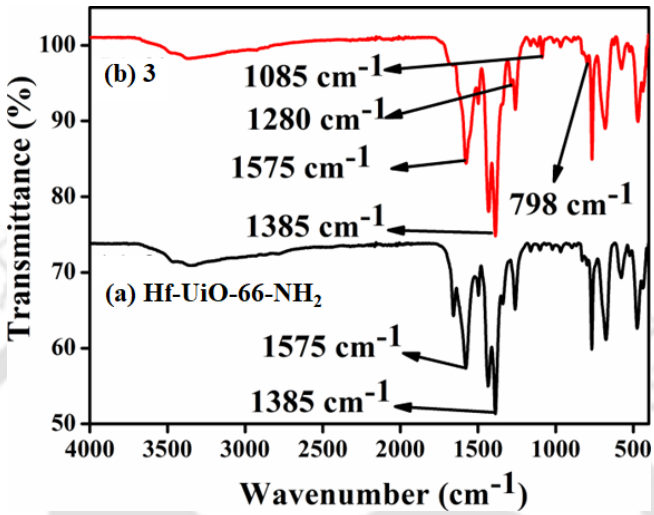

Figure 4.7 ATR-IR spectra of Hf-UiO-66-NH_2 and **3**.

The FE-SEM images of **3** and Hf-UiO-66-NH_2 demonstrate similar particles, which confirmed no change in the crystallinity of the material after post-synthetic modification (Figure 4.8). The successful post-synthetic modification was again supported by the EDX elemental analysis. The EDX elemental analysis of **3** confirmed the presence of Hf (5.1%), elements. At the same time, the TEM-EDS elemental analysis of **3** confirmed the presence of Hf (4.6 %) and S (4.5 %) elements (Figure 4.9 and 4.11). The TEM-EDS mapping was also carried out for Hf-UiO-66-NH_2 and **3** which displayed the homogenous distribution of all the desired elements (Figure 4.10 and 4.12). The presence of the additional sulfur atom in **3** confirmed the incorporation of the isothiocyanate group into the free amine of Hf-UiO-66-NH_2. The homogenous distribution of desired elements in the elemental mapping of **3** suggests that methyl isothiocyanate molecule was not physically adsorbed on the surface of Hf-UiO-66-NH_2 but it was bonded with the –NH_2 group of Hf-UiO-66-NH_2.

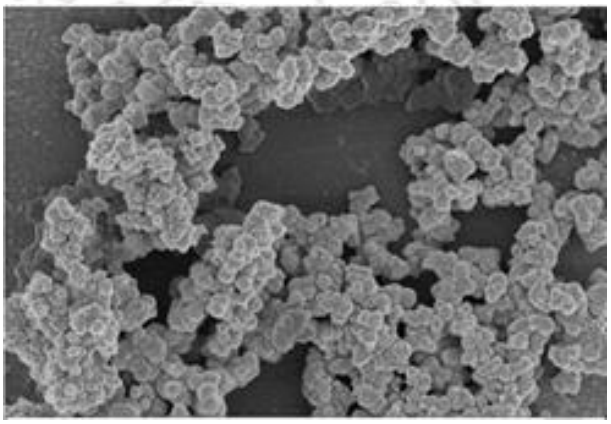

Figure 4.8 FE-SEM image of **3**.

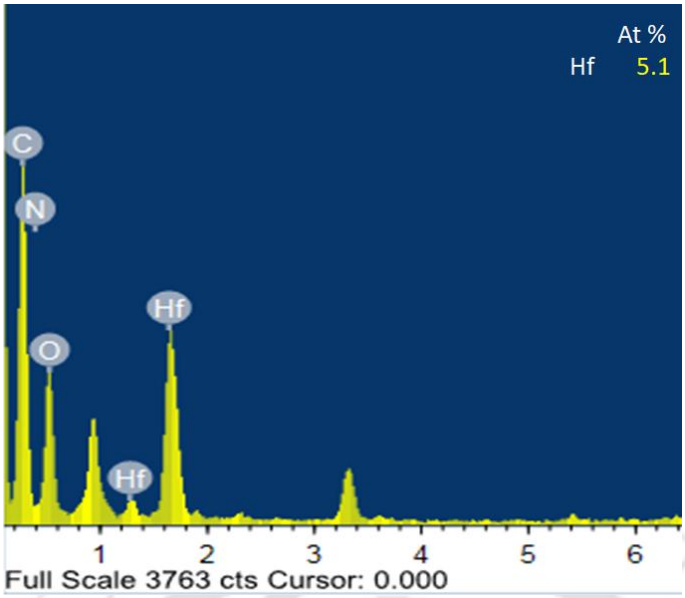

Figure 4.9. TEM-EDX spectrum of Hf-UiO-66-NH_2.

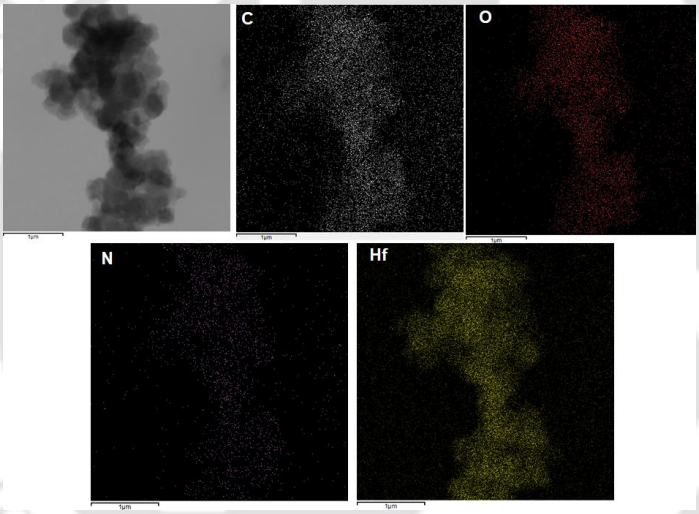

Figure 4.10 TEM-EDS elemental mapping of Hf-UiO-66-NH_2.

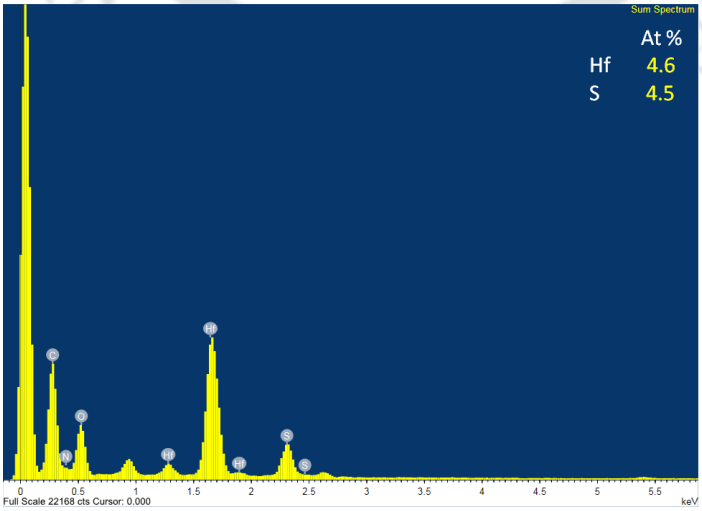

Figure 4.11 TEM-EDX spectrum of **3**.

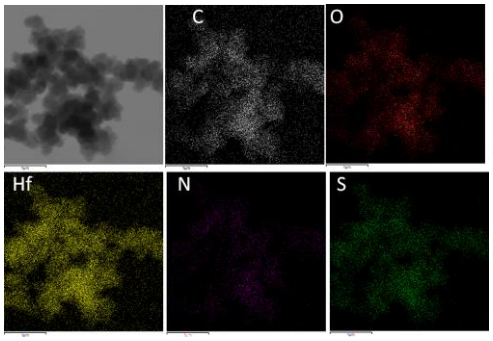

Figure 4.12 TEM-EDX mapping of **3**.

Further, the PXRD analysis of **3** and Hf-UiO-66-NH_2 was performed to confirm their phase purity and crystallinity. Both materials showed similar PXRD patterns like the simulated one (Figure 4.13). The PXRD experiment demonstrated that the above-synthesized materials **3** and Hf-UiO-66-NH_2 belong to the UiO-66 topology. The Pawley fit and indexing data (Figure 4.14 Table 4.1) of the slow scan PXRD data of **3** again supported this observation. The Pawley fit data showed that the PXRD pattern of **3** exactly fits with the simulated pattern with negligible errors (R_p = 1.0% and R_{wp} = 1.6%) (Figure 4.14).

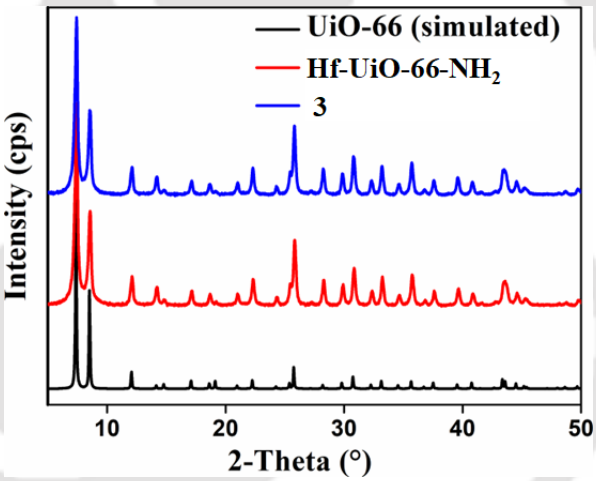

Figure 4.13 PXRD patterns of UiO-66 (simulated), Hf-UiO-66-NH_2 and **3**.

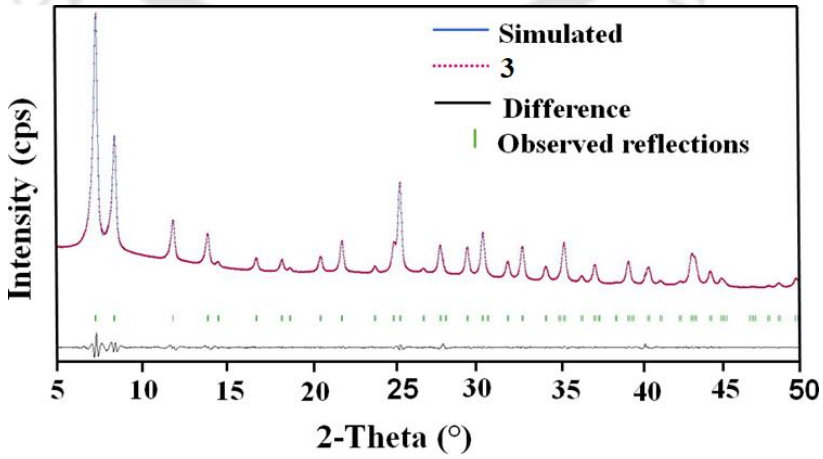

Figure 4.14 Pawley fit plot for the PXRD pattern of **3** (R_{wp} and R_p are 1.6% and 2.3%, respectively).

Table 4.1 Indexing parameters of simulated UiO-66 and **3**.

Compound name	**3** (this work)	UiO-66 (reported)[430]
Crystal System	Cubic	Cubic
a = b = c (Å)	20.743 (5)	20.700 (2)
α = β= γ (°)	90	90
V (Å^3)	8924.6 (35)	8870.3 (2)
Radiation	Cu Kα1	Cu Kα1

The chemical robustness of the material was also examined by stirring the materials in DCM, DMF, H_2O, pH 2 and pH 12 solutions. The materials were filtered and the PXRD patterns of the recovered materials were measured individually. The PXRD pattern of recovered materials precisely matched with the PXRD pattern of **3** (Figure 4.15). It concludes that the crystallinity of the material remained unchanged even after 24 h of stirring. Therefore, the probe **3** is stable enough for the application of sensing purpose in a variety of solvent media.

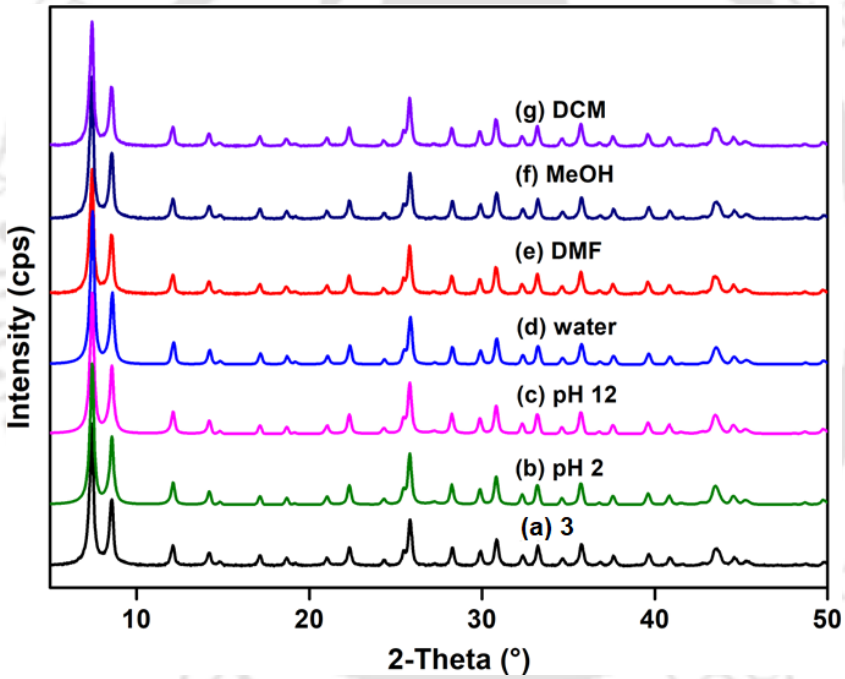

Figure 4.15 PXRD pattern of **3** (black) and PXRD patterns of the recovered samples after stirring in (b) pH 2 solution (green), (c) pH 12 solution (pink), (d) water (blue), (e) DMF (red), (f) MeOH (deep blue), (g) DCM (violet).

The thermogravimetric (TG) experiments for both **3** and Hf-UiO-66-NH_2 were performed to know the material's thermal stability. Initially, there was a weight loss of 2.9% in the TG curve of Hf-UiO-66-NH_2 due to the removal of 3 molecules of water per unit formula at 130 °C (Figure 4.16). The second weight loss was attributed to the loss of framework structure at 400 °C. The absence of breakpoint due to DMF in the TG trace confirmed the proper activation of Hf-UiO-66-NH_2. The material **3** also displayed a similar TG-curve with an initial weight loss of 3.7% due to the loss 1.5 molecules of water per unit formula and the second weight loss due to linker dislocation from the framework structure started from 350 °C to 400 °C. The

framework destruction of Hf-UiO-66-NH_2 occurred at a slightly lower temperature compared to **3** due to linker defect that arose at the time of post-synthetic modification.

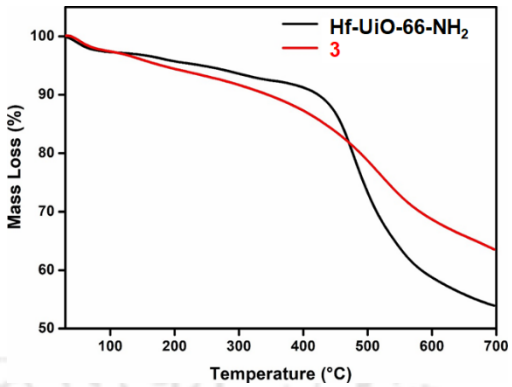

Figure 4.16 TG curves of **3** and Hf-UiO-66-NH_2 measured under N_2 atmosphere.

N_2 sorption analysis of material **3** was carried out at -196 °C using liquid nitrogen. The found surface area for **3** was 498 m^2/g. We noticed a decreased surface area of **3** compared to the surface area (784 m^2/g) of previously Hf-UiO-66-NH_2 (Figure 4.17).[431] The reduced surface area is attributed to the post-synthetic modification. Because of post-synthetic transformation, the extra functionality of methyl isothiocyanate occupied the pores of Hf-UiO-66-NH_2, which caused the decrease in the surface area of **3** The decreased surface area of **3** again supports the successful incorporation of methyl isothiocyanate moiety to the free amine of Hf-UiO-66-NH_2 (Figure 4.18).

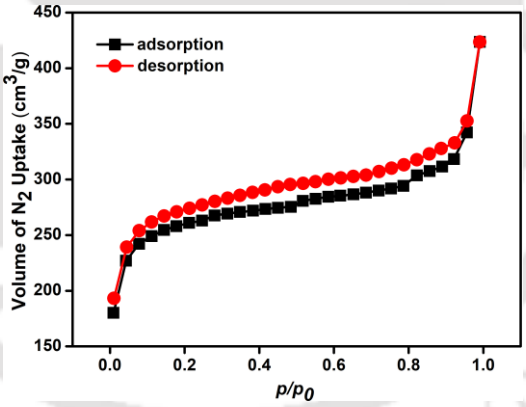

Figure 4.17 N_2 sorption isotherms of Hf-UiO-66-NH_2 measured at -196 °C.

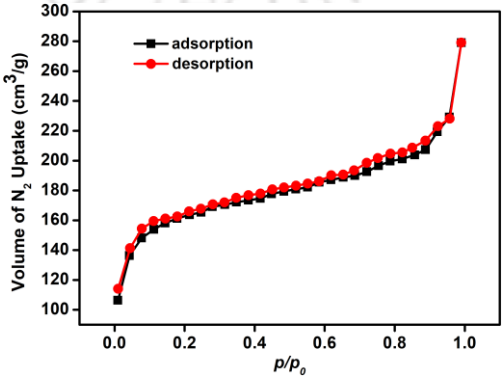

Figure 4.18 N_2 sorption isotherms of **3** measured at -196 °C.

4.3.2 Structural Description

The PXRD pattern of synthesized **3** material agrees that the material belongs to the UiO-66 class like **3**. Again, the material's phase purity, crystallinity and topology were supported by Pawley fit and indexing. Due to the strong binding between the oxophilic hard Zr(IV) centers with the oxygen of carboxylate groups of linkers, the MOFs bearing Zr(IV) ions are usually robust. The hard-hard interaction gives rise to a chemically robust material. Initially, a secondary building unit (SBU) is formed by the bonding of six Zr(IV) ions to four of the oxygen and four hydroxy groups in μ_3-bridging mode to afford one cuboctahedron oxo cluster.[432] Twelve of the BDC linkers bound to the SBU to give face-centered cubic topology with an approximate cell length of around 20.7 Å (Figure 4.19a-b).[433] The cell parameter of **3** was found to be 20.74 Å by indexing of its slow scan PXRD data. The overall face-centered cubic framework possesses small tetrahedral cages and large octahedral cages.

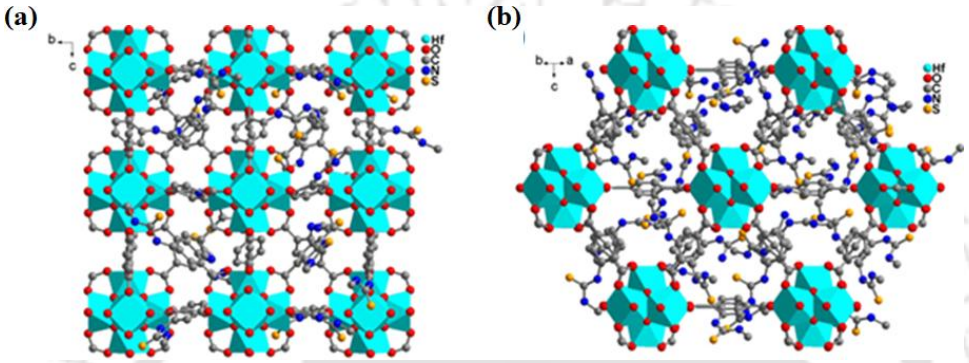

Figure 4.19 Simulated structure of **3** with Hf atoms shown as cyan polyhedra.

4.3.3 Fluorescence Sensing of Hg^{2+} and Hydrazine

The use of mercury and hydrazine in industrial processes and their release into the environment creates numerous health-related issues. Therefore, the selective detection of industrially important toxic analytes is highly required for a healthy environment. Consequently, we synthesized a 2-(3-methylthioureido)terephthalic) acid functionalized targeted system for the selective detection of mercury and hydrazine. All the fluorescence experiments for the sensing of mercury were performed using a MOF suspension in DMF (1 mg/mL) and the analytes were prepared in water. The MOF suspension was prepared by taking 1 mg of MOF in 1 mL of water. The mixture was sonicated for about 30 min and kept undisturbed for 12 h. Afterward, the mixture was centrifuged and only the supernatant suspension was collected by decanting from the centrifuge tube and separating the excess MOF powder adhered below. In this way, we prepared the stable MOF suspension. A systematic fluorescence experiment was performed using 2700 µL of DMF and 300 µL of the above-prepared MOF suspension and then adding 300 µL of 10 mM aqueous analyte solution. For the detection of hydrazine, similar procedure as mercury was followed with slight modification. Both MOF suspension and analyte solution were prepared in water and all the fluorescence spectra were recorded using 2700 µL of water and 300 µL of MOF suspension and thereafter adding 300 µL of 10 mM aqueous analyte solution. For all the fluorescence experiments for the detection of both mercury and hydrazine, fluorescence light of 360 nm wavelength was used for excitation and the emission spectra were recorded between 380 and 600 nm. The excitation and emission spectra of MOF suspension are displayed in Figure 4.20.

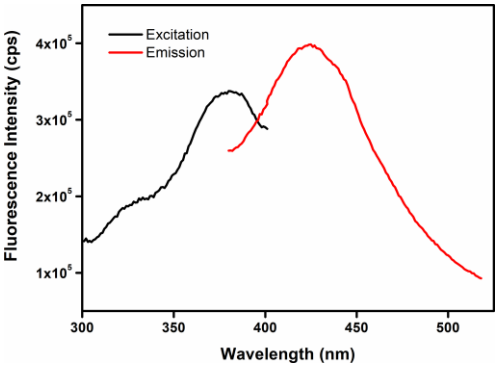

Figure 4.20 Fluorescence excitation and emission spectra of **3**.

A volume dependent fluorescence detection experiment was carried out by adding 50 µL of 10 mM aqueous Hg^{2+} solution to 3000 µL MOF suspension in each step. A sudden quenching in fluorescence emission intensity was observed after every incremental step and finally, a saturation of the quenching process was noticed after the addition of 300 µL of aqueous Hg^{2+} solution, as shown in Figure 4.21a. A similar volume-dependent sensing experiment was carried out by adding 50 µL of 10 mM aqueous hydrazine solution to 3000 µL of aqueous MOF suspension in each step. An immediate turn-on in fluorescence emission intensity was noticed after each incremental addition and finally, a saturation in fluorescence intensity was detected after the addition of 300 µL of 10 mM aqueous hydrazine solution, as displayed in Figure 4.21b**.** The detection of targeted analytes should be reproducible and repeatable, which is a good characteristic of the ideal sensor material. Therefore, we carried out batch experiments multiple times on the same day and different days. The experimental results presented in Tables 4.2 and 4.3 confirmed that the sensing processes are reproducible and repeatable for providing the same results towards both the analytes with high precision and accuracy.

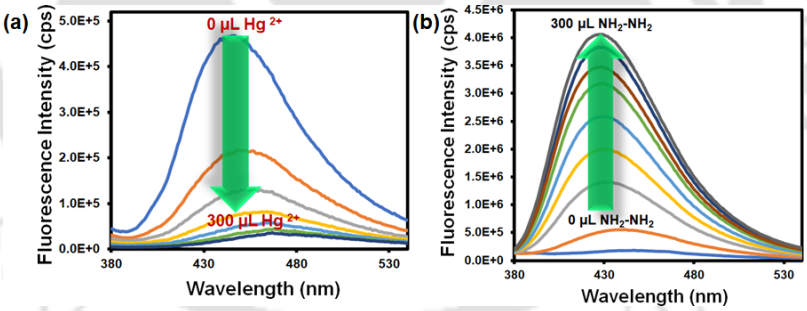

Figure 4.21 Change in fluorescence emission intensity of probe **3** after the incremental addition of 300 µL of aqueous 10 mM Hg^{2+} (a) and hydrazine (b) solution.

The time-dependent experiment was performed to know the sensitivity of detection. To find the detection time, 300 µL of 10 mM aqueous Hg^{2+} solution was added to a 3000 µL of MOF suspension and the fluorescence emission intensity was recorded after every 10 s intervals. We found that after 10 s, there was saturation in fluorescence intensity and no further appreciable quenching occurred up to 1 min (Figure 4.22a and 4.22b**)**. A similar procedure was adopted to find the probe's response time for hydrazine detection. In this case, we found that the turn-on nature of fluorescence intensity of **3** became saturated after 50 s (Figure 4.22c and 4.22d). Therefore, the probe **3** is highly sensitive with a very low detection time as compared to other MOF-based mercury and hydrazine sensors displayed in Tables 4.6 and 4.7. The fluorescence fold increment and quenching efficiency after adding 300 µL of hydrazine and Hg^{2+} solution was calculated using the formulas: I/I_0 and $((I_0\text{-}I)/I_0) \times 100$, respectively ($I_0$ is the fluorescence

intensity of the probe before the addition of the target analyte and *I* is the fluorescence intensity of the probe after the addition of the target analyte). We found a 28-fold increment in the fluorescence intensity of the probe after the addition of 300 µL of 10 mM hydrazine solution. After the addition of 300 µL of 10 mM Hg^{2+} solution, the fluorescence intensity of the probe quenched up to 92%. The appreciable change in the original fluorescence intensity of the probe by both the targeted analytes made our material a different and more efficient sensor.

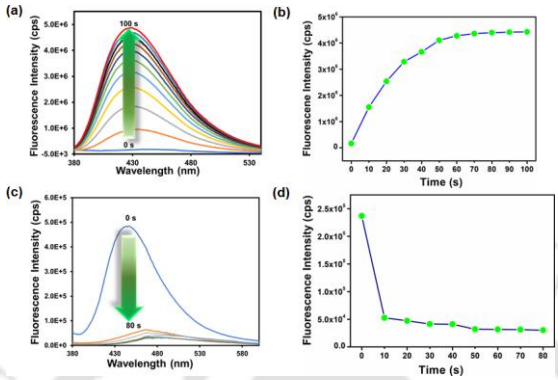

Figure 4.22 Time dependent fluorescence emission intensity of probe **3** after the addition of 300 µL of 10 mM aqueous solution of hydrazine (a) and Hg^{2+} (c). Fluorescence intensity versus time plot for hydrazine (b) and Hg^{2+} (d).

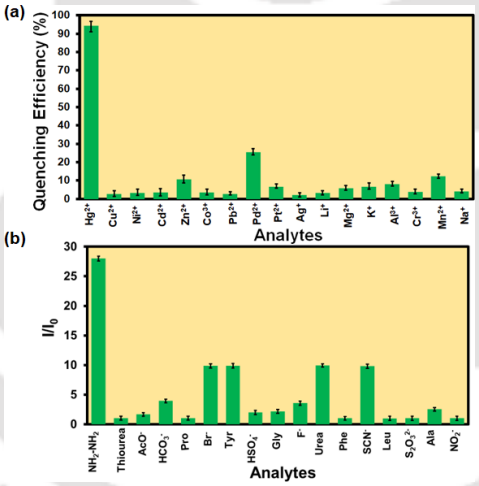

Figure 4.23 (a) Comparative selectivity bar plots of probe **3** towards Hg^{2+} (a) and hydrazine (b) with their respective congeners (plots are shown with standard deviations of three measurements).

The selectivity of the probe over the other competitive analytes was thoroughly investigated. To a MOF suspension of 3000 µL, 300 µL of 10 mM of aqueous competitive analyte solutions (Ag^{+}, K^{+}, Li^{+}, Cd^{2+}, Zn^{2+}, Cu^{2+}, Mg^{2+}, Mn^{2+}, Pb^{2+}, Ni^{2+}, Na^{+}, Pt^{2+}, Pd^{2+}, Al^{3+}, $Cr^{3+}$and Co^{3+}) were added in individual experiments and the fluorescence intensity was recorded (Figure 4a). We found a quenching efficiency of 92% in the case of Hg^{2+}, whereas for other analytes, the quenching efficiency only remained below 25% (Figure 4.23a). A similar experiment was performed using an aqueous MOF suspension and competitive analytes (ala, gly, leu, tyr, pro, urea, thiourea, phe, Br^{-}, F^{-}, CH_3COO^{-}, HSO_4^{-}, NCS^{-}, HCO_3^{-}, $S_2O_3^{2-}$ and NO_2^{-}) of hydrazine (Figure 4.23b). We found an immediate 29-fold increment in fluorescence intensity when hydrazine was added to an aqueous MOF suspension. However, a minor enhancement in fluorescence intensity was noticed for other competitive analytes of hydrazine. The above

experiments confirmed that the probe **3** is highly selective over other competitive analytes for the selective detection of Hg^{2+} and hydrazine, as shown in Figure 4.23b. An ideal probe should not only detect the target analyte selectively, but the detection process should also be repeatable and with a minimum allowed standard error. Therefore, the selectivity experiment was carried out three times and the error in the 2D-bar plot is presented as the standard deviation in Figure 4.23a and Figure 4.23b. The minor standard deviations confirmed that our probe is reproducible in providing the exact results repeatedly.

We evaluated the selectivity of our probe to hydrazine and Hg^{2+} in a complex medium in the presence of other competitive analytes. A three-step procedure was carried out for the selectivity experiments. In the first step, the fluorescence emission intensity of MOF suspension was recorded. In the second step, 300 µL of 10 mM aqueous solution of a competitive analyte was added and the fluorescence spectrum was recorded. In the last step, 300 µL of 10 mM aqueous Hg^{2+} solution was added and fluorescence emission intensity was recorded. The same experiment was repeated for all the competitive analytes of Hg^{2+}. Similar experimental procedures were adopted for all the competitive analytes of hydrazine as well. The obtained results showed that probe **3** can detect both Hg^{2+} and hydrazine selectively in the presence of respective competitors. As displayed in Figure 4.24a and Figure 4.24b, there is no such competitor analyte to question the selectivity of probe **3** for detecting both the targeted analytes (Hg^{2+} and hydrazine).

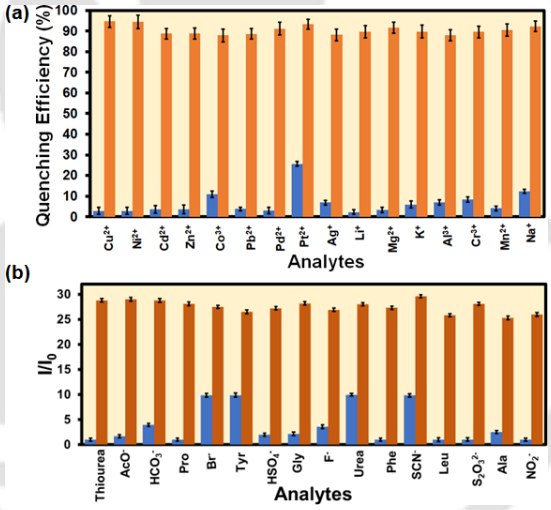

Figure 4.24 The comparative selectivity bar plot (with standard deviations) of probe **3** towards Hg^{2+} (a) and hydrazine (b) in the presence of their respective congeners. The brown bars represent the quenching efficiency towards Hg^{2+} and fold increment in the case of hydrazine and the blue bars belong to the competitive analytes.

The low values of limit of detection (LOD) is one of the essential properties of an ideal sensor. Therefore, we performed the fluorescence sensing experiment of **3** of our probe towards detecting mercury and hydrazine in the concentration of analytes as low as possible. After a systematic investigation, we calculated the LOD values using the formula of $3\sigma/k$. Here, σ is the standard deviation of the blank fluorescence intensities of only MOF suspension and k is the slope of the curve (linear fit curve between fluorescence intensity and concentration) (Figures 4.25 to 4.26). The LOD values of probe **3** were 1.9 ± 0.25 nM and 4.0 ± 0.37 nM for hydrazine and Hg^{2+} detection, respectively. The obtained LOD values are lower in comparison with any MOF-based sensors of mercury and hydrazine to date (Tables 4.6 and 4.7). The selectivity, sensitivity and lower LOD value of our probe **3** toward detecting mercury and hydrazine make it an ideal sensor.

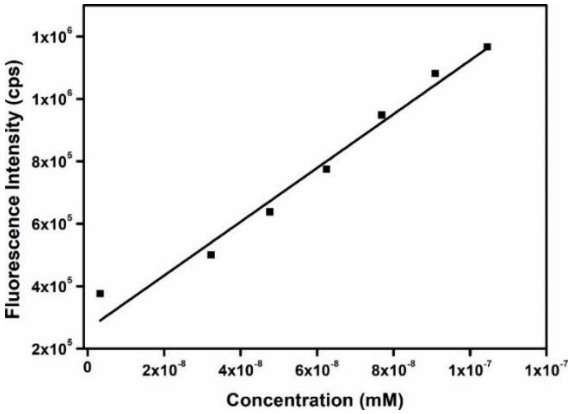

Figure 4.25 Change in the fluorescence intensity of **3** in water as a function of concentration of hydrazine (with error bars).

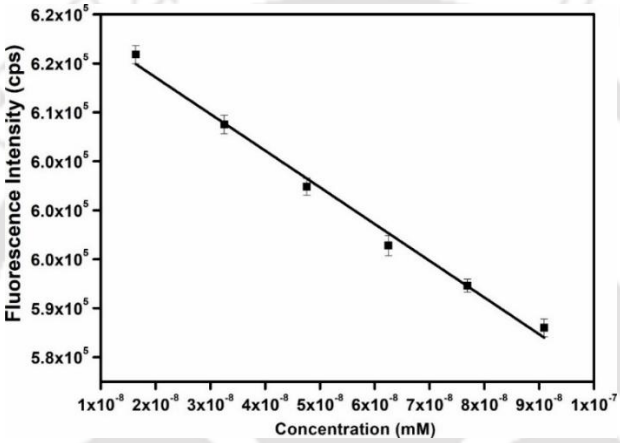

Figure 4.26 Change in the fluorescence intensity of **3** as a function of concentration of Hg^{2+} (with error bars).

To understand the quenching process of the probe by Hg^{2+}, we plotted the Stern-Volmer plot. The Stern-Volmer plot in Figure 4.48 displays that at lower concentration, the plot is linear, but at higher concentration, it became steeper. The above observation concluded that the quenching process might be due to static or dynamic pathway.[434] Therefore, we carried out the time-resolved fluorescence lifetime experiment. Again, the Stern-Volmer constant (K_{sv}) obtained from the slope of the plot between I_0/I versus the concentration of mercury confirmed that the quenching process must be due to strong interaction between the probe and mercury as the K_{sv} value is much higher (7.49×10^5 M^{-1}). The 3D-Stern-Volmer plot, also presented in Figure 4.27, shows that the material is highly selective for mercury over other analytes in a wide concentration range.

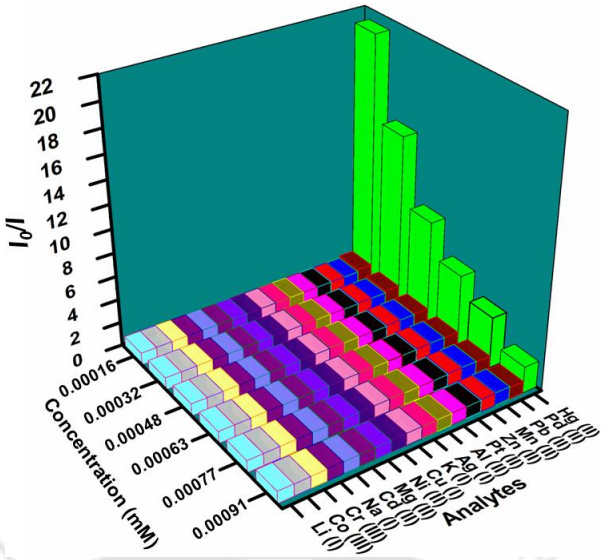

Figure 4.27 3D Stern-Volmer plot for the detection of Hg^{2+}.

The recyclability of the probe for the sensing of mercury was examined by washing it with DMF and water after each cycle of the sensing process. We performed the recyclability experiment up to seven cycles which showed that the probe is equally efficient in detecting Hg^{2+} up to seventh cycles, as shown in Figure 4.28.

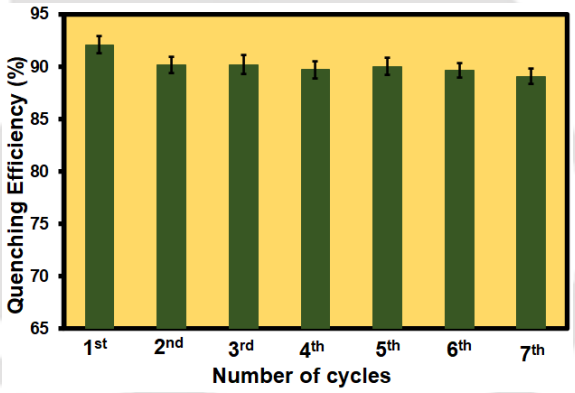

Figure 4.28 Recyclability of probe **3** towards the detection of Hg^{2+} for 7 cycles with almost equal quenching efficiency up to 7^{th} cycle.

The sensing of hydrazine in different water specimens was studied in a systematic way. A MOF suspension was prepared in each water specimen (river water, seawater, lake water, tap water and distilled water). A series of aqueous hydrazine solutions of 3.33 mM, 6.66 mM and 10 mM concentrations were prepared and utilized for sensing experiments. The fluorescence experiment was carried out in a general manner by recording the fluorescence emission intensity before and after the addition of different concentrations of hydrazine. The obtained results shown in Figure 4.29a proved that our probe has the efficiency in detecting hydrazine even from a complex water specimen system. These results indicate that the probe can work for real-field application purposes.

Again, the detection of hydrazine in different pH solutions was examined. The obtained results in Figure 4.29b indicates that our probe could detect hydrazine in a wide pH range (pH 4 to pH 12). At pH 2, the presence of an acidic medium immediately protonated the added hydrazine

and hindered its attack on the thiocarbonyl group. Therefore, a negligible turn-on in fluorescence emission intensity noticed after the addition of hydrazine to MOF suspension.

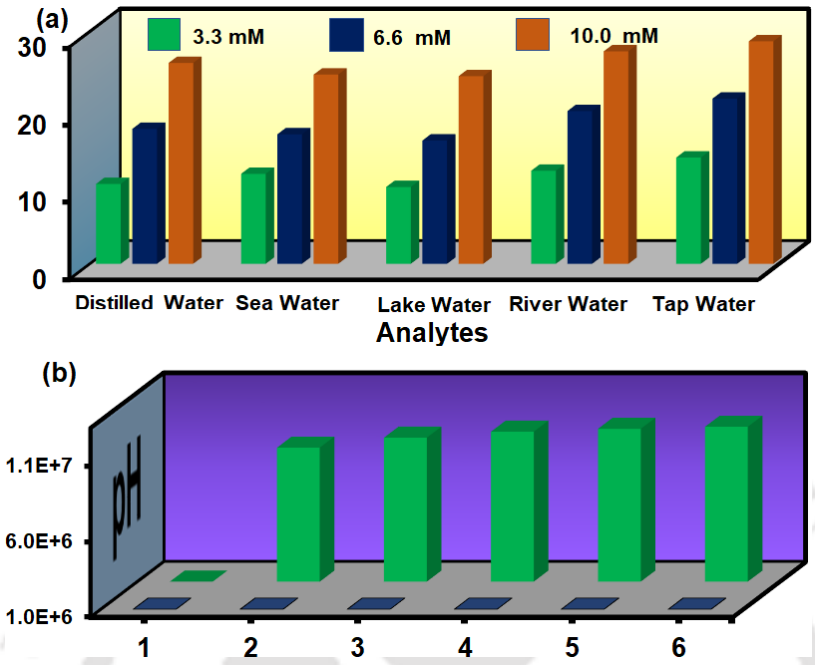

Figure 4.29 (a) Detection of hydrazine in environmental water specimens at different concentrations. (b) Detection of hydrazine in various pH solutions.

A naked eye detection method was adopted by adding hydrazine and mercury to the cuvettes containing MOF suspension under a fluorescence lamp. A turn-on blue fluorescence light was observed after the addition of hydrazine, whereas after the addition of mercury, a turn-off in fluorescence was observed under the fluorescence lamp. A cotton composite-based device was also designed by coating MOF powder onto the surface of a cotton cloth. For preparing the MOF-cotton composite, at first, cotton pieces were washed with ethanol and acetone and dried. The clean cotton pieces were immersed in MOF suspension in ethanol. The cotton pieces were stirred in MOF suspension slowly for 24 h. Then, the pieces were removed and dried in an oven. The dried MOF-cotton composite was utilised further for real-field sensing purposes. The cotton possesses free hydroxy groups on its surface and the Hf-atom of **3** is oxophilic in nature. Therefore, the MOF material was bound to the hydroxy groups on the surface of cotton to produce a useful cotton-composite material, which has great utilization for real-field sensing application purposes. After adding mercury and hydrazine to the MOF-coated cotton composite, similar turn-off and turn-on phenomena in fluorescence intensity were noticed (Figure 4.30). The simple cotton composite-based naked eye sensing device made of our material applicable in real-world sensing purpose.

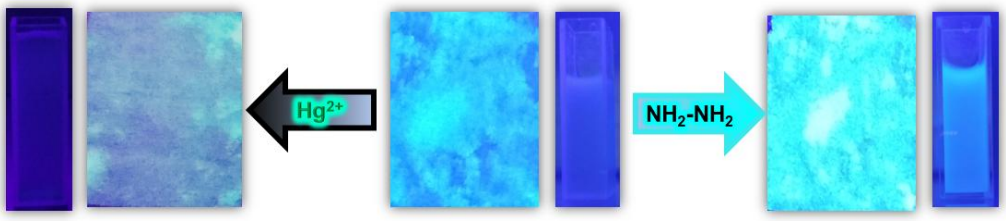

Figure 4.30 Naked eye detection of Hg^{2+} and hydrazine by MOF-coated cotton composite under fluorescence lamp.

Table 4.2 Intra-day and inter-day precession towards detection of Hg^{2+} towards with standard deviation and relative standard deviation.

Volume of Hg^{2+} Solution Added	Intra-Day Fluorescence Emission Intensity (cps)			Mean (χ)	Standard Deviation (σ)	Relative Standard Deviation (RSD)
0 µL	461358.6	462046.4	461947.9	461784.3	371.9	0.081
50 µL	214541.7	215282.9	216689.2	215504.6	1090.8	0.506
100 µL	124669.3	125729.4	126317.4	125572.0	835.3	0.665
150 µL	77811.0	77153.8	77527.4	77497.4	329.6	0.425
200 µL	48169.6	48736.6	48896.6	48600.9	382.0	0.786
250 µL	33920.7	33296.7	33558.1	33591.8	313.4	0.933
300 µL	22522.4	22841.6	22217.5	22527.1	312.1	1.385
Volume of Hg^{2+} solution added	Inter-Day Fluorescence Emission Intensity (cps)			Mean (χ)	Standard Deviation (σ)	Relative Standard Deviation (RSD)
0 µL	461358.6	462579.4	460047.9	461328.6	1266.0	0.274
50 µL	214541.7	220282.9	218689.7	217837.9	2963.8	1.361
100 µL	124669.3	126532.4	125212.4	125471.4	958.2	0.764
150 µL	77811.0	78039.8	76513.3	77454.7	823.2	1.061
200 µL	48169.6	48254.6	49038.6	48487.6	479.1	0.988
250 µL	33920.7	32485.2	34061.1	33489.0	872.1	2.604
300 µL	22522.4	21832.6	23424.5	22593.2	798.3	3.533

Table 4.3 Intra-day and inter-day precession towards detection of hydrazine with standard deviation and relative standard deviation.

Volume of Hydrazine Solution Added	Intra-Day Fluorescence Emission Intensity (cps)			Mean (χ)	Standard Deviation (σ)	Relative Standard Deviation (RSD)
0 µL	164150.3	163163.2	163084.1	163465.9	594.1	0.363
50 µL	560246.9	562283.7	563234.3	561921.6	1526.2	0.272
100 µL	1406800.8	1402152.4	1408004.7	1405652.1	3090.1	0.220
150 µL	2516240.9	2513823.7	2508612.3	2512891.8	3898.2	0.155
200 µL	3628730.1	3623210.1	3625432.7	3625790.9	2777.3	0.077
250 µL	4351430.3	4356219.3	4359842.8	4355830.7	4219.8	0.097
300 µL	5075660.6	5084791.6	5078214.6	5079555.4	4711.1	0.093
Volume of hydrazine Solution Added	Inter-Day Fluorescence Emission Intensity (cps)			Mean (χ)	Standard Deviation (σ)	Relative Standard Deviation (RSD)
0 µL	164150.3	162578.7	163897.5	163608.8	920.4	0.563
50 µL	560246.9	562237.3	558721.9	560402.04	1762.8	0.315
100 µL	1406800.8	1415758.9	1413975.5	1412178.1	4742.2	0.336
150 µL	2516240.9	2508278.4	2509391.8	2511303.4	4311.3	0.1717
200 µL	3628730.1	3609873.7	3619854.5	3614486.1	5033.2	0.139
250 µL	4351430.3	4360429.6	4349852.3	4353904.0	5706.2	0.1311
300 µL	5075660.6	5100874.7	4997528.2	5058021.0	53884	1.0653

4.3.4 Mechanism of Hydrazine Sensing

A systematic experimental investigation was performed to find the reason behind the selective turn-on detection of hydrazine by probe **3**. The PXRD analysis of the probe was performed after one cycle of sensing experiment and the retention of the exact PXRD pattern before and after sensing confirmed that the turn-on behaviour of the probe was not due to structural destruction of the MOF material (Figure 4.31). The recyclability experiment was performed using the recovered material after the first cycle of the sensing experiment. The fluorescence spectrum of the recovered probe showed a turn-on nature before adding hydrazine solution. The above result confirmed that a new species was generated due to the reaction between the functional group of the probe and hydrazine. Therefore, the fluorescence turn-on occurred by a reaction-based pathway.

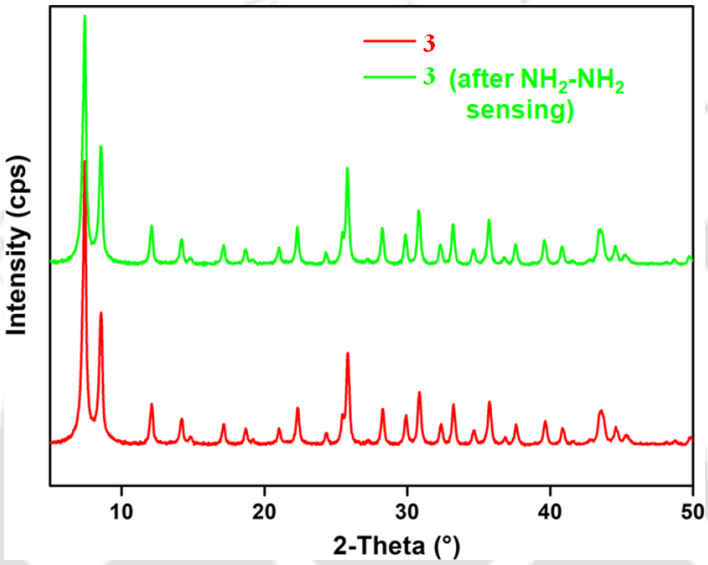

Figure 4.31 PXRD patterns of **3** before (red) and after (green) sensing of hydrazine.

To know the exact active center of the reaction, we carried out sensing experiments with Hf-UiO-66-NH_2 MOF. The obtained result showed that after adding hydrazine solution to Hf-UiO-66-NH_2 suspensions, there was little change in fluorescence emission intensity. The above result indicated that the reaction between the thiocarbonyl group of the probe and hydrazine is the reason behind the fluorescence turn-on behavior. Again, we repeated the fluorescence sensing experiment utilizing a Hf-BDC-$NHCON(CH_3)_2$ MOF in place of our probe **3**. In this case, a similar fluorescence turn-on behavior like probe **3** was noticed (Figure 9). The probe Hf-BDC-$NHCON(CH_3)_2$ is not selective for other competitive analytes like (NCS^-, HSO_4^-, $S_2O_3^{2-}$ etc. Hf-BDC-$NHCON(CH_3)_2$ showed a similar turn-on behaviour like hydrazine). The higher electrophilicity of Hf-BDC-$NHCON(CH_3)_2$ is the cause of the absence of selectivity, whereas, with probe **3**, the moderate electrophilicity of thiocarbonyl group helps to detect hydrazine without having any selectivity issue. The α-effect of hydrazine causes the nucleophilic attack on the thiocarbonyl group. It breaks the conjugation from the aromatic part of the linker resulting in an enhancement in fluorescence emission intensity. Further proof of reaction-based nucleophilic attack to the thiocarbonyl functionality of the linker was supported by the ^1H NMR and ^{13}C NMR spectra. The aromatic peaks in ^1H NMR spectrum of hydrazine-treated **3** displayed an up-field chemical shift due to an increase in electron density on the benzene ring (Figure 4.32). In ^{13}C NMR spectrum, the disappearance of the peak at 175 ppm and the appearance of the 149 ppm peak is a strong evidence of the nucleophilic attack by hydrazine (Figure 4.33**)**. Again, the UV-Vis spectra of probe **3** before and after the addition of

hydrazine was examined. We noticed a considerable change in the absorbance spectrum after adding hydrazine. It also supports that the enhancement in fluorescence emission intensity of the probe **3** after adding hydrazine might be due to a reaction-based pathway (Figure 4.35).

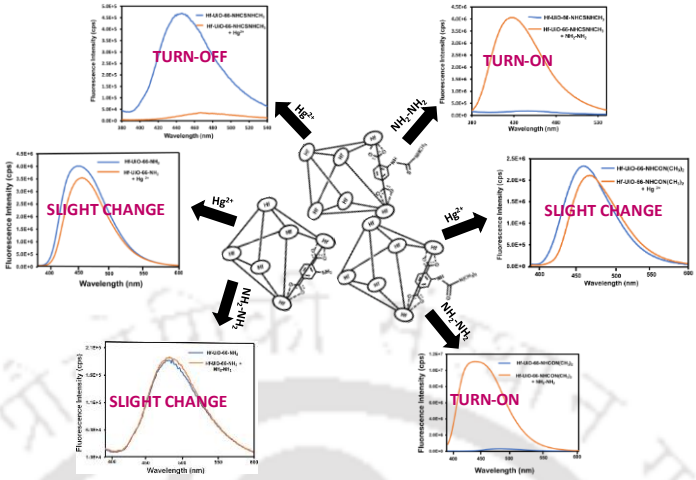

Figure 4.32 Schematic representation of the change in fluorescence emission intensity of Hf-UiO-66-NH_2, **3** and Hf-UiO-66-$NHCON(CH_3)_2$ before and after the addition of Hg^{2+} and hydrazine.

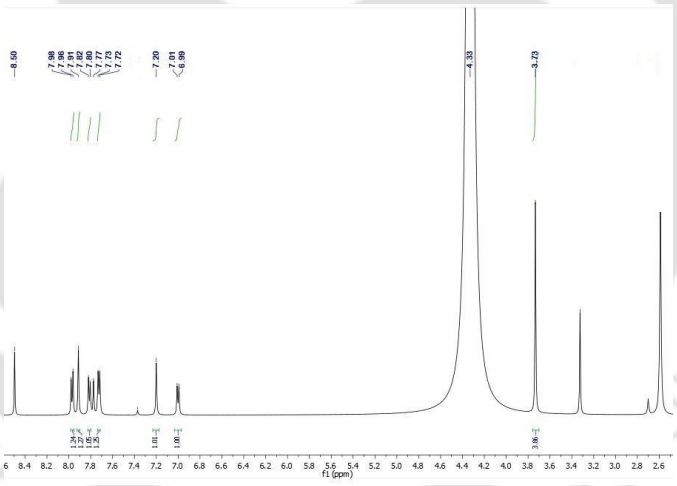

Figure 4.33 Digested ^1H NMR spectrum of **3** after treatment with hydrazine.

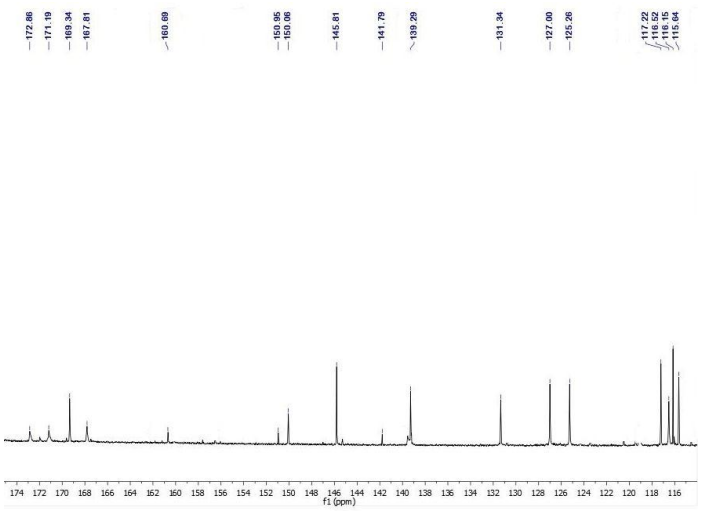

Figure 4.34 Digested ^{13}C NMR spectrum of **3** after treatment with hydrazine.

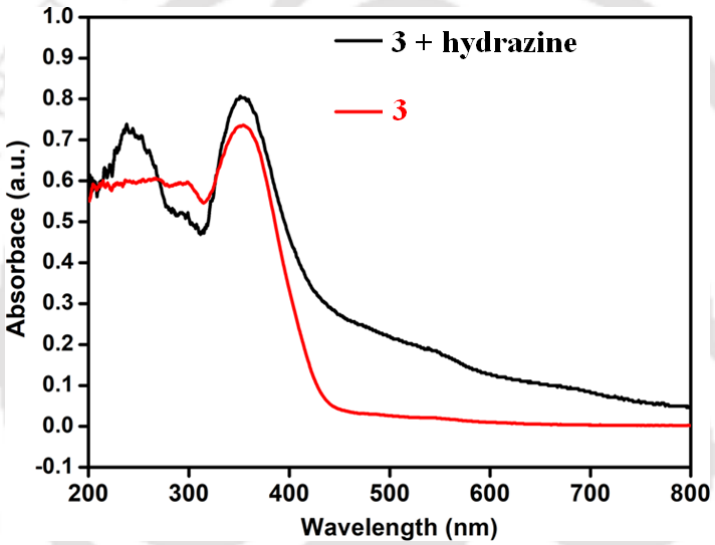

Figure 4.35. UV-Vis spectrum of **3** before (black) and after (red) sensing of hydrazine Ein solid state.

EDX elemental analysis of the recovered probe after hydrazine sensing confirmed the absence of sulfur atoms, indicating a nucleophilic attack by hydrazine on the thiocarbonyl group of the probe and thereby causing loss of sulfur in the form of hydrogen sulfide (H_2S) (Figure 4.36). To confirm the removal of sulfur in the form of H_2S, we used a previously reported azide-based H_2S sensor, Nap-but, for H_2S detection.[435] The H_2S sensor was spiked with our MOF suspension and the fluorescence spectrum was recorded. The same was also utilized by Bhabak et al. to detect the H_2S from their reaction medium.[436] After the addition of hydrazine to the above mixture, we noticed a prominent enhancement in fluorescence intensity, which confirmed the release of H_2S from our probe due to the attack of hydrazine on the thiocarbonyl part of our probe (Figure 4.37). When we added hydrazine to a mixture of our probe and lead acetate in water, we noticed immediate black precipitation due to the formation of lead sulfide (Figure 4.38).[437] The source of sulfur must be due to the detachment of sulfur from our probe. As we know that lead acetate is very reactive towards H_2S to form lead sulfate. The color of lead sulfate is black, and we noticed black sediment in the mixed suspension after adding hydrazine. All the above experimental data strongly supported the nucleophilic attack of

hydrazine to the thiocarbonyl center of our probe. It caused the enhancement in fluorescence emission intensity after adding hydrazine to the probe.

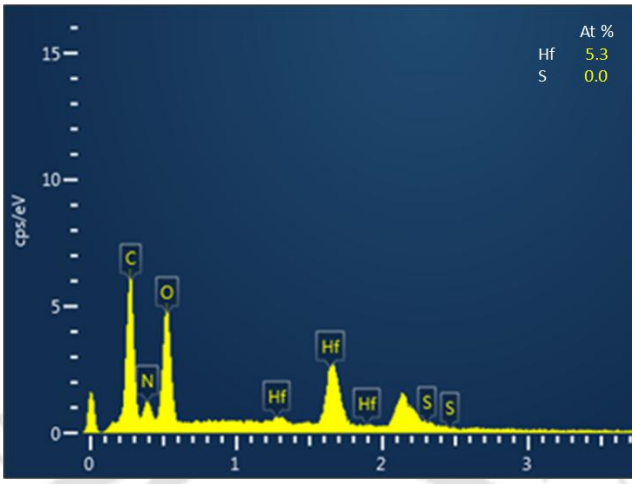

Figure 4.36 EDX spectrum of recovered **3** after sensing of hydrazine.

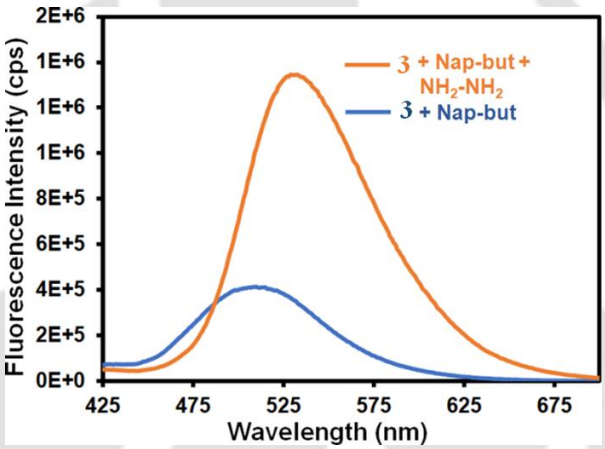

Figure 4.37 Change in fluorescence emission intensity of **Nap-but** (H_2S sensor) in the presence of probe **3** and after addition of hydrazine.

Figure 4.39 Change in colour of **3** + $Pb(CH_3COO)_2$ aqueous mixture after the addition of hydrazine.

4.3.5 Mechanism of Hg^{2+} Sensing

A significant quenching in the fluorescence spectrum of **3** by mercury inspired us to explore the sensing mechanism of our probe towards mercury. The fluorescence quenching mechanism is very crucial from a chemist's perspective. Therefore, we conducted a series of experiments to find the exact reason behind the quenching process. As we mentioned above, the probe is recyclable and the PXRD pattern remained unchanged after sensing (Figure 4.40), proving that the fluorescence quenching process is neither due to a reaction-based process nor due to structural destruction of framework structure. Further, the EDX spectrum of the probe after sensing and thorough washing did not show Hg^{2+} or loss of any element, which also supported the above statement that the quenching process is neither due to a reaction-based process nor due to structural destruction of the framework (Figure 4.41). The washing process was carried out by stirring the recovered sample in water for 24 h, followed by filtration and drying for further use. The recovered sample after the sensing of Hg^{2+} without washing showed the presence of Hg^{2+} in the EDS (TEM) spectrum and elemental mapping, which confirmed the weak complexation between the probe and Hg^{2+} (Figure 4.42 and 4.43).

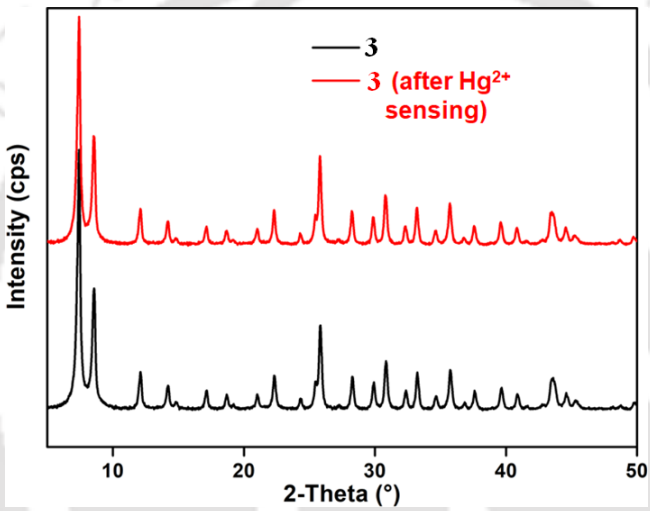

Figure 4.40 PXRD pattern of **3** before (black) and after (red) the addition of aqueous solution of Hg^{2+}.

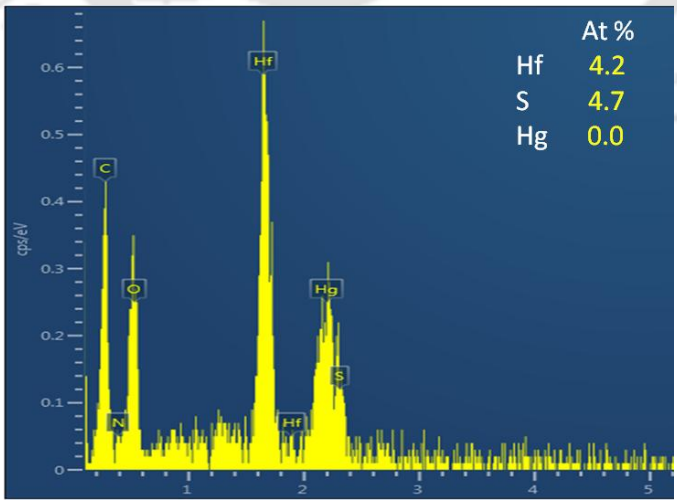

Figure 4.41 TEM-EDX spectrum of **3** after Hg^{2+} sensing after through washing.

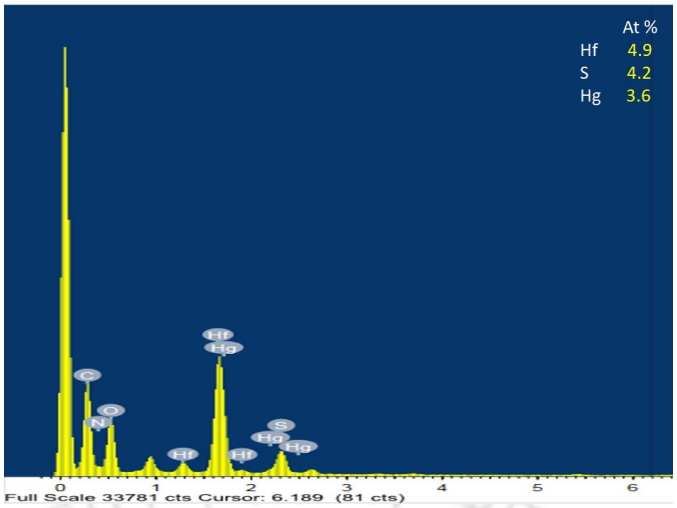

Figure 4.42 TEM-EDX spectrum of **3** after Hg^{2+} sensing and without through washing.

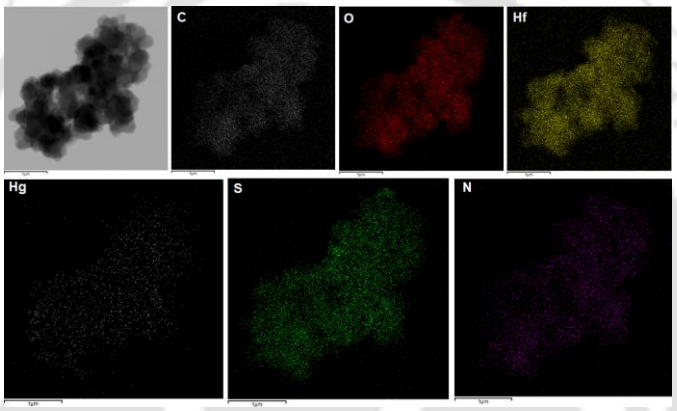

Figure 4.43 TEM-EDX mapping of **3** after Hg^{2+} sensing and without washing.

Furthermore, we carried out the fluorescence lifetime study of probe **3** before and after adding Hg^{2+}. The fluorescence lifetime of the probe remained almost the same before and after adding mercury solution to the MOF suspension (Figure 4.44 and Table 4.4). Therefore, the quenching process was not due to a dynamic pathway that kicked out the possibility of fluorescence resonance energy transfer mechanism. The above result confirmed that the fluorescence quenching process occurred through a static quenching pathway, i.e., due to the ground state complexation between the probe and mercury, which allows the electron transfer from the probe to the vacant orbital of mercury. As reported by many previous works, the sulfur atom of the thiocarbonyl group is the center for interaction with mercury, and in our case, the sulfur of the probe may be the center for soft-soft interaction with the mercury.[438] Therefore, we performed X-ray photoelectron spectroscopy to find the exact active center of complexation. We executed the XPS analysis of **3** before and after interaction with mercury. The binding energies of the 2S orbital of sulfur were 161.96 and 163.09 eV before the interaction with mercury. They became 162.46 and 163.58 eV after the interaction with mercury, providing a direct support for interaction of mercury with sulfur. The mercury-sulfur interaction allows the transfer of electrons from the probe to mercury and thereby causes quenching in the fluorescence intensity of the probe (Figure 4.45). The presence of the XPS characteristic peak of mercury is also direct proof of the interaction between the sulfur atom of the probe and Hg^{2+} (Figure 4.46).[439] The solid state UV-Vis spectrum of our material before and after the addition

of Hg^{2+} showed an 24 nm red shift which is a strong evidence of ground state complexation between our probe and Hg^{2+} (Figure 4.47).

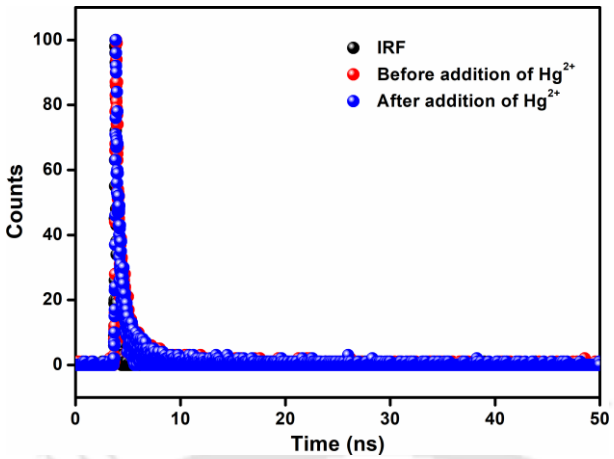

Figure 4.44 Fluorescence life-time decay curve of probe **3** before and after the addition of Hg^{2+}.

Table 4.4 Fluorescence life time change (in ns) of probe **3** before and after the addition of 300 μL of aqueous Hg^{2+} solution.

Volume of Hg^{2+} solution added (μL)	B_1	a_1	τ_1 (ns)	$\langle\tau\rangle^*$ (ns)	χ^2
0	0.0782	1	0.476	0.476	1.054
300	0.0741	1	0.479	0.479	1.001

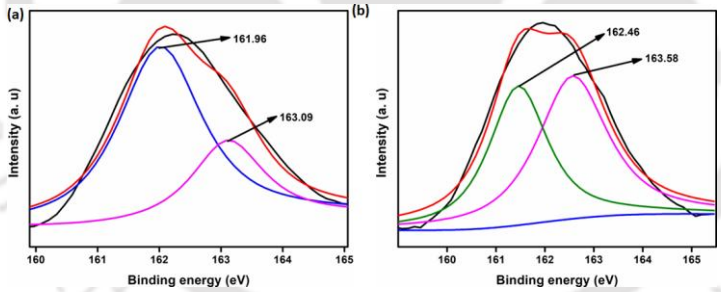

Figure 4.45 Fitted XPS spectra of S (2s) before (a) and after (b) treatment of Hg^{2+} with **3**.

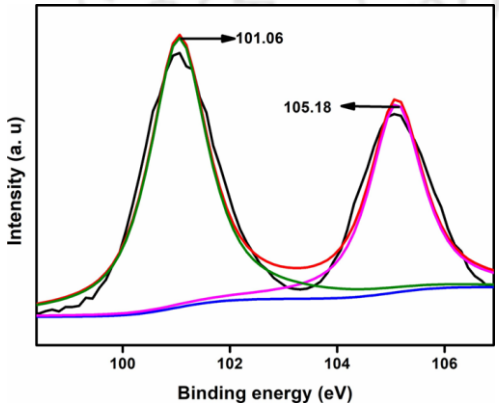

Figure 4.46 Fitted XPS spectra of Hg (4f) after treatment of Hg^{2+} with **3**.

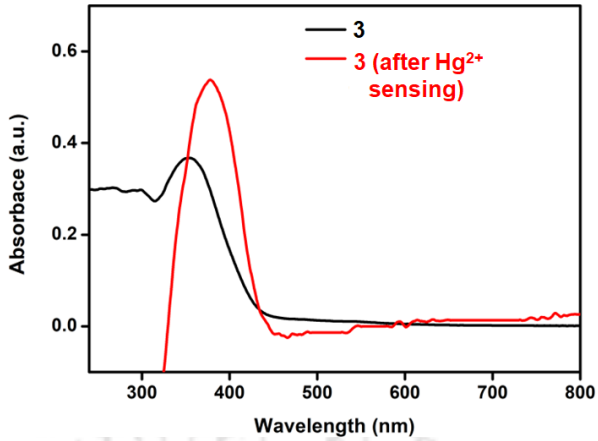

Figure 4.47 Solid-state UV-Vis spectrum of **3** before (black) and after (red) sensing of Hg^{2+}.

Further confirmation of molecular interaction was obtained from a systematic temperature dependant fluorescence experiment of our probe in the presence of different concentrations of mercury in varying temperature range (298-343 K). The K_{sv} value was obtained at different temperatures from the linear fit plot of I/I_0 versus the concentration of mercury (Figure 4.48). There was a decrease in K_{sv} value with an increase in temperature, as shown in Table 1. The reduction in K_{sv} value with a temperature rise also supports the soft-soft interaction between mercury and the sulfur atom of our probe.

The bimolecular binding constant (K_a) at different temperatures was obtained from the intercept of the plot of $\log[(I_0–I)/I]$ versus log[Q] using the modified Stern-Volmer equation (Figure 4.49): $\log[(I_0–I)/I] = \log K_a M + n \log[Q]$. The decrease in the magnitude of the binding constant again supported the fact that the quenching process was due to the soft-soft interaction between mercury and the sulfur atom of our probe (Table 1). By increasing the temperature of the system, the randomness of the system increases and the interaction becomes weak, because of which the value of the binding constant decreased with the increase in temperature.

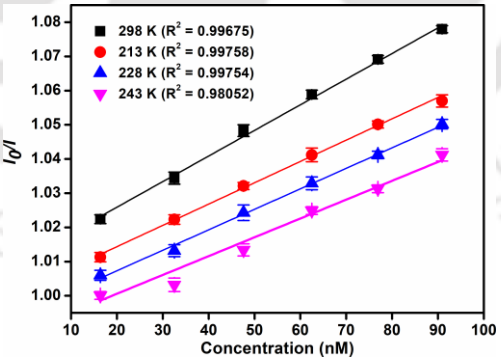

Figure 4.48 Stern-Volmer plots (with error bars) for fluorescence quenching of **3** by Hg^{2+} at different temperatures.

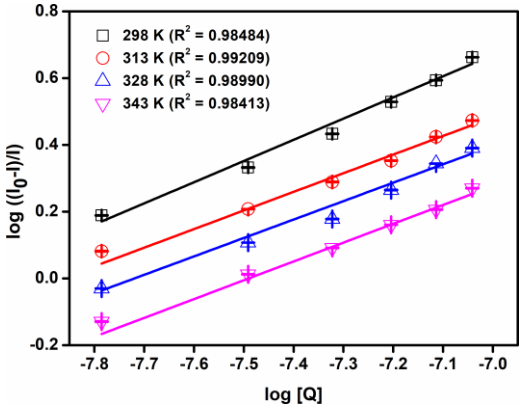

Figure 4.49 Modified Stern-Volmer plots (with error bars) between log((I_0-I)/I) and log [Q].

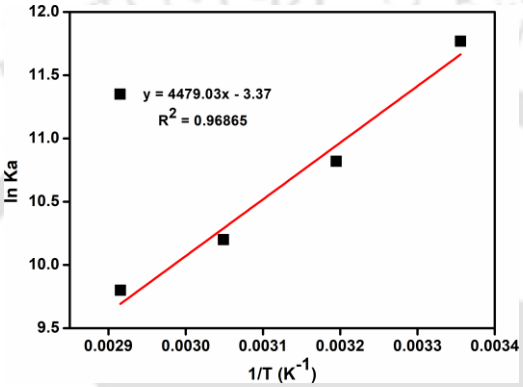

Figure 4.50 Van't Hoff plot for interaction of **3** with Hg^{2+}.

Table 4.5 Thermodynamic parameters obtained from Stern-Volmer, modified Stern-Volmer and Van't Hoff equations obtained from temperature-dependent fluorescence titration experiments in the presence of Hg^{2+} ion.

T (K)	$K_{sv} \times 10^5$ (L mol^{-1})	$K_a \times 10^5$ (L mol^{-1})	ΔG (kJ mol^{-1})	ΔH (kJ mol^{-1})	ΔS (J mol^{-1}K^{-1})
298	7.49	1.29	-28.89	-37.24	-28.02
313	6.23	0.49	-28.47		
328	5.99	0.26	-28.05		
343	5.51	0.19	-27.63		

The thermodynamic parameters, i.e., enthalpy change (ΔH) and entropy change (ΔS) were obtained from the slope and intercept of log K_a versus 1/T plot, respectively (Figure S4.50). As we know that the difference in enthalpy and entropy could help in predicting the interaction process. The positive value of ΔH and ΔS suggests the hydrophobic interaction, whereas the negative value of ΔH and positive value of ΔS suggests the electrostatic interaction. In our case, both the thermodynamic parameters are negative, indicating the molecular interaction.

$$\text{Ln } K_a = -\Delta H/RT + \Delta S/R$$

Further, we calculated the free energy change (ΔG) at different temperatures using the obtained value of ΔH and ΔS and the following thermodynamic formula. The obtained value of ΔG at various temperature were negative, which confirmed the interaction process was

spontaneous and exothermic.[440] The decrease in the magnitude of ΔG with rise in temperature also agrees with the K_a values obtained at various temperatures.

$\Delta G = \Delta H - T\Delta S$

Further, we carried out control fluorescence experiments using Hf-UiO-66-NH_2 and Hf-UiO-66-$NHCON(CH_3)_2$ MOF materials in place of our probe. A negligible quenching in fluorescence emission intensity was observed after adding mercury solution to Hf-UiO-66-NH_2 and Hf-UiO-66-$NHCON(CH_3)_2$ MOF suspensions (Figure 10). The experiments again confirmed that the interaction between the sulfur atom of the probe and mercury is the reason behind the fluorescence quenching process.

Table 4.6 Comparison of the response time, detection limit and sensing media used for the reported fluorescent chemosensors of hydrazine in the literature.

Sl. No.	Sensor Material	Sensing Medium	Mode of Detection	LOD	Detection Time	Ref.
1	Zr-UiO-66-OSO_2-Ph-NO_2	water	turn-on	52.6 nM	2 min	243
2	Zr-UiO-66-$(OCOCH_3)_2$	water	turn-on	78.8 nM	seconds	441
3	UiO-66-phmd	HEPES buffer	turn-on	0.87 µM	20 min	442
4	BTI	HEPES buffer	turn-on	2.9 ppb	20 min	443
5	HyP-1	PBS buffer	turn-on	0.035 ppb	1 h	444
6	P1	PRS buffer	turn-on	1.79 nM	40 s	445
7	BPB	HEPES buffer	turn-off	1.87 µM	-	446
8	Naphsulf-O	PBS buffer	turn-on	22 nM	40 min	447
9	BBHC	PBS buffer	turn-on	0.43 µM	1 min	448
10	CFAc	PBS buffer	ratio-metric	0.0474 µM	-	449
11	BI-E	PBS buffer	turn-on	0.057 µM	1 min	450
12	NA-N_2H_4	HEPES buffer	ratio-metric	9.4 nM	15 min	451
13	TAPHP	HEPES buffer	ratio-metric	0.3 µM	60 min	452
14	AB-NDI	DMSO	turn-on	-	-	453
15	TNQ	PBS buffer	ratio-metric	-	-	454
16	HBTM	PBS buffer	turn-on	29 µM	55 min	455
17	NAC	HEPES buffer	turn-on	4.5 µM	4 min	456
18	DPA	DMSO/ PBS buffer	turn-on	1.9 nM	8 min	457
19	probe 1 and 2	HEPES buffer	turn-on	0.17 µM 0.24 µM	3 min	458
20	SF-Azo compounds	CH_3OH/H_2O (v/v = 1:1)	turn-on	2.33 mM	18-42 min	459
21	levulinated hydroxyl-coumarin 1	acetate buffer	turn-on	2.46 µM	15 min	460
22	Compound 6a	HEPES/ DMSO (1:1, v/v)	turn-on	0.19 µM	-	461
23	NS-N_2H_4	PBS/ DMSO (v/v = 2/1)	turn-on	-	240 min	462

24	PBF	$CH_3CN–H_2O$ (6: 4, v/v)	turn-on	0.41 μM	1 min	[463]
25	**$[Hf_6O_4(OH)_4(C_{10}H_8N_2O_4S)_{3.3}(C_8H_5NO_4)_2]\cdot H_2O$ (3)**	**H_2O**	**turn-on**	**1.9 nM**	**0.8 min**	**this work**

Table 4.7 Comparison of the response time, detection limit and sensing media used for the reported sensors of Hg^{2+} in the literature using fluorometric method.

Sl. No.	Sensor Material	Sensing Medium	Detection Limit (nM)	Response Time (min)	Ref.
1	Thiosemicarbazone	acetate buffer	770	-	[464]
2	GT capped AgNPs	water	0.037	0-60	[465]
3	Azo Crown ether	methanol	13900	-	[466]
4	Rhodamine 6 G based	THF/Water	30.37	-	[467]
5	Tetraphenyl ethylene based AIE probe	water	63	-	[468]
6	Squaraine based fluorescent probe	Ethanol/Water	21.9	3	[469]
7	Rhodamine appended terphenyl	THF	500	30	[470]
8	Double naphthalene Schiff base	DMSO	55.9	80	[471]
9	2-Hydroxy benzothiazole modified rhodol	THF:HEPES	270	-	[472]
10	Nitrogen-doped carbon quantum dots	water	230	15	[473]
11	$[Ni(3\text{-}bpd)_2(NCS)_2]_n$	water	-	120	[474]
12	[PCN-221]	water	10	1	[475]
13	[Cu(Dcbb)(Bpe)]·Cl	HEPES buffer	3.2 and 3.3	30	[476]
14	UiO-66@ Butyne	water	10.9	3	[238]
15	Ln(TATAB) ,$(DMF)_4$ $(H_2O)(MeOH)_{0.5}$	water	4.4	-	[477]
16	Eu^{3+}/CDs@MOF-253	water	47.88	3	[478]
17	$[Cu(Cdcbp)(H_2O)_2\cdot 2H_2O]_n$	water	2.3	2	[479]
18	Al-MOF (TAM)	water	2.94	0.5	[480]
19	[Cu(Cbdcp)(Dps) $(H_2O)_3]\cdot 6H_2On$	HEPES buffer	2.6	10	[481]
20	Cd−EDDA	water	2	0.25	[482]
21	tetrahydrodibenzo phenanthridine derivatives	DMSO/THF	0.91 0.041	1	[483]
22	$[Zn(L)(BBI).(H_2O)_2]$ $[Cd(L)(TPOM)_{0.75}]\cdot xS$	water	-		[484]
33	IITG-5a	water	5	1	[485]
34	**$[Hf_6O_4(OH)_4(C_{10}H_8N_2O_4S)_{3.3}(C_8H_5NO_4)_2]\cdot H_2O$ (3)**	**H_2O**	**4**	**0.16**	**this work**

4.4 Conclusion

The detection capacity of Hg^{2+} and hydrazine by our probe was presented systematically with a proper explanation of the mechanism behind the change in fluorescence emission intensities. The lower detection limit, fast response, recyclability and reproducibility with high precession made our probe reliable over the other reported probes for Hg^{2+} and hydrazine sensing. The cotton-based MOF composite is advantageous over the paper-strip device due to its low-cost and recyclable nature. The probe detects Hg^{2+} and hydrazine in the presence of a wide variety of competitive analysts. The high turn-on in fluorescence emission intensity (28-fold increment) due to hydrazine and for Hg^{2+} high quenching efficiency (92%) made our probe ideal due to the noticeable change in signal. The probe can also detect hydrazine from environmental water samples and a wide range of pH solutions. The detection mechanisms of Hg^{2+} and hydrazine were explained in a systematic manner using appropriate analytical characterization methods, which is an essential criterion for a good sensor material. The overall work presented here will help scientists working in the field of MOF-based sensors due to the reliable and reproducible nature of our probe.

4.5 References

1. F. A. Cotton, G. Wilkinson, C. Murillo and M. Bochmann, *John Wiley and Sons, Inc; New York*, 1999, **6**, 590-629.
2. C. T. Driscoll, R. P. Mason, H. M. Chan, D. J. Jacob and N. Pirrone, *Environ. Sci. Technol.*, 2013, **47**, 4967–4983.
3. M. E. Brigham, D. A. Wentz, G. R. Aiken and D. P. Krabbenhoft, *Environ. Sci. Technol.*, 2009, **43**, 2720–2725.
4. M. Li, A. T. Schartup, A. P. Valberg, J. D. Ewald, D. P. Krabbenhoft, R. Yin, P. H. Balcom and E. M. Sunderland, *Environ. Sci. Technol.*, 2016, **50**, 11559–11568.
5. R. K. B. Barvin, P. Prakash, V. Ganesh and B. Jeyaprabha, *Int. J. Environ. Res. Public Health*, 2013, **13**, 1015–1023.
6. S. Ghosh, F. Steinke, A. Rana and S. Biswas, *Inorg. Chem. Front.*, 2022, **9**, 859-869.
7. L. P. Kuhn, *J. Am. Chem. Soc.*, 1951, **73**, 1510–1512.
8. J. B. Levy, G. V. Elbe, R. Friedman, T. Wallin and S. J. Adams, *Adv. Propellant Chem.*, 1966, **54**, 55-72.
9. A. R. Katritzky, *J. Am. Chem. Soc.*, 2002, **124**, 6504.
10. J. Singh, K. R. B. Singh, M. Kumar, R. Verma, R. Verma, P. Malik, S. Srivastava, R. P. Singh and D. Kumar, *Mater. Adv.*, 2021, **2**, 6665-6675.
11. M. Sun, L. Bai and D. Q. Liu, *J. Pharm. Biomed. Anal.*, 2009, **49**, 529– 533.
12. E. Bakker and M. T. Diaz, *Anal. Chem.*, 2002, **74**, 2781–2800.
13. L. Eilert, A. Schallmey and F. Kaspar, *Anal. Chem.*, 2022, **94**, 3432–3435.
14. M. Michalak, M. Kurel, J. Jedraszko, D. Toczydlowska, G. Wittstock, M. Opallo and W. Nogala, *Anal. Chem.*, 2015, **87**, 11641–11645.
15. Y. Wu, X. Liu, Q. Wu, J. Yi and G. Zhang, *Anal. Chem.*, 2017, **89**, 7084–7089.
16. A. Rana, S. Nandi and S. Biswas, *New J. Chem.*, 2022, **46**, 10477-10483.
17. A. Rana, C. Gogoi, S. Ghosh, S. Nandi, S. Kumar, U. Manna and S. Biswas, *New J. Chem.*, 2021, **45**, 20193-20200.
18. S.Ghosh, F. Steinke, A. Rana, M. Alam and S. Biswas, *Eur. J. Inorg. Chem.*, 2021, **2021**, 3846-3851.
19. Q. Fan, J. Li, Y. Zhu, Z. Yang, T. Shen, Y. Guo, L. Wang, T. Mei, J. Wang and X. Wang, *ACS Appl. Mater. Interfaces*, 2020, **12**, 4797–4803.

20. G. Mao, G. Wu, M. Chen, C. Y. C. Yan and X. Zhang, *Anal. Chem.*, 2022, **94**, 6665–6671.
21. M. Li, T. Chen, J. J. Gooding and J. Liu, *ACS Sens.*, 2019, **4**, 1732–1748.
22. V. Schroeder, S. Savagatrup, S. L. M. He and T. M. Swager, *Chem. Rev.*, 2019, **119**, 599–663.
23. A. K. Singh, A. V. Nair and N. D. P. Singh, *Anal. Chem.* , 2022, **94**, 177–192.
24. A. Recchimurzo, C. Micheletti, G. Uccello-Barretta and F. Balzano, *J. Org. Chem.*, 2021, **86**, 7381-7389.
25. C. Rao and R. Venkataraghavan, *Spectrochim. Acta*, 1989, **45**, 299-305.
26. S. Jakobsen, D. Gianolio, D. S. Wragg, M. H. Nilsen, H. Emerich, S. Bordiga, C. Lamberti, U. Olsbye, M. Tilset and K. P. Lillerud, *Phys. Rev. B*, 2012, **86**, 125429.
27. Z. Hu, A. Nalaparaju, Y. Peng, J. Jiang and D. Zhao, *Inorg. Chem.*, 2016, **55**, 1134-1141.
28. J. Winarta, B. Shan, S. M. Mcintyre, L. Ye, C. Wang, J. Liu and B. Mu, *Cryst. Growth Des.*, 2019, **20**, 1347-1362.
29. L. Valenzano, B. Civalleri, S. Chavan, S. Bordiga, M. H. Nilsen, S. Jakobsen, K. P. Lillerud and C. Lamberti, *Chem. Mater.*, 2011, **23**, 1700-1718.
30. S. Mukherjee, S. Ghosh and S. Biswas, *Inorg. Chem. Front.*, 2022, **9**, 6288-6298.
31. Z. Wu, D. Liang and X. Tang, *Anal. Chem.*, 2016, **88**, 9213-9218.
32. S. K. Mahato, D. Bhattacherjee and K. P. Bhabak, *ChemComm*, 2020, **56**, 7769-7772.
33. J.-H. Cha, D.-H. Kim, S.-J. Choi, W.-T. Koo and I.-D. Kim, *Anal. Chem.*, 2018, **90**, 8769-8775.
34. C. Tang, Y. Qin, C. Ni and J. Zou, *ACS Appl. Polym. Mater.*, 2022, **4**, 849-858.
35. G. Marimuthu, M. Arivanandhan and C. Vedhi, *Synth. React. Inorg. Met.-Org. Nano-Met. Chem.*, 2015, **45**, 217-224.
36. M. Maity, S. Dolui and N. C. Maiti, *Phys. Chem. Chem. Phys.*, 2015, **17**, 31216-31227.
37. S. Ghosh and S. Biswas, *Microporous Mesoporous Mater.*, 2022, **329**, 111552.
38. S. Nandi, M. SK and S. Biswas, *Dalton Trans.*, 2020, **49**, 2830-2834.
39. M. SK, M. R. U. Z. Khan, A. Das, S. Nandi, V. TrivedI and S. Biswas, *Dalton Trans.*, 2019, **48**, 12615-12621.
40. R. Maji, A. K. Mahapatra, K. Maiti, S. Mondal, S. S. Ali, P. Sahoo, S. Mandal, M. R. Uddin, S. Goswami, C. K. Quah and H.-K. Fun, *RSC Adv.*, 2016, **6**, 70855-70862.
41. Y. Jung, I. G. Ju, Y. H. Choe, Y. Kim, S. Park, Y.-M. Hyun, M. S. Oh and D. Kim, *ACS Sens.*, 2019, **4**, 441-449.
42. S. Shweta, A. Kumar, S. K. Asthana, A. Prakash, J. K. Roy, I. Tiwari and K. K. Upadhyay, *RSC Adv.*, 2016, **6**, 94959-99496.
43. A. K. Mahapatra, R. Maji, K. Maiti, S. K. Manna, S. Mondal, S. S. Ali, S. Manna, P. Sahoo, S. Mandal, M. R. Uddin and D. Mandal, *RSC Adv.*, 2015, **5**, 58228-58236.
44. W. Chen, W. Liu, X.-J. Liu, Y.-Q. Kuang, R.-Q. Yu and J.-H.Jiang, *Talanta*, 2017, **162**, 225-231.
45. S. Paul, R. Nandi, K. Ghoshal, M. Bhattacharyya and D. K. Maiti, *New J. Chem.*, 2019, **43**, 3303-3330.
46. Z. Zhang, Z. Zhuang, L. L. Song, X. Lin, S. Zhang, G. Zheng and F. Zhan, *J. Photochem. Photobiol. A*, 2018, **358**, 10-16.
47. J. Ma, J. Fan, H. Li, Q. Yao, J. Xia, J. Wang and X. Peng, *Dyes Pigm.*, 2017, **138**, 39-46.
48. X. Xia, F. Zeng, P. Zhang, J. Lyu, Y. Huang and S. Wu, *Sens. Actuators B*, 2017, **227**, 411-418.
49. Z. Luo, B. Liu, T. Qin, K. Zhu, C. Zhao, C. Pan and L. Eang, *Sens. Actuators B*, 2018, **263**, 229-236.

50. D. Zhou, Y. Wang, J. Jia, W. Yu, B. Qu, X. Li and X. Sun, *Chem. Commun.*, 2015, **51**, 10656-10659.
51. S. Yu, S. Wang, H. Yu, Y. Feng, S. Zhang, M. Zhu, H. Yin and X. Meng, *Sens. Actuators B*, 2015, **220**, 1338-1345.
52. Z. Chen, X. Zhong, W. Qu, T. Shi, H. Liu, H. He, X. Zhang and S. Wang, *Tetrahedron Lett.*, 2017, **58**, 2596-2601.
53. S. Goswami, A. K. Das, U. Saha, S. Maity, K. Khanra and N. Bhattacharyya, *Org. Biomol. Chem.*, 2015, **13**, 2134-2139.
54. Y. Zhang, Y. Huang, Y. Yue, J. Chao, F. Huo and C. Yin, *Sens. Actuators B*, 2018, **273**, 944-950.
55. B. Roy, S. Halder, A. Guha and S. Bandyopadhyay, *Anal. Chem.*, 2017, **89**, 10625-10636.
56. M. C. Shin, Y. Lee, S. B. Park and E. Kim, *ACS Omega*, 2019, **4**, 14875-14885.
57. M. G. Choi, J. Hwang, J. O. Moon, J. Sung and S.-K. Chang, *Org. Lett.*, 2011, **13**, 5260-5263.
58. D. Purohit, C. P. Sharma, A. Raghuvanshi, A. Jain, K. S.Rawat, N. M.Gupta, J. Singh, M. Sachdev and A. Goel, *Chem. Eur.J.*, 2019, **25**, 4660-4664.
59. J.-Y. Wang, Z.-R. Liu, M. Ren and W. Lin, *Sci. Rep.*, 2017, **7**, 1-8.
60. S. Goswami, S. Paul and A. Manna, *New J. Chem.*, 2015, **39**, 2300-2305.
61. Y. Yu, L.-R. Lin, K.-B. Yang, X. Zhong, R.-B. Huang and L.-S. Zheng, *Talanta*, 2006, **69**, 103-106.
62. P. G. Mahajan, N. C. Dige, B. D. Vanjare, A. R. Phull, S. J. Kim and K. H. Lee, *J. Lumin.*, 2019, **206**, 624-633.
63. Y.-C. Hsieh, J.-L. Chir, H.-H. Wu, P.-S. Chang and A.-T. Wu, *Carbohydr. Res.*, 2009, **344**, 2236-2239.
64. B. D. Vanjare, P. G. Mahajan, H.-I. Ryoo, N. C. Dige, N. G. Choi, Y. Han, S. J. Kim, C.-H. Kim and K. H. Lee, *Sens. Actuators B Chem.*, 2021, **330**, 129308.
65. V. Bhalla, R. Tejpal and M. Kumar, *Sens. Actuators B: Chem.*, 2010, **151**, 180-185.
66. B. Yuan, D.-X. Wang, L.-N. Zhu, Y.-L. Lan, M. Cheng, L.-M. Zhang, J.-Q. Chu, X.-Z. Li and D.-M. Kong, *Chem. Sci.*, 2019, **10**, 4220-4226.
67. S.-Y. Lin, H.-J. Zhu, W.-J. Xu, G.-M. Wang and N.-Y. Fu, *Chin. Chem. Lett.*, 2014, **25**, 1291-1295.
68. T.-b. Wei, G.-y. Gao, W.-j. Qu, B.-b. Shi, Q. Lin, H. Yao and Y.-m. Zhang, *Sens. Actuators B: Chem.*, 2014, **199**, 142-147.
69. S. Chen, W. Wang, M. Yan, Q. Tu, S.-W. Chen, T. Li, M.-S. Yuan and J. Wang, *Sens. Actuators B: Chem.*, 2018, **255**, 2086-2094.
70. R. Zhang and W. Chen, *Biosens. Bioelectron.*, 2014, **55**, 83-90.
71. S. Halder, J. Mondal, J. Ortega-Castro, A. Frontera and P. Roy, *Dalton Trans.*, 2017, **46**, 1943-1950.
72. E. Moradi, R. Rahimi and V. Safarifard, *J. Solid State Chem. Sci.*, 2020, **286**, 121277.
73. P.-P. Hu, N. Liu, K.-Y. Wu, L.-Y. Zhai, B.-P. Xie, B. Sun, W.-J. Duan, W.-H. Zhang and J.-X. Chen, *Inorg. Chem.*, 2018, **57**, 8382-8389.
74. P. Samanta, A. V. Desai, S. Sharma, P. Chandra and S. K. Ghosh, *Inorg. Chem.*, 2018, **57**, 2360-2364.
75. T. Xia, T. Song, G. Zhang, Y. Cui, Y. Yang, Z. Wang and G. Qian, *Chem. Eur. J.*, 2016, **22**, 18429-18434.
76. X.-Y. Xu and B. Yan, *J. Mater. Chem. C*, 2016, **4**, 1543-1549.
77. N.-H. Huang, R.-T. Li, C. Fan, K.-Y. Wu, Z. Zhang and J.-X. Chen, *J. Inorg. Biochem.*, 2019, **197**, 110690.

78. A. Radwan, I. M. El-Sewify, A. Shahat, H. M. Azzazy, M. M. Khalil and M. F. El-Shahat, *ACS Sustain. Chem. Eng.*, 2020, **8**, 15097-15107.
79. N.-H. Huang, Y. Liu, R.-T. Li, J. Chen, P.-P. Hu, D. J. Young, J.-X. Chen and W.-H. Zhang, *Analyst*, 2020, **145**, 2779-2788.
80. P. Wu, Y. Liu, Y. Liu, J. Wang, Y. Li, W. Liu and J. Wang, *Inorg. Chem.*, 2015, **54**, 11046-11048.
81. M. Ponram, U. Balijapalli, B. Sambath, S. K. Iyer, B. Venkatachalapathy, R. Cingaram and K. N. Sundaramurthy, *New J. Chem.*, 2018, 8530-8536.
82. Y. Zhao, X. Xu, L. Qiu, X. Kang, L. Wen and B. Zhang, *ACS Appl. Mater. Interfaces*, 2017, **9**, 15164-15175.
83. Y. Yang, G. Ren, W. Yang, X. Qin, D. Gu, Z. Liang, D.-Y. Guo and P. Qinhe, *Polyhedron*, 2021, **194**, 114923.

Design of Functionalized Luminescent MOF Sensor for Precise Monitoring of Tuberculosis Drug and Neonicotinoid Pesticide from Human Body-Fluids and Food Samples to Protect Health and Environment

Selectively detecting pharmaceutical drugs and pesticides from drinking water and environmental water sources with an ultralow detection limit by a simple handling method remains challenging. To circumvent such challenges, we prepared an aluminium metal-organic framework (MOF) using 2-(((2-hydroxy naphthalene-1-yl)methyl)amino)terephthalic acid (H_2L^4) linker. We explored the potential of the guest-free MOF for fluorescence detection of a largely utilized neonicotinoid category of pesticide called nitenpyram and a very common antibiotic drug used for curing tuberculosis namely rifampicin. It is the first MOF-based fluorescent sensor capable of detecting nitenpyram and rifampicin by fluorescent turn-off mode. This probe has lower detection limit (LOD for rifampicin: 11.7 nM and nitenpyram: 13.8 nM) as compared to formerly reported probes of nitenpyram and rifampicin sensing. It can detect nitenpyram and rifampicin instantaneously (within 5 s). The ultrafast nature of this probe made it superior to the previously reported time-consuming probes. This sensor material is recyclable for five times for sensing nitenpyram and rifampicin, boosting its cost-effectiveness and sustainability. This chemically robust MOF material was utilized for the fluorometric detection of both analytes in drinking water and environmental water samples. The probe can also precisely quantify rifampicin from human blood serum, urine, and nitenpyram from soil and food samples (rice and corn). The mechanistic aspects of the detection events have been unveiled with the help of systematic experimental techniques and molecular simulations. In addition, the repeatability and reproducibility of the probe to sense both analytes were demonstrated. The overall work presents an inexpensive and compatible multiple-usable photoluminescent sensor of nitenpyram and rifampicin to address real-world issues.

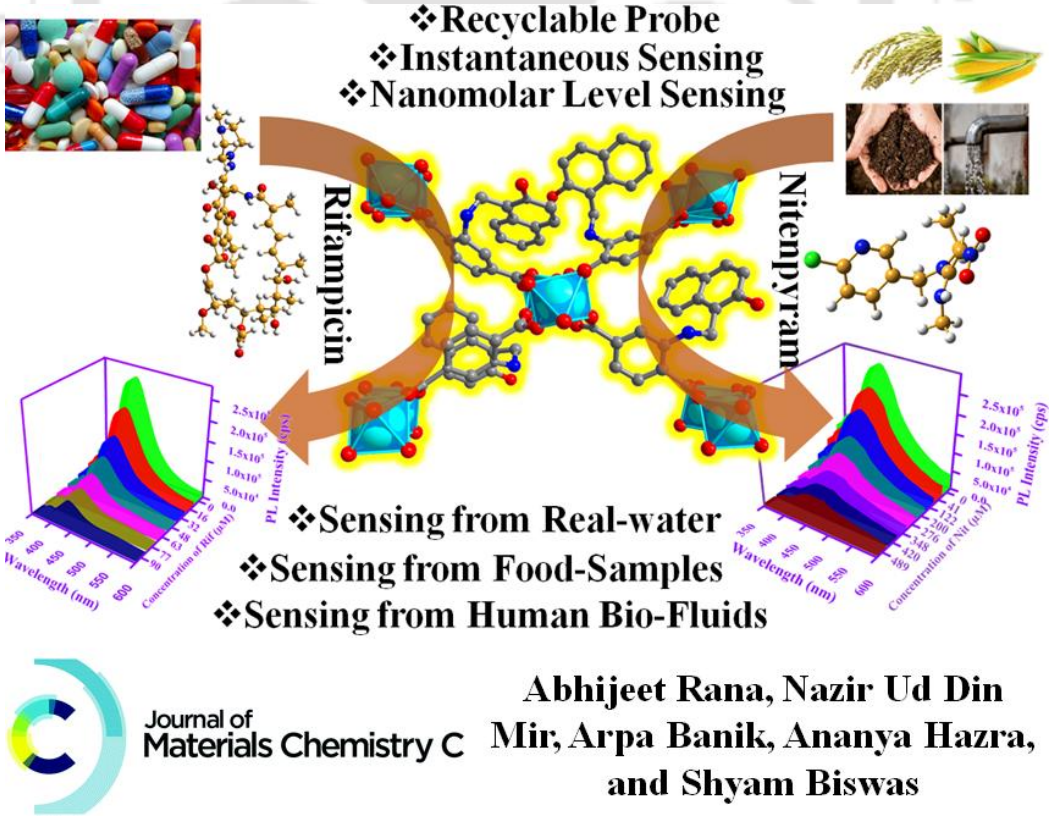

5.1 Introduction

Detection of pesticides has become increasingly significant in recent years due to their negative influence on non-targeted animals and humans. Nitenpyram ((E)-N-[(6-Chloropyridin-3-yl)methyl]-N-ethyl-N′-methyl-2-nitroethene-1,1-diamine) is a neonicotinoid insecticide that is commonly used to protect crops from crop-destroying insects in agricultural fields and veterinary use to treat adult flea infestations.[486] The Japanese Takeda Company invented this significant family of pyridine chemicals in 1989. It is very harmful to insects because it primarily inhibits the central nervous system of the targeted insecticide. It is highly water soluble and environmentally stable with a hydrolytic half-life of 415 days at pH 7. Therefore, it could easily assimilated into animal and human body through food chain.[487] Long-term exposure of this insecticide may negatively impact mammals (including humans), causing genotoxicity, neurotoxicity and endocrine disruption.[488] It can also cause environmental pollution.[489] The exposure of nitenpyram to honey bees decreases their lifetimes, which are one of the prime members of natural pollination process. The decrease in the honey bee population directly affects the production rate of agricultural products.[490] Therefore, the monitoring of such pesticide in environment (soil, natural water and food samples) is essential.

Like pesticides, monitoring of pharmaceutical drug waste in different environmental water specimens has also become important to stop environmental pollution. Rifampicin (RIF, IUPAC: 3-[(4-methyl-1-pyrazinyl)imino]methyl), an essential semi-synthetic antibacterial drug belonging to the rifamycin group, is used to cure tuberculosis, leprosy, inactive meningitis, cholestatic pruritus and HIV.[491] It inhibits the production of bacterial DNA-dependent RNA polymerase.[492] Rifampicin was discovered in 1965 from the soil bacterium. Long-term use of rifampicin can cause adverse impacts on human health (hepatotoxicity, fever, allergic reactions) and the environment.[493] The exposure of rifampicin to a healthy human can lead to the development of antibiotic resistance. The latter creates severe medical issues, as the bacteria will no longer be affected by the previous antibiotics.[494] Dogs are also adversely affected by rifampicin, which causes hepatotoxicity in them.[495] Therefore, detecting and monitoring such pharmaceutically active drugs are essential to protect health of humans and animals.

The development of health science, crop protection and agricultural research accelerated the production and consumption of drugs, pesticides or insecticides. The overdoses of drugs and excess consumption of pesticides, herbicides and insecticides cause their accumulation in water bodies. The excess concentration of such chemicals and drugs directly affects the health of plants, animals and humans. Therefore, to minimize the toxicity caused by rifampicin and nitenpyram, it is very important to develop some analytical methods for detecting and determining the concentration of these insecticides and drug compounds in drinking water and environmental water sources. The widely used methods to detect these artificial chemicals are gas/liquid chromatography,[496-497] thin layer chromatography,[498] high-performance liquid chromatography (HPLC),[499] mass spectrometry,[500-501] photometry, biological detection techniques, hyperpolarization and Raman spectroscopy due to their sensitivity and precision.[502] However, these methods are time-consuming and expensive. In contrast, with high sensitivity, less cost and user-compatibility, fluorescence sensing has become a more reliable way to detect nitenpyram and rifampicin.

Zhang *et al.* developed a La(III)/Ta(III) mixed-metal fluorescent MOF for the selective recognition of nitenpyram, but the probe has a high value of detection limit (0.63 M).[272] Yang et al., on the other hand, developed a functional Zr-MOF (FMOF) to select nitenpyram with a lower detection limit (0.11 μM).[503] The presence of nitenpyram at lower concentrations (such as nanomolar) is also hazardous. While both the probes described by Zhang and Yang et al. have good selectivity, their probes are not sensitive enough to detect nanomolar concentrations

of nitenpyram. On the other hand, the probe presented in this report can detect nanomolar concentration of nitenpyram (LOD = 13.8 nM).

Cai *et al.* synthesized a folic acid-protected copper nanocluster (FA-CuNC) for rifampicin detection in methanol.[504] Because of the high LOD (0.07 μM) and sensing in methanol (not a suitable sensing medium), the FA-CuNC's real-field application is limited. Chen *et al.* also synthesized gold nanocluster for fluorescence detection of rifampicin in water. Although Chen *et al.* could overcome the issue of organic solvent and preferentially sense rifampicin in an aqueous medium, their probe has a high detection limit of 0.09 μM.[505] To address the issue of organic solvent and sensitivity, we prepared an environmentally friendly functional Al-MOF capable of detecting rifampicin in an aqueous medium with nanomolar sensitivity.

Herein, we report a 2-(((2-hydroxy naphthalene-2-yl)methyl)amino)terephthalic acid (H_2L linker) and Al(III) based metal-organic framework for the nanomolar detection and monitoring of rifampicin and nitenpyram. The probe can detect both analytes (rifampicin and nitenpyram) selectively, even in the presence of their congeners without significant interferences. The detection time for nitenpyram and rifampicin is only 5 s. The ultrafast nature of the probe towards detecting both analytes made it unique for real field applications as it could detect these analytes instantaneously. The MOF material can detect both analytes at very low concentrations. The LOD for nitenpyram and rifampicin detection is 13.8 nM and 11.7 nM, respectively. These values are lower than the sensors reported to date for the nitenpyram and rifampicin (Table 5.11 and 5.12). Our probe's low detection limit made it advantageous over other reported sensors. This MOF can also detect rifampicin and nitenpyram from environmental water samples (lake, tap, river and distilled water) to safeguard human health and the environment. This luminescent MOF can also precisely quantify rifampicin from human blood serum and urine, and nitenpyram from soil and food samples.

5.2 Experimental Section

5.2.1 Synthesis of [Al(OH)(L)]·0.5H_2O (4)

A homogenous suspension of $AlCl_3 \cdot 6H_2O$ (56 mg, 0.15 mmol) and H_2L linker (50 mg, 0.15 mmol) in water was prepared in a Teflon lined autoclave by sonicating for 20 min. The uniform combination of metal salt and linker was then exposed to 150 °C for 24 h in a hot air oven. After 24 h, the autoclave was slowly cooled to room temperature and then the obtained brown residue was washed thoroughly with water, DMF and acetone and put in an oven for 24 h at 100 °C. The as-synthesized material was termed **4**. The as-synthesized form of the material was then solvent-exchanged by stirring in methanol for 24 h and then vacuum dried at 120 °C for 24 h. The solvent-free vacant pore form of the material was termed **4'**. The obtained yield was 45.3 g (77.8%). The calculated elemental % was C: 60.16%, N: 3.69, H: 3.72 and obtained elemental microanalysis was C: 60.01%, N: 3.59, H: 3.64.

5.3 Results and Discussion

5.3.1 Structural Elucidation of 4

The PXRD pattern of as-synthesized MOF matches with the PXRD profile of MIL-53 MOF (Figure 5.1). Again, the Pawley fitting was performed by taking the PXRD pattern of as-synthesized MOF compared to the crystal structure of previously reported pristine MOF. The obtained Pawley-fit is displayed in Figure 5.2, which suggests good agreement with the parent MOF with very low R_{wp} (2.6%) and R_p (1.8%) values. The parent MOF was first reported by Férey et al.[506] It comprises unfunctionalized 1,4-benzezenedicaboxylic acid linker and Al(III) as metal center.

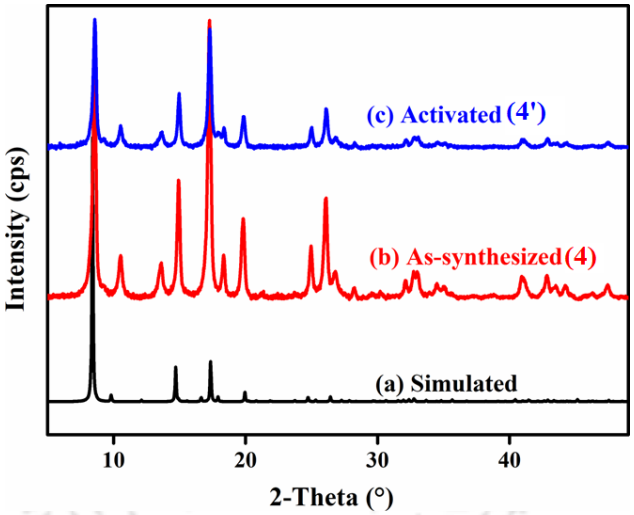

Figure 5.1 (a) PXRD patterns of MIL-53, (b) as-synthesized **4** and (c) activated **4'**.

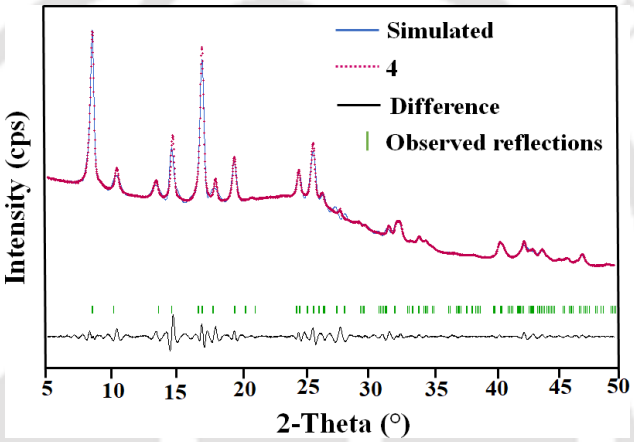

Figure 5.2 Pawley fit for the PXRD pattern of as-synthesized **4** (R_p = 2.62, R_{wp} = 1.76).

Table 2.1 Unit cell parameters of MIL-53(Al) and **4**.

Compound Name	[Al(OH)(L)]·0.5H_2O (**4**) (this work)	MIL-53(Al) (reported)
Crystal System	Orthorhombic P	Orthorhombic P
a ≠ b ≠ c (Å)	16.654 ≠ 12.890 ≠ 6.610 (9)	16.675 ≠ 12.813 ≠ 6.608 (2)
α = β = γ (°)	90	90
V (Å^3)	1419.1 (17)	1411.8 (2)
Radiation	Cu Kα1	Cu Kα1

Again, the indexing of the slow scan PXRD profile of the synthesized MOF confirmed that all the PXRD peaks are due to the orthorhombic form of the parent MOF. The obtained indexing data also display the close resemblance of the unit cell parameters of the synthesized MOF with the parent MOF (Table 5.1). The MOF possesses AlO_6 octahedra consisting of four oxygen from carboxylate of four different terephthalate linkers and two μ_2-OH groups, and aluminium is the central metal atom. A chain of inorganic AlO_6 octahedra is formed with the help of bridging hydroxy groups (Figure 5.3b). The inorganic chain is connected using terephthalate linkers to give a 3D porous framework. The 3D framework possesses rhombic-shaped 1D

channels, as shown in Figure 5.3a. The porosity of the material was affected due to the bulky naphthalene group occupying the rhombic channels, reducing the material's surface area.

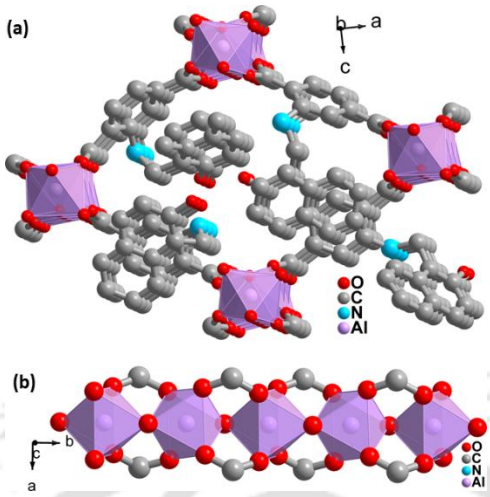

Figure 5.3 (a) 3D network structure of **4**. (b) 1D inorganic linear chain in the structure of **4**.

5.3.2 Functional Group Investigation

ATR-IR measurements of **4** and **4′** revealed that the -COO- group's asymmetrical and symmetrical stretching vibrations (1574 cm^{-1} and 1439 cm^{-1}) are lower than free carboxylic acid in the linker. The effective attachment of the -COO- group to the Al(III) ion aided in this shift of stretching frequency. The amide carbonyl group of the adsorbed DMF molecules is responsible for the peak at 1656 cm^{-1} in 1.[267] The identical peak, however, is absent in the activated form of material **4'**, confirming the proper activation process (Figure 5.4).

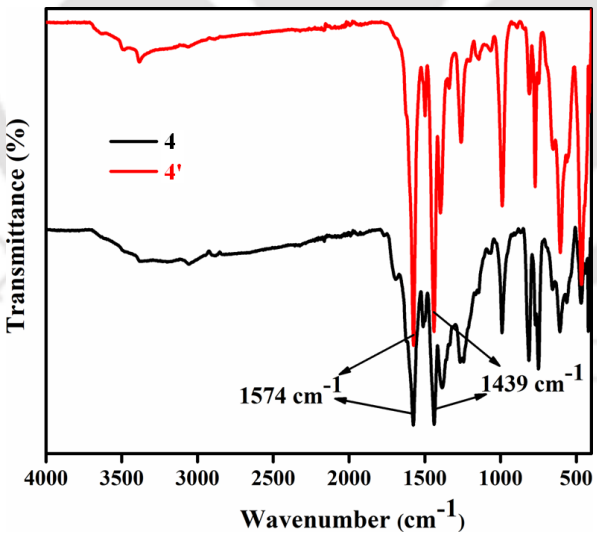

Figure 5.4 ATR-IR spectrum of **4** and **4'**.

5.3.3 Compositional and Morphological Investigation of 4′

The homogenous rod shape of the particles, as displayed in the FE-SEM images, confirmed the purity and homogeneity of **4′** (Figure 5.5). The existence of the necessary elements was confirmed by the EDX spectrum of **4′** (Figure 5.6) (C: 75.2, O: 15.2, N: 4.9, Al: 4.4%). The EDX elemental mapping validated the homogeneous distribution of desired elements all over the material (Figure 5.7). Again, to confirm the phase purity we have performed X-ray

photoelectron spectroscopy (XPS) analysis. The high-resolution XPS analysis of **4′** in Figure 5.8 confirmed the presence of two peaks for Al-2p peaks due to the Al-O bond of the carboxylate oxygen of the linker and the Al-O bond of the inorganic sub-units.[507] The Al-coordinated oxygen peak came near 532 eV and the absence of any peak for oxygen above 533 eV confirmed that there was no free carboxylate remaining in the MOF material.[507] The obtained result from XPS also confirmed that the material is pure enough for further applications.

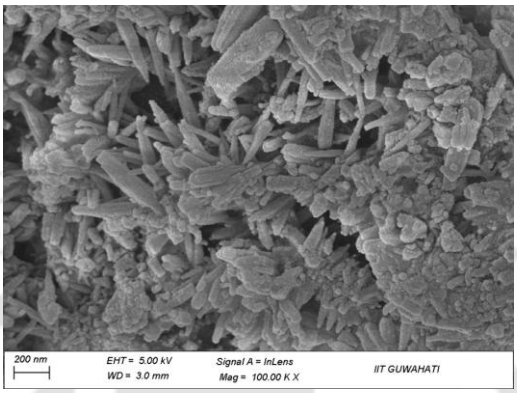

Figure 5.5 FE-SEM image of **4'**.

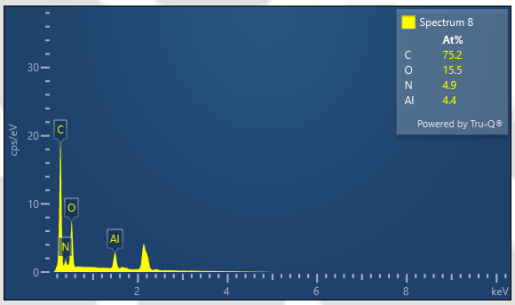

Figure 5.6 EDX spectrum of **4'** showing the distribution of the desired elements in atomic percentage.

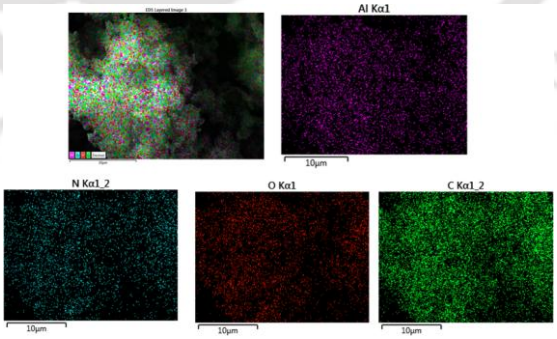

Figure 5.7 EDX elemental mapping **4'** showing the homogenous distribution of all the desired elements.

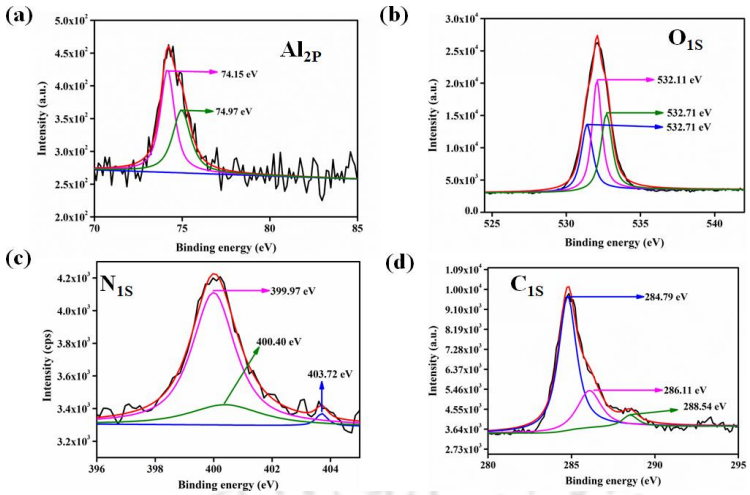

Figure 5.8 High-resolution XPS spectra of Al (2p), O (1s), N (1s) and C (1s) orbitals of **4'**.

5.3.4 Examination of Physicochemical Stability

The thermal stability of **1** and **1′** in an oxygen environment was examined at a heating rate of 4 °C min^{-1} (Figure 5.9). The TG curve of **1** demonstrated a weight loss of 2.2% at 105 °C due to the loss of 0.5 water molecules per formula unit. After 360 °C, the dissociation of linkers from metal centers resulted in a sudden mass loss. Following that, we found an almost flat TG curve for the activated material (**1′**) up to 360 °C, indicating the absence of any solvent molecule in **1′**. According to the findings, the activated and as-synthesized versions of the material are stable in an oxygen atmosphere up to 360 °C.

The stability of **1′** in acidic and alkaline pH and organic solvents was demonstrated by stirring it in the respective solutions for 24 h.[508] Afterward, it was filtered, and the PXRD pattern was recorded. The PXRD pattern of the recovered sample of **1′** was precisely similar to the activated form of the material, confirming the stability of the material in such chemically harsh conditions (Figure 5.10).

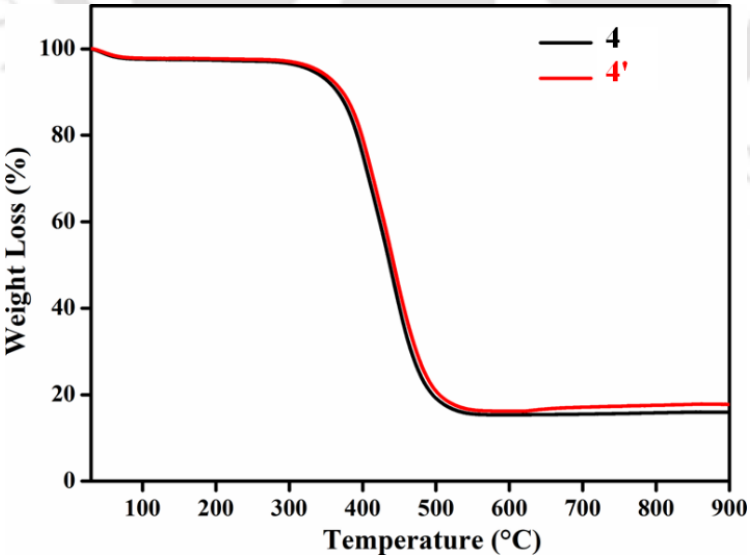

Figure 5.9 Thermogravimetric analysis curve of **4** (black) and **4'** (red) measured under O_2 atmosphere.

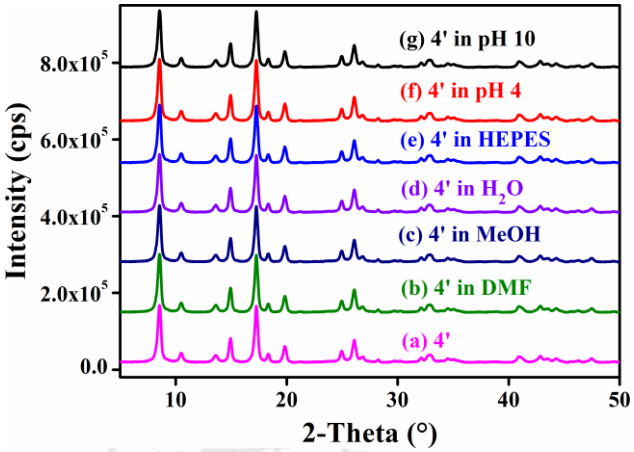

Figure 5.10 PXRD patterns of **4'** after stirring in different organic solvents and pH media for 24 h.

5.3.5 Investigation of Porosity of 4′

The MOF's high surface area and porosity are critical properties for their application in various sectors. As a result, we conducted a N_2 adsorption analysis of **4′** at -196 °C. The specific BET surface area and pore volume of **4′** were 50 m^2/g and 0.31 cm^3/g (at p/p_0 = 0.5), respectively. The functionalization of MOF by a bulky 2-hydroxy naphthalene group reduces the available pore for the adsorption of N_2 gas, which resulted in a decreased surface area of **4′** in comparison to parent MOF (Figure 5.11).[509-510]

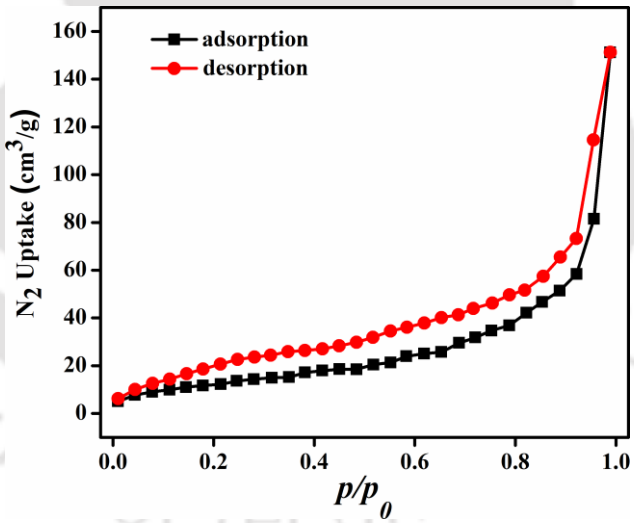

Figure 5.11 Nitrogen adsorption and desorption isotherms of **4'** recorded at –196 °C.

5.3.6 Photoluminescence (PL) Detection of Rifampicin

Rifampicin is a widely used tuberculosis medication. Excess biomedical and pharmaceutical use and unwanted disposal into the environment aid in the distribution of this drug in the natural environment. The presence of rifampicin in natural water sources may endanger the health of animals, including humans. Because of the abovementioned issues, in this study, we synthesized a luminescent MOF probe. By changing its light absorption and emission properties through functional tuning, we applied it for the selective detection of rifampicin.

The MOF suspension was prepared by dispersing 10 mg of MOF in 10 mL of water, sonicating it for 1 h, and then leaving it undisturbed for 24 h to settle the surplus colloidal MOF particles. The suspension of MOF was characterized using a dynamic light scattering experiment in an aqueous medium. The obtained result displays that the MOF particles were present in the sensing medium in monodispersed form with an average particle size of 1500 nM (Figure 5.12).[511-512] After obtaining a stable MOF suspension, 2800 µL of mili-Q water and 200 µL of the MOF suspension were used for all sensing studies. An aqueous solution of 1 mM rifampicin was prepared. The aqueous suspension of the probe was excited with fluorescence light at 330 nm and the PL intensity was measured in a wavelength range of 350 to 600 nm for all sensing experiments (Figure 5.13).

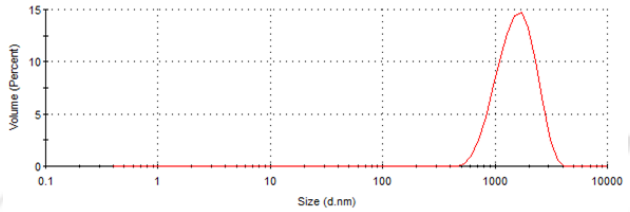

Figure 5.12 Particle size distribution curve of **4'** in aqueous medium from DLS measurement.

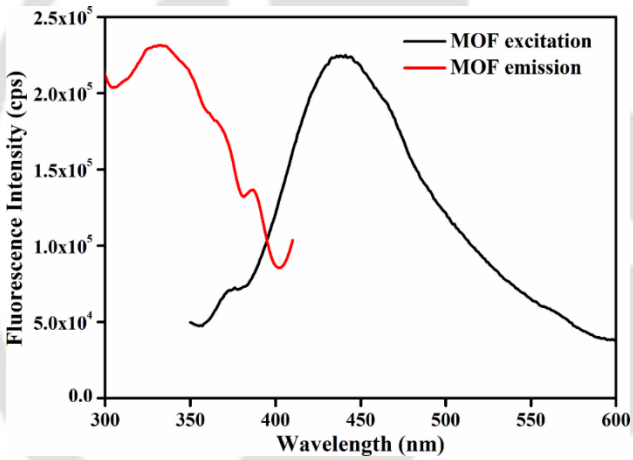

Figure 5.13 Excitation and emission spectra of **4'** in water.

Rifampicin sensing was accomplished by the gradual addition of 50 µL of 1 mM aqueous solution of rifampicin to a quartz cuvette containing 2800 µL of mili-Q water and 200 µL of MOF suspension. The PL emission intensity was measured after each progressive augmentation. The probe's PL emission intensity was suppressed after each addition step, and saturation in PL emission intensity was observed (93% quenching) after adding 300 µL of 1 mM rifampicin (Figure 5.14a).

One of the key features of every probe is its short period of analyte detection. As a result, we conducted a time-dependent fluorescence titration experiment to investigate the detection time of our probe for rifampicin sensing. We introduced 300 µL of 1 mM rifampicin to an aqueous MOF suspension and measured the PL emission intensity over time. After introducing the rifampicin solution, we noted a quick quenching and saturation of the PL emission intensity of our probe within 5 s (Figure 5.14b and 5.14c). As a result, the detection time for rifampicin was estimated to be 5 s. A fluorescence kinetic experiment was executed to confirm the detection time for rifampicin sensing. The kinetic study was carried out by exciting the probe at 330 nm and collecting PL emission intensity at the emission maxima, i.e., at 430 nm, before

and after the addition of rifampicin. After adding rifampicin, we noticed a rapid drop in PL emission intensity at 430 nm within 5 s. The kinetic fluorescence experiment also confirmed that the probe requires only 5 s to detect rifampicin (Figure 5.14d). Our sensor's rapid nature boosted its real-world applicability by detecting the drug instantly. Among all known works on rifampicin sensing, our probe is the fastest.

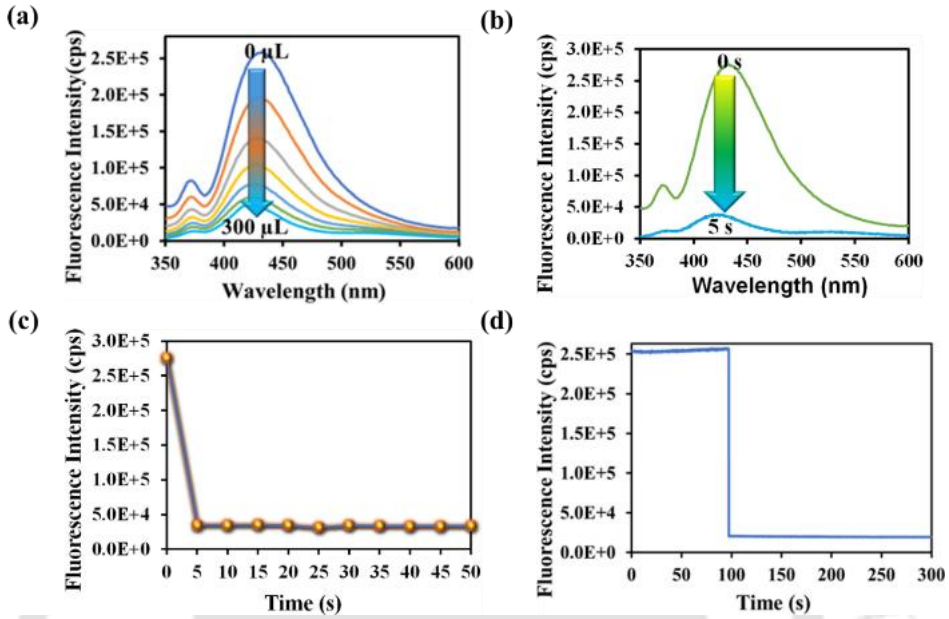

Figure 5.14 (a) PL emission intensity plot for **4′** with incrementally added rifampicin. (b) Time-dependent PL emission intensity of **4′** in the presence of 300 µL of 1 mM rifampicin. (c) PL emission intensity of the probe with variation in time after adding 300 µL, 1 mM rifampicin. (d) Fluorescence kinetic study of the probe by recording the PL intensity at 430 nm with variation in time after the addition of 300 µL, 1 mM rifampicin.

Numerous sensors are available for detecting drug molecules, but most of them suffer from selectivity over the congeners. As a result, an ideal probe must have selectivity over the congeners of the targeted analyte. In order to test the selectivity of rifampicin over other analytes, 300 µL of 1 mM aqueous analyte solution was added to a cuvette containing MOF suspension. We have observed that the I/I_0 value for competing analytes is close to **1**, while the I/I_0 value for rifampicin is 0.1 (Figure 5.15a). For competitive analytes, the unity value of I/I_0 indicates that the PL intensity remained essentially constant both before and after the analyte was added to the MOF suspension. However, the I/I_0 became nearer to zero for rifampicin due to a drastic fall in PL intensity of the MOF after the addition of rifampicin.

The on-field applicability of a probe requires the probe's selectivity toward the sensing of a targeted analyte even when competing analytes are present. Therefore, we conducted a three-step selectivity experiment. At first, the PL emission intensity of MOF was measured, and then one of the competitive analytes was introduced to the MOF suspension and the PL spectrum was recorded. Finally, the targeted analyte, i.e., rifampicin, was introduced to the MOF suspension containing a competitive analyte and the intensity of PL emission was measured. We observed that adding a competitive analyte could not alter the PL emission intensity of MOF. With the addition of a competing analyte, the I/I_0 value stayed close to one (Figure 5.15b). However, it almost reached zero after the addition of rifampicin, which confirmed that our probe could detect rifampicin even in the presence of the competitive congeners.

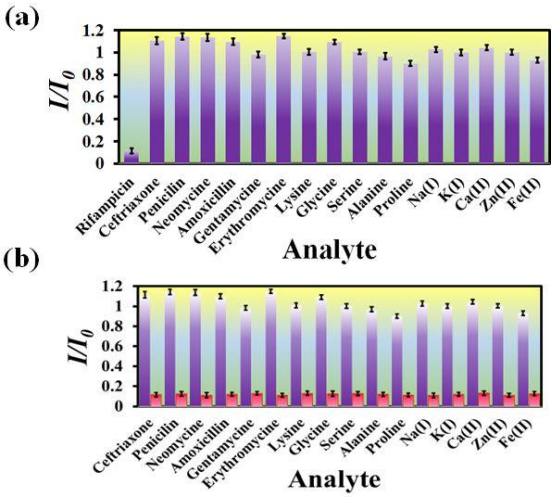

Figure 5.15 (a) Selectivity plot for rifampicin over its congeners. (b) Selectivity plot for rifampicin in the coexistence of the competitive analytes.

One of the critical factors for an ideal sensor for its real-field usability is the sensitivity of detection. As a result, rifampicin was detected at a lower concentration. The detection limit was derived using the formula $3\sigma/k$, where k is the slope of the linear-fit plot of the concentration of rifampicin versus PL emission intensity of MOF and σ is the standard deviation of ten blank readings of MOF suspension (Figure 5.16). Rifampicin's LOD value was found to be 11.7 nM. Our probe has a far lower sensitivity than the previously reported probes for rifampicin sensing (Table 5.11). In contrast to other sensors, our probe's lower detection limit distinguishes this material and makes it more appropriate than others for practical use.

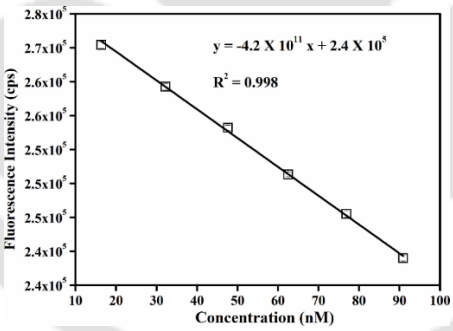

Figure 5.16 Plot of concentration of rifampicin versus fluorescence intensity of **4′**.

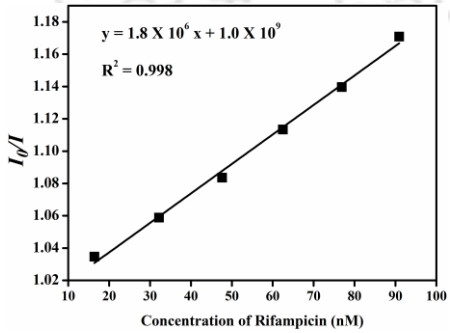

Figure 5.16 Stern-Volmer plot for **4′** with the incremental addition of rifampicin solution.

The Stern-Volmer constant (K_{sv}) was determined using the Stern-Volmer equation (K_{sv}[Q] + 1 = I_0/I). I and I_0 are the PL intensities of **4′** in the absence and presence of various analytes, respectively, and 'Q' is the analyte concentration (Figure 5.17). The high K_{sv} value for rifampicin sensing (1.8×10^6 M^{-1}) substantiated our probe's sensitivity to rifampicin. Figure 5.17a depicts the 3D S-V graphs for all of the examined analytes. The 3D S-V graphs demonstrated rifampicin's exceptional selectivity over a wide range of other congeners.

The capacity to reuse a sensor due to its recyclability offers a benefit over one-time-usable sensors. The sensor's multiple-time reusability reduces expenses by many folds compared to single-use probes. Therefore, we have demonstrated the recyclability of our probe towards rifampicin. After each sensing experiment, the probe was rinsed adequately with fresh water, and identical fluorescence titration studies were repeated to investigate the recyclability behavior. Figure 5.17b displays that following the addition of rifampicin, the PL intensity was suppressed significantly and after the washing step, the probe's fluorescence property was recovered after each sensing cycle. The recyclability experiment was conducted five times and the results confirmed that the quenching efficiency remained nearly the same even after the fifth cycle. The above results demonstrated that the probe could be useful for at least five cycles.

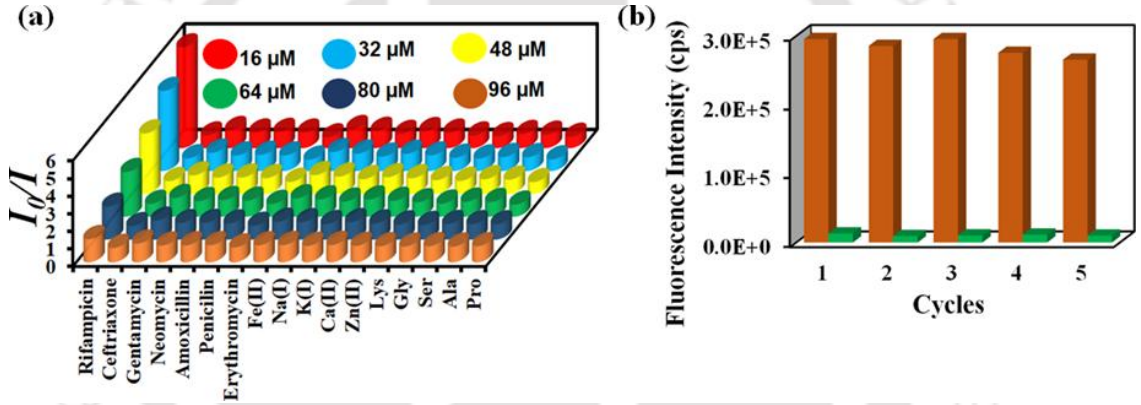

Figure 5.17 (a) 3D Stern-Volmer plot for detection of rifampicin by **4′**. (b) Recyclability of **4′** towards rifampicin sensing.

5.3.7 Rifampicin Sensing from Real Water Samples

Due to the extremely long half-life of disintegration of medications, their presence in natural water sources creates a variety of health hazards. Therefore, we conducted rifampicin sensing in environmental water samples to protect living things. The PL intensity of the MOF suspension was measured in the presence of varying amounts of rifampicin in environmental water samples (lake water, ocean, river water, and tap water). The MOF's PL emission intensity decreased as rifampicin concentration increased. The ability of the probe to find rifampicin in samples of naturally occurring environmental water demonstrates the applicability of our probe in real-world applications. (Figure 5.18).

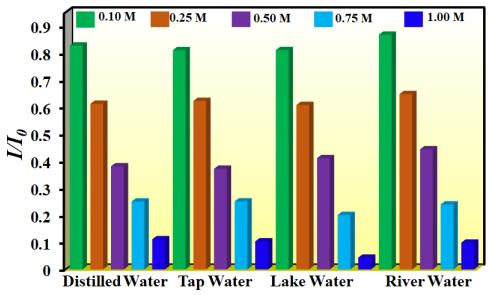

Figure 5.18 Bar plot depicting the detection of rifampicin from real water specimens by **4′**.

5.3.8 Rifampicin Sensing from Biological Fluids

An excess of rifampicin in the body can cause toxicity and in extreme cases, death.[513] Therefore, we conducted PL titration experiments to quantify rifampicin in human blood serum and urine. Rifampicin is stable in pure water, but it begins to degrade when it comes into the blood. Farina et al. discovered that adding ascorbic acid to a rifampicin solution could boost its stability for up to 3 days in ambient conditions.[514] As a result, we prepared a mixture of ascorbic acid and rifampicin in human blood serum and urine separately. Rifampicin was quantified in both the mixtures using the PL titration technique. The obtained results revealed that there was no change in the PL intensity of MOF in the presence of only ascorbic acid, but the PL intensity was significantly quenched in the presence of both rifampicin and ascorbic acid (Figure 5.19 and 5.20), which strongly recommend that the quenching effect is solely due to rifampicin. Table 5.2 and 5.3 present the good recovery percentage of rifampicin from human blood serum and urine, confirming that our probe could detect rifampicin from human blood serum and urine with high accuracy and precession.

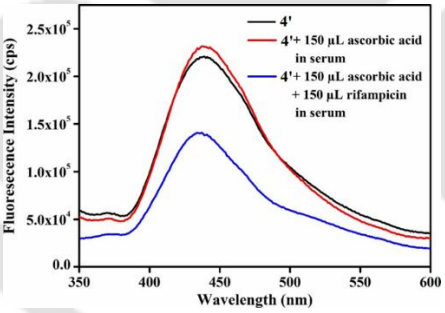

Figure 5.19 Fluorescence intensity of **4′** in human blood serum in presence of only ascorbic acid (red) and mixture of ascorbic acid and rifampicin (blue).

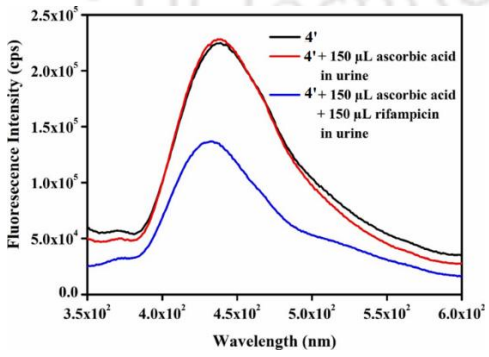

Figure 5.20 Fluorescence sensing of **4′** in human urine in presence of only ascorbic acid (red) and mixture of ascorbic acid and rifampicin (blue).

Table 5.2 Detection of rifampicin from human blood serum using **4′**.

Rifampicin Spiked (mol L^{-1})	Rifampicin Found (mol L^{-1})	Recovery (%)
9.804×10-6	9.541×10-6	97.3
2.206×10-5	2.322×10-5	105.3
3.271×10-5	3.222×10-5	98.5

Table 5.3 Detection of rifampicin from human urine using **4′**.

Rifampicin Spiked (mol L^{-1})	Rifampicin Found (mol L^{-1})	Recovery (%)
9.804×10-6	9.311×10-6	94.9
2.206×10-5	2.361×10-5	107.0
3.271×10-5	3.073×10-5	93.9

5.3.9 PL Detection of Nitenpyram

Nitenpyram is one of the world's most widely used neonicotinoid insecticides, and it is also utilized in veterinary medicine. The presence of nitenpyram in high concentrations is hazardous to non-targeted organisms. One of the most important criteria for ensuring a healthy society is monitoring such harmful compounds in the natural environment. Therefore, we performed the same PL titration studies in an aqueous medium for nitenpyram sensing as we did for rifampicin sensing.

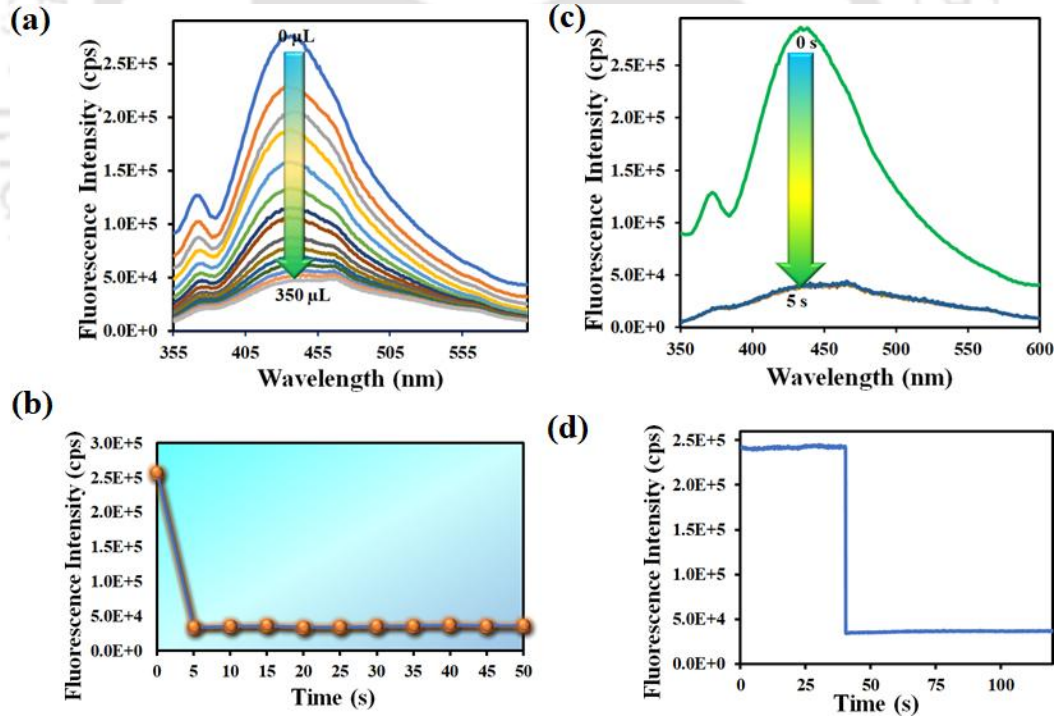

Figure 5.21 PL emission intensity plot for **4′** with incrementally added nitenpyram. (b) Time-dependent PL emission intensity of **4′** in 350 µL of 1 mM nitenpyram. (c) The PL emission intensity of the probe by changing the time after adding 350 µL, 1 mM nitenpyram. (d) Fluorescence kinetic study of the probe by recording the PL intensity at 430 nm by changing the time after the addition of 350 µL, 1 mM nitenpyram.

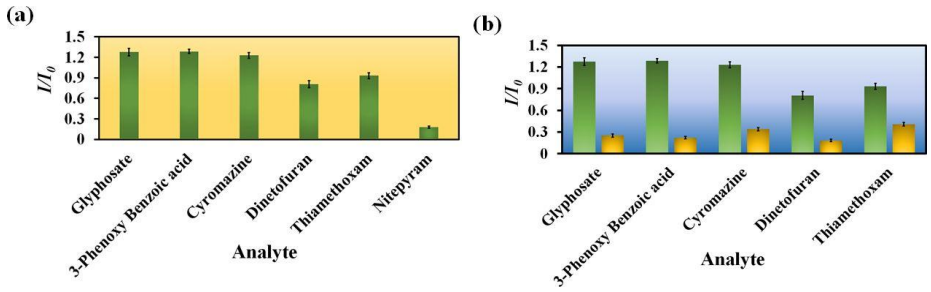

Figure 5.22 (a) Selectivity plot for nitenpyram over its congeners. (b) Selectivity plot for nitenpyram in the coexistence of the competitive analytes.

The PL emission intensity of the aqueous suspension of **4′** displayed 95% quenching rapidly (5 s) in the presence of 350 µL of 5 mM nitenpyram solution (Figure 5.21a-5.21c). Furthermore, A PL kinetic experiment was also performed to verify the actual detection time of nitenpyram by **4′**. The PL kinetic experiment confirmed that our probe could detect nitenpyram in less than 5 s (Figure 5.21d). The detection of nitenpyram was also performed in the co-existence of other congeners. We observed that **4′** possesses excellent selectivity towards nitenpyram in comparison to other competitors (Figure 5.22a-5.22b). The LOQ and LOD values for nitenpyram detection were determined using the same experimental approach used for rifampicin (Figure 5.23). The LOQ and LOD values were 45.9 nM and 13.8 nM for nitenpyram, respectively. Our probe's nanomolar LOD and LOQ value confirmed its great sensitivity towards nitenpyram sensing for real-world application. Moreover, the high value of S-V constant (K_{sv} = 3.2 × 10^6 M^{-1}) for nitenpyram sensing established our probe's great sensitivity and selectivity (Figure 5.24 and Figure 5.25a).

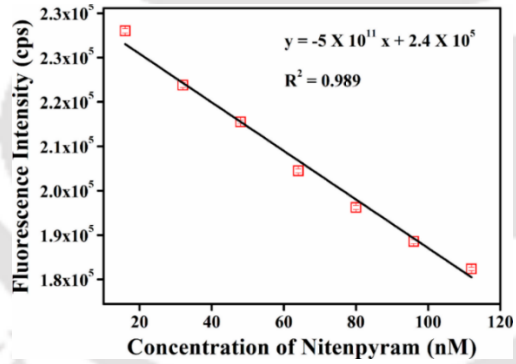

Figure 5.23 Plot of concentration of nitenpyram versus fluorescence intensity of **4'**.

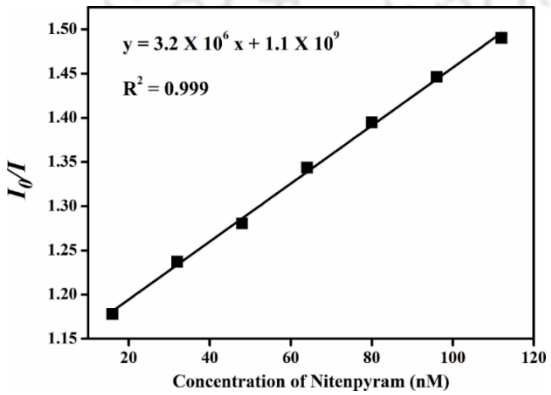

Figure 5.24 Stern-Volmer plot for **4′** with the incremental addition of nitenpyram solution.

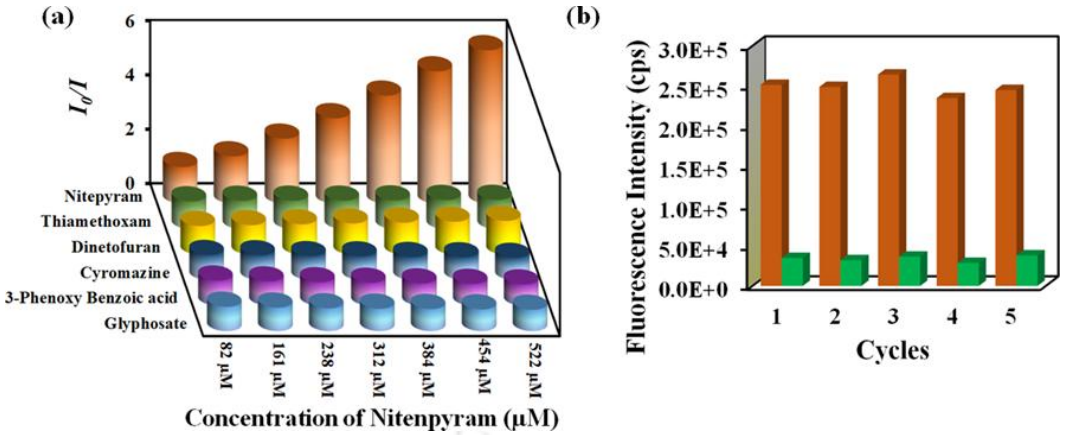

Figure 5.25 (a) 3D Stern-Volmer plot for detecting nitenpyram by **4′**. (b) Recyclability of **4′** towards nitenpyram sensing.

The reusability of **4′** for the sensing of nitenpyram was examined similarly to those described above for rifampicin sensing. The recyclability plot in Figure 5.25b confirmed that **4′** could detect nitenpyram at least up to five cycles with excellent efficacy.

5.3.10 Nitenpyram Sensing from Real Water Samples

Nitenpyram is a water-soluble pesticide. Its excessive use in crop fields could elevate its concentration in natural water sources, which is a warning towards a safe environment. Therefore, we have carried out a series of PL sensing experiments, taking various concentrations of nitenpyram in natural water specimens (lake, river, tap and distilled water). The obtained result inferred that our probe could detect nitenpyram from natural water sources without interference (Figure 5.26).

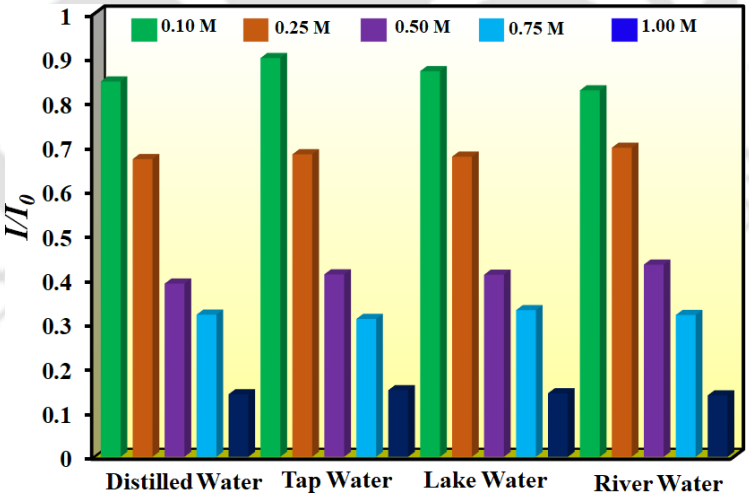

Figure 5.26 Bar plot depicting the detection of nitenpyram from real-water specimens by **4′**.

5.3.11 Nitenpyram Sensing from Soil and Food Samples

The excessive use of pesticides (nitenpyram) could also contaminate soil and crops due to its high-water solubility. The presence of such harmful pesticides in soil and food samples will hamper the natural biological cycle inside the body of affected animals. As a result, we performed nitenpyram detection in soil and food samples (rice and corn). The results revealed that **4′** can identify nitenpyram from soil and food samples with high accuracy and precision (Tables 5.4-5.6).

Table 5.4 Detection of nitenpyram from soil using **4′**.

Nitenpyram Spiked (mol L^{-1})	Nitenpyram Found (mol L^{-1})	Recovery (%)
3.922×10-5	3.891×10-5	99.2
8.612×10-5	8.873×10-5	103.0
1.308×10-4	1.278×10-4	97.7

Table 5.5 Detection of nitenpyram from rice using **4′**.

Nitenpyram Spiked (mol L^{-1})	Nitenpyram Found (mol L^{-1})	Recovery (%)
3.922×10-5	4.103×10-5	104.6
8.612×10-5	8.838×10-5	102.6
1.308×10-4	1.295×10-4	99.0

Table 5.6 Detection of nitenpyram from corn using **4′**.

Nitenpyram Spiked (mol L^{-1})	Nitenpyram Found (mol L^{-1})	Recovery (%)
3.922×10-5	4.137×10-5	105.5
8.612×10-5	8.986×10-5	104.3
1.308×10-4	1.292×10-4	98.8

5.3.12 Reproducibility of PL Sensing

We conducted the sensing experiments several times, both on the same and other days. The inter-day and intra-day fluorescence detection assays demonstrated that the MOF could detect rifampicin and nitenpyram with excellent precision and accuracy repeatedly (Table 5.7 and 5.8).

Table 5.7 Evaluation of intra-day, inter-day accuracy and precision parameters for change in fluorescence intensity of **4'** after incremental addition of 1 mM aqueous solution of rifampicin respectively.

Volume of Rifampicin Added	Intra-Day Fluorescence Emission Intensity (cps)			Mean (χ)	Standard Deviation (σ)	Relative Standard Deviation (RSD)
0 µL	254237	254252.2	253221.7	253903.6	482.2357	0.189
50 µL	175498.7	174478.8	174518.7	174832.1	471.6866	0.269
100 µL	118513.9	117911.6	117516.2	117980.6	410.2253	0.347
150 µL	94002.16	92999.91	93421.4	93474.4	410.8826	0.439
200 µL	58046.29	57995.36	59007.22	58349.6	465.4527	0.797
250 µL	34017.82	32945.46	33290.2	33417.8	446.9949	1.337
300 µL	19585.53	19193.82	19977.2	19585.5	319.8304	1.632
Volume of Rifampicin Added	Inter-Day Fluorescence Emission Intensity (cps)			Mean (χ)	Standard Deviation (σ)	Relative Standard Deviation (RSD)
0 µL	258754.5	258237	260565.8	258519.1	860.1	0.333
50 µL	176351.4	175998.7	177585.9	176478.7	554.6	0.314
100 µL	120955.8	120713.9	121802.5	120624.1	448.4	0.372

150 µL	94451.1	94262.2	95112.2	94641.81	409.8	0.433
200 µL	58062.4	57946.3	58468.8	58492.52	415.7	0.711
250 µL	33685.2	33617.8	33920.9	33674.66	385.3	1.144
300 µL	19624.8	19585.5	19762.2	19390.83	238.5	1.230

Table 5.8 Evaluation of intra-day, inter-day accuracy and precision parameters for change in fluorescence intensity of **4'** after incremental addition of 1 mM aqueous solution of nitenpyram respectively.

Volume of Nitenpyram Added	Intra-Day Fluorescence Emission Intensity (cps)			Mean (χ)	Standard Deviation (σ)	Relative Standard Deviation (RSD)
0 µL	250900	251952	251548	251466.5	433.2	0.172
50 µL	186805	187120	187689	187204.9	365.8	0.195
100 µL	144381	143941	143317	143879.8	436.2	0.303
150 µL	104934	105012	105918	105287.8	446.6	0.424
200 µL	69925.6	69025.3	68896.6	69282.5	457.8	0.660
250 µL	43523.8	42912.1	42558.3	42998.1	398.8	0.927
300 µL	21536.6	20914.3	21817.5	21422.8	377.4	1.762
Volume of Nitenpyram Added	Inter-Day Fluorescence Emission Intensity (cps)			Mean (χ)	Standard Deviation (σ)	Relative Standard Deviation (RSD)
0 µL	250900	252859.5	251296.4	251685.3	845.9	0.336
50 µL	186805	187868.9	187501.5	187391.9	441.1133	0.235
100 µL	144381	144517.2	143174.1	144023.9	603.5273	0.419
150 µL	104734	105811.8	105432.1	105325.8	446.5384	0.423
200 µL	69925.6	69301.4	68727.7	69318.23	489.1841	0.705
250 µL	43523.8	42515.74	43183.75	43074.43	418.7348	0.972
300 µL	21536.6	21715.68	20907.96	21386.75	346.3592	1.619

5.3.13 Mechanism of Fluorescence Quenching by Rifampicin

Using a variety of analytical techniques, the mechanism of fluorescence quenching by rifampicin was fully explored. To understand the influence of rifampicin on the crystallinity of the MOF, PXRD investigation was conducted before and after rifampicin sensing. PXRD examination confirmed that the crystallinity of MOF remained unchanged (Figure 5.27), confirming that the change in PL emission intensity of MOF in the presence of rifampicin is not due to structural change of MOF. The ATR-IR and EDX analyses were performed before and after treatment with rifampicin. The obtained ATR-IR and EDX spectra of MOF before and after treatment of rifampicin remained the same (Figure 5.28-5.29). Again, **4′** is recyclable towards the rifampicin sensing as mentioned above in Fig. 4b. All the above-mentioned results confirmed that the fluorescence sensing process could not be due to formation of any ground state complex or any reaction between the MOF and rifampicin.

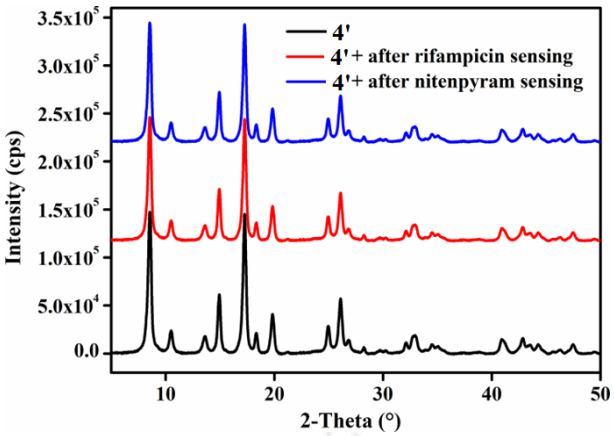

Figure 5.27 PXRD patterns of**4′** before sensing (black), after rifampicin sensing (red) and after nitenpyram sensing (blue).

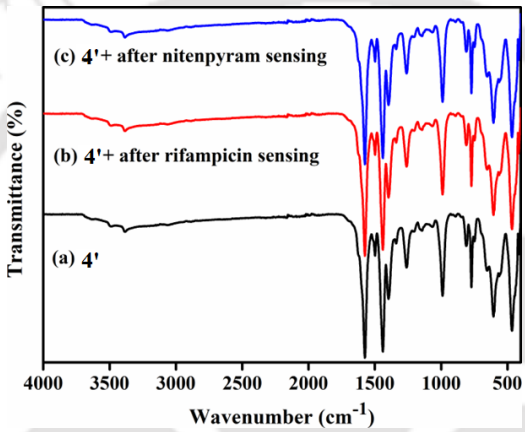

Figure 5.28 ATR-IR spectra of **4′** before sensing (black), after rifampicin sensing (red) and after nitenpyram sensing (blue).

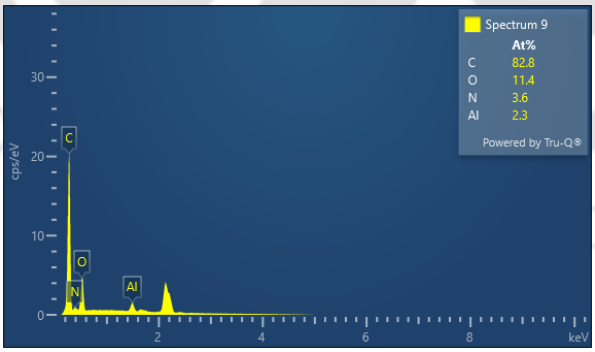

Figure 5.29 EDX elemental spectrum of **4′** after rifampicin sensing.

The elimination of reaction-based processes compelled us to consider non-reaction type fluorescence quenching techniques (IFE, PET, FRET and so on). We started with an excited-state lifetime investigation of **4′** in the presence and absence of rifampicin. The excited state lifetime of **4′** was 11.8 ns in the absence of rifampicin, but it was reduced to 8.0 ns with the addition of rifampicin (Figure 5.30 and Table 5.9). The decrease in the probe's lifetime in the presence of rifampicin suggests that the PL quenching is caused by a dynamic process. The IFE mechanism is ruled out by the dynamic process of fluorescence quenching. In addition, to better understand the process of PL quenching by rifampicin, we plotted the UV-Vis spectra of all

analytes, including rifampicin, as well as the PL emission of MOF (Figure 5.31). The overlap plot confirmed that there is enough overlap between the MOF emission spectrum and the rifampicin absorbance spectrum for energy transfer from the excited state of the probe to the analyte. According to the findings displayed above, the quenching of MOF's PL intensity may be caused due to the FRET process. Again, the UV-Vis spectra of other analytes of rifampicin do not display significant overlap with the emission spectrum of MOF which is the reason behind the selectivity of rifampicin over other congeners.

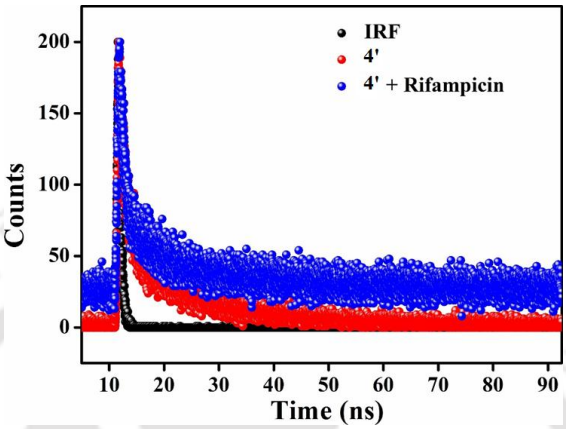

Figure 5.30 Time-resolved fluorescence lifetime decay plot for **4′** in presence and absence of rifampicin.

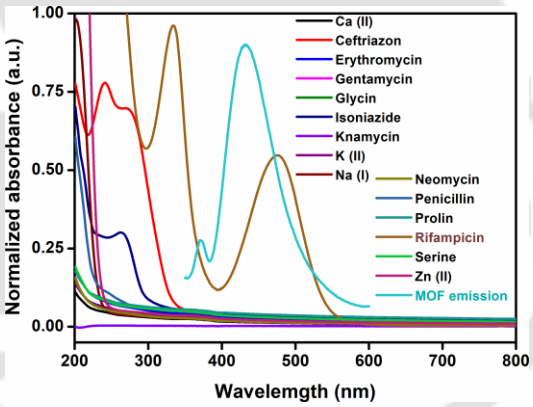

Figure 5.31 Overlap plot for UV-Vis spectra of all the analytes for rifampicin sensing with the fluorescence emission spectrum of **4′**.

Table 5.9 Excited-state lifetime of **4′** in presence and absence of rifampicin.

Volume of Rifampicin Solution Added (μL)	B_1 (%)	B_2 (%)	T_1 (ns)	T_2 (ns)	$\langle\tau\rangle^*$ (ns)	χ^2
0	11.5	88.5	1.3	13.2	11.8	1.19
350	22.5	77.5	0.9	10.1	8.0	1.10

In addition, we have performed the DFT energy level calculation for rifampicin and H_2L linker using Gaussian 6.0 software and B3LYP function with 631G ++ basic set. We found that the HOMO and LUMO of linker are located at -5.82 eV and -2.16 eV, and rifampicin at -4.92 eV and -2.82 eV (Figure 5.32). The PL quenching will only be possible through PET based path if the donor's (probe) LUMO is higher in energy than the acceptor's (analyte: rifampicin) LUMO.

The energy of the LUMO of linker and rifampicin provided above indicates that there is a possibility of photoinduced electron transfer from linker to rifampicin.[515]

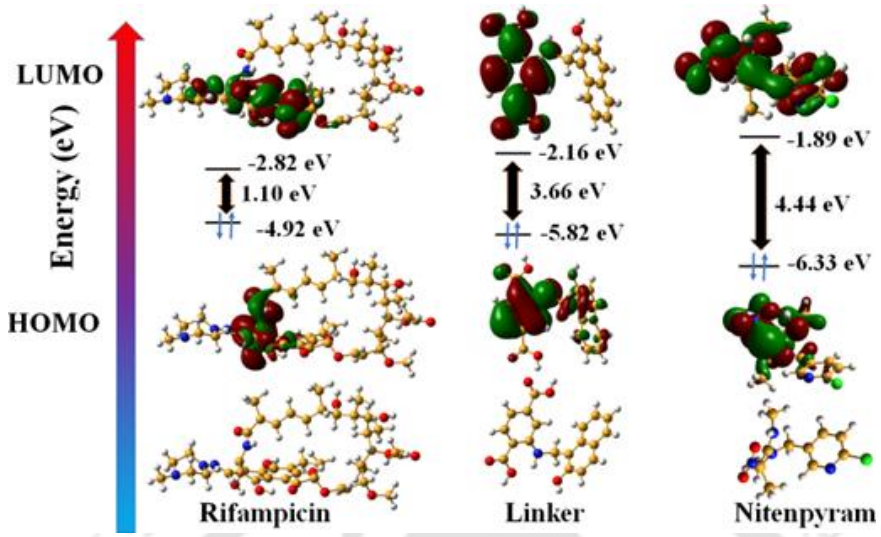

Figure 5.32 DFT based HOMO and LUMO energy levels of linker, rifampicin and nitenpyram.

All the above results obtained from the rigorous analytical techniques and theoretical calculations strongly indicate that the quenching of PL intensity of MOF by rifampicin is due to combined FRET and PET mechanisms.

5.3.14 Mechanism of Nitenpyram Sensing

The PXRD, ATR-IR and EDX elemental investigation of **4′** before and after nitenpyram sensing were measured and found to be precisely similar (Figure 5.27-5.28 and 5.33). The similarity in PXRD pattern of **4′** before and after nitenpyram sensing inferred that nitenpyram's quenching of PL emission intensity of MOF was not because of any structural change of **4′**. The resemblance of ATR-IR peaks and retention of all the elements of **4′** before and after nitenpyram sensing indicate that the PL quenching of **4′** by nitenpyram might be due to some non-reaction-based pathway (IFE, FRET or PET) instead of any reaction or ground state complexation between MOF and nitenpyram. Furthermore, the recyclability of the probe toward nitenpyram sensing also supported the non-reaction type PL quenching.

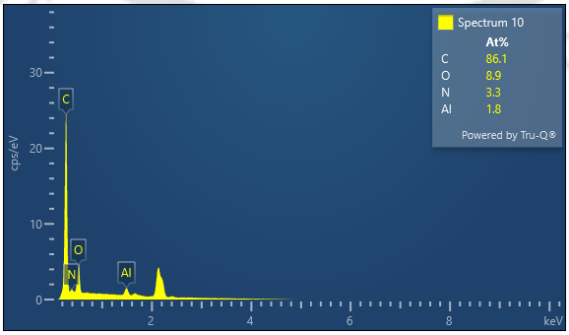

Figure 5.33 EDX elemental spectrum of **4′** after nitenpyram sensing.

To determine the precise mechanism of PL quenching by nitenpyram, we measured the excited state PL lifetime of **4′** in the absence and presence of nitenpyram. In the absence of nitenpyram, the probe's lifetime is 11.8 ns, but it reduces to 6.7 ns (Figure 5.34 and Table 5.10) after adding

nitenpyram. The decrease in lifetime of our probe in the presence of nitenpyram revealed that PL quenching occurs via a dynamic mechanism. The dynamic nature of PL quenching by nitenpyram excluded the possibility of IFE process. As a result, we calculated the energy of HOMO and LUMO orbitals of nitenpyram and the linker molecule to understand the possibility of photoinduced electron transfer. The quenching of PL emission intensity of MOF by nitenpyram is only possible when the photoexcited electron from the LUMO of the linker transfers to the LUMO of the nitenpyram. But, in the case of nitenpyram, the LUMO is energetically higher than the LUMO of the linker, which is a forbidden condition for PET process to occur between the probe and nitenpyram.

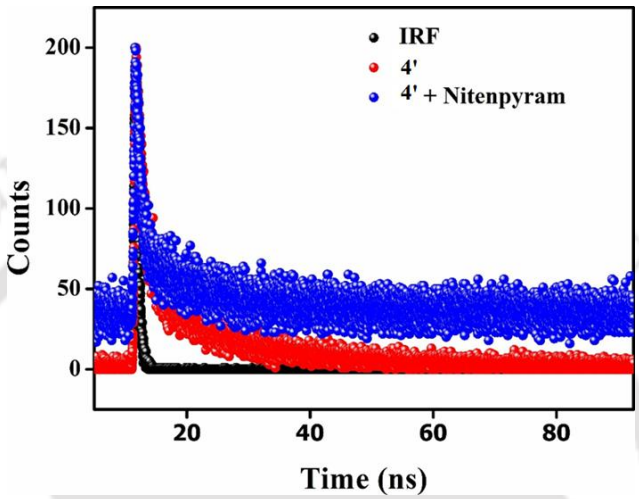

Figure 5.34 Time-resolved fluorescence lifetime decay plot for **4′** in presence and absence of nitenpyram.

Table 5.10 Excited-state lifetime of **4′** in presence and absence of nitenpyram.

Volume of Nitenpyram Solution Added (μL)	B_1 (%)	B_2 (%)	T_1 (ns)	T_2 (ns)	$<\tau>^*$ (ns)	χ^2
0	11.5	88.5	1.3	13.2	11.8	1.19
300	63.4	36.6	10.4	0.3	6.7	1.09

The results of the aforementioned experiments ruled out the feasibility of PET and IFE. Therefore, we concentrated on the possibility of the FRET process. It is already known that FRET-based quenching takes place when there is enough overlap between the PL emission spectrum of the donor and UV-Vis absorbance spectrum of the acceptor, which mediates the transfer of energy through a dynamic process.[516] Because of that, the PL emission spectrum of MOF was plotted with the UV-Vis absorption spectra of all the analytes, including nitenpyram (Figure 5.35). The acquired results demonstrated that, among all of the analytes, only nitenpyram's UV-Vis absorption spectrum overlaps with the PL emission spectrum of MOF. The dynamic nature of PL quenching, as well as the overlap of the absorption (nitenpyram) and emission spectrum (MOF) demonstrated that FRET is the sole reason of nitenpyram sensing.

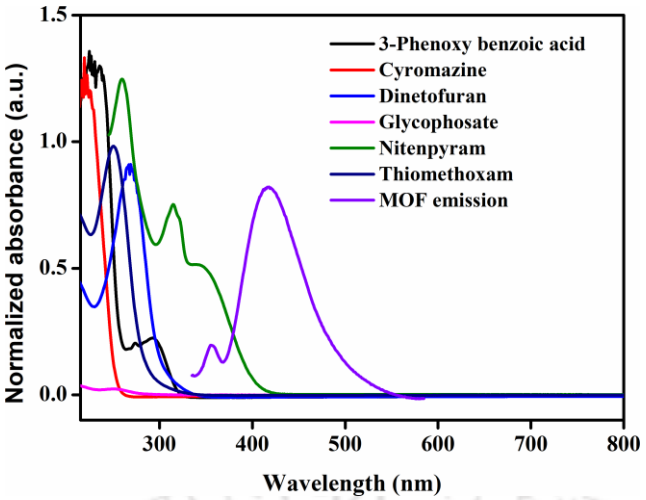

Figure 5.35 Overlap plot for UV-Vis spectra of analytes for nitenpyram sensing with the fluorescence emission spectrum of **4′**.

Table 5.11 Comparison table for fluorescence sensing performance of rifampicin by **4'** with previously reported materials.

Sl. No.	Sensor Material	Sensing Medium	LOD	Response Time (s)	K_{sv} (M^{-1})	Ref.
1	FA-Cu NCs	methanol	0.07 µM	20 s	5.1×10^4	487
2	BSA-Au NCs	water	0.09 µM	1800	-	488
3	G-NSCDs	water	0.06 µM	1800	1.2×10^4	489
4	GSH-CdTe/ZnS QDs	water	0.06 µM	900	4.4×10^4	490
5	Ce-N-CQDs	water	96 nM	300	-	491
6	**[Al(OH)(L)]·0.5H$_2$O (4')**	**water**	**11.7 nM**	**5**	**1.8×10^6**	**this work**

Table 5.12 Comparison table for MOF based fluorescence sensing performance of nitenpyram with **4'**.

Sl. No.	Sensor Material	Sensing Medium	LOD	Response Time (s)	K_{sv} (M^{-1})	Ref.
1	[In$_3$Tb$_3$O$_3$(TATAB)$_4$ (H$_2$O)$_6$]·12DMF·12H$_2$O	water	0.63 µM	-	1.5×10^4	492
2	FMOF	water	0.11 µM	1200	-	493
3	Dye@MOFs	water	0.27 µM	-	-	494
4	EY@Zr-MOF	water	1.18 µM	-	3.5×10^4	495
5	**[Al(OH)(L)]·0.5H$_2$O (4')**	**water**	**13.8 nM**	**5 s**	**3.2×10^4**	**this work**

5.4 Conclusion

The preparation, complete characterization and utilization of a 2-hydroxy naphthaldehyde functionalized aluminium MOF for the detection of a popular antibiotic drug for tuberculosis (rifampicin) and a neonicotinoid pesticide (nitenpyram) are presented herein. This is the first luminescent MOF to detect rifampicin through a fluorescence process. The luminescent, recyclable and chemically stable MOF can detect rifampicin at an ultra-low concentration (11.7 nM) in an aqueous medium. The probe's detection limit is much lower than the previously reported probes of rifampicin, which establishes its real-world usefulness. It is also the first-ever luminescent MOF-based sensor to detect the nanomolar concentration of nitenpyram via

a fluorescence turn-off procedure. This probe can recognize up to 13.8 nM concentration of nitenpyram, which confirms its superior sensitivity over the other fluorescent-based nitenpyram sensors. Moreover, it can selectively recognize both these analytes instantaneously (5 s), which is an important property of this probe. Rifampicin and nitenpyram were also detected from natural water sources (lake, river, tap and distilled water) for health and environmental protection. Furthermore, this probe was utilized to precisely quantify rifampicin from human biological fluids (blood serum and urine) and nitenpyram from soil and food samples (rice and corn). The detection of rifampicin and nitenpyram were checked several times to establish the reproducibility and repeatability of the probe to detect both these analytes with high precision and accuracy. The recyclability of the probe up to five cycles was confirmed, which underscores its cost-effectiveness and sustainability. Finally, we have systematically explored the mechanism of PL quenching of by rifampicin and nitenpyram with the help of modern analytical instruments. The FRET and PET processes are combinedly responsible in the case of rifampicin sensing, whereas the FRET process is responsible for nitenpyram sensing. The overall work presents a systematic detection and monitoring of an essential class of tuberculosis drug (rifampicin) and a neonicotinoid pesticide (nitenpyram) to protect the health of animals, including humans and our environment.

5.6 References

1. M. Rust, M. Waggoner, N. Hinkle, D. Stansfield and S. Barnett, *J. Med. Entomol.*, 2003, **40**, 678-681.
2. H. Wang, L. Pan, Y. Liu, Y. Ye and S. Yao, *J. Electroanal. Chem.*, 2020, **862**, 113955.
3. W. Liu, Z. Li, X. Cui, F. Luo, C. Zhou, J. Zhang and L. Xing, *Toxicol. Appl. Pharmacol.*, 2022, **446**, 116065.
4. S. Yan, W. Sun, S. Tian, Z. Meng, J. Diao, Z. Zhou, L. Li and W. Zhu, *J. Environ. Sci.*, 2024, **137**, 120-130.
5. M. A. I. Ahmed, C. F. A. Vogel and G. Malafaia, *Sci. Total Environ.*, 2022, **804**, 150254.
6. M. Grobbelaar, G. E. Louw, S. L. Sampson, P. D. van Helden, P. R. Donald and R. M. Warren, *Infect. Genet. Evol.*, 2019, **74**, 103937.
7. E. A. Campbell, N. Korzheva, A. Mustaev, K. Murakami, S. Nair, A. Goldfarb and S. A. Darst, *Cell*, 2001, **104**, 901-912.
8. C. Shen, Q. Meng, G. Zhang and W. Hu, *Br. J. Pharmacol.*, 2008, **153**, 784-791.
9. Q. Xu, G. Owens and Z. Chen, *J. Clean. Prod.*, 2020, **264**, 121617.
10. J. Bajwa, M. Charach and D. Duclos, *Vet. Dermatol.*, 2013, **24**, 570-e136.
11. A. Srivastava, D. Waterhouse, A. Ardrey and S. A. Ward, *J. Pharm. Biomed. Anal.*, 2012, **70**, 523-528.
12. B. Milz, I. B. Idros and B. Spangenberg, *J. Liq. Chromatogr. Relat. Technol.*, 2012, **35**, 1404-1414.
13. M. F. Khan, S. A. Rita, M. S. Kayser, M. S. Islam, S. Asad, R. Bin Rashid, M. A. Bari, M. M. Rahman, D. A. Al Aman and N. I. Setu, *Front. Chem.*, 2017, **5**, 27.
14. S. Ge, Y. Wang, Q. Song, L. Chen, Y. Zhang and D. Hu, *Food Addit. Contam. Part A*, 2020, **37**, 955-962.
15. Ž. Temova Rakuša, R. Roškar, A. Klančar Andrejc, T. Trdan Lušin, N. Faganeli, I. Grabnar, A. Mrhar, A. Kristl and J. Trontelj, *Int. J. Anal. Chem.*, 2019, **2019**.
16. T. Yoshida, H. Murakawa and K. Toda, *J Pestic Sci*, 2013, **38**, 27-32.
17. Q. Wang, Y. Liu, Y. Bai, S. Yao, Z. Wei, M. Zhang, L. Wang and L. Wang, *Anal. Chim. Acta*, 2019, **1049**, 170-178.
18. A. Li, Q. Chu, H. Zhou, Z. Yang, B. Liu and J. Zhang, *Inorg. Chem. Front.*, 2021, **8**, 2341-2348.

19. J. Liu, W. H. Xiong, L. Y. Ye, W. S. Zhang and H. Yang, *J. Agric. Food Chem.*, 2020, **68**, 5572-5578.
20. Y. Zhang, Q. Deng, C. Tang, M. Zhang, Z. Huang and Z. Cai, *Spectrochim. Acta - A: Mol. Biomol. Spectrosc.*, 2023, **286**, 121944.
21. K. Chatterjee, C. W. Kuo, A. Chen and P. Chen, *J. Nanobiotechnology*, 2015, **13**, 1-9.
22. T. Loiseau, C. Serre, C. Huguenard, G. Fink, F. Taulelle, M. Henry, T. Bataille and G. Férey, *Chem. Eur. J.*, 2004, **10**, 1373-1382.
23. A. Rana and S. Biswas, *Inorg. Chem. Front.*, 2023, **10**, 2742-2753.
24. C. M. Moran, J. N. Joshi, R. M. Marti, S. E. Hayes and K. S. Walton, *J. Am. Chem. Soc.*, 2018, **140**, 9148-9153.
25. A. Rana, S. Ghosh and S. Biswas, *Inorg. Chem. Front.*, 2023, **10**, 612-620.
26. M. Allahbakhshi, N. M. Mahmoodi, M. Mosaferi, H. Kazemian and H. Aslani, *Surf. Interfaces*, 2022, **35**, 102471.
27. P. Chakraborty, A. Rana, S. Mukherjee and S. Biswas, *Inorg. Chem.*, 2022, **62**, 802-809.
28. A. Nath, D. V. Gaikwad and S. Mandal, *Dalton Trans.*, 2023, **52**, 4303-4308.
29. A. Nath, G. M. Thomas, S. Hans, S. R. Vennapusa and S. Mandal, *Inorg. Chem.*, 2022, **61**, 2227-2233.
30. A. Sridhar, Y. Sandeep, C. Krishnakishore, P. Sriramnaveen, Y. Manjusha and V. Sivakumar, *Indian J. Nephrol.*, 2012, **22**, 385.
31. A. Santoveña-Estévez, J. Suárez-González, A. R. Cáceres-Pérez, Z. Ruiz-Noda, S. Machado-Rodríguez, M. Echezarreta, M. Soriano and J. B. Fariña, *Pharmaceutics*, 2020, **12**, 195.
32. S. Mukherjee, S. Ghosh and S. Biswas, *Inorg. Chem. Front.*, 2022, **9**, 6288-6298.
33. A. Rana, S. Nandi and S. Biswas, *New J. Chem.*, 2022, **46**, 10477-10483.

Conclusion

Metal-organic frameworks are a unique class of materials that combine both organic and inorganic components, forming highly porous, crystalline coordination networks. Their intrinsic porosity has been widely leveraged for applications such as gas storage, separation, and the management of both miscible and immiscible liquids. Moreover, MOFs have demonstrated remarkable utility in the selective separation of organic and inorganic compounds that are soluble in various solvents. This versatility stems from the inherent ability to easily functionalize MOFs, making them highly efficient materials for heterogeneous catalysis, proton conduction, and numerous other applications. Recently, the scientific community has taken significant interest in MOFs for their potential in detecting and accurately quantifying bio-active and toxic chemicals. This growing focus arises from the strategic incorporation of specific chemical functionalities into MOF frameworks, enabling them to selectively interact with analytes. When applied to the detection of environmental toxins and biological molecules, MOFs offer significant advantages. However, to closely simulate real-world environmental conditions, studies must be carried out in aqueous environments. Unfortunately, the synthesis of MOFs that maintain their stability in water, while still offering high sensitivity and selectivity for specific analytes, continues to be a major challenge in current research.

This thesis seeks to address this challenge by focusing on the design, synthesis, and characterization of aqua-stable MOFs. A particular emphasis is placed on developing comprehensive sensing methodologies for detecting inorganic, agricultural pollutants and pharmaceutical chemicals in aqueous media. Furthermore, the potential for utilizing MOFs in the removal of oil-based pollutants from water bodies was explored. Specifically, a superhydrophobic MOF-coated polypropylene and sponge composite and silk membrane were investigated for their ability to selectively remove oil, organic pollutant, from environmental water sources. To achieve these goals, the synthesis of aqua-stable MOFs was approached by using Zr(IV) and Al(III) metal ions, known for their strong coordination ability, alongside organic linkers that contain hard carboxylate groups. These components contribute to the formation of robust MOF structures capable of withstanding aqueous environments. The frameworks were further tailored through functionalization with specific chemical groups either during the synthesis process (via specially designed linkers) or through post-synthetic modifications. These modifications imbue the MOFs with recognition sites that are highly selective for specific analytes, enabling precise detection of environmental toxins and pharmaceutical chemicals. Additionally, these functional groups provided the necessary hydrophobicity, allowing the MOFs to effectively capture lipophilic substances such as oil spills, thereby demonstrating their potential for environmental cleanup applications.

In my first work, I have presented the detailed synthesis, characterization and application of a new hydrophobic Hf(IV) based MOF with DUT-52 structure bearing the rigid 1-(2,2,2-trifluoroacetamido)naphthalene-3,7-dicarboxylic acid (H_2L^1) ligand was prepared and its solid structures were characterized with the help of X-ray powder diffraction technique. The other characterization methods like thermogravimetric analysis and Fourier transform infrared spectroscopy were applied to verify the phase purity of the compound. Indexing of the slow scan PXRD pattern was carried out in comparison with the parent DUT-52 MOF in order to know the lattice parameters of our as-synthesized MOF material. As-synthesized (**1**) and activated (**1′**) compounds are thermally stable up to 310 °C in air atmosphere. The BET surface area of **1′** was found to be 884 $m^2 g^{-1}$**.** The in-situ synthesis of this hydrophobic MOF was again prepared and immobilized on the surface of PP fabric of a N95 mask. The surface immobilization of PP fabric of a N95 mask was confirmed by FT-IR, EDX, FESEM, water contact angle measurement (WCA) and BET surface area measurement. The surface area of

PP fabric before and after immobilization was found to be 0 and 257 m^2 g^{-1}. The contact angle before and after surface modification was found to be 0° and 160° respectively. The superhydrophobic PP fabric (**1′@PP**) possesses remarkable efficiency towards both heavy and light oil separation from oil-water mixture (95 to 99 %). The efficiency of oil-water separation remained unaltered even in harsh conditions like in different environmental water samples and pH solutions. The hydrophobic nature of synthesized MOF material inspired us to examine its self-cleaning nature. The material displays good self-cleaning nature for various real field applications.

My second work outlines the synthesis and characterization of a superhydrophobic Zr-UiO-66 (**2'**) metal-organic framework was synthesized palamitamidoterephthalic acid (H_2L^2, (H_2L^2: BDC-NH-CO-$(CH_2)_{14}$-CH_3)) linker and zirconium salt. Using the fluorine-free superhydrophobic **2'** MOF a robust **2'@sponge** composite and an **2'@silk** membrane were designed using PDMS-co-PMHS polymer. Initially, the sponge was coated with polydopamine hydrochloride (PDA) followed by dipping into the suspension of PDMS-co-PMHS polymer and **2'**. An enhancement in water contact angle (WCA) from 106 ± 1 to 169 ± 1 was found by the surface drafting of **2'** particles. The superhydrophobic composite and membrane displayed a remarkable oil-water separation with 70-time recyclability and a very fast flux rate. The separation efficiency of both the composite and membrane is over 99 % and the composite has an absorption capacity of 43.8-97.2 $g \cdot g^{-1}$ and the membrane has a flux rate of 58263-47416 $Lm^{-2}h^{-1}$ for different oils. The membrane and composite are maintaining their native property of hydrophobicity and crystallinity of drafted MOF particles even after 70 times of oil-water separation experiments. Both the composite and membrane maintain the self-cleaning and anti-fouling properties in soil and dye suspension. The mechanism of oil-water separation was also supported by the ESP diagram of all the possible molecules present in crude oil. The separation of crude oil was also performed. The recyclability of the material towards crude oil was also 70 times. The fluorine-free eco-friendly nature, recyclability harsh conditions and applicability towards the separation of crude oil made this work unique in the field of oil-water separation.

My next work summarized the construction of a new hafnium (Hf) metal-organic framework and bearing the rigid amine functionalized 2-aminoterephthalic acid (H_2BDC-NH_2) ligand was prepared and thereafter, post-synthetically modified with methylisocyanate to introduce a thioureido functionalization. The solid structure of MOF was characterized with the help of X-ray powder diffraction technique. Other characterization methods like thermogravimetric analysis and Fourier transform infrared spectroscopy were applied to verify the phase purity of the compound. The activated (**3**) compound is thermally stable up to 400 °C in N_2 atmosphere, whereas the stability of **3'** was between 350 to 400 °C. The BET surface area of **3'** was found to be 512 m^2g^{-1}. Fluorescence titration experiments showed that **3'** exhibits highly selective and sensitive fluorescence turn-off and turn-on behavior towards mercury (Hg^{2+}) and hydrazine (NH_2-NH_2) respectively. A good feature of a chemical sensor is to produce a detectable change towards the target analytes and with our probe, a 91% quenching and 28-fold increment in fluorescence emission intensity were observed for Hg^{2+} and NH_2-NH_2 respectively. The interference experiments suggested that other cations did not interfere with detecting Hg^{2+} and, the probe was sufficiently selective towards NH_2-NH_2 over the competitive analytes. Moreover, short response times (10 s and 50 s) were shown by the probe **3'** for Hg^{2+} and NH_2-NH_2 detection, respectively. The detection limits were found to be 4.0 nM and 1.9 nM, by our probe for Hg^{2+} and NH_2-NH_2, respectively, which is lower than the maximum acceptable concentration of Hg^{2+} ion as regulated by WHO and US environment protection agency. The response time and LOD of our probe are much lower than the other previously reported probes for Hg^{2+} and NH_2-NH_2 to date. Probe **3'** can also be effectively used for on-site detection of Hg^{2+} and NH_2-NH_2 by using portable MOF-coated cotton composite. The experimental studies

about the possible sensing mechanism revealed that the soft-soft interaction between the sulfur atom of the probe and Hg^{2+} is the reason behind the turn-off behavior of our probe in the presence of Hg^{2+}. The nucleophilic attack of hydrazine to the moderate electrophilic thiourea center of our probe caused a drastic increment in fluorescence emission intensity.

In my last work, I have demonstrated the synthesis of a functional Al(III) MIL-53 MOF-based sensor for rifampicin and nitenpyram detection. Pharmaceutical drugs and pesticides have lethal effects even in deficient concentrations. Our probe has an ultralow detection limit towards the sensing of nitenpyram (13.8 nM) and rifampicin (11.7 nM), which is an essential advantage of our probe to detect such lower concentration of nitenpyram and rifampicin for real-world application over the previously reported probes. The overdoses of drugs (rifampicin) into the human body could have toxic effects. Therefore, an ideal probe should be able to detect the targeted analyte from human body fluids. This issue could be addressed with the help of our probe, as it can detect and monitor rifampicin from human blood serum and urine with good accuracy and precision. The presence of pesticides and drugs in environmental waters could harm the health of humans and animals, too. As a result, we performed the detection of nitenpyram and rifampicin from environmental water samples (lake, river, tap and distilled water). Moreover, nitenpyram could also contaminate the soil and agricultural products (crops). Therefore, we have precisely quantified this neonicotinoid pesticide (nitenpyram) from soil and food samples (corn and rice) with the help of our probe. This probe could detect both these analytes (rifampicin and nitenpyram) multiple times due to its recyclable nature, which is an advantage over the single-use probes from an economical point of view. Systematic analytical experiments were performed to understand the exact mechanism of fluorescence quenching. We believe that this work will provide a detailed idea from the synthesis of functional luminescent MOF to the application of selective sensing of rifampicin and nitenpyram. It could be useful for the biomedical remediation and safeguarding of human health.

In conclusion, this thesis highlights the development and application of novel hydrophobic MOFs for diverse and impactful uses in environmental and analytical fields. The synthesis of new Hf(IV) and Zr-based MOFs demonstrated exceptional performance in oil-water separation, showcasing their high stability, superhydrophobic properties, and recyclability, even under harsh conditions. Additionally, the functionalization of these MOFs with specific ligands facilitated selective and sensitive detection of hazardous substances, such as mercury, hydrazine, rifampicin, and nitenpyram, at ultra-low concentrations, surpassing the capabilities of previous probes. The successful integration of these MOFs into composite materials, including membranes and fabrics, further expanded their practical applications for real-world challenges like pollution and contamination. The findings highlights the potential of these MOFs for advancing environmental remediation, sensing technologies, and human health protection, while also contributing to the broader field of functional material design.

Future Aspects

Looking ahead, the focus of my future research will be on overcoming the challenges related to the stability of MOFs in extreme pH conditions. Although many aqua MOFs have been synthesized by enhancing coordination bonds and utilizing high oxidation state metal ions, their stability in highly acidic and basic environments is still a significant concern. To address this, I plan to synthesize MOFs that exhibit robust stability under both acidic and basic conditions, which will greatly expand their potential applications in various industrial and environmental processes. One of the primary directions of my future work will be the exploration of MOFs incorporating redox-active metal ions, such as Cr(III), Cu(II), Ni(II), Zn(II), and Cd(II). These metal ions can play a key role in enhancing the electrocatalytic

properties of MOFs, which are crucial for applications in energy conversion, fuel cells, and batteries. By investigating these materials, I aim to contribute to the development of highly efficient electrocatalysts for renewable energy technologies, such as hydrogen production through water splitting and CO_2 reduction. Additionally, I am interested in exploring MOFs that contain photoactive metal ions and linkers, which have the potential for use in photocatalytic applications. Photocatalysis is a promising field for energy harvesting, environmental remediation, and organic synthesis, and MOFs with photoactive properties could significantly improve the efficiency of these processes. By combining metal ions with photoactive linkers, I hope to develop materials that can harness light energy for sustainable chemical transformations, including water splitting, CO_2 reduction, and pollutant degradation. A critical challenge in the field of MOFs is the vulnerability of certain materials, especially those containing hard metal ions, to degradation or ion exchange in the presence of certain ions like PO_4^{3-}, and AsO_4^{3-}. These limitations restrict the use of some MOFs in sensing and adsorption applications. To overcome these issues, I plan to investigate alternative coordinating sites, such as phthalimide, acetoxy, boronic acid, maleimide, and allyloxy groups, which could provide enhanced stability and expand the functionality of MOFs. By exploring these alternative coordination chemistries, I aim to design more robust and versatile MOFs that can overcome the current limitations in sensing, separation, and catalytic applications. Looking further ahead, I believe that the foundation laid by renowned researchers like Prof. Robson and Prof. Yagi, along with their teams, has greatly advanced the understanding and development of MOFs. However, the journey is far from over. The potential for new and innovative MOFs continues to grow, with the possibility of discovering new metal-organic architectures that offer unprecedented properties for a wide range of applications. The collaboration between metal ions and organic linkers has proven to be a rich source of fascinating chemistry, and I strongly believe that the future of MOF research holds even more exciting discoveries. As a contributor to this ongoing journey, I am eager to push the boundaries of MOF chemistry and help unravel the full potential of these materials. With the rapid expansion of research in this field, I am optimistic that the future will bring new insights and breakthroughs that will have a profound impact on energy, environmental, and industrial technologies. I consider myself fortunate to be part of this dynamic and evolving field, and I look forward to continuing to explore the exciting possibilities of MOFs in the years to come.

ELSEVIER LICENSE
TERMS AND CONDITIONS

Feb 13, 2025

This Agreement between Abijeet Rana ("You") and Elsevier ("Elsevier") consists of your license details and the terms and conditions provided by Elsevier and Copyright Clearance Center.

License Number	5966871367406
License date	Feb 13, 2025
Licensed Content Publisher	Elsevier
Licensed Content Publication	Materials Today Chemistry
Licensed Content Title	Ce-MOF-based superhydrophobic polyurethane sponge reinforced by cellulose for efficient oil-water separation
Licensed Content Author	J.-F. Meng,B.-Y. Song, F. Li,T.-H Li
Licensed Content Date	Mar 1, 2023
Licensed Content Volume	28
Licensed Content Issue	n/a
Licensed Content Pages	1
Start Page	101371
End Page	0
Type of Use	reuse in a thesis/dissertation

Portion	figures/tables/illustrations
Number of figures/tables/illustrations	12
Format	both print and electronic
Are you the author of this Elsevier article?	No
Will you be translating?	No
Title of new work	Development of Water-Stable Metal-Organic Frameworks for Oil-Water Separation and Toxic Chemical Sensing
Institution name	IIT Guwahati
Expected presentation date	Jul 2025
Portions	Graphical abstract
The Requesting Person / Organization to Appear on the License	Abijeet Rana
Requestor Location	Mr. Abijeet Rana IIT Guwahati Guwahati, Assam 781039 India
Order reference number	12
Publisher Tax ID	GB 494 6272 12
Total	0.00 USD
Terms and Conditions	

INTRODUCTION

1. The publisher for this copyrighted material is Elsevier. By clicking "accept" in connection with completing this licensing transaction, you agree that the following terms and conditions apply to this transaction (along with the Billing and Payment terms and conditions established by Copyright Clearance Center, Inc. ("CCC"), at the time that you opened your RightsLink account and that are available at any time at https://myaccount.copyright.com).

GENERAL TERMS

2. Elsevier hereby grants you permission to reproduce the aforementioned material subject to the terms and conditions indicated.

3. Acknowledgement: If any part of the material to be used (for example, figures) has appeared in our publication with credit or acknowledgement to another source, permission must also be sought from that source. If such permission is not obtained then that material may not be included in your publication/copies. Suitable acknowledgement to the source must be made, either as a footnote or in a reference list at the end of your publication, as follows:

"Reprinted from Publication title, Vol /edition number, Author(s), Title of article / title of chapter, Pages No., Copyright (Year), with permission from Elsevier [OR APPLICABLE SOCIETY COPYRIGHT OWNER]." Also Lancet special credit - "Reprinted from The Lancet, Vol. number, Author(s), Title of article, Pages No., Copyright (Year), with permission from Elsevier."

4. Reproduction of this material is confined to the purpose and/or media for which permission is hereby given. The material may not be reproduced or used in any other way, including use in combination with an artificial intelligence tool (including to train an algorithm, test, process, analyse, generate output and/or develop any form of artificial intelligence tool), or to create any derivative work and/or service (including resulting from the use of artificial intelligence tools).

5. Altering/Modifying Material: Not Permitted. However figures and illustrations may be altered/adapted minimally to serve your work. Any other abbreviations, additions, deletions and/or any other alterations shall be made only with prior written authorization of Elsevier Ltd. (Please contact Elsevier's permissions helpdesk here). No modifications can be made to any Lancet figures/tables and they must be reproduced in full.

6. If the permission fee for the requested use of our material is waived in this instance, please be advised that your future requests for Elsevier materials may attract a fee.

7. Reservation of Rights: Publisher reserves all rights not specifically granted in the combination of (i) the license details provided by you and accepted in the course of this licensing transaction, (ii) these terms and conditions and (iii) CCC's Billing and Payment terms and conditions.

8. License Contingent Upon Payment: While you may exercise the rights licensed immediately upon issuance of the license at the end of the licensing process for the transaction, provided that you have disclosed complete and accurate details of your proposed use, no license is finally effective unless and until full payment is received from you (either by publisher or by CCC) as provided in CCC's Billing and Payment terms and conditions. If full payment is not received on a timely basis, then any license preliminarily granted shall be deemed automatically revoked and shall be void as if never granted. Further, in the event that you breach any of these terms and conditions or any of CCC's Billing and Payment terms and conditions, the license is automatically revoked and shall be void as if never granted. Use of materials as described in a revoked license, as well as any use of the materials beyond the scope of an unrevoked license, may constitute copyright infringement and publisher reserves the right to take any and all action to protect its copyright in the materials.

9. Warranties: Publisher makes no representations or warranties with respect to the licensed material.

10. Indemnity: You hereby indemnify and agree to hold harmless publisher and CCC, and their respective officers, directors, employees and agents, from and against any and all claims arising out of your use of the licensed material other than as specifically authorized pursuant to this license.

11. No Transfer of License: This license is personal to you and may not be sublicensed, assigned, or transferred by you to any other person without publisher's written permission.

12. No Amendment Except in Writing: This license may not be amended except in a writing signed by both parties (or, in the case of publisher, by CCC on publisher's behalf).

13. Objection to Contrary Terms: Publisher hereby objects to any terms contained in any purchase order, acknowledgment, check endorsement or other writing prepared by you, which terms are inconsistent with these terms and conditions or CCC's Billing and Payment terms and conditions. These terms and conditions, together with CCC's Billing and Payment terms and conditions (which are incorporated herein), comprise the entire agreement between you and publisher (and CCC) concerning this licensing transaction. In the event of any conflict between your obligations established by these terms and conditions and those established by CCC's Billing and Payment terms and conditions, these terms and conditions shall control.

14. Revocation: Elsevier or Copyright Clearance Center may deny the permissions described in this License at their sole discretion, for any reason or no reason, with a full refund payable to you. Notice of such denial will be made using the contact information provided by you. Failure to receive such notice will not alter or invalidate the denial. In no event will Elsevier or Copyright Clearance Center be responsible or liable for any costs, expenses or damage incurred by you as a result of a denial of your permission request, other than a refund of the amount(s) paid by you to Elsevier and/or Copyright Clearance Center for denied permissions.

LIMITED LICENSE

The following terms and conditions apply only to specific license types:

15. **Translation**: This permission is granted for non-exclusive world **English** rights only unless your license was granted for translation rights. If you licensed translation rights you may only translate this content into the languages you requested. A professional translator must perform all translations and reproduce the content word for word preserving the integrity of the article.

16. **Posting licensed content on any Website**: The following terms and conditions apply as follows: Licensing material from an Elsevier journal: All content posted to the web site must maintain the copyright information line on the bottom of each image; A hyper-text must be included to the Homepage of the journal from which you are licensing at http://www.sciencedirect.com/science/journal/xxxxx or the Elsevier homepage for books at http://www.elsevier.com; Central Storage: This license does not include permission for a scanned version of the material to be stored in a central repository such as that provided by Heron/XanEdu.

Licensing material from an Elsevier book: A hyper-text link must be included to the Elsevier homepage at http://www.elsevier.com . All content posted to the web site must maintain the copyright information line on the bottom of each image.

Posting licensed content on Electronic reserve: In addition to the above the following clauses are applicable: The web site must be password-protected and made available only

to bona fide students registered on a relevant course. This permission is granted for 1 year only. You may obtain a new license for future website posting.

17. **For journal authors:** the following clauses are applicable in addition to the above:

Preprints:

A preprint is an author's own write-up of research results and analysis, it has not been peer-reviewed, nor has it had any other value added to it by a publisher (such as formatting, copyright, technical enhancement etc.).

Authors can share their preprints anywhere at any time. Preprints should not be added to or enhanced in any way in order to appear more like, or to substitute for, the final versions of articles however authors can update their preprints on arXiv or RePEc with their Accepted Author Manuscript (see below).

If accepted for publication, we encourage authors to link from the preprint to their formal publication via its DOI. Millions of researchers have access to the formal publications on ScienceDirect, and so links will help users to find, access, cite and use the best available version. Please note that Cell Press, The Lancet and some society-owned have different preprint policies. Information on these policies is available on the journal homepage.

Accepted Author Manuscripts: An accepted author manuscript is the manuscript of an article that has been accepted for publication and which typically includes author-incorporated changes suggested during submission, peer review and editor-author communications.

Authors can share their accepted author manuscript:

- immediately
  - via their non-commercial person homepage or blog
  - by updating a preprint in arXiv or RePEc with the accepted manuscript
  - via their research institute or institutional repository for internal institutional uses or as part of an invitation-only research collaboration work-group
  - directly by providing copies to their students or to research collaborators for their personal use
  - for private scholarly sharing as part of an invitation-only work group on commercial sites with which Elsevier has an agreement
- After the embargo period
  - via non-commercial hosting platforms such as their institutional repository
  - via commercial sites with which Elsevier has an agreement

In all cases accepted manuscripts should:

- link to the formal publication via its DOI
- bear a CC-BY-NC-ND license - this is easy to do
- if aggregated with other manuscripts, for example in a repository or other site, be shared in alignment with our hosting policy not be added to or enhanced in any way to appear more like, or to substitute for, the published journal article.

Published journal article (JPA): A published journal article (PJA) is the definitive final record of published research that appears or will appear in the journal and embodies all value-adding publishing activities including peer review co-ordination, copy-editing, formatting, (if relevant) pagination and online enrichment.

Policies for sharing publishing journal articles differ for subscription and gold open access articles:

Subscription Articles: If you are an author, please share a link to your article rather than the full-text. Millions of researchers have access to the formal publications on ScienceDirect, and so links will help your users to find, access, cite, and use the best available version.

Theses and dissertations which contain embedded PJAs as part of the formal submission can be posted publicly by the awarding institution with DOI links back to the formal publications on ScienceDirect.

If you are affiliated with a library that subscribes to ScienceDirect you have additional private sharing rights for others' research accessed under that agreement. This includes use for classroom teaching and internal training at the institution (including use in course packs and courseware programs), and inclusion of the article for grant funding purposes.

Gold Open Access Articles: May be shared according to the author-selected end-user license and should contain a CrossMark logo, the end user license, and a DOI link to the formal publication on ScienceDirect.

Please refer to Elsevier's posting policy for further information.

18. **For book authors** the following clauses are applicable in addition to the above: Authors are permitted to place a brief summary of their work online only. You are not allowed to download and post the published electronic version of your chapter, nor may you scan the printed edition to create an electronic version. **Posting to a repository:** Authors are permitted to post a summary of their chapter only in their institution's repository.

19. **Thesis/Dissertation**: If your license is for use in a thesis/dissertation your thesis may be submitted to your institution in either print or electronic form. Should your thesis be published commercially, please reapply for permission. These requirements include permission for the Library and Archives of Canada to supply single copies, on demand, of the complete thesis and include permission for Proquest/UMI to supply single copies, on demand, of the complete thesis. Should your thesis be published commercially, please reapply for permission. Theses and dissertations which contain embedded PJAs as part of the formal submission can be posted publicly by the awarding institution with DOI links back to the formal publications on ScienceDirect.

Elsevier Open Access Terms and Conditions

You can publish open access with Elsevier in hundreds of open access journals or in nearly 2000 established subscription journals that support open access publishing. Permitted third party re-use of these open access articles is defined by the author's choice of Creative Commons user license. See our open access license policy for more information.

Terms & Conditions applicable to all Open Access articles published with Elsevier:

Any reuse of the article must not represent the author as endorsing the adaptation of the article nor should the article be modified in such a way as to damage the author's honour or reputation. If any changes have been made, such changes must be clearly indicated.

The author(s) must be appropriately credited and we ask that you include the end user license and a DOI link to the formal publication on ScienceDirect.

If any part of the material to be used (for example, figures) has appeared in our publication with credit or acknowledgement to another source it is the responsibility of the

user to ensure their reuse complies with the terms and conditions determined by the rights holder.

Additional Terms & Conditions applicable to each Creative Commons user license:

CC BY: The CC-BY license allows users to copy, to create extracts, abstracts and new works from the Article, to alter and revise the Article and to make commercial use of the Article (including reuse and/or resale of the Article by commercial entities), provided the user gives appropriate credit (with a link to the formal publication through the relevant DOI), provides a link to the license, indicates if changes were made and the licensor is not represented as endorsing the use made of the work. The full details of the license are available at http://creativecommons.org/licenses/by/4.0.

CC BY NC SA: The CC BY-NC-SA license allows users to copy, to create extracts, abstracts and new works from the Article, to alter and revise the Article, provided this is not done for commercial purposes, and that the user gives appropriate credit (with a link to the formal publication through the relevant DOI), provides a link to the license, indicates if changes were made and the licensor is not represented as endorsing the use made of the work. Further, any new works must be made available on the same conditions. The full details of the license are available at http://creativecommons.org/licenses/by-nc-sa/4.0.

CC BY NC ND: The CC BY-NC-ND license allows users to copy and distribute the Article, provided this is not done for commercial purposes and further does not permit distribution of the Article if it is changed or edited in any way, and provided the user gives appropriate credit (with a link to the formal publication through the relevant DOI), provides a link to the license, and that the licensor is not represented as endorsing the use made of the work. The full details of the license are available at http://creativecommons.org/licenses/by-nc-nd/4.0. Any commercial reuse of Open Access articles published with a CC BY NC SA or CC BY NC ND license requires permission from Elsevier and will be subject to a fee.

Commercial reuse includes:

- Associating advertising with the full text of the Article
- Charging fees for document delivery or access
- Article aggregation
- Systematic distribution via e-mail lists or share buttons

Posting or linking by commercial companies for use by customers of those companies.

20. **Other Conditions**:

v1.10

Questions? customercare@copyright.com.

ELSEVIER LICENSE
TERMS AND CONDITIONS

Feb 13, 2025

This Agreement between Abijeet Rana ("You") and Elsevier ("Elsevier") consists of your license details and the terms and conditions provided by Elsevier and Copyright Clearance Center.

License Number	5966900981916
License date	Feb 13, 2025
Licensed Content Publisher	Elsevier
Licensed Content Publication	Coordination Chemistry Reviews
Licensed Content Title	Potential applications of metal-organic frameworks
Licensed Content Author	Ryan J. Kuppler,Daren J. Timmons,Qian-Rong Fang,Jian-Rong Li,Tegan A. Makal,Mark D. Young,Daqiang Yuan,Dan Zhao,Wenjuan Zhuang,Hong-Cai Zhou
Licensed Content Date	Dec 1, 2009
Licensed Content Volume	253
Licensed Content Issue	23-24
Licensed Content Pages	25
Start Page	3042
End Page	3066
Type of Use	reuse in a thesis/dissertation

Portion	figures/tables/illustrations
Number of figures/tables/illustrations	1
Format	both print and electronic
Are you the author of this Elsevier article?	No
Will you be translating?	No
Title of new work	Development of Water-Stable Metal-Organic Frameworks for Oil-Water Separation and Toxic Chemical Sensing
Institution name	IIT Guwahati
Expected presentation date	Jul 2025
Portions	2
The Requesting Person / Organization to Appear on the License	Abijeet Rana
Requestor Location	Mr. Abijeet Rana IIT Guwahati Guwahati, Assam 781039 India
Order reference number	16
Publisher Tax ID	GB 494 6272 12
Total	0.00 USD
Terms and Conditions	

INTRODUCTION

1. The publisher for this copyrighted material is Elsevier. By clicking "accept" in connection with completing this licensing transaction, you agree that the following terms and conditions apply to this transaction (along with the Billing and Payment terms and conditions established by Copyright Clearance Center, Inc. ("CCC"), at the time that you opened your RightsLink account and that are available at any time at https://myaccount.copyright.com).

GENERAL TERMS

2. Elsevier hereby grants you permission to reproduce the aforementioned material subject to the terms and conditions indicated.

3. Acknowledgement: If any part of the material to be used (for example, figures) has appeared in our publication with credit or acknowledgement to another source, permission must also be sought from that source. If such permission is not obtained then that material may not be included in your publication/copies. Suitable acknowledgement to the source must be made, either as a footnote or in a reference list at the end of your publication, as follows:

"Reprinted from Publication title, Vol /edition number, Author(s), Title of article / title of chapter, Pages No., Copyright (Year), with permission from Elsevier [OR APPLICABLE SOCIETY COPYRIGHT OWNER]." Also Lancet special credit - "Reprinted from The Lancet, Vol. number, Author(s), Title of article, Pages No., Copyright (Year), with permission from Elsevier."

4. Reproduction of this material is confined to the purpose and/or media for which permission is hereby given. The material may not be reproduced or used in any other way, including use in combination with an artificial intelligence tool (including to train an algorithm, test, process, analyse, generate output and/or develop any form of artificial intelligence tool), or to create any derivative work and/or service (including resulting from the use of artificial intelligence tools).

5. Altering/Modifying Material: Not Permitted. However figures and illustrations may be altered/adapted minimally to serve your work. Any other abbreviations, additions, deletions and/or any other alterations shall be made only with prior written authorization of Elsevier Ltd. (Please contact Elsevier's permissions helpdesk here). No modifications can be made to any Lancet figures/tables and they must be reproduced in full.

6. If the permission fee for the requested use of our material is waived in this instance, please be advised that your future requests for Elsevier materials may attract a fee.

7. Reservation of Rights: Publisher reserves all rights not specifically granted in the combination of (i) the license details provided by you and accepted in the course of this licensing transaction, (ii) these terms and conditions and (iii) CCC's Billing and Payment terms and conditions.

8. License Contingent Upon Payment: While you may exercise the rights licensed immediately upon issuance of the license at the end of the licensing process for the transaction, provided that you have disclosed complete and accurate details of your proposed use, no license is finally effective unless and until full payment is received from you (either by publisher or by CCC) as provided in CCC's Billing and Payment terms and conditions. If full payment is not received on a timely basis, then any license preliminarily granted shall be deemed automatically revoked and shall be void as if never granted. Further, in the event that you breach any of these terms and conditions or any of CCC's Billing and Payment terms and conditions, the license is automatically revoked and shall be void as if never granted. Use of materials as described in a revoked license, as well as any use of the materials beyond the scope of an unrevoked license, may constitute copyright infringement and publisher reserves the right to take any and all action to protect its copyright in the materials.

9. Warranties: Publisher makes no representations or warranties with respect to the licensed material.

10. Indemnity: You hereby indemnify and agree to hold harmless publisher and CCC, and their respective officers, directors, employees and agents, from and against any and all claims arising out of your use of the licensed material other than as specifically authorized pursuant to this license.

11. No Transfer of License: This license is personal to you and may not be sublicensed, assigned, or transferred by you to any other person without publisher's written permission.

12. No Amendment Except in Writing: This license may not be amended except in a writing signed by both parties (or, in the case of publisher, by CCC on publisher's behalf).

13. Objection to Contrary Terms: Publisher hereby objects to any terms contained in any purchase order, acknowledgment, check endorsement or other writing prepared by you, which terms are inconsistent with these terms and conditions or CCC's Billing and Payment terms and conditions. These terms and conditions, together with CCC's Billing and Payment terms and conditions (which are incorporated herein), comprise the entire agreement between you and publisher (and CCC) concerning this licensing transaction. In the event of any conflict between your obligations established by these terms and conditions and those established by CCC's Billing and Payment terms and conditions, these terms and conditions shall control.

14. Revocation: Elsevier or Copyright Clearance Center may deny the permissions described in this License at their sole discretion, for any reason or no reason, with a full refund payable to you. Notice of such denial will be made using the contact information provided by you. Failure to receive such notice will not alter or invalidate the denial. In no event will Elsevier or Copyright Clearance Center be responsible or liable for any costs, expenses or damage incurred by you as a result of a denial of your permission request, other than a refund of the amount(s) paid by you to Elsevier and/or Copyright Clearance Center for denied permissions.

LIMITED LICENSE

The following terms and conditions apply only to specific license types:

15. **Translation**: This permission is granted for non-exclusive world **English** rights only unless your license was granted for translation rights. If you licensed translation rights you may only translate this content into the languages you requested. A professional translator must perform all translations and reproduce the content word for word preserving the integrity of the article.

16. **Posting licensed content on any Website**: The following terms and conditions apply as follows: Licensing material from an Elsevier journal: All content posted to the web site must maintain the copyright information line on the bottom of each image; A hyper-text must be included to the Homepage of the journal from which you are licensing at http://www.sciencedirect.com/science/journal/xxxxx or the Elsevier homepage for books at http://www.elsevier.com; Central Storage: This license does not include permission for a scanned version of the material to be stored in a central repository such as that provided by Heron/XanEdu.

Licensing material from an Elsevier book: A hyper-text link must be included to the Elsevier homepage at http://www.elsevier.com . All content posted to the web site must maintain the copyright information line on the bottom of each image.

Posting licensed content on Electronic reserve: In addition to the above the following clauses are applicable: The web site must be password-protected and made available only

to bona fide students registered on a relevant course. This permission is granted for 1 year only. You may obtain a new license for future website posting.

17. **For journal authors:** the following clauses are applicable in addition to the above:

Preprints:

A preprint is an author's own write-up of research results and analysis, it has not been peer-reviewed, nor has it had any other value added to it by a publisher (such as formatting, copyright, technical enhancement etc.).

Authors can share their preprints anywhere at any time. Preprints should not be added to or enhanced in any way in order to appear more like, or to substitute for, the final versions of articles however authors can update their preprints on arXiv or RePEc with their Accepted Author Manuscript (see below).

If accepted for publication, we encourage authors to link from the preprint to their formal publication via its DOI. Millions of researchers have access to the formal publications on ScienceDirect, and so links will help users to find, access, cite and use the best available version. Please note that Cell Press, The Lancet and some society-owned have different preprint policies. Information on these policies is available on the journal homepage.

Accepted Author Manuscripts: An accepted author manuscript is the manuscript of an article that has been accepted for publication and which typically includes author-incorporated changes suggested during submission, peer review and editor-author communications.

Authors can share their accepted author manuscript:

- immediately
  - via their non-commercial person homepage or blog
  - by updating a preprint in arXiv or RePEc with the accepted manuscript
  - via their research institute or institutional repository for internal institutional uses or as part of an invitation-only research collaboration work-group
  - directly by providing copies to their students or to research collaborators for their personal use
  - for private scholarly sharing as part of an invitation-only work group on commercial sites with which Elsevier has an agreement
- After the embargo period
  - via non-commercial hosting platforms such as their institutional repository
  - via commercial sites with which Elsevier has an agreement

In all cases accepted manuscripts should:

- link to the formal publication via its DOI
- bear a CC-BY-NC-ND license - this is easy to do
- if aggregated with other manuscripts, for example in a repository or other site, be shared in alignment with our hosting policy not be added to or enhanced in any way to appear more like, or to substitute for, the published journal article.

Published journal article (JPA): A published journal article (PJA) is the definitive final record of published research that appears or will appear in the journal and embodies all value-adding publishing activities including peer review co-ordination, copy-editing, formatting, (if relevant) pagination and online enrichment.

Policies for sharing publishing journal articles differ for subscription and gold open access articles:

Subscription Articles: If you are an author, please share a link to your article rather than the full-text. Millions of researchers have access to the formal publications on ScienceDirect, and so links will help your users to find, access, cite, and use the best available version.

Theses and dissertations which contain embedded PJAs as part of the formal submission can be posted publicly by the awarding institution with DOI links back to the formal publications on ScienceDirect.

If you are affiliated with a library that subscribes to ScienceDirect you have additional private sharing rights for others' research accessed under that agreement. This includes use for classroom teaching and internal training at the institution (including use in course packs and courseware programs), and inclusion of the article for grant funding purposes.

Gold Open Access Articles: May be shared according to the author-selected end-user license and should contain a CrossMark logo, the end user license, and a DOI link to the formal publication on ScienceDirect.

Please refer to Elsevier's posting policy for further information.

18. **For book authors** the following clauses are applicable in addition to the above: Authors are permitted to place a brief summary of their work online only. You are not allowed to download and post the published electronic version of your chapter, nor may you scan the printed edition to create an electronic version. **Posting to a repository:** Authors are permitted to post a summary of their chapter only in their institution's repository.

19. **Thesis/Dissertation**: If your license is for use in a thesis/dissertation your thesis may be submitted to your institution in either print or electronic form. Should your thesis be published commercially, please reapply for permission. These requirements include permission for the Library and Archives of Canada to supply single copies, on demand, of the complete thesis and include permission for Proquest/UMI to supply single copies, on demand, of the complete thesis. Should your thesis be published commercially, please reapply for permission. Theses and dissertations which contain embedded PJAs as part of the formal submission can be posted publicly by the awarding institution with DOI links back to the formal publications on ScienceDirect.

Elsevier Open Access Terms and Conditions

You can publish open access with Elsevier in hundreds of open access journals or in nearly 2000 established subscription journals that support open access publishing. Permitted third party re-use of these open access articles is defined by the author's choice of Creative Commons user license. See our open access license policy for more information.

Terms & Conditions applicable to all Open Access articles published with Elsevier:

Any reuse of the article must not represent the author as endorsing the adaptation of the article nor should the article be modified in such a way as to damage the author's honour or reputation. If any changes have been made, such changes must be clearly indicated.

The author(s) must be appropriately credited and we ask that you include the end user license and a DOI link to the formal publication on ScienceDirect.

If any part of the material to be used (for example, figures) has appeared in our publication with credit or acknowledgement to another source it is the responsibility of the

user to ensure their reuse complies with the terms and conditions determined by the rights holder.

Additional Terms & Conditions applicable to each Creative Commons user license:

CC BY: The CC-BY license allows users to copy, to create extracts, abstracts and new works from the Article, to alter and revise the Article and to make commercial use of the Article (including reuse and/or resale of the Article by commercial entities), provided the user gives appropriate credit (with a link to the formal publication through the relevant DOI), provides a link to the license, indicates if changes were made and the licensor is not represented as endorsing the use made of the work. The full details of the license are available at http://creativecommons.org/licenses/by/4.0.

CC BY NC SA: The CC BY-NC-SA license allows users to copy, to create extracts, abstracts and new works from the Article, to alter and revise the Article, provided this is not done for commercial purposes, and that the user gives appropriate credit (with a link to the formal publication through the relevant DOI), provides a link to the license, indicates if changes were made and the licensor is not represented as endorsing the use made of the work. Further, any new works must be made available on the same conditions. The full details of the license are available at http://creativecommons.org/licenses/by-nc-sa/4.0.

CC BY NC ND: The CC BY-NC-ND license allows users to copy and distribute the Article, provided this is not done for commercial purposes and further does not permit distribution of the Article if it is changed or edited in any way, and provided the user gives appropriate credit (with a link to the formal publication through the relevant DOI), provides a link to the license, and that the licensor is not represented as endorsing the use made of the work. The full details of the license are available at http://creativecommons.org/licenses/by-nc-nd/4.0. Any commercial reuse of Open Access articles published with a CC BY NC SA or CC BY NC ND license requires permission from Elsevier and will be subject to a fee.

Commercial reuse includes:

- Associating advertising with the full text of the Article
- Charging fees for document delivery or access
- Article aggregation
- Systematic distribution via e-mail lists or share buttons

Posting or linking by commercial companies for use by customers of those companies.

20. **Other Conditions:**

v1.10

Questions? customercare@copyright.com.

ELSEVIER LICENSE
TERMS AND CONDITIONS

Feb 13, 2025

This Agreement between Abijeet Rana ("You") and Elsevier ("Elsevier") consists of your license details and the terms and conditions provided by Elsevier and Copyright Clearance Center.

License Number	5966900981916
License date	Feb 13, 2025
Licensed Content Publisher	Elsevier
Licensed Content Publication	Coordination Chemistry Reviews
Licensed Content Title	Potential applications of metal-organic frameworks
Licensed Content Author	Ryan J. Kuppler,Daren J. Timmons,Qian-Rong Fang,Jian-Rong Li,Tegan A. Makal,Mark D. Young,Daqiang Yuan,Dan Zhao,Wenjuan Zhuang,Hong-Cai Zhou
Licensed Content Date	Dec 1, 2009
Licensed Content Volume	253
Licensed Content Issue	23-24
Licensed Content Pages	25
Start Page	3042
End Page	3066
Type of Use	reuse in a thesis/dissertation

Portion	figures/tables/illustrations
Number of figures/tables/illustrations	1
Format	both print and electronic
Are you the author of this Elsevier article?	No
Will you be translating?	No
Title of new work	Development of Water-Stable Metal-Organic Frameworks for Oil-Water Separation and Toxic Chemical Sensing
Institution name	IIT Guwahati
Expected presentation date	Jul 2025
Portions	2
The Requesting Person / Organization to Appear on the License	Abijeet Rana
Requestor Location	Mr. Abijeet Rana IIT Guwahati Guwahati, Assam 781039 India
Order reference number	16
Publisher Tax ID	GB 494 6272 12
Total	0.00 USD
Terms and Conditions	

INTRODUCTION

1. The publisher for this copyrighted material is Elsevier. By clicking "accept" in connection with completing this licensing transaction, you agree that the following terms and conditions apply to this transaction (along with the Billing and Payment terms and conditions established by Copyright Clearance Center, Inc. ("CCC"), at the time that you opened your RightsLink account and that are available at any time at https://myaccount.copyright.com).

GENERAL TERMS

2. Elsevier hereby grants you permission to reproduce the aforementioned material subject to the terms and conditions indicated.

3. Acknowledgement: If any part of the material to be used (for example, figures) has appeared in our publication with credit or acknowledgement to another source, permission must also be sought from that source. If such permission is not obtained then that material may not be included in your publication/copies. Suitable acknowledgement to the source must be made, either as a footnote or in a reference list at the end of your publication, as follows:

"Reprinted from Publication title, Vol /edition number, Author(s), Title of article / title of chapter, Pages No., Copyright (Year), with permission from Elsevier [OR APPLICABLE SOCIETY COPYRIGHT OWNER]." Also Lancet special credit - "Reprinted from The Lancet, Vol. number, Author(s), Title of article, Pages No., Copyright (Year), with permission from Elsevier."

4. Reproduction of this material is confined to the purpose and/or media for which permission is hereby given. The material may not be reproduced or used in any other way, including use in combination with an artificial intelligence tool (including to train an algorithm, test, process, analyse, generate output and/or develop any form of artificial intelligence tool), or to create any derivative work and/or service (including resulting from the use of artificial intelligence tools).

5. Altering/Modifying Material: Not Permitted. However figures and illustrations may be altered/adapted minimally to serve your work. Any other abbreviations, additions, deletions and/or any other alterations shall be made only with prior written authorization of Elsevier Ltd. (Please contact Elsevier's permissions helpdesk here). No modifications can be made to any Lancet figures/tables and they must be reproduced in full.

6. If the permission fee for the requested use of our material is waived in this instance, please be advised that your future requests for Elsevier materials may attract a fee.

7. Reservation of Rights: Publisher reserves all rights not specifically granted in the combination of (i) the license details provided by you and accepted in the course of this licensing transaction, (ii) these terms and conditions and (iii) CCC's Billing and Payment terms and conditions.

8. License Contingent Upon Payment: While you may exercise the rights licensed immediately upon issuance of the license at the end of the licensing process for the transaction, provided that you have disclosed complete and accurate details of your proposed use, no license is finally effective unless and until full payment is received from you (either by publisher or by CCC) as provided in CCC's Billing and Payment terms and conditions. If full payment is not received on a timely basis, then any license preliminarily granted shall be deemed automatically revoked and shall be void as if never granted. Further, in the event that you breach any of these terms and conditions or any of CCC's Billing and Payment terms and conditions, the license is automatically revoked and shall be void as if never granted. Use of materials as described in a revoked license, as well as any use of the materials beyond the scope of an unrevoked license, may constitute copyright infringement and publisher reserves the right to take any and all action to protect its copyright in the materials.

9. Warranties: Publisher makes no representations or warranties with respect to the licensed material.

10. Indemnity: You hereby indemnify and agree to hold harmless publisher and CCC, and their respective officers, directors, employees and agents, from and against any and all claims arising out of your use of the licensed material other than as specifically authorized pursuant to this license.

11. No Transfer of License: This license is personal to you and may not be sublicensed, assigned, or transferred by you to any other person without publisher's written permission.

12. No Amendment Except in Writing: This license may not be amended except in a writing signed by both parties (or, in the case of publisher, by CCC on publisher's behalf).

13. Objection to Contrary Terms: Publisher hereby objects to any terms contained in any purchase order, acknowledgment, check endorsement or other writing prepared by you, which terms are inconsistent with these terms and conditions or CCC's Billing and Payment terms and conditions. These terms and conditions, together with CCC's Billing and Payment terms and conditions (which are incorporated herein), comprise the entire agreement between you and publisher (and CCC) concerning this licensing transaction. In the event of any conflict between your obligations established by these terms and conditions and those established by CCC's Billing and Payment terms and conditions, these terms and conditions shall control.

14. Revocation: Elsevier or Copyright Clearance Center may deny the permissions described in this License at their sole discretion, for any reason or no reason, with a full refund payable to you. Notice of such denial will be made using the contact information provided by you. Failure to receive such notice will not alter or invalidate the denial. In no event will Elsevier or Copyright Clearance Center be responsible or liable for any costs, expenses or damage incurred by you as a result of a denial of your permission request, other than a refund of the amount(s) paid by you to Elsevier and/or Copyright Clearance Center for denied permissions.

LIMITED LICENSE

The following terms and conditions apply only to specific license types:

15. **Translation**: This permission is granted for non-exclusive world **English** rights only unless your license was granted for translation rights. If you licensed translation rights you may only translate this content into the languages you requested. A professional translator must perform all translations and reproduce the content word for word preserving the integrity of the article.

16. **Posting licensed content on any Website**: The following terms and conditions apply as follows: Licensing material from an Elsevier journal: All content posted to the web site must maintain the copyright information line on the bottom of each image; A hyper-text must be included to the Homepage of the journal from which you are licensing at http://www.sciencedirect.com/science/journal/xxxxx or the Elsevier homepage for books at http://www.elsevier.com; Central Storage: This license does not include permission for a scanned version of the material to be stored in a central repository such as that provided by Heron/XanEdu.

Licensing material from an Elsevier book: A hyper-text link must be included to the Elsevier homepage at http://www.elsevier.com . All content posted to the web site must maintain the copyright information line on the bottom of each image.

Posting licensed content on Electronic reserve: In addition to the above the following clauses are applicable: The web site must be password-protected and made available only

to bona fide students registered on a relevant course. This permission is granted for 1 year only. You may obtain a new license for future website posting.

17. **For journal authors:** the following clauses are applicable in addition to the above:

Preprints:

A preprint is an author's own write-up of research results and analysis, it has not been peer-reviewed, nor has it had any other value added to it by a publisher (such as formatting, copyright, technical enhancement etc.).

Authors can share their preprints anywhere at any time. Preprints should not be added to or enhanced in any way in order to appear more like, or to substitute for, the final versions of articles however authors can update their preprints on arXiv or RePEc with their Accepted Author Manuscript (see below).

If accepted for publication, we encourage authors to link from the preprint to their formal publication via its DOI. Millions of researchers have access to the formal publications on ScienceDirect, and so links will help users to find, access, cite and use the best available version. Please note that Cell Press, The Lancet and some society-owned have different preprint policies. Information on these policies is available on the journal homepage.

Accepted Author Manuscripts: An accepted author manuscript is the manuscript of an article that has been accepted for publication and which typically includes author-incorporated changes suggested during submission, peer review and editor-author communications.

Authors can share their accepted author manuscript:

- immediately
  - via their non-commercial person homepage or blog
  - by updating a preprint in arXiv or RePEc with the accepted manuscript
  - via their research institute or institutional repository for internal institutional uses or as part of an invitation-only research collaboration work-group
  - directly by providing copies to their students or to research collaborators for their personal use
  - for private scholarly sharing as part of an invitation-only work group on commercial sites with which Elsevier has an agreement
- After the embargo period
  - via non-commercial hosting platforms such as their institutional repository
  - via commercial sites with which Elsevier has an agreement

In all cases accepted manuscripts should:

- link to the formal publication via its DOI
- bear a CC-BY-NC-ND license - this is easy to do
- if aggregated with other manuscripts, for example in a repository or other site, be shared in alignment with our hosting policy not be added to or enhanced in any way to appear more like, or to substitute for, the published journal article.

Published journal article (JPA): A published journal article (PJA) is the definitive final record of published research that appears or will appear in the journal and embodies all value-adding publishing activities including peer review co-ordination, copy-editing, formatting, (if relevant) pagination and online enrichment.

Policies for sharing publishing journal articles differ for subscription and gold open access articles:

Subscription Articles: If you are an author, please share a link to your article rather than the full-text. Millions of researchers have access to the formal publications on ScienceDirect, and so links will help your users to find, access, cite, and use the best available version.

Theses and dissertations which contain embedded PJAs as part of the formal submission can be posted publicly by the awarding institution with DOI links back to the formal publications on ScienceDirect.

If you are affiliated with a library that subscribes to ScienceDirect you have additional private sharing rights for others' research accessed under that agreement. This includes use for classroom teaching and internal training at the institution (including use in course packs and courseware programs), and inclusion of the article for grant funding purposes.

Gold Open Access Articles: May be shared according to the author-selected end-user license and should contain a CrossMark logo, the end user license, and a DOI link to the formal publication on ScienceDirect.

Please refer to Elsevier's posting policy for further information.

18. **For book authors** the following clauses are applicable in addition to the above: Authors are permitted to place a brief summary of their work online only. You are not allowed to download and post the published electronic version of your chapter, nor may you scan the printed edition to create an electronic version. **Posting to a repository:** Authors are permitted to post a summary of their chapter only in their institution's repository.

19. **Thesis/Dissertation**: If your license is for use in a thesis/dissertation your thesis may be submitted to your institution in either print or electronic form. Should your thesis be published commercially, please reapply for permission. These requirements include permission for the Library and Archives of Canada to supply single copies, on demand, of the complete thesis and include permission for Proquest/UMI to supply single copies, on demand, of the complete thesis. Should your thesis be published commercially, please reapply for permission. Theses and dissertations which contain embedded PJAs as part of the formal submission can be posted publicly by the awarding institution with DOI links back to the formal publications on ScienceDirect.

Elsevier Open Access Terms and Conditions

You can publish open access with Elsevier in hundreds of open access journals or in nearly 2000 established subscription journals that support open access publishing. Permitted third party re-use of these open access articles is defined by the author's choice of Creative Commons user license. See our open access license policy for more information.

Terms & Conditions applicable to all Open Access articles published with Elsevier:

Any reuse of the article must not represent the author as endorsing the adaptation of the article nor should the article be modified in such a way as to damage the author's honour or reputation. If any changes have been made, such changes must be clearly indicated.

The author(s) must be appropriately credited and we ask that you include the end user license and a DOI link to the formal publication on ScienceDirect.

If any part of the material to be used (for example, figures) has appeared in our publication with credit or acknowledgement to another source it is the responsibility of the

user to ensure their reuse complies with the terms and conditions determined by the rights holder.

Additional Terms & Conditions applicable to each Creative Commons user license:

CC BY: The CC-BY license allows users to copy, to create extracts, abstracts and new works from the Article, to alter and revise the Article and to make commercial use of the Article (including reuse and/or resale of the Article by commercial entities), provided the user gives appropriate credit (with a link to the formal publication through the relevant DOI), provides a link to the license, indicates if changes were made and the licensor is not represented as endorsing the use made of the work. The full details of the license are available at http://creativecommons.org/licenses/by/4.0.

CC BY NC SA: The CC BY-NC-SA license allows users to copy, to create extracts, abstracts and new works from the Article, to alter and revise the Article, provided this is not done for commercial purposes, and that the user gives appropriate credit (with a link to the formal publication through the relevant DOI), provides a link to the license, indicates if changes were made and the licensor is not represented as endorsing the use made of the work. Further, any new works must be made available on the same conditions. The full details of the license are available at http://creativecommons.org/licenses/by-nc-sa/4.0.

CC BY NC ND: The CC BY-NC-ND license allows users to copy and distribute the Article, provided this is not done for commercial purposes and further does not permit distribution of the Article if it is changed or edited in any way, and provided the user gives appropriate credit (with a link to the formal publication through the relevant DOI), provides a link to the license, and that the licensor is not represented as endorsing the use made of the work. The full details of the license are available at http://creativecommons.org/licenses/by-nc-nd/4.0. Any commercial reuse of Open Access articles published with a CC BY NC SA or CC BY NC ND license requires permission from Elsevier and will be subject to a fee.

Commercial reuse includes:

- Associating advertising with the full text of the Article
- Charging fees for document delivery or access
- Article aggregation
- Systematic distribution via e-mail lists or share buttons

Posting or linking by commercial companies for use by customers of those companies.

20. **Other Conditions:**

v1.10

Questions? customercare@copyright.com.

CCC Marketplace

Order Number: 1577928
Order Date: 13 Feb 2025

Payment Information

Abijeet Rana
arana@iitg.ac.in
Payment method: Invoice

Billing Address:
Mr. Abijeet Rana
IIT Guwahati
Guwahati, Assam 781039
India

+91 9040166787
arana@iitg.ac.in

Customer Location:
Mr. Abijeet Rana
IIT Guwahati
Guwahati, Assam 781039
India

Order Details

1. Chemical Society reviews

Billing Status: Open

Article: Tuning the structure and function of metal-organic frameworks via linker design.

Order License ID	1577928-1	**Type of Use**	Republish in a thesis/dissertation
Order detail status	Completed		
ISSN	1460-4744	**Publisher**	ROYAL SOCIETY OF CHEMISTRY
		Portion	Image/photo/illustration

0.00 USD
Republication Permission

LICENSED CONTENT

Publication Title	Chemical Society reviews	**Publication Type**	e-journal
Article Title	Tuning the structure and function of metal-organic frameworks via linker design.	**Start Page**	5561
		End Page	5593
		Issue	16
Author / Editor	Royal Society of Chemistry (Great Britain)	**Volume**	43
Date	01/01/1972	**URL**	http://www.rsc.org/csr
Language	English		
Country	United Kingdom of Great Britain and Northern Ireland		
Rightsholder	Royal Society of Chemistry		

REQUEST DETAILS

Portion Type	Image/photo/illustration	**Distribution**	Worldwide
Number of Images / Photos / Illustrations	1	**Translation**	Original language of publication
Format (select all that apply)	Print, Electronic	**Copies for the Disabled?**	No
		Minor Editing Privileges?	No
Who Will Republish the Content?	Not-for-profit entity	**Incidental Promotional Use?**	No
Duration of Use	Life of current edition	**Currency**	USD
Lifetime Unit Quantity	Up to 250,000		
Rights Requested	Main product		

NEW WORK DETAILS

Title	Development of Water-Stable Metal-Organic Frameworks for Oil-Water Separation and Toxic Chemical Sensing	**Institution Name**	IIT Guwahati
		Expected Presentation Date	2025-07-13

Instructor Name	Abhijeet Rana

ADDITIONAL DETAILS

Order Reference Number	17	**The Requesting Person / Organization to Appear on the License**	Abijeet Rana

REQUESTED CONTENT DETAILS

Title, Description or Numeric Reference of the Portion(s)	Development of Water-Stable Metal-Organic Frameworks for Oil-Water Separation and Toxic Chemical Sensing	**Title of the Article / Chapter the Portion Is From**	Tuning the structure and function of metal-organic frameworks via linker design.
Editor of Portion(s)	Lu, Weigang; Wei, Zhangwen; Gu, Zhi-Yuan; Liu, Tian-Fu; Park, Jinhee; Park, Jihye; Tian, Jian; Zhang, Muwei; Zhang, Qiang; Gentle III, Thomas; Bosch, Mathieu; Zhou, Hong-Cai	**Author of Portion(s)**	Lu, Weigang; Wei, Zhangwen; Gu, Zhi-Yuan; Liu, Tian-Fu; Park, Jinhee; Park, Jihye; Tian, Jian; Zhang, Muwei; Zhang, Qiang; Gentle III, Thomas; Bosch, Mathieu; Zhou, Hong-Cai
Volume / Edition	43 / ONLINE	**Issue, if Republishing an Article From a Serial**	16
Page or Page Range of Portion	5561-5593	**Publication Date of Portion**	2014-08-21

Total Items: 1

Subtotal: 0.00 USD

Order Total: 0.00 USD

Marketplace Permissions General Terms and Conditions

The following terms and conditions ("General Terms"), together with any applicable Publisher Terms and Conditions, govern User's use of Works pursuant to the Licenses granted by Copyright Clearance Center, Inc. ("CCC") on behalf of the applicable Rightsholders of such Works through CCC's applicable Marketplace transactional licensing services (each, a "Service").

1) **Definitions.** For purposes of these General Terms, the following definitions apply:

"License" is the licensed use the User obtains via the Marketplace platform in a particular licensing transaction, as set forth in the Order Confirmation.

"Order Confirmation" is the confirmation CCC provides to the User at the conclusion of each Marketplace transaction. "Order Confirmation Terms" are additional terms set forth on specific Order Confirmations not set forth in the General Terms that can include terms applicable to a particular CCC transactional licensing service and/or any Rightsholder-specific terms.

"Rightsholder(s)" are the holders of copyright rights in the Works for which a User obtains licenses via the Marketplace platform, which are displayed on specific Order Confirmations.

"Terms" means the terms and conditions set forth in these General Terms and any additional Order Confirmation Terms collectively.

"User" or "you" is the person or entity making the use granted under the relevant License. Where the person accepting the Terms on behalf of a User is a freelancer or other third party who the User authorized to accept the General Terms on the User's behalf, such person shall be deemed jointly a User for purposes of such Terms.

"Work(s)" are the copyright protected works described in relevant Order Confirmations.

2) **Description of Service.** CCC's Marketplace enables Users to obtain Licenses to use one or more Works in accordance with all relevant Terms. CCC grants Licenses as an agent on behalf of the copyright rightsholder identified in the relevant Order Confirmation.

3) **Applicability of Terms.** The Terms govern User's use of Works in connection with the relevant License. In the event of any conflict between General Terms and Order Confirmation Terms, the latter shall govern. User acknowledges that Rightsholders have complete discretion whether to grant any permission, and whether to place any limitations on any grant, and that CCC has no right to supersede or to modify any such discretionary act by a Rightsholder.

4) **Representations; Acceptance.** By using the Service, User represents and warrants that User has been duly authorized by the User to accept, and hereby does accept, all Terms.

5) **Scope of License; Limitations and Obligations.** All Works and all rights therein, including copyright rights, remain the sole and exclusive property of the Rightsholder. The License provides only those rights expressly set forth in the terms and conveys no other rights in any Works

6) **General Payment Terms.** User may pay at time of checkout by credit card or choose to be invoiced. If the User chooses to be invoiced, the User shall: (i) remit payments in the manner identified on specific invoices, (ii) unless otherwise specifically stated in an Order Confirmation or separate written agreement, Users shall remit payments upon receipt of the relevant invoice from CCC, either by delivery or notification of availability of the invoice via the Marketplace platform, and (iii) if the User does not pay the invoice within 30 days of receipt, the User may incur a service charge of 1.5% per month or the maximum rate allowed by applicable law, whichever is less. While User may exercise the rights in the License immediately upon receiving the Order Confirmation, the License is automatically revoked and is null and void, as if it had never been issued, if CCC does not receive complete payment on a timely basis.

7) **General Limits on Use.** Unless otherwise provided in the Order Confirmation, any grant of rights to User (i) involves only the rights set forth in the Terms and does not include subsequent or additional uses, (ii) is non-exclusive and non-transferable, and (iii) is subject to any and all limitations and restrictions (such as, but not limited to, limitations on duration of use or circulation) included in the Terms. Upon completion of the licensed use as set forth in the Order Confirmation, User shall either secure a new permission for further use of the Work(s) or immediately cease any new use of the Work(s) and shall render inaccessible (such as by deleting or by removing or severing links or other locators) any further copies of the Work. User may only make alterations to the Work if and as expressly set forth in the Order Confirmation. No Work may be used in any way that is unlawful, including without limitation if such use would violate applicable sanctions laws or regulations, would be defamatory, violate the rights of third parties (including such third parties' rights of copyright, privacy, publicity, or other tangible or intangible property), or is otherwise illegal, sexually explicit, or obscene. In addition, User may not conjoin a Work with any other material that may result in damage to the reputation of the Rightsholder. Any unlawful use will render any licenses hereunder null and void. User agrees to inform CCC if it becomes aware of any infringement of any rights in a Work and to cooperate with any reasonable request of CCC or the Rightsholder in connection therewith.

8) **Third Party Materials.** In the event that the material for which a License is sought includes third party materials (such as photographs, illustrations, graphs, inserts and similar materials) that are identified in such material as having been used by permission (or a similar indicator), User is responsible for identifying, and seeking separate licenses (under this Service, if available, or otherwise) for any of such third party materials; without a separate license, User may not use such third party materials via the License.

9) **Copyright Notice.** Use of proper copyright notice for a Work is required as a condition of any License granted under the Service. Unless otherwise provided in the Order Confirmation, a proper copyright notice will read substantially as follows: "Used with permission of [Rightsholder's name], from [Work's title, author, volume, edition number and year of copyright]; permission conveyed through Copyright Clearance Center, Inc." Such notice must be provided in a reasonably legible font size and must be placed either on a cover page or in another location that any person, upon gaining access to the material which is the subject of a permission, shall see, or in the case of republication Licenses, immediately adjacent to the Work as used (for example, as part of a by-line or footnote) or in the place where substantially all other credits or notices for the new work containing the republished Work are located. Failure to include the required notice results in loss to the Rightsholder and CCC, and the User shall be liable to pay liquidated damages for each such failure equal to twice the use fee specified in the Order Confirmation, in addition to the use fee itself and any other fees and charges specified.

10) **Indemnity.** User hereby indemnifies and agrees to defend the Rightsholder and CCC, and their respective employees and directors, against all claims, liability, damages, costs, and expenses, including legal fees and expenses, arising out of any use of a Work beyond the scope of the rights granted herein and in the Order Confirmation, or any use of a Work which has been altered in any unauthorized way by User, including claims of defamation or infringement of rights of copyright, publicity, privacy, or other tangible or intangible property.

11) **Limitation of Liability.** UNDER NO CIRCUMSTANCES WILL CCC OR THE RIGHTSHOLDER BE LIABLE FOR ANY DIRECT, INDIRECT, CONSEQUENTIAL, OR INCIDENTAL DAMAGES (INCLUDING WITHOUT LIMITATION DAMAGES FOR LOSS OF BUSINESS PROFITS OR INFORMATION, OR FOR BUSINESS INTERRUPTION) ARISING OUT OF THE USE OR INABILITY TO USE A WORK, EVEN IF ONE OR BOTH OF THEM HAS BEEN ADVISED OF THE POSSIBILITY OF SUCH DAMAGES. In any event, the total liability of the Rightsholder and CCC (including their respective employees and directors) shall not exceed the total amount actually paid by User for the relevant License. User assumes full liability for the actions and omissions of its principals, employees, agents, affiliates, successors, and assigns.

12) **Limited Warranties.** THE WORK(S) AND RIGHT(S) ARE PROVIDED "AS IS." CCC HAS THE RIGHT TO GRANT TO USER THE RIGHTS GRANTED IN THE ORDER CONFIRMATION DOCUMENT. CCC AND THE RIGHTSHOLDER DISCLAIM ALL OTHER WARRANTIES RELATING TO THE WORK(S) AND RIGHT(S), EITHER EXPRESS OR IMPLIED, INCLUDING WITHOUT LIMITATION IMPLIED WARRANTIES OF MERCHANTABILITY OR FITNESS FOR A PARTICULAR PURPOSE. ADDITIONAL RIGHTS MAY BE REQUIRED TO USE ILLUSTRATIONS, GRAPHS, PHOTOGRAPHS, ABSTRACTS, INSERTS, OR OTHER PORTIONS OF THE WORK (AS OPPOSED TO THE ENTIRE WORK) IN A MANNER CONTEMPLATED BY USER; USER UNDERSTANDS AND AGREES THAT NEITHER CCC NOR THE RIGHTSHOLDER MAY HAVE SUCH ADDITIONAL RIGHTS TO GRANT.

13) **Effect of Breach.** Any failure by User to pay any amount when due, or any use by User of a Work beyond the scope of the License set forth in the Order Confirmation and/or the Terms, shall be a material breach of such License. Any breach not cured within 10 days of written notice thereof shall result in immediate termination of such License without further notice. Any unauthorized (but licensable) use of a Work that is terminated immediately upon notice thereof may be liquidated by payment of the Rightsholder's ordinary license price therefor; any unauthorized (and unlicensable) use that is not terminated immediately for any reason (including, for example, because materials containing the Work cannot reasonably be recalled) will be subject to all remedies available at law or in equity, but in no event to a payment of less than three times the Rightsholder's ordinary license price for the most closely analogous licensable use plus Rightsholder's and/or CCC's costs and expenses incurred in collecting such payment.

14) **Additional Terms for Specific Products and Services.** If a User is making one of the uses described in this Section 14, the additional terms and conditions apply:

a) ***Print Uses of Academic Course Content and Materials (photocopies for academic coursepacks or classroom handouts).*** For photocopies for academic coursepacks or classroom handouts the following additional terms apply:

i) The copies and anthologies created under this License may be made and assembled by faculty members individually or at their request by on-campus bookstores or copy centers, or by off-campus copy shops and other similar entities.

ii) No License granted shall in any way: (i) include any right by User to create a substantively non-identical copy of the Work or to edit or in any other way modify the Work (except by means of deleting material immediately preceding or following the entire portion of the Work copied) (ii) permit "publishing ventures" where any particular anthology would be systematically marketed at multiple institutions.

iii) Subject to any Publisher Terms (and notwithstanding any apparent contradiction in the Order Confirmation arising from data provided by User), any use authorized under the academic pay-per-use service is limited as follows:

A) any License granted shall apply to only one class (bearing a unique identifier as assigned by the institution, and thereby including all sections or other subparts of the class) at one institution;

B) use is limited to not more than 25% of the text of a book or of the items in a published collection of essays, poems or articles;

C) use is limited to no more than the greater of (a) 25% of the text of an issue of a journal or other periodical or (b) two articles from such an issue;

D) no User may sell or distribute any particular anthology, whether photocopied or electronic, at more than one institution of learning;

E) in the case of a photocopy permission, no materials may be entered into electronic memory by User except in order to produce an identical copy of a Work before or during the academic term (or analogous period) as to which any particular permission is granted. In the event that User shall choose to retain materials that are the subject of a photocopy permission in electronic memory for purposes of producing identical copies more than one day after such retention (but still within the scope of any permission granted), User must notify CCC of such fact in the applicable permission request and such retention shall constitute one copy actually sold for purposes of calculating permission fees due; and

F) any permission granted shall expire at the end of the class. No permission granted shall in any way include any right by User to create a substantively non-identical copy of the Work or to edit or in any other way modify the Work (except by means of deleting material immediately preceding or following the entire portion of the Work copied).

iv) Books and Records; Right to Audit. As to each permission granted under the academic pay-per-use Service, User shall maintain for at least four full calendar years books and records sufficient for CCC to determine the numbers of copies made by User under such permission. CCC and any representatives it may designate shall have the right to audit such books and records at any time during User's ordinary business hours, upon two days' prior notice. If any such audit shall determine that User shall have underpaid for, or underreported, any photocopies sold or by three percent (3%) or more, then User shall bear all the costs of any such audit; otherwise, CCC shall bear the costs of any such audit. Any amount determined by such audit to have been underpaid by User shall immediately be paid to CCC by User, together with interest thereon at the rate of 10% per annum from the date such amount was originally due. The provisions of this paragraph shall survive the termination of this License for any reason.

b) ***Digital Pay-Per-Uses of Academic Course Content and Materials (e-coursepacks, electronic reserves, learning management systems, academic institution intranets).*** For uses in e-coursepacks, posts in electronic reserves, posts in learning management systems, or posts on academic institution intranets, the following additional terms apply:

i) The pay-per-uses subject to this Section 14(b) include:

A) **Posting e-reserves, course management systems, e-coursepacks for text-based content,** which grants authorizations to import requested material in electronic format, and allows electronic access to this material to members of a designated college or university class, under the direction of an instructor designated by the college or university, accessible only under appropriate electronic controls (e.g., password);

B) **Posting e-reserves, course management systems, e-coursepacks for material consisting of photographs or other still images not embedded in text,** which grants not only the authorizations described in Section 14(b)(i)(A) above, but also the following authorization: to include the requested material in course materials for use consistent with Section 14(b)(i)(A) above, including any necessary resizing, reformatting or modification of the resolution of such requested material (provided that such modification does not alter the underlying editorial content or meaning of the requested material, and provided that the resulting modified content is used solely within the scope of, and in a manner consistent with, the particular authorization described in the Order Confirmation and the Terms), but not including any other form of manipulation, alteration or editing of the requested material;

C) **Posting e-reserves, course management systems, e-coursepacks or other academic distribution for audiovisual content,** which grants not only the authorizations described in Section 14(b)(i)(A) above, but also the following authorizations: (i) to include the requested material in course materials for use consistent with Section 14(b)(i)(A) above; (ii) to display and perform the requested material to such members of such class in the physical classroom or remotely by means of streaming media or other video formats; and (iii) to "clip" or reformat the requested material for purposes of time or content management or ease of delivery, provided that such "clipping" or reformatting does not alter the underlying editorial content or meaning of the requested material and that the resulting material is used solely within the scope of, and in a manner consistent with, the particular authorization described in the Order Confirmation and the Terms.

Unless expressly set forth in the relevant Order Conformation, the License does not authorize any other form of manipulation, alteration or editing of the requested material.

ii) Unless expressly set forth in the relevant Order Confirmation, no License granted shall in any way: (i) include any right by User to create a substantively non-identical copy of the Work or to edit or in any other way modify the Work (except by means of deleting material immediately preceding or following the entire portion of the Work copied or, in the case of Works subject to Sections 14(b)(1)(B) or (C) above, as described in such Sections) (ii) permit "publishing ventures" where any particular course materials would be systematically marketed at multiple institutions.

iii) Subject to any further limitations determined in the Rightsholder Terms (and notwithstanding any apparent contradiction in the Order Confirmation arising from data provided by User), any use authorized under the electronic course content pay-per-use service is limited as follows:

A) any License granted shall apply to only one class (bearing a unique identifier as assigned by the institution, and thereby including all sections or other subparts of the class) at one institution;

B) use is limited to not more than 25% of the text of a book or of the items in a published collection of essays, poems or articles;

C) use is limited to not more than the greater of (a) 25% of the text of an issue of a journal or other periodical or (b) two articles from such an issue;

D) no User may sell or distribute any particular materials, whether photocopied or electronic, at more than one institution of learning;

E) electronic access to material which is the subject of an electronic-use permission must be limited by means of electronic password, student identification or other control permitting access solely to students and instructors in the class;

F) User must ensure (through use of an electronic cover page or other appropriate means) that any person, upon gaining electronic access to the material, which is the subject of a permission, shall see:

- a proper copyright notice, identifying the Rightsholder in whose name CCC has granted permission,
- a statement to the effect that such copy was made pursuant to permission,
- a statement identifying the class to which the material applies and notifying the reader that the material has been made available electronically solely for use in the class, and
- a statement to the effect that the material may not be further distributed to any person outside the class, whether by copying or by transmission and whether electronically or in paper form, and User must also ensure that such cover page or other means will print out in the event that the person accessing the material chooses to print out the material or any part thereof.

G) any permission granted shall expire at the end of the class and, absent some other form of authorization, User is thereupon required to delete the applicable material from any electronic storage or to block electronic access to the applicable material.

iv) Uses of separate portions of a Work, even if they are to be included in the same course material or the same university or college class, require separate permissions under the electronic course content pay-per-use Service. Unless otherwise provided in the Order Confirmation, any grant of rights to User is limited to use completed no later than the end of the academic term (or analogous period) as to which any particular permission is granted.

v) Books and Records; Right to Audit. As to each permission granted under the electronic course content Service, User shall maintain for at least four full calendar years books and records sufficient for CCC to determine the numbers of copies made by User under such permission. CCC and any representatives it may designate shall have the right to audit such books and records at any time during User's ordinary business hours, upon two days' prior notice. If any such audit shall determine that User shall have underpaid for, or underreported, any electronic copies used by three percent (3%) or more, then User shall bear all the costs of any such audit; otherwise, CCC shall bear the costs of any such audit. Any amount determined by such audit to have been underpaid by User shall immediately be paid to CCC by User, together with interest thereon at the rate of 10% per annum from the date such amount was originally due. The provisions of this paragraph shall survive the termination of this license for any reason.

c) ***Pay-Per-Use Permissions for Certain Reproductions (Academic photocopies for library reserves and interlibrary loan reporting) (Non-academic internal/external business uses and commercial document delivery).*** The License expressly excludes the uses listed in Section (c)(i)-(v) below (which must be subject to separate license from the applicable Rightsholder) for: academic photocopies for library reserves and interlibrary loan reporting; and non-academic internal/external business uses and commercial document delivery.

i) electronic storage of any reproduction (whether in plain-text, PDF, or any other format) other than on a transitory basis;

ii) the input of Works or reproductions thereof into any computerized database;

iii) reproduction of an entire Work (cover-to-cover copying) except where the Work is a single article;

iv) reproduction for resale to anyone other than a specific customer of User;

v) republication in any different form. Please obtain authorizations for these uses through other CCC services or directly from the rightsholder.

Any license granted is further limited as set forth in any restrictions included in the Order Confirmation and/or in these Terms.

d) ***Electronic Reproductions in Online Environments (Non-Academic-email, Intranet, Internet and Extranet).*** For "electronic reproductions", which generally includes e-mail use (including instant messaging or other electronic transmission to a defined group of recipients) or posting on an Intranet, extranet or Intranet site (including any display or performance incidental thereto), the following additional terms apply:

i) Unless otherwise set forth in the Order Confirmation, the License is limited to use completed within 30 days for any use on the Internet, 60 days for any use on an Intranet or extranet and one year for any other use, all as measured from the "republication date" as identified in the Order Confirmation, if any, and otherwise from the date of the Order Confirmation.

ii) User may not make or permit any alterations to the Work, unless expressly set forth in the Order Confirmation (after request by User and approval by Rightsholder); provided, however, that a Work consisting of photographs or other still images not embedded in text may, if necessary, be resized, reformatted or have its resolution modified without additional express permission, and a Work consisting of audiovisual content may, if necessary, be "clipped" or reformatted for purposes of time or content management or ease of delivery (provided that any such resizing, reformatting, resolution modification or "clipping" does not alter the underlying editorial content or meaning of the Work used, and that the resulting material is used solely within the scope of, and in a manner consistent with, the particular License described in the Order Confirmation and the Terms.

15) **Miscellaneous.**

a) User acknowledges that CCC may, from time to time, make changes or additions to the Service or to the Terms, and that Rightsholder may make changes or additions to the Rightsholder Terms. Such updated Terms will replace the prior terms and conditions in the order workflow and shall be effective as to any subsequent Licenses but shall not apply to Licenses already granted and paid for under a prior set of terms.

b) Use of User-related information collected through the Service is governed by CCC's privacy policy, available online at www.copyright.com/about/privacy-policy/.

c) The License is personal to User. Therefore, User may not assign or transfer to any other person (whether a natural person or an organization of any kind) the License or any rights granted thereunder; provided, however, that, where applicable, User may assign such License in its entirety on written notice to CCC in the event of a transfer of all or substantially all of User's rights in any new material which includes the Work(s) licensed under this Service.

d) No amendment or waiver of any Terms is binding unless set forth in writing and signed by the appropriate parties, including, where applicable, the Rightsholder. The Rightsholder and CCC hereby object to any terms contained in any writing prepared by or on behalf of the User or its principals, employees, agents or affiliates and purporting to govern or otherwise relate to the License described in the Order Confirmation, which terms are in any way inconsistent with any Terms set forth in the Order Confirmation, and/or in CCC's standard operating procedures, whether such writing is prepared prior to, simultaneously with or subsequent to the Order Confirmation, and whether such writing appears on a copy of the Order Confirmation or in a separate instrument.

e) The License described in the Order Confirmation shall be governed by and construed under the law of the State of New York, USA, without regard to the principles thereof of conflicts of law. Any case, controversy, suit, action, or proceeding arising out of, in connection with, or related to such License shall be brought, at CCC's sole discretion, in any federal or state court located in the County of New York, State of New York, USA, or in any federal or state court whose geographical jurisdiction covers the location of the Rightsholder set forth in the Order Confirmation. The parties expressly submit to the personal jurisdiction and venue of each such federal or state court.

Last updated October 2022

RightsLink

SPRINGER NATURE

A Study of the Fabrication of Different-Dimensional Metal–Organic Frameworks and Their Hybrid Composites for Novel Applications

Author: Asima Imtiyaz et al
Publication: Journal of Inorganic and Organometallic Polymers and Materials
Publisher: Springer Nature
Date: Jul 4, 2023

Order Completed

Thank you for your order.

This Agreement between Abhijeet Rana ("You") and Springer Nature ("Springer Nature") consists of your license details and the terms and conditions provided by Springer Nature and Copyright Clearance Center.

Your confirmation email will contain your order number for future reference.

License Number	5967010846868
License date	Feb 13, 2025

Printable Details

Licensed Content

Licensed Content Publisher	Springer Nature
Licensed Content Publication	Journal of Inorganic and Organometallic Polymers and Materials
Licensed Content Title	A Study of the Fabrication of Different-Dimensional Metal–Organic Frameworks and Their Hybrid Composites for Novel Applications
Licensed Content Author	Asima Imtiyaz et al
Licensed Content Date	Jul 4, 2023

Order Details

Type of Use	Thesis/Dissertation
Requestor Type	academic/university or research institute
Format	print and electronic
Portion	figures/tables/illustrations
Number of figures/tables/illustrations	1
Will you be translating?	no
Circulation/distribution	50000 or greater
Author of this Springer Nature content	no

About Your Work

Title of new work	Development of Water-Stable Metal-Organic Frameworks for Oil-Water Separation and Toxic Chemical Sensing
Institution name	IIT Guwahati
Expected presentation date	Jul 2025

Additional Data

Portions	4
The Requesting Person / Organization to Appear on the License	Abhijeet Rana

Requestor Location

Mr. Abijeet Rana
IIT Guwahati

Requestor Location

Guwahati, Assam 781039
India

Tax Details

Billing Information

Billing Type Invoice

Abijeet Rana
IIT Guwahati

Billing address

Guwahati, India 781039

Order Reference Number

Order reference number 111

Total: 0.00 USD

CLOSE WINDOW ORDER MORE

ELSEVIER LICENSE
TERMS AND CONDITIONS

Feb 13, 2025

This Agreement between Abijeet Rana ("You") and Elsevier ("Elsevier") consists of your license details and the terms and conditions provided by Elsevier and Copyright Clearance Center.

License Number	5967041465173
License date	Feb 13, 2025
Licensed Content Publisher	Elsevier
Licensed Content Publication	Coordination Chemistry Reviews
Licensed Content Title	When defects turn into virtues: The curious case of zirconium-based metal-organic frameworks
Licensed Content Author	Marco Taddei
Licensed Content Date	Jul 15, 2017
Licensed Content Volume	343
Licensed Content Issue	n/a
Licensed Content Pages	24
Start Page	1
End Page	24
Type of Use	reuse in a thesis/dissertation

Portion	figures/tables/illustrations
Number of figures/tables/illustrations	2
Format	both print and electronic
Are you the author of this Elsevier article?	No
Will you be translating?	No
Title of new work	Development of Water-Stable Metal-Organic Frameworks for Oil-Water Separation and Toxic Chemical Sensing
Institution name	IIT Guwahati
Expected presentation date	Jul 2025
Portions	2
The Requesting Person / Organization to Appear on the License	Abijeet Rana
Requestor Location	Mr. Abijeet Rana IIT Guwahati Guwahati, Assam 781039 India
Order reference number	115
Publisher Tax ID	GB 494 6272 12
Total	0.00 USD
Terms and Conditions	

INTRODUCTION

1. The publisher for this copyrighted material is Elsevier. By clicking "accept" in connection with completing this licensing transaction, you agree that the following terms and conditions apply to this transaction (along with the Billing and Payment terms and conditions established by Copyright Clearance Center, Inc. ("CCC"), at the time that you opened your RightsLink account and that are available at any time at https://myaccount.copyright.com).

GENERAL TERMS

2. Elsevier hereby grants you permission to reproduce the aforementioned material subject to the terms and conditions indicated.

3. Acknowledgement: If any part of the material to be used (for example, figures) has appeared in our publication with credit or acknowledgement to another source, permission must also be sought from that source. If such permission is not obtained then that material may not be included in your publication/copies. Suitable acknowledgement to the source must be made, either as a footnote or in a reference list at the end of your publication, as follows:

"Reprinted from Publication title, Vol /edition number, Author(s), Title of article / title of chapter, Pages No., Copyright (Year), with permission from Elsevier [OR APPLICABLE SOCIETY COPYRIGHT OWNER]." Also Lancet special credit - "Reprinted from The Lancet, Vol. number, Author(s), Title of article, Pages No., Copyright (Year), with permission from Elsevier."

4. Reproduction of this material is confined to the purpose and/or media for which permission is hereby given. The material may not be reproduced or used in any other way, including use in combination with an artificial intelligence tool (including to train an algorithm, test, process, analyse, generate output and/or develop any form of artificial intelligence tool), or to create any derivative work and/or service (including resulting from the use of artificial intelligence tools).

5. Altering/Modifying Material: Not Permitted. However figures and illustrations may be altered/adapted minimally to serve your work. Any other abbreviations, additions, deletions and/or any other alterations shall be made only with prior written authorization of Elsevier Ltd. (Please contact Elsevier's permissions helpdesk here). No modifications can be made to any Lancet figures/tables and they must be reproduced in full.

6. If the permission fee for the requested use of our material is waived in this instance, please be advised that your future requests for Elsevier materials may attract a fee.

7. Reservation of Rights: Publisher reserves all rights not specifically granted in the combination of (i) the license details provided by you and accepted in the course of this licensing transaction, (ii) these terms and conditions and (iii) CCC's Billing and Payment terms and conditions.

8. License Contingent Upon Payment: While you may exercise the rights licensed immediately upon issuance of the license at the end of the licensing process for the transaction, provided that you have disclosed complete and accurate details of your proposed use, no license is finally effective unless and until full payment is received from you (either by publisher or by CCC) as provided in CCC's Billing and Payment terms and conditions. If full payment is not received on a timely basis, then any license preliminarily granted shall be deemed automatically revoked and shall be void as if never granted. Further, in the event that you breach any of these terms and conditions or any of CCC's Billing and Payment terms and conditions, the license is automatically revoked and shall be void as if never granted. Use of materials as described in a revoked license, as well as any use of the materials beyond the scope of an unrevoked license, may constitute copyright infringement and publisher reserves the right to take any and all action to protect its copyright in the materials.

9. Warranties: Publisher makes no representations or warranties with respect to the licensed material.

10. Indemnity: You hereby indemnify and agree to hold harmless publisher and CCC, and their respective officers, directors, employees and agents, from and against any and all claims arising out of your use of the licensed material other than as specifically authorized pursuant to this license.

11. No Transfer of License: This license is personal to you and may not be sublicensed, assigned, or transferred by you to any other person without publisher's written permission.

12. No Amendment Except in Writing: This license may not be amended except in a writing signed by both parties (or, in the case of publisher, by CCC on publisher's behalf).

13. Objection to Contrary Terms: Publisher hereby objects to any terms contained in any purchase order, acknowledgment, check endorsement or other writing prepared by you, which terms are inconsistent with these terms and conditions or CCC's Billing and Payment terms and conditions. These terms and conditions, together with CCC's Billing and Payment terms and conditions (which are incorporated herein), comprise the entire agreement between you and publisher (and CCC) concerning this licensing transaction. In the event of any conflict between your obligations established by these terms and conditions and those established by CCC's Billing and Payment terms and conditions, these terms and conditions shall control.

14. Revocation: Elsevier or Copyright Clearance Center may deny the permissions described in this License at their sole discretion, for any reason or no reason, with a full refund payable to you. Notice of such denial will be made using the contact information provided by you. Failure to receive such notice will not alter or invalidate the denial. In no event will Elsevier or Copyright Clearance Center be responsible or liable for any costs, expenses or damage incurred by you as a result of a denial of your permission request, other than a refund of the amount(s) paid by you to Elsevier and/or Copyright Clearance Center for denied permissions.

LIMITED LICENSE

The following terms and conditions apply only to specific license types:

15. **Translation**: This permission is granted for non-exclusive world **English** rights only unless your license was granted for translation rights. If you licensed translation rights you may only translate this content into the languages you requested. A professional translator must perform all translations and reproduce the content word for word preserving the integrity of the article.

16. **Posting licensed content on any Website**: The following terms and conditions apply as follows: Licensing material from an Elsevier journal: All content posted to the web site must maintain the copyright information line on the bottom of each image; A hyper-text must be included to the Homepage of the journal from which you are licensing at http://www.sciencedirect.com/science/journal/xxxxx or the Elsevier homepage for books at http://www.elsevier.com; Central Storage: This license does not include permission for a scanned version of the material to be stored in a central repository such as that provided by Heron/XanEdu.

Licensing material from an Elsevier book: A hyper-text link must be included to the Elsevier homepage at http://www.elsevier.com . All content posted to the web site must maintain the copyright information line on the bottom of each image.

Posting licensed content on Electronic reserve: In addition to the above the following clauses are applicable: The web site must be password-protected and made available only

to bona fide students registered on a relevant course. This permission is granted for 1 year only. You may obtain a new license for future website posting.

17. **For journal authors:** the following clauses are applicable in addition to the above:

Preprints:

A preprint is an author's own write-up of research results and analysis, it has not been peer-reviewed, nor has it had any other value added to it by a publisher (such as formatting, copyright, technical enhancement etc.).

Authors can share their preprints anywhere at any time. Preprints should not be added to or enhanced in any way in order to appear more like, or to substitute for, the final versions of articles however authors can update their preprints on arXiv or RePEc with their Accepted Author Manuscript (see below).

If accepted for publication, we encourage authors to link from the preprint to their formal publication via its DOI. Millions of researchers have access to the formal publications on ScienceDirect, and so links will help users to find, access, cite and use the best available version. Please note that Cell Press, The Lancet and some society-owned have different preprint policies. Information on these policies is available on the journal homepage.

Accepted Author Manuscripts: An accepted author manuscript is the manuscript of an article that has been accepted for publication and which typically includes author-incorporated changes suggested during submission, peer review and editor-author communications.

Authors can share their accepted author manuscript:

- immediately
  - via their non-commercial person homepage or blog
  - by updating a preprint in arXiv or RePEc with the accepted manuscript
  - via their research institute or institutional repository for internal institutional uses or as part of an invitation-only research collaboration work-group
  - directly by providing copies to their students or to research collaborators for their personal use
  - for private scholarly sharing as part of an invitation-only work group on commercial sites with which Elsevier has an agreement
- After the embargo period
  - via non-commercial hosting platforms such as their institutional repository
  - via commercial sites with which Elsevier has an agreement

In all cases accepted manuscripts should:

- link to the formal publication via its DOI
- bear a CC-BY-NC-ND license - this is easy to do
- if aggregated with other manuscripts, for example in a repository or other site, be shared in alignment with our hosting policy not be added to or enhanced in any way to appear more like, or to substitute for, the published journal article.

Published journal article (JPA): A published journal article (PJA) is the definitive final record of published research that appears or will appear in the journal and embodies all value-adding publishing activities including peer review co-ordination, copy-editing, formatting, (if relevant) pagination and online enrichment.

Policies for sharing publishing journal articles differ for subscription and gold open access articles:

Subscription Articles: If you are an author, please share a link to your article rather than the full-text. Millions of researchers have access to the formal publications on ScienceDirect, and so links will help your users to find, access, cite, and use the best available version.

Theses and dissertations which contain embedded PJAs as part of the formal submission can be posted publicly by the awarding institution with DOI links back to the formal publications on ScienceDirect.

If you are affiliated with a library that subscribes to ScienceDirect you have additional private sharing rights for others' research accessed under that agreement. This includes use for classroom teaching and internal training at the institution (including use in course packs and courseware programs), and inclusion of the article for grant funding purposes.

Gold Open Access Articles: May be shared according to the author-selected end-user license and should contain a CrossMark logo, the end user license, and a DOI link to the formal publication on ScienceDirect.

Please refer to Elsevier's posting policy for further information.

18. **For book authors** the following clauses are applicable in addition to the above: Authors are permitted to place a brief summary of their work online only. You are not allowed to download and post the published electronic version of your chapter, nor may you scan the printed edition to create an electronic version. **Posting to a repository:** Authors are permitted to post a summary of their chapter only in their institution's repository.

19. **Thesis/Dissertation**: If your license is for use in a thesis/dissertation your thesis may be submitted to your institution in either print or electronic form. Should your thesis be published commercially, please reapply for permission. These requirements include permission for the Library and Archives of Canada to supply single copies, on demand, of the complete thesis and include permission for Proquest/UMI to supply single copies, on demand, of the complete thesis. Should your thesis be published commercially, please reapply for permission. Theses and dissertations which contain embedded PJAs as part of the formal submission can be posted publicly by the awarding institution with DOI links back to the formal publications on ScienceDirect.

Elsevier Open Access Terms and Conditions

You can publish open access with Elsevier in hundreds of open access journals or in nearly 2000 established subscription journals that support open access publishing. Permitted third party re-use of these open access articles is defined by the author's choice of Creative Commons user license. See our open access license policy for more information.

Terms & Conditions applicable to all Open Access articles published with Elsevier:

Any reuse of the article must not represent the author as endorsing the adaptation of the article nor should the article be modified in such a way as to damage the author's honour or reputation. If any changes have been made, such changes must be clearly indicated.

The author(s) must be appropriately credited and we ask that you include the end user license and a DOI link to the formal publication on ScienceDirect.

If any part of the material to be used (for example, figures) has appeared in our publication with credit or acknowledgement to another source it is the responsibility of the

user to ensure their reuse complies with the terms and conditions determined by the rights holder.

Additional Terms & Conditions applicable to each Creative Commons user license:

CC BY: The CC-BY license allows users to copy, to create extracts, abstracts and new works from the Article, to alter and revise the Article and to make commercial use of the Article (including reuse and/or resale of the Article by commercial entities), provided the user gives appropriate credit (with a link to the formal publication through the relevant DOI), provides a link to the license, indicates if changes were made and the licensor is not represented as endorsing the use made of the work. The full details of the license are available at http://creativecommons.org/licenses/by/4.0.

CC BY NC SA: The CC BY-NC-SA license allows users to copy, to create extracts, abstracts and new works from the Article, to alter and revise the Article, provided this is not done for commercial purposes, and that the user gives appropriate credit (with a link to the formal publication through the relevant DOI), provides a link to the license, indicates if changes were made and the licensor is not represented as endorsing the use made of the work. Further, any new works must be made available on the same conditions. The full details of the license are available at http://creativecommons.org/licenses/by-nc-sa/4.0.

CC BY NC ND: The CC BY-NC-ND license allows users to copy and distribute the Article, provided this is not done for commercial purposes and further does not permit distribution of the Article if it is changed or edited in any way, and provided the user gives appropriate credit (with a link to the formal publication through the relevant DOI), provides a link to the license, and that the licensor is not represented as endorsing the use made of the work. The full details of the license are available at http://creativecommons.org/licenses/by-nc-nd/4.0. Any commercial reuse of Open Access articles published with a CC BY NC SA or CC BY NC ND license requires permission from Elsevier and will be subject to a fee.

Commercial reuse includes:

- Associating advertising with the full text of the Article
- Charging fees for document delivery or access
- Article aggregation
- Systematic distribution via e-mail lists or share buttons

Posting or linking by commercial companies for use by customers of those companies.

20. **Other Conditions:**

v1.10

Questions? customercare@copyright.com.

RightsLink

ACS Publications

Structures, Sorption Characteristics, and Nonlinear Optical Properties of a New Series of Highly Stable Aluminum MOFs

Author: Helge Reinsch, Monique A. van der Veen, Barbara Gil, et al
Publication: Chemistry of Materials
Publisher: American Chemical Society
Date: Jan 1, 2013

PERMISSION/LICENSE IS GRANTED FOR YOUR ORDER AT NO CHARGE

This type of permission/license, instead of the standard Terms and Conditions, is sent to you because no fee is being charged for your order. Please note the following:

- Permission is granted for your request in both print and electronic formats, and translations.
- If figures and/or tables were requested, they may be adapted or used in part.
- Please print this page for your records and send a copy of it to your publisher/graduate school.
- Appropriate credit for the requested material should be given as follows: "Reprinted (adapted) with permission from {COMPLETE REFERENCE CITATION}. Copyright {YEAR} American Chemical Society." Insert appropriate information in place of the capitalized words.
- One-time permission is granted only for the use specified in your RightsLink request. No additional uses are granted (such as derivative works or other editions). For any uses, please submit a new request.

If credit is given to another source for the material you requested from RightsLink, permission must be obtained from that source.

BACK CLOSE WINDOW

CCC Marketplace

Order Number: 1578082
Order Date: 13 Feb 2025

Payment Information

Abijeet Rana
arana@iitg.ac.in
Payment method: Invoice

Billing Address:
Mr. Abijeet Rana
IIT Guwahati
Guwahati, Assam 781039
India

+91 9040166787
arana@iitg.ac.in

Customer Location:
Mr. Abijeet Rana
IIT Guwahati
Guwahati, Assam 781039
India

Order Details

1. CrystEngComm

Billing Status: Open

Article: Metal-organic Frameworks (MOFs) as Fluorescence Sensors: Principles, Development and Prospects

Order License ID	1578082-1	**Type of Use**	Republish in a thesis/dissertation
Order detail status	Completed		
ISSN	1466-8033	**Publisher**	ROYAL SOCIETY OF CHEMISTRY
		Portion	Image/photo/illustration

0.00 USD
Republication Permission

LICENSED CONTENT

Publication Title	CrystEngComm	**Publication Type**	e-journal
Article Title	Metal-organic Frameworks (MOFs) as Fluorescence Sensors: Principles, Development and Prospects	**Start Page**	7881
		End Page	7901
		Issue	45
Author / Editor	Royal Society of Chemistry (Great Britain)	**Volume**	24
		URL	http://www.rsc.org/Publishing/Journals/ce/index.asp
Date	01/01/1999		
Language	English		
Country	United Kingdom of Great Britain and Northern Ireland		
Rightsholder	Royal Society of Chemistry		

REQUEST DETAILS

Portion Type	Image/photo/illustration	**Distribution**	Worldwide
Number of Images / Photos / Illustrations	1	**Translation**	Original language of publication
Format (select all that apply)	Print, Electronic	**Copies for the Disabled?**	No
		Minor Editing Privileges?	No
Who Will Republish the Content?	Not-for-profit entity	**Incidental Promotional Use?**	No
Duration of Use	Life of current edition	**Currency**	USD
Lifetime Unit Quantity	Up to 750,000		
Rights Requested	Main product		

NEW WORK DETAILS

Title	Development of Water-Stable Metal-Organic Frameworks for Oil-Water Separation and Toxic Chemical Sensing	**Institution Name**	IIT Guwahati
		Expected Presentation Date	2025-07-13
Instructor Name	Abhijeet Rana		

ADDITIONAL DETAILS

Order Reference Number	120	**The Requesting Person / Organization to Appear on the License**	Abhijeet Rana

REQUESTED CONTENT DETAILS

Title, Description or Numeric Reference of the Portion(s)	Development of Water-Stable Metal-Organic Frameworks for Oil-Water Separation and Toxic Chemical Sensing	**Title of the Article / Chapter the Portion Is From**	Metal-organic Frameworks (MOFs) as Fluorescence Sensors: Principles, Development and Prospects
Editor of Portion(s)	Wu, Tingting; Gao, Xiang-Jing; Ge, Fa-Yuan; Zheng, Hegen	**Author of Portion(s)**	Wu, Tingting; Gao, Xiang-Jing; Ge, Fa-Yuan; Zheng, Hegen
Volume / Edition	24	**Issue, if Republishing an Article From a Serial**	45
Page or Page Range of Portion	7881-7901	**Publication Date of Portion**	2022-01-01

Total Items: 1

Subtotal: 0.00 USD

Order Total: 0.00 USD

Marketplace Permissions General Terms and Conditions

The following terms and conditions ("General Terms"), together with any applicable Publisher Terms and Conditions, govern User's use of Works pursuant to the Licenses granted by Copyright Clearance Center, Inc. ("CCC") on behalf of the applicable Rightsholders of such Works through CCC's applicable Marketplace transactional licensing services (each, a "Service").

1) **Definitions.** For purposes of these General Terms, the following definitions apply:

"License" is the licensed use the User obtains via the Marketplace platform in a particular licensing transaction, as set forth in the Order Confirmation.

"Order Confirmation" is the confirmation CCC provides to the User at the conclusion of each Marketplace transaction. "Order Confirmation Terms" are additional terms set forth on specific Order Confirmations not set forth in the General Terms that can include terms applicable to a particular CCC transactional licensing service and/or any Rightsholder-specific terms.

"Rightsholder(s)" are the holders of copyright rights in the Works for which a User obtains licenses via the Marketplace platform, which are displayed on specific Order Confirmations.

"Terms" means the terms and conditions set forth in these General Terms and any additional Order Confirmation Terms collectively.

"User" or "you" is the person or entity making the use granted under the relevant License. Where the person accepting the Terms on behalf of a User is a freelancer or other third party who the User authorized to accept the General Terms on the User's behalf, such person shall be deemed jointly a User for purposes of such Terms.

"Work(s)" are the copyright protected works described in relevant Order Confirmations.

2) **Description of Service.** CCC's Marketplace enables Users to obtain Licenses to use one or more Works in accordance with all relevant Terms. CCC grants Licenses as an agent on behalf of the copyright rightsholder identified in the relevant Order Confirmation.

3) **Applicability of Terms.** The Terms govern User's use of Works in connection with the relevant License. In the event of any conflict between General Terms and Order Confirmation Terms, the latter shall govern. User acknowledges that Rightsholders have complete discretion whether to grant any permission, and whether to place any limitations on any grant, and that CCC has no right to supersede or to modify any such discretionary act by a Rightsholder.

4) **Representations; Acceptance.** By using the Service, User represents and warrants that User has been duly authorized by the User to accept, and hereby does accept, all Terms.

5) **Scope of License; Limitations and Obligations.** All Works and all rights therein, including copyright rights, remain the sole and exclusive property of the Rightsholder. The License provides only those rights expressly set forth in the terms and conveys no other rights in any Works

6) **General Payment Terms.** User may pay at time of checkout by credit card or choose to be invoiced. If the User chooses to be invoiced, the User shall: (i) remit payments in the manner identified on specific invoices, (ii) unless otherwise specifically stated in an Order Confirmation or separate written agreement, Users shall remit payments upon receipt of the relevant invoice from CCC, either by delivery or notification of availability of the invoice via the Marketplace platform, and (iii) if the User does not pay the invoice within 30 days of receipt, the User may incur a service charge of 1.5% per month or the maximum rate allowed by applicable law, whichever is less. While User may exercise the rights in the License immediately upon receiving the Order Confirmation, the License is automatically revoked and is null and void, as if it had never been issued, if CCC does not receive complete payment on a timely basis.

7) **General Limits on Use.** Unless otherwise provided in the Order Confirmation, any grant of rights to User (i) involves only the rights set forth in the Terms and does not include subsequent or additional uses, (ii) is non-exclusive and non-transferable, and (iii) is subject to any and all limitations and restrictions (such as, but not limited to, limitations on duration of use or circulation) included in the Terms. Upon completion of the licensed use as set forth in the Order Confirmation, User shall either secure a new permission for further use of the Work(s) or immediately cease any new use of the Work(s) and shall render inaccessible (such as by deleting or by removing or severing links or other locators) any further copies of the Work. User may only make alterations to the Work if and as expressly set forth in the Order Confirmation. No Work may be used in any way that is unlawful, including without limitation if such use would violate applicable sanctions laws or regulations, would be defamatory, violate the rights of third parties (including such third parties' rights of copyright, privacy, publicity, or other tangible or intangible property), or is otherwise illegal, sexually explicit, or obscene. In addition, User may not conjoin a Work with any other material that may result in damage to the reputation of the Rightsholder. Any unlawful use will render any licenses hereunder null and void. User agrees to inform CCC if it becomes aware of any infringement of any rights in a Work and to cooperate with any reasonable request of CCC or the Rightsholder in connection therewith.

8) **Third Party Materials.** In the event that the material for which a License is sought includes third party materials (such as photographs, illustrations, graphs, inserts and similar materials) that are identified in such material as having been used by permission (or a similar indicator), User is responsible for identifying, and seeking separate licenses (under this Service, if available, or otherwise) for any of such third party materials; without a separate license, User may not use such third party materials via the License.

9) **Copyright Notice.** Use of proper copyright notice for a Work is required as a condition of any License granted under the Service. Unless otherwise provided in the Order Confirmation, a proper copyright notice will read substantially as follows: "Used with permission of [Rightsholder's name], from [Work's title, author, volume, edition number and year of copyright]; permission conveyed through Copyright Clearance Center, Inc." Such notice must be provided in a reasonably legible font size and must be placed either on a cover page or in another location that any person, upon gaining access to the material which is the subject of a permission, shall see, or in the case of republication Licenses, immediately adjacent to the Work as used (for example, as part of a by-line or footnote) or in the place where substantially all other credits or notices for the new work containing the republished Work are located. Failure to include the required notice results in loss to the Rightsholder and CCC, and the User shall be liable to pay liquidated damages for each such failure equal to twice the use fee specified in the Order Confirmation, in addition to the use fee itself and any other fees and charges specified.

10) **Indemnity.** User hereby indemnifies and agrees to defend the Rightsholder and CCC, and their respective employees and directors, against all claims, liability, damages, costs, and expenses, including legal fees and expenses, arising out of any use of a Work beyond the scope of the rights granted herein and in the Order Confirmation, or any use of a Work which has been altered in any unauthorized way by User, including claims of defamation or infringement of rights of copyright, publicity, privacy, or other tangible or intangible property.

11) **Limitation of Liability.** UNDER NO CIRCUMSTANCES WILL CCC OR THE RIGHTSHOLDER BE LIABLE FOR ANY DIRECT, INDIRECT, CONSEQUENTIAL, OR INCIDENTAL DAMAGES (INCLUDING WITHOUT LIMITATION DAMAGES FOR LOSS OF BUSINESS PROFITS OR INFORMATION, OR FOR BUSINESS INTERRUPTION) ARISING OUT OF THE USE OR INABILITY TO USE A WORK, EVEN IF ONE OR BOTH OF THEM HAS BEEN ADVISED OF THE POSSIBILITY OF SUCH DAMAGES. In any event, the total liability of the Rightsholder and CCC (including their respective employees and directors) shall not exceed the total amount actually paid by User for the relevant License. User assumes full liability for the actions and omissions of its principals, employees, agents, affiliates, successors, and assigns.

12) **Limited Warranties.** THE WORK(S) AND RIGHT(S) ARE PROVIDED "AS IS." CCC HAS THE RIGHT TO GRANT TO USER THE RIGHTS GRANTED IN THE ORDER CONFIRMATION DOCUMENT. CCC AND THE RIGHTSHOLDER DISCLAIM ALL OTHER WARRANTIES RELATING TO THE WORK(S) AND RIGHT(S), EITHER EXPRESS OR IMPLIED, INCLUDING WITHOUT LIMITATION IMPLIED WARRANTIES OF MERCHANTABILITY OR FITNESS FOR A PARTICULAR PURPOSE. ADDITIONAL RIGHTS MAY BE REQUIRED TO USE ILLUSTRATIONS, GRAPHS, PHOTOGRAPHS, ABSTRACTS, INSERTS, OR OTHER PORTIONS OF THE WORK (AS OPPOSED TO THE ENTIRE WORK) IN A MANNER CONTEMPLATED BY USER; USER UNDERSTANDS AND AGREES THAT NEITHER CCC NOR THE RIGHTSHOLDER MAY HAVE SUCH ADDITIONAL RIGHTS TO GRANT.

13) **Effect of Breach.** Any failure by User to pay any amount when due, or any use by User of a Work beyond the scope of the License set forth in the Order Confirmation and/or the Terms, shall be a material breach of such License. Any breach not cured within 10 days of written notice thereof shall result in immediate termination of such License without further notice. Any unauthorized (but licensable) use of a Work that is terminated immediately upon notice thereof may be liquidated by payment of the Rightsholder's ordinary license price therefor; any unauthorized (and unlicensable) use that is not terminated immediately for any reason (including, for example, because materials containing the Work cannot reasonably be recalled) will be subject to all remedies available at law or in equity, but in no event to a payment of less than three times the Rightsholder's ordinary license price for the most closely analogous licensable use plus Rightsholder's and/or CCC's costs and expenses incurred in collecting such payment.

14) **Additional Terms for Specific Products and Services.** If a User is making one of the uses described in this Section 14, the additional terms and conditions apply:

a) ***Print Uses of Academic Course Content and Materials (photocopies for academic coursepacks or classroom handouts).*** For photocopies for academic coursepacks or classroom handouts the following additional terms apply:

i) The copies and anthologies created under this License may be made and assembled by faculty members individually or at their request by on-campus bookstores or copy centers, or by off-campus copy shops and other similar entities.

ii) No License granted shall in any way: (i) include any right by User to create a substantively non-identical copy of the Work or to edit or in any other way modify the Work (except by means of deleting material immediately preceding or following the entire portion of the Work copied) (ii) permit "publishing ventures" where any particular anthology would be systematically marketed at multiple institutions.

iii) Subject to any Publisher Terms (and notwithstanding any apparent contradiction in the Order Confirmation arising from data provided by User), any use authorized under the academic pay-per-use service is limited as follows:

A) any License granted shall apply to only one class (bearing a unique identifier as assigned by the institution, and thereby including all sections or other subparts of the class) at one institution;

B) use is limited to not more than 25% of the text of a book or of the items in a published collection of essays, poems or articles;

C) use is limited to no more than the greater of (a) 25% of the text of an issue of a journal or other periodical or (b) two articles from such an issue;

D) no User may sell or distribute any particular anthology, whether photocopied or electronic, at more than one institution of learning;

E) in the case of a photocopy permission, no materials may be entered into electronic memory by User except in order to produce an identical copy of a Work before or during the academic term (or analogous period) as to which any particular permission is granted. In the event that User shall choose to retain materials that are the subject of a photocopy permission in electronic memory for purposes of producing identical copies more than one day after such retention (but still within the scope of any permission granted), User must notify CCC of such fact in the applicable permission request and such retention shall constitute one copy actually sold for purposes of calculating permission fees due; and

F) any permission granted shall expire at the end of the class. No permission granted shall in any way include any right by User to create a substantively non-identical copy of the Work or to edit or in any other way modify the Work (except by means of deleting material immediately preceding or following the entire portion of the Work copied).

iv) Books and Records; Right to Audit. As to each permission granted under the academic pay-per-use Service, User shall maintain for at least four full calendar years books and records sufficient for CCC to determine the numbers of copies made by User under such permission. CCC and any representatives it may designate shall have the right to audit such books and records at any time during User's ordinary business hours, upon two days' prior notice. If any such audit shall determine that User shall have underpaid for, or underreported, any photocopies sold or by three percent (3%) or more, then User shall bear all the costs of any such audit; otherwise, CCC shall bear the costs of any such audit. Any amount determined by such audit to have been underpaid by User shall immediately be paid to CCC by User, together with interest thereon at the rate of 10% per annum from the date such amount was originally due. The provisions of this paragraph shall survive the termination of this License for any reason.

b) ***Digital Pay-Per-Uses of Academic Course Content and Materials (e-coursepacks, electronic reserves, learning management systems, academic institution intranets).*** For uses in e-coursepacks, posts in electronic reserves, posts in learning management systems, or posts on academic institution intranets, the following additional terms apply:

i) The pay-per-uses subject to this Section 14(b) include:

A) **Posting e-reserves, course management systems, e-coursepacks for text-based content,** which grants authorizations to import requested material in electronic format, and allows electronic access to this material to members of a designated college or university class, under the direction of an instructor designated by the college or university, accessible only under appropriate electronic controls (e.g., password);

B) **Posting e-reserves, course management systems, e-coursepacks for material consisting of photographs or other still images not embedded in text,** which grants not only the authorizations described in Section 14(b)(i)(A) above, but also the following authorization: to include the requested material in course materials for use consistent with Section 14(b)(i)(A) above, including any necessary resizing, reformatting or modification of the resolution of such requested material (provided that such modification does not alter the underlying editorial content or meaning of the requested material, and provided that the resulting modified content is used solely within the scope of, and in a manner consistent with, the particular authorization described in the Order Confirmation and the Terms), but not including any other form of manipulation, alteration or editing of the requested material;

C) **Posting e-reserves, course management systems, e-coursepacks or other academic distribution for audiovisual content,** which grants not only the authorizations described in Section 14(b)(i)(A) above, but also the following authorizations: (i) to include the requested material in course materials for use consistent with Section 14(b)(i)(A) above; (ii) to display and perform the requested material to such members of such class in the physical classroom or remotely by means of streaming media or other video formats; and (iii) to "clip" or reformat the requested material for purposes of time or content management or ease of delivery, provided that such "clipping" or reformatting does not alter the underlying editorial content or meaning of the requested material and that the resulting material is used solely within the scope of, and in a manner consistent with, the particular authorization described in the Order Confirmation and the Terms.

Unless expressly set forth in the relevant Order Conformation, the License does not authorize any other form of manipulation, alteration or editing of the requested material.

ii) Unless expressly set forth in the relevant Order Confirmation, no License granted shall in any way: (i) include any right by User to create a substantively non-identical copy of the Work or to edit or in any other way modify the Work (except by means of deleting material immediately preceding or following the entire portion of the Work copied or, in the case of Works subject to Sections 14(b)(1)(B) or (C) above, as described in such Sections) (ii) permit "publishing ventures" where any particular course materials would be systematically marketed at multiple institutions.

iii) Subject to any further limitations determined in the Rightsholder Terms (and notwithstanding any apparent contradiction in the Order Confirmation arising from data provided by User), any use authorized under the electronic course content pay-per-use service is limited as follows:

A) any License granted shall apply to only one class (bearing a unique identifier as assigned by the institution, and thereby including all sections or other subparts of the class) at one institution;

B) use is limited to not more than 25% of the text of a book or of the items in a published collection of essays, poems or articles;

C) use is limited to not more than the greater of (a) 25% of the text of an issue of a journal or other periodical or (b) two articles from such an issue;

D) no User may sell or distribute any particular materials, whether photocopied or electronic, at more than one institution of learning;

E) electronic access to material which is the subject of an electronic-use permission must be limited by means of electronic password, student identification or other control permitting access solely to students and instructors in the class;

F) User must ensure (through use of an electronic cover page or other appropriate means) that any person, upon gaining electronic access to the material, which is the subject of a permission, shall see:

- a proper copyright notice, identifying the Rightsholder in whose name CCC has granted permission,
- a statement to the effect that such copy was made pursuant to permission,
- a statement identifying the class to which the material applies and notifying the reader that the material has been made available electronically solely for use in the class, and
- a statement to the effect that the material may not be further distributed to any person outside the class, whether by copying or by transmission and whether electronically or in paper form, and User must also ensure that such cover page or other means will print out in the event that the person accessing the material chooses to print out the material or any part thereof.

G) any permission granted shall expire at the end of the class and, absent some other form of authorization, User is thereupon required to delete the applicable material from any electronic storage or to block electronic access to the applicable material.

iv) Uses of separate portions of a Work, even if they are to be included in the same course material or the same university or college class, require separate permissions under the electronic course content pay-per-use Service. Unless otherwise provided in the Order Confirmation, any grant of rights to User is limited to use completed no later than the end of the academic term (or analogous period) as to which any particular permission is granted.

v) Books and Records; Right to Audit. As to each permission granted under the electronic course content Service, User shall maintain for at least four full calendar years books and records sufficient for CCC to determine the numbers of copies made by User under such permission. CCC and any representatives it may designate shall have the right to audit such books and records at any time during User's ordinary business hours, upon two days' prior notice. If any such audit shall determine that User shall have underpaid for, or underreported, any electronic copies used by three percent (3%) or more, then User shall bear all the costs of any such audit; otherwise, CCC shall bear the costs of any such audit. Any amount determined by such audit to have been underpaid by User shall immediately be paid to CCC by User, together with interest thereon at the rate of 10% per annum from the date such amount was originally due. The provisions of this paragraph shall survive the termination of this license for any reason.

c) ***Pay-Per-Use Permissions for Certain Reproductions (Academic photocopies for library reserves and interlibrary loan reporting) (Non-academic internal/external business uses and commercial document delivery).*** The License expressly excludes the uses listed in Section (c)(i)-(v) below (which must be subject to separate license from the applicable Rightsholder) for: academic photocopies for library reserves and interlibrary loan reporting; and non-academic internal/external business uses and commercial document delivery.

i) electronic storage of any reproduction (whether in plain-text, PDF, or any other format) other than on a transitory basis;

ii) the input of Works or reproductions thereof into any computerized database;

iii) reproduction of an entire Work (cover-to-cover copying) except where the Work is a single article;

iv) reproduction for resale to anyone other than a specific customer of User;

v) republication in any different form. Please obtain authorizations for these uses through other CCC services or directly from the rightsholder.

Any license granted is further limited as set forth in any restrictions included in the Order Confirmation and/or in these Terms.

d) ***Electronic Reproductions in Online Environments (Non-Academic-email, intranet, internet and extranet).*** For "electronic reproductions", which generally includes e-mail use (including instant messaging or other electronic transmission to a defined group of recipients) or posting on an Intranet, extranet or Intranet site (including any display or performance incidental thereto), the following additional terms apply:

i) Unless otherwise set forth in the Order Confirmation, the License is limited to use completed within 30 days for any use on the Internet, 60 days for any use on an Intranet or extranet and one year for any other use, all as measured from the "republication date" as identified in the Order Confirmation, if any, and otherwise from the date of the Order Confirmation.

ii) User may not make or permit any alterations to the Work, unless expressly set forth in the Order Confirmation (after request by User and approval by Rightsholder); provided, however, that a Work consisting of photographs or other still images not embedded in text may, if necessary, be resized, reformatted or have its resolution modified without additional express permission, and a Work consisting of audiovisual content may, if necessary, be "clipped" or reformatted for purposes of time or content management or ease of delivery (provided that any such resizing, reformatting, resolution modification or "clipping" does not alter the underlying editorial content or meaning of the Work used, and that the resulting material is used solely within the scope of, and in a manner consistent with, the particular License described in the Order Confirmation and the Terms.

15) **Miscellaneous.**

a) User acknowledges that CCC may, from time to time, make changes or additions to the Service or to the Terms, and that Rightsholder may make changes or additions to the Rightsholder Terms. Such updated Terms will replace the prior terms and conditions in the order workflow and shall be effective as to any subsequent Licenses but shall not apply to Licenses already granted and paid for under a prior set of terms.

b) Use of User-related information collected through the Service is governed by CCC's privacy policy, available online at www.copyright.com/about/privacy-policy/.

c) The License is personal to User. Therefore, User may not assign or transfer to any other person (whether a natural person or an organization of any kind) the License or any rights granted thereunder; provided, however, that, where applicable, User may assign such License in its entirety on written notice to CCC in the event of a transfer of all or substantially all of User's rights in any new material which includes the Work(s) licensed under this Service.

d) No amendment or waiver of any Terms is binding unless set forth in writing and signed by the appropriate parties, including, where applicable, the Rightsholder. The Rightsholder and CCC hereby object to any terms contained in any writing prepared by or on behalf of the User or its principals, employees, agents or affiliates and purporting to govern or otherwise relate to the License described in the Order Confirmation, which terms are in any way inconsistent with any Terms set forth in the Order Confirmation, and/or in CCC's standard operating procedures, whether such writing is prepared prior to, simultaneously with or subsequent to the Order Confirmation, and whether such writing appears on a copy of the Order Confirmation or in a separate instrument.

e) The License described in the Order Confirmation shall be governed by and construed under the law of the State of New York, USA, without regard to the principles thereof of conflicts of law. Any case, controversy, suit, action, or proceeding arising out of, in connection with, or related to such License shall be brought, at CCC's sole discretion, in any federal or state court located in the County of New York, State of New York, USA, or in any federal or state court whose geographical jurisdiction covers the location of the Rightsholder set forth in the Order Confirmation. The parties expressly submit to the personal jurisdiction and venue of each such federal or state court.

Last updated October 2022

Sign in/Register

pH-Stable Luminescent Metal–Organic Frameworks for the Selective Detection of Aqueous-Phase FeIII and CrVI Ions

Author: Shyam Chand Pal, Debolina Mukherjee, Madhab C. Das
Publication: Inorganic Chemistry
Publisher: American Chemical Society
Date: Aug 1, 2022

PERMISSION/LICENSE IS GRANTED FOR YOUR ORDER AT NO CHARGE

This type of permission/license, instead of the standard Terms and Conditions, is sent to you because no fee is being charged for your order. Please note the following:

- Permission is granted for your request in both print and electronic formats, and translations.
- If figures and/or tables were requested, they may be adapted or used in part.
- Please print this page for your records and send a copy of it to your publisher/graduate school.
- Appropriate credit for the requested material should be given as follows: "Reprinted (adapted) with permission from {COMPLETE REFERENCE CITATION}. Copyright {YEAR} American Chemical Society." Insert appropriate information in place of the capitalized words.
- One-time permission is granted only for the use specified in your RightsLink request. No additional uses are granted (such as derivative works or other editions). For any uses, please submit a new request.

If credit is given to another source for the material you requested from RightsLink, permission must be obtained from that source.

BACK CLOSE WINDOW

ELSEVIER LICENSE
TERMS AND CONDITIONS

Feb 20, 2025

This Agreement between Abijeet Rana ("You") and Elsevier ("Elsevier") consists of your license details and the terms and conditions provided by Elsevier and Copyright Clearance Center.

License Number	5972900220643
License date	**Feb 20, 2025**
Licensed Content Publisher	Elsevier
Licensed Content Publication	Environmental Research
Licensed Content Title	MOF-based composites as photoluminescence sensing platforms for pesticides: Applications and mechanisms
Licensed Content Author	Romina Yousefi,Shadi Asgari,Ali Banitalebi Dehkordi,Ghodsi Mohammadi Ziarani,Alireza Badiei,Fatemeh Mohajer,Rajender S. Varma,Siavash Iravani
Licensed Content Date	Jun 1, 2023
Licensed Content Volume	226
Licensed Content Issue	n/a
Licensed Content Pages	1
Start Page	115664
End Page	0

Type of Use	reuse in a thesis/dissertation
Portion	figures/tables/illustrations
Number of figures/tables/illustrations	1
Format	both print and electronic
Are you the author of this Elsevier article?	No
Will you be translating?	No
Title of new work	Development of Water-Stable Metal-Organic Frameworks for Oil-Water Separation and Toxic Chemical Sensing
Institution name	IIT Guwahati
Expected presentation date	Jul 2025
Portions	FIG. 1
The Requesting Person / Organization to Appear on the License	Abijeet Rana
Requestor Location	Mr. Abijeet Rana IIT Guwahati Guwahati, Assam 781039 India
Order reference number	124
Publisher Tax ID	GB 494 6272 12
Total	0.00 USD
Terms and Conditions	

INTRODUCTION

1. The publisher for this copyrighted material is Elsevier. By clicking "accept" in connection with completing this licensing transaction, you agree that the following terms and conditions apply to this transaction (along with the Billing and Payment terms and conditions established by Copyright Clearance Center, Inc. ("CCC"), at the time that you opened your RightsLink account and that are available at any time at https://myaccount.copyright.com).

GENERAL TERMS

2. Elsevier hereby grants you permission to reproduce the aforementioned material subject to the terms and conditions indicated.

3. Acknowledgement: If any part of the material to be used (for example, figures) has appeared in our publication with credit or acknowledgement to another source, permission must also be sought from that source. If such permission is not obtained then that material may not be included in your publication/copies. Suitable acknowledgement to the source must be made, either as a footnote or in a reference list at the end of your publication, as follows:

"Reprinted from Publication title, Vol /edition number, Author(s), Title of article / title of chapter, Pages No., Copyright (Year), with permission from Elsevier [OR APPLICABLE SOCIETY COPYRIGHT OWNER]." Also Lancet special credit - "Reprinted from The Lancet, Vol. number, Author(s), Title of article, Pages No., Copyright (Year), with permission from Elsevier."

4. Reproduction of this material is confined to the purpose and/or media for which permission is hereby given. The material may not be reproduced or used in any other way, including use in combination with an artificial intelligence tool (including to train an algorithm, test, process, analyse, generate output and/or develop any form of artificial intelligence tool), or to create any derivative work and/or service (including resulting from the use of artificial intelligence tools).

5. Altering/Modifying Material: Not Permitted. However figures and illustrations may be altered/adapted minimally to serve your work. Any other abbreviations, additions, deletions and/or any other alterations shall be made only with prior written authorization of Elsevier Ltd. (Please contact Elsevier's permissions helpdesk here). No modifications can be made to any Lancet figures/tables and they must be reproduced in full.

6. If the permission fee for the requested use of our material is waived in this instance, please be advised that your future requests for Elsevier materials may attract a fee.

7. Reservation of Rights: Publisher reserves all rights not specifically granted in the combination of (i) the license details provided by you and accepted in the course of this licensing transaction, (ii) these terms and conditions and (iii) CCC's Billing and Payment terms and conditions.

8. License Contingent Upon Payment: While you may exercise the rights licensed immediately upon issuance of the license at the end of the licensing process for the transaction, provided that you have disclosed complete and accurate details of your proposed use, no license is finally effective unless and until full payment is received from you (either by publisher or by CCC) as provided in CCC's Billing and Payment terms and conditions. If full payment is not received on a timely basis, then any license preliminarily granted shall be deemed automatically revoked and shall be void as if never granted. Further, in the event that you breach any of these terms and conditions or any of CCC's Billing and Payment terms and conditions, the license is automatically revoked and shall be void as if never granted. Use of materials as described in a revoked license, as

well as any use of the materials beyond the scope of an unrevoked license, may constitute copyright infringement and publisher reserves the right to take any and all action to protect its copyright in the materials.

9. Warranties: Publisher makes no representations or warranties with respect to the licensed material.

10. Indemnity: You hereby indemnify and agree to hold harmless publisher and CCC, and their respective officers, directors, employees and agents, from and against any and all claims arising out of your use of the licensed material other than as specifically authorized pursuant to this license.

11. No Transfer of License: This license is personal to you and may not be sublicensed, assigned, or transferred by you to any other person without publisher's written permission.

12. No Amendment Except in Writing: This license may not be amended except in a writing signed by both parties (or, in the case of publisher, by CCC on publisher's behalf).

13. Objection to Contrary Terms: Publisher hereby objects to any terms contained in any purchase order, acknowledgment, check endorsement or other writing prepared by you, which terms are inconsistent with these terms and conditions or CCC's Billing and Payment terms and conditions. These terms and conditions, together with CCC's Billing and Payment terms and conditions (which are incorporated herein), comprise the entire agreement between you and publisher (and CCC) concerning this licensing transaction. In the event of any conflict between your obligations established by these terms and conditions and those established by CCC's Billing and Payment terms and conditions, these terms and conditions shall control.

14. Revocation: Elsevier or Copyright Clearance Center may deny the permissions described in this License at their sole discretion, for any reason or no reason, with a full refund payable to you. Notice of such denial will be made using the contact information provided by you. Failure to receive such notice will not alter or invalidate the denial. In no event will Elsevier or Copyright Clearance Center be responsible or liable for any costs, expenses or damage incurred by you as a result of a denial of your permission request, other than a refund of the amount(s) paid by you to Elsevier and/or Copyright Clearance Center for denied permissions.

LIMITED LICENSE

The following terms and conditions apply only to specific license types:

15. **Translation**: This permission is granted for non-exclusive world **English** rights only unless your license was granted for translation rights. If you licensed translation rights you may only translate this content into the languages you requested. A professional translator must perform all translations and reproduce the content word for word preserving the integrity of the article.

16. **Posting licensed content on any Website**: The following terms and conditions apply as follows: Licensing material from an Elsevier journal: All content posted to the web site must maintain the copyright information line on the bottom of each image; A hyper-text must be included to the Homepage of the journal from which you are licensing at http://www.sciencedirect.com/science/journal/xxxxx or the Elsevier homepage for books at http://www.elsevier.com; Central Storage: This license does not include permission for a scanned version of the material to be stored in a central repository such as that provided by Heron/XanEdu.

Licensing material from an Elsevier book: A hyper-text link must be included to the Elsevier homepage at http://www.elsevier.com . All content posted to the web site must maintain the copyright information line on the bottom of each image.

Posting licensed content on Electronic reserve: In addition to the above the following clauses are applicable: The web site must be password-protected and made available only to bona fide students registered on a relevant course. This permission is granted for 1 year only. You may obtain a new license for future website posting.

17. **For journal authors:** the following clauses are applicable in addition to the above:

Preprints:

A preprint is an author's own write-up of research results and analysis, it has not been peer-reviewed, nor has it had any other value added to it by a publisher (such as formatting, copyright, technical enhancement etc.).

Authors can share their preprints anywhere at any time. Preprints should not be added to or enhanced in any way in order to appear more like, or to substitute for, the final versions of articles however authors can update their preprints on arXiv or RePEc with their Accepted Author Manuscript (see below).

If accepted for publication, we encourage authors to link from the preprint to their formal publication via its DOI. Millions of researchers have access to the formal publications on ScienceDirect, and so links will help users to find, access, cite and use the best available version. Please note that Cell Press, The Lancet and some society-owned have different preprint policies. Information on these policies is available on the journal homepage.

Accepted Author Manuscripts: An accepted author manuscript is the manuscript of an article that has been accepted for publication and which typically includes author-incorporated changes suggested during submission, peer review and editor-author communications.

Authors can share their accepted author manuscript:

- immediately
  - via their non-commercial person homepage or blog
  - by updating a preprint in arXiv or RePEc with the accepted manuscript
  - via their research institute or institutional repository for internal institutional uses or as part of an invitation-only research collaboration work-group
  - directly by providing copies to their students or to research collaborators for their personal use
  - for private scholarly sharing as part of an invitation-only work group on commercial sites with which Elsevier has an agreement
- After the embargo period
  - via non-commercial hosting platforms such as their institutional repository
  - via commercial sites with which Elsevier has an agreement

In all cases accepted manuscripts should:

- link to the formal publication via its DOI
- bear a CC-BY-NC-ND license - this is easy to do
- if aggregated with other manuscripts, for example in a repository or other site, be shared in alignment with our hosting policy not be added to or enhanced in any way to appear more like, or to substitute for, the published journal article.

Published journal article (JPA): A published journal article (PJA) is the definitive final record of published research that appears or will appear in the journal and embodies all value-adding publishing activities including peer review co-ordination, copy-editing, formatting, (if relevant) pagination and online enrichment.

Policies for sharing publishing journal articles differ for subscription and gold open access articles:

Subscription Articles: If you are an author, please share a link to your article rather than the full-text. Millions of researchers have access to the formal publications on ScienceDirect, and so links will help your users to find, access, cite, and use the best available version.

Theses and dissertations which contain embedded PJAs as part of the formal submission can be posted publicly by the awarding institution with DOI links back to the formal publications on ScienceDirect.

If you are affiliated with a library that subscribes to ScienceDirect you have additional private sharing rights for others' research accessed under that agreement. This includes use for classroom teaching and internal training at the institution (including use in course packs and courseware programs), and inclusion of the article for grant funding purposes.

Gold Open Access Articles: May be shared according to the author-selected end-user license and should contain a CrossMark logo, the end user license, and a DOI link to the formal publication on ScienceDirect.

Please refer to Elsevier's posting policy for further information.

18. **For book authors** the following clauses are applicable in addition to the above: Authors are permitted to place a brief summary of their work online only. You are not allowed to download and post the published electronic version of your chapter, nor may you scan the printed edition to create an electronic version. **Posting to a repository:** Authors are permitted to post a summary of their chapter only in their institution's repository.

19. **Thesis/Dissertation**: If your license is for use in a thesis/dissertation your thesis may be submitted to your institution in either print or electronic form. Should your thesis be published commercially, please reapply for permission. These requirements include permission for the Library and Archives of Canada to supply single copies, on demand, of the complete thesis and include permission for Proquest/UMI to supply single copies, on demand, of the complete thesis. Should your thesis be published commercially, please reapply for permission. Theses and dissertations which contain embedded PJAs as part of the formal submission can be posted publicly by the awarding institution with DOI links back to the formal publications on ScienceDirect.

Elsevier Open Access Terms and Conditions

You can publish open access with Elsevier in hundreds of open access journals or in nearly 2000 established subscription journals that support open access publishing. Permitted third party re-use of these open access articles is defined by the author's choice of Creative Commons user license. See our open access license policy for more information.

Terms & Conditions applicable to all Open Access articles published with Elsevier:

Any reuse of the article must not represent the author as endorsing the adaptation of the article nor should the article be modified in such a way as to damage the author's honour or reputation. If any changes have been made, such changes must be clearly indicated.

The author(s) must be appropriately credited and we ask that you include the end user license and a DOI link to the formal publication on ScienceDirect.

If any part of the material to be used (for example, figures) has appeared in our publication with credit or acknowledgement to another source it is the responsibility of the user to ensure their reuse complies with the terms and conditions determined by the rights holder.

Additional Terms & Conditions applicable to each Creative Commons user license:

CC BY: The CC-BY license allows users to copy, to create extracts, abstracts and new works from the Article, to alter and revise the Article and to make commercial use of the Article (including reuse and/or resale of the Article by commercial entities), provided the user gives appropriate credit (with a link to the formal publication through the relevant DOI), provides a link to the license, indicates if changes were made and the licensor is not represented as endorsing the use made of the work. The full details of the license are available at http://creativecommons.org/licenses/by/4.0.

CC BY NC SA: The CC BY-NC-SA license allows users to copy, to create extracts, abstracts and new works from the Article, to alter and revise the Article, provided this is not done for commercial purposes, and that the user gives appropriate credit (with a link to the formal publication through the relevant DOI), provides a link to the license, indicates if changes were made and the licensor is not represented as endorsing the use made of the work. Further, any new works must be made available on the same conditions. The full details of the license are available at http://creativecommons.org/licenses/by-nc-sa/4.0.

CC BY NC ND: The CC BY-NC-ND license allows users to copy and distribute the Article, provided this is not done for commercial purposes and further does not permit distribution of the Article if it is changed or edited in any way, and provided the user gives appropriate credit (with a link to the formal publication through the relevant DOI), provides a link to the license, and that the licensor is not represented as endorsing the use made of the work. The full details of the license are available at http://creativecommons.org/licenses/by-nc-nd/4.0. Any commercial reuse of Open Access articles published with a CC BY NC SA or CC BY NC ND license requires permission from Elsevier and will be subject to a fee.

Commercial reuse includes:

- Associating advertising with the full text of the Article
- Charging fees for document delivery or access
- Article aggregation
- Systematic distribution via e-mail lists or share buttons

Posting or linking by commercial companies for use by customers of those companies.

20. **Other Conditions:**

v1.10

Questions? customercare@copyright.com.

Publications

1. Cu(I)-Anchored Amine-Rich Covalent-Organic Polymer for Sustainable Utilization of CO_2 in the Synthesis of Valuable Chemicals and C-C Bond Formation Reactions, **A. Rana**, S. Mukherjee, K. A. Sundari, A. Dhakshinamoorthy, S. Biswas, ChemCatChem, 2025, doi:10.1002/cctc.202401503.
2. Amine-Anchored Nanoscale Covalent-Organic Framework for Detecting Kynurenine and Mitoxantrone from Biofluids and Environmental Water, **A Rana**, S Ghosh, P Mandal, AN Panda, S Biswas, ACS Applied Polymer Materials 6, 14812-14823.
3. Superhydrophobic Metal-Organic Framework Based Composite Featuring Removal of Hydrophobic Drug and Pesticide and Antibacterial Activities, **A. Rana**, S. Ghosh, A. Patel, A. Das, A. Bhunia, D. Manna, D. Volkmer, S. Biswas, Inorg. Chem., 2024, 63, 15311-15322.
4. Functional-Group Assisted Fluorescence Sensing Platform for Nanomolar Level Detection of Antineoplastic Drug and Neurotransmitter from Environmental Water and Human Bio-fluids, **A. Rana**, G. Mishra, S. Biswas, Inorg. Chem., 2024, 63, 4502-4510.
5. Design of Functionalized Luminescent MOF Sensor for Precise Monitoring of Tuberculosis Drug and Neonicotinoid Pesticide from Human Body-Fluids and Food Samples to Protect Health and Environment, **A. Rana**, N. U. Mir, A. Banik, A. Hazra, S. Biswas, J. Mater. Chem. C, 2024, 12, 1030-1039.
6. Metal-Organic Framework Based Fluorescence Sensor for Detection of Pharmaceutical Active Compounds, S. Ghosh[ǂ], **A. Rana**[ǂ], S. Biswas. Chem. Mater., 2024,36,99-131. (ǂ = equal contribution)
7. Electrophilicity Modulated Targeted Luminescence of MOF Coated Cotton Composite for Dual Analyte Detection in Aqueous Medium, **A. Rana**, S. Biswas, Inorg. Chem. Front., 2023, 10, 2742-2753.
8. An eco-friendly approach by nonfluorous self-cleaning metal-organic framework composite and membrane for oil-water separation, **A. Rana**[ǂ], S. Ghosh[ǂ], S. Biswas, Inorg. Chem. Front., 2023, 10, 612-620
9. Superhydrophobic Self-Cleaning Composite of MOF with Polypropylene Fabric for Efficient Removal of Oils from Oil-Water Mixtures and Emulsions, C. Gogoi[ǂ], **A. Rana**[ǂ], S. Ghosh[ǂ], R. Fopase, L. M. Pandey, S. Biswas, ACS Appl. Nano Mater., 2022, 5, 10003-10014.
10. A self-cleaning hydrophobic MOF based composite for highly efficient and recyclable separation of oil from water and emulsion, S. Ghosh[ǂ], **A. Rana**[ǂ], S. Kumar, C. Gogoi, S. Mukherjee, U. Manna, S. Biswas, Mater. Chem. Front., 2022, 6, 2051-2060.
11. A sulfonic acid functionalized zirconium-based metal organic framework for the selective detection of copper(II) ion, **A. Rana**, S. Nandi, S. Biswas, New J. Chem., 2022, 46, 10477-10483.
12. Rapid Recognition of Fatal Cyanide in Water in a Wide pH Range by a Trifluoroacetamido Based Metal-Organic Framework, **A. Rana**, C. Gogoi, S. Ghosh, S. Nandi, S. Kumar, U. Manna, S. Biswas, New J. Chem., 2021, 45, 20193-20200.
13. Superhydrophobicity aided highly specific and efficient removal of hydrophobic pharmaceutical wastes from environmental water and remarkable bacterial anti-

adhesion unveiled by nanosized, metal-organic framework composites, S. Ghosh, **A. Rana**, A. Patel, D. Manna, S. Biswas, Environ. Sci. Nano, 2024, 11, 1233-1244.

14. Hf-Based MOF for Rapid and Selective Sensing of a Nerve Agent Simulant and an Aminophenol: Insights from Experiment and Theory, S. Ghosh, R. Lipin, A. Ngoipala, N. Ruser, D. Venturi, **A. Rana**, M. Vandichel, S. Biswas, Inorg. Chem., 2023, 62, 14632-14646.
15. A Metal-Organic Framework Based Chemosensor for Ultrafast and Ultrasensitive Detection of Pd^{2+} ion in Water, Real Specimens and Test Strips, P. Chakraborty, **A. Rana**, S. Mukherjee, S. Biswas, Inorg. Chem., 2023, 62, 802-809.
16. Friedlander condensation reaction catalysed by hafnium-based metal-organic framework, S. Ghosh, J. Krishnan, V. Karthik, **A. Rana**, A. Dhakshinamoorthy, S. Biswas, Mol. Catal., 2022, 533, 112748.
17. Diamine functionalized Zr-based metal-organic framework for fluorescence sensing of free chlorine in aqueous phase and Knoevenagel condensation, C. Gogoi, N. Nagarjun, **A. Rana**, A. Dhakshinamoorthy, S. Biswas, Dalton Trans., 2022, 51, 6964-6975.
18. A fluorescent zirconium organic framework displaying rapid and nanomolar level detection of Hg(II) and nitroantibiotics, S. Ghosh, F. Steinke, **A. Rana**, S. Biswas, Inorg. Chem. Front., 2022, 9, 859-869.
19. A metal-organic framework with allyloxy functionalization for aqueous-phase fluorescence recognition of Pd(II) ion, S. Ghosh, F. Steinke, **A. Rana**, M. Alam, S. Biswas, Eur. J. Inorg. Chem., 2021, 3846.

Conferences Attended

1. Northeast Research Conclave (NERC-2024), 2022, 20th -22nd May 2024, Poster Presentation, Certificate.
2. P. C. Roy Memorial International Conference on Contemporary Ideas, Innovation & Initiatives in Chemical Sciences (CI3CS-2023), 2023, 23rd August–24th August, Poster Presentation, Certificate & Best Poster Presentation Prize.
3. Internation Conference on Modern Trends in Inorganic Chemistry (MTIC-XX), 2023, 14th December-17th December, Poster Presentation, Certificate.
4. Chemical Research Society of India-Americal Research Society (CRSI-ACS) Early Career Researchers Symposium 2024, 22nd -23rd October 2024, Poster Presentation, Certificate and & Best Poster Presentation Prize.
5. Frontier in Chemical Science (FICS-2024) 2024, 2nd December-4th December, Poster Presentation, Certificate.

THE END